STRUCTURAL AND PETROLOGICAL INVESTIGATIONS OF THE PRETORIA SALTPAN IMPACT CRATER AND SURROUNDING AREA

Dion Brandt

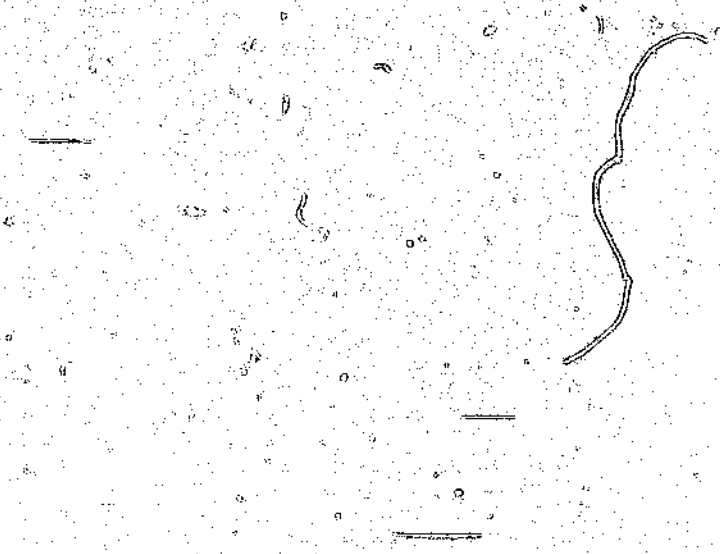

Degree awarded with distinction on 19 May 1994.

Thesis submitted to the Faculty of Science,
University of the Witwatersrand, in fulfilment of
the requirements for the degree of
Master of Science.

Johannesburg, 1994

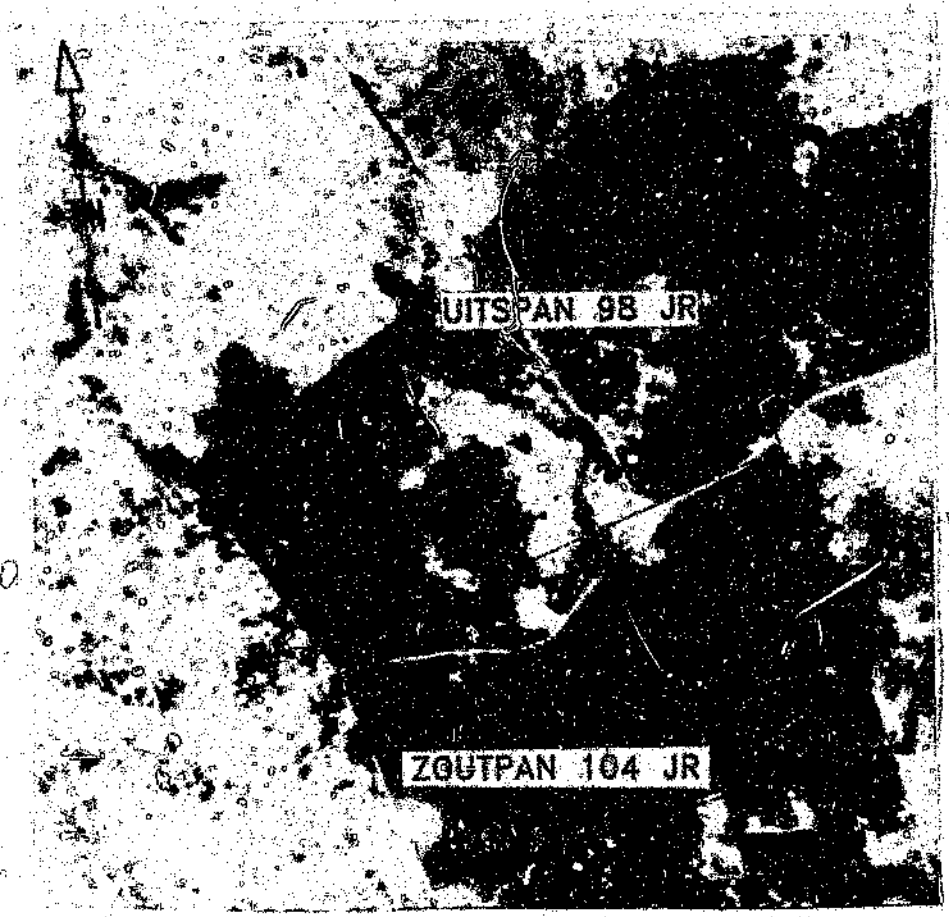

Landsat image of the Pretoria Saltpan (Zoutpan) crater.
The rim-to-rim diameter is 1.13 kilometres.

ABSTRACT

The origin of the 1.13 kilometres-in-diameter Pretoria Saltpan crater, which is situated some 40 kilometres north-north-west of Pretoria, has been a matter of controversy for the last century. Two models have been proposed for the origin of this structure, favouring either a cryptovolcanic or a meteorite impact origin. Occurrences of alkaline rocks were previously used as an argument in favour of a volcanic origin. A more detailed investigation, requiring a multi-disciplinary approach of the crater, began in 1988, when a borehole was drilled to a depth of 200 metres near the centre of the crater. Shock metamorphic effects were recognised in the core, which are generally believed to be diagnostic for impact processes. The age of this impact event was recently determined at 220±52 ka. Young and well-preserved impact craters similar to the Pretoria Saltpan are rare. Therefore, the Saltpan crater provided an excellent opportunity for the structural analysis of such a crater. Further work was required with respect to the distribution of the lithologies and the occurrence of alkaline rocks in an otherwise granitic terrane. The geology of the crater environs and the possibility that mafic and alkaline lithologies could be a regional phenomenon and not be restricted to the crater, have been disregarded in previous work. Detailed lithological mapping and sampling for petrographic and chemical analysis of rocks from the well-exposed crater rim as well as the isolated exposures outside of the crater was carried out. A second, smaller, circular depression (400 metre diameter) to the southwest of the main crater was discovered and is suggestive of a twin or satellite crater. Geophysical studies were carried out over the main crater and this possible satellite crater.

Detailed mapping revealed that most of the intrusives exposed along the crater rim have no radial or peripheral disposition with respect to the crater centre. In most cases the intrusives have been faulted both radially and concentrically by a post-intrusive event, presumably the cratering event. Closer to the crater floor, the granite was found to dip gently inwards. Towards the rim crest the granite dips outwards to varying degrees, indicative of upturning. Ejecta debris is found in an inverted stratigraphic sequence, that is the older granite debris overlies the younger Karoo sediments at various localities around the rim. The mid-section of the rim consists of an anticline, which is locally

displaced along inward dipping faults. Overall, the Pretoria Saltpan crater is structurally similar to the Odessa impact crater, Texas, with some similarity and strikingly similar dimensions to Meteor Crater, Arizona.

The various lithologies from the crater and environs (including samples from the Pienaars River Alkaline Complex) were studied petrographically, including electron microprobe analysis. Geochemical analyses, including Rb-Sr dating, were carried out on the various lithologies. These results are strongly suggestive of a common source for the intrusives from within and outside the crater, that were all formed at about 1.30-1.34 Ga ago.

A negative gravity anomaly (-3.2 mgal) obtained over the main crater, as well as the magnetic signature, are in agreement with the signatures expected for an impact crater of these dimensions. The small circular feature to the southeast does not show any characteristic geophysical signatures. However, the lack of a positive gravity and of any magnetic anomaly rules out the possibility of a magnetic volcanic pipe. As it is the only such feature in the entire area it should not be overlooked as a possible twin or satellite crater.

This study has indicated that the Pretoria Saltpan crater occurs in an area of alkaline activity, the age of which has been tentatively determined at about 1.30-1.34 Ga. The cratering event is significantly younger at about 220,000 a ago. The petrographic and structural observations on the crater, as well as the new geological data, are all in keeping with an impact origin for the Pretoria Saltpan structure.

DECLARATION

I declare that this research represents my own work carried out under the supervision of Dr. W.U. Reimold from the Economic Geology Research Unit, at the University of the Witwatersrand. No part of this research has been submitted, or is being submitted, for a degree at any other university.

Signed at Johannesburg on the 7th day of January 1994

Dion Brandt

ACKNOWLEDGEMENTS

The Barringer Crater Company is thanked for their contribution to the financial support of these studies. I am indebted to the Senior Bursary Travel Fund, the Department of Geology (in particular the Head: Professor T.S. McCarthy) and my supervisor Dr W.U. Reimold for a travel grant and additional financial contributions that enabled me to attend an overseas conference (24th Lunar and Planetary Science Conference) in Houston, March 1993. The gains from this conference contributed significantly to my research and therefore to my MSc. degree.

A special thanks to the Geophysical Department, especially Dr. R.J. Durrheim for his stimulating discussion, constructive criticisms and enthusiastic participation and assistance with the geophysical field work. To the 1992 Geophysical Honours students and my brother Paul Brandt, who assisted with various aspects of my field work.

Dr. C.B. Smith and his team from the Isotope Research Unit of the Bernard Price Institute are thanked for their assistance and patience during the period in which the Rb-Sr dating was carried out. Dr. F. Walraven is thanked for allowing the inclusion of his unpublished Rb-Sr dating results carried out on a crater rim lamprophyre. His results contributed to and supported the results of this study. Lynda Whitfield is thanked for her assistance in the drafting of various figures for this thesis. Professor T.C. Partridge is thanked for making available aerial photographs for aerial photographic interpretation, and for constructive discussions and criticisms related to this study. Prof. C. Koeberl from the Institute of Geochemistry, University of Vienna, is thanked for providing the results of instrumental neutron activation analysis of selected samples.

My extended gratitude to my supervisor Dr. W.U. Reimold who enthusiastically and actively guided the research.

A special thanks to my wife, Jane Nichola Brandt, for assistance in the field and support throughout the study period.

CONTENTS

LIST OF FIGURES

LIST OF TABLES

CHAPTER 1 INTRODUCTION

The detailed geologic study of impact craters is relatively new and is a direct result of space exploration in the last three decades together with the discovery of techniques for identifying impact craters. To date, hypervelocity impact processes have been widely accepted as having played and still playing a major role in the evolution of terrestrial planets (e.g., Roddy et al., 1980; Melosh, 1989). The evidence of this process is most abundant and is best exemplified on planetary bodies which have retained portions of their earliest, >3.8 Ga, crust (Grieve and Pesonen, 1992). Although this is not the case on the earth, it is known that the earth bears many scars from collisions with large meteorites in the geologic past: it has been estimated (Grieve, 1980; Frey, 1980) that prior to 3.8 Ga ago, 2,500-3,000 structures with diameter > 100 kilometres and 25 structures with diameter > 1,000 kilometres were formed on Earth. In contrast to other terrestrial planets, the number of identified impact craters on the Earth is relatively small (approximately 150), but is the main source of ground truth observations on the geologic effects of impact in the inner solar system (Grieve and Pesonen, 1992). These authors emphasized that the geologic control is generally good and permits detailed analysis for such effects as structural changes, the physical and chemical nature of impact melting, the response of isotopic systems, and the nature and extent of meteoritic contamination. The geologic study of impact craters came with the development of a reliable set of criteria for their recognition, known collectively as shock metamorphism (for example, French and Short, 1968; Stöffler, 1972; Sharpton and Grieve, 1990).

At present, one of the most discussed subjects in earth sciences is the catastrophic event that marks the Cretaceous/Tertiary (K/T) boundary, and which led to a well documented mass extinction. Its possible connection to the impact of an asteroid or comet is not a new idea (De Laubenfels, 1956; McLaren, 1970; Urey, 1973). An intensive study regarding this possibility started with the discovery of iridium and siderophile element enrichments in the thin sedimentary layer at the boundary (Alvarez et al., 1980; reviewed by Sharpton and Grieve, 1990). In addition to geochemical evidence at this boundary, shocked mineral grains have been detected within K/T boundary sediments

at many sites worldwide (e.g., Bohor et al., 1984, 1987). Assessing the intriguing proposition that the course of life can be strongly influenced by collisions with extraterrestrial bodies, the need arises to identify, study, and further understand the processes involved in producing impact structures.

Impact craters can generally be classified into two main groups according to their shape and size: a) simple, bowl shaped craters with a diameter of less than 2 kilometres in sedimentary rocks, or less than 4 kilometres in crystalline target rocks (Dence et al., 1977), and b) larger complex craters with a central uplift and possibly ring or modified ring structures.

The Pretoria Saltpan crater (Figure 1.1) is a simple, bowl-shaped crater located in the southern portion of the Bushveld Complex, some 40 km north-northwest of Pretoria, at 25°24'30" S and 28°04'59" E in the Transvaal Province of South Africa (see Figure 1.2). The crater position is approximately 20 kilometres to the west of the town of Hammanskraal and the margin of the Pienaars River Alkaline Complex (Figure 3.2). The near-circular structure has a 1.13 kilometre rim-to-rim diameter and exhibits a well-preserved, uptilted granite rim, which is largely overlain by granitic breccia. The breccia overlies Karoo sediment in places, indicating a post-Karoo age for the cratering event. The rim is elevated by 60 metres above the surrounding plains, with an elevation of 119 metres above the crater floor. The preservation of the rim indicates a young age for the crater. An extensive blanket of ejecta breccia is superimposed onto most of the rim and surrounding terrain (Figure 3.14).

The origin of the Pretoria Saltpan crater has been a matter of controversy for the last century. Two models have been proposed, that is, a cryptovolcanic or meteorite impact origin. It is partly due to this controversy that much research has been carried out on this structure. The coincidence of the spatial occurrence of the crater with that of mafic and alkaline intrusives has been the main argument against the impact interpretation.

In 1988 a borehole was drilled to obtain the necessary information to determine the true origin of the crater and to document and study the accumulated, undisturbed crater

sediments for palaeoenvironmental changes since the formation of the crater (Scott, 1988; Partridge et al., 1993). The drillcore (Figure 2.1) revealed an internal stratigraphy comprising about 90 metres of crater sediments that are underlain by 53 metres of unconsolidated granitic breccia (Reimold et al., 1992; Partridge et al., 1993).

The continental sedimentary sequence provided a high-resolution palaeoenvironmental record for the southern mid-latitudes. Numerous shock metamorphosed grains, and glass and melt breccia fragments, were found in the granitic breccia and allowed the confirmation of an impact origin for the Saltpan (Reimold et al., 1991, 1992). While the drillcore provided good vertical control of the crater fill, the crater itself had only been studied superficially, before the drillcore became available (Feuchtwanger, 1973).

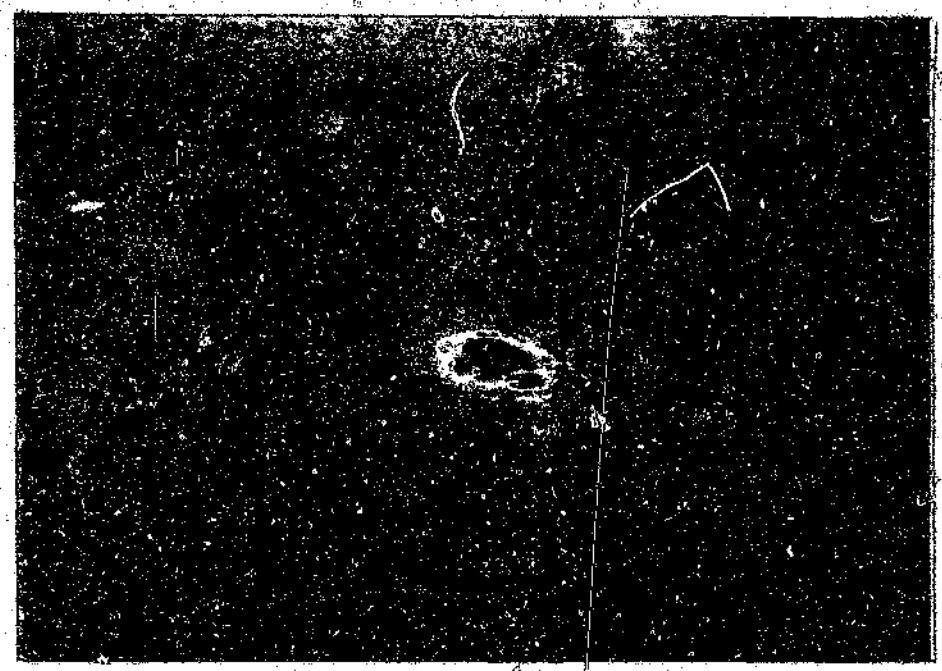

Figure 1.1 Aerial view of the Pretoria Saltpan crater towards the west.

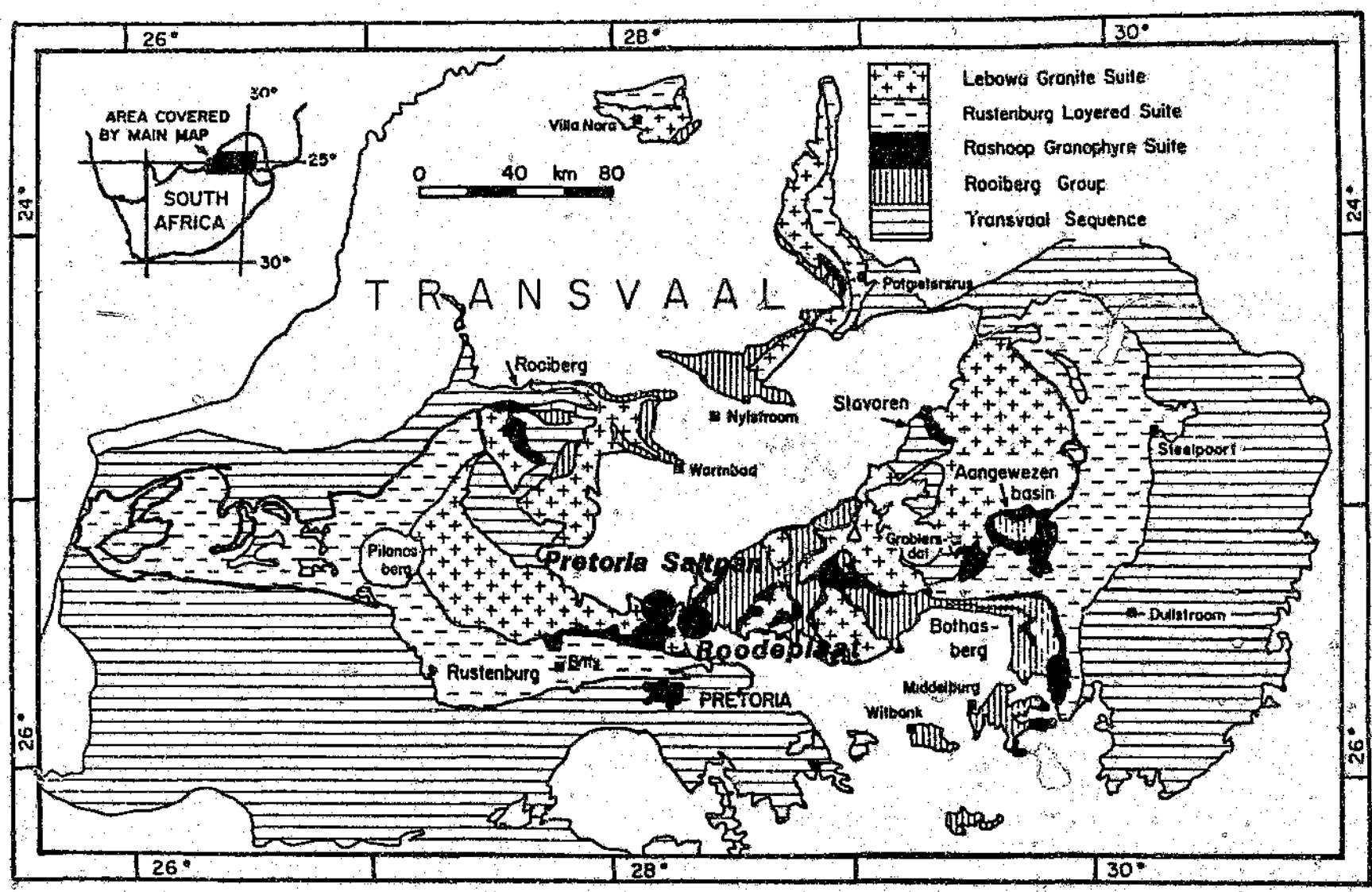

Figure 1.2 Map showing the locality of the Pretoria Saltpan crater in relation to the Bushveld Complex (modified after Walraven et al., 1987). Also shown are the localities of Pilanesberg and the Roodeplaat Complex.

The areas outside of the rim and the possibility of occurrences of mafic and alkaline rocks in both the wider region and within the crater have been disregarded in previous work. Although very limited, previous chronological results suggest that the volcanic rocks found in the crater are some 1.3 Ga older than the crater itself, the disposition of the controversial interpretation of the intrusives needed to be investigated. Further geochronological analysis was required with the improved understanding of the occurrences of the various intrusives. Trace element analysis was required to reveal which rock types contributed to the high siderophile element abundances detected in the crater fill breccias, and to understand any relationships the intrusives from the crater site may have with the rocks from the crater environs and the Pienaars River Alkaline Complex.

Among the 150 terrestrial impact structures recognised to date only two in the size range of up to 4 kilometres in diameter, in crystalline target rocks, are sufficiently well exposed to allow a detailed geological analysis. Both of these structures, Brent Crater and West Hawk Lake, located in Canada, are several hundred million years old. In contrast, the Pretoria Saltpan crater is ca. 220 000 years old (Storzer et al., 1993; Koeberl et al., 1994b) and has therefore been far better preserved than these other structures. The world's best studied impact crater, Meteor Crater in Arizona (approximately 50 000 years old), is formed in a sedimentary target terrain. The size of Meteor Crater is similar to that of the Pretoria Saltpan crater, but the latter was formed in a granitic basement which was overlain by only a thin cover of Karoo sedimentary rocks. A comparison with Meteor Crater and Odessa Crater, Texas would also aid in the structural understanding and an understanding of the processes involved in producing a crater such as the Pretoria Saltpan crater.

Detailed mapping of the crater rim and its environs, together with comparative petrographic and chemical studies on samples from the crater and its environs, were carried out to investigate the possibility of an association of the basic and alkaline intrusives with the cratering event. A detailed structural analysis would contribute to a better understanding of the cratering processes and would reveal the presence of deformation effects and the distribution of shock effects in a small structure in crystalline

rock. Such an analysis allows for a comparison of a structure formed in a crystalline target to the well-studied Meteor Crater, Arizona, which occurs in sedimentary target rocks. For the first time, using the additional information obtained from this study, a comparative structural, petrological and chemical analysis was possible.

With the aid of the stratigraphy provided by the drill-core, better modelling of geophysical data was possible. Furthermore, a gravity survey of higher resolution was needed to better understand the three-dimensional subsurface structure and the crater-fill configuration. No magnetic survey has been carried out before over the Saltpan crater. A second, smaller depression to the southeast of the main crater, which was not recognised before and could represent a twin or satellite crater to the main crater, was investigated geophysically using magnetic, gravity, seismic and resistivity methods.

CHAPTER 2 PREVIOUS WORK

2.1 STRUCTURE AND PETROLOGY

The Pretoria Saltpan was first described as a unique feature of "volcanic origin" by the travel-writer Jeppe (1868). A detailed account of its surface form or morphology was given by the British writer Anthony Trollope (1878). The geology of the crater was first studied in detail by Wagner (1922), who concluded that it had been produced by a volcanic explosion. His assumptions were mainly based on the presence of various mafic and alkaline rock types, found within the crater rim which he associated with volcanism. One such product was a carbonatite, found on the inner slopes of the crater. Wagner (1922) also concluded that the crater was of an explosive volcanic origin on the basis of the rim structure, which he interpreted as a sunken caldera with a typical ring fault (to be discussed in Chapter 4) comparable to that of known calderas. The ejecta breccia found on the outer rim was described by Wagner (1922, p. 38-39) as follows: "It occurs as a sheet of varying thickness dipping outward in all directions at a low angle, and rests either on granite, or, as in the southern part of the ridge, on 'grit.'... It is uncemented, contains no trace of lava, scoriae, or lapilli, and is made up entirely of large and small angular and subangular blocks of red and pink granite, and other rocks piled irregularly on one another." Wagner (1922) also stated that he could find no definite evidence for or against the hypothesis that the carbonatite is a product of a magma responsible for the proposed explosive volcanism. He does, however, discuss the saline brines in the crater fill sediments as a possible product of volcanism. Bond (1946) maintained that the saline brines have just the composition that would result from evaporation of the normal ground water of the Bushveld granite in a closed basin. Ashton and Schoeman (1983) carried out limnological studies on the Pretoria Saltpan lake and concluded that where evaporation exceeds precipitation, closed lakes such as that at the Saltpan become saline, particularly if they receive inflows sufficient to maintain a standing body of water.

Later, a connection between the carbonatite found at the structure and volcanism was discussed by others. For example, Verwoerd (1967) reported many other occurrences of

carbonatite within a 50 kilometre radius of the Pretoria Saltpan in his detailed account of the occurrence, chemistry and petrology of carbonatites in South Africa and South West Africa (Namibia). He suggests that carbonatites encountered in the Roodeplaat and Derdepoort areas (Figure 3.2) are related occurrences and further speculates that the Pretoria Saltpan Crater could be the southernmost representative of the East African carbonatite-type volcanoes and thus was not a member of the Roodeplaat Group (part of the Pienaars River Alkaline Complex).

Rohleder (1933) was the first to suggest an impact origin for the Pretoria Saltpan crater. As early as 1946, the Saltpan crater was listed in a compilation of possible terrestrial impact craters (Leonard, 1946), and since then individual workers have repeatedly discussed this possibility without ever producing unambiguous evidence in support of this hypothesis.

According to Milton and Naeser (1971), the structure, as originally mapped by Wagner (1922), exhibits deformation of the pre-cratering sheeting joints in the rim granite by "an abundance of folds and thrust faults on a scale of decimetres," with orientations indicating horizontal or low-angle couples. They concluded that these minor deformation structures in the rim were strongly indicative of an impact origin, because of their similarity to structures which they observed in other impact craters. They therefore based their conclusion that the Pretoria Saltpan crater is of impact origin on the morphological resemblance to known impact craters, the absence of similar, volcanic crater structures in the region, the apparent young age of the structure, and the absence of associated volcanic products which could be related to the cratering event. They also presented fission track ages for zircon and apatite crystals in the crater carbonatites of 1.9 and 0.6 m.y. respectively, which they concluded to be incompatible with the youthful morphology of the crater.

Feuchtwanger (1973) remapped the crater for a B.Sc Honours dissertation and also supported a volcanic origin because of new findings of various alkaline and peralkaline volcanic rock types on the inner crater rim. Wallace (1979) carried out whole-rock geochemical and electron microprobe investigations on some of the intrusives occurring

at the structure. He reported a highly alkalic nature of the clinopyroxenes and feldspars in an "augitite", three carbonatites, and four "aegirine-biotite porphyries", which he attributes to the rocks having been derived from a complex alkaline-carbonatite magma originating at a minimum depth of 7-9.5 kilometres. He also assumes that these rocks have no correlatives in the surrounding region.

McNerny et al. (1992) described the field relationships, petrology and geochemistry of a suite of lamprophyric rocks and breccias of the Greenview lamprophyric breccia vent along the southern margin of the Pienaars River Alkaline Complex. Their results indicate that a complicated sequence of events involving several episodes of explosive lamprophyric intrusion of more than one magma type and generation was required to produce the observed complex vent structure.

2.2 GEOPHYSICS

The only geophysical work previously carried out at the crater is a gravity survey by Fudali et al. (1973). The gravity profiles across the crater floor revealed a strong residual, negative anomaly asymmetrical with regard to the crater centre. This was interpreted by them as an off-centre basin, occupied by several hundred feet of low-density sediments. They interpreted the crater fill as consisting of two components: a lower zone of brecciated granite, which was assumed to contribute insignificantly to the observed gravity low topped by low-density sediments which were primarily responsible for the negative anomaly. Fudali et al. (1973) concluded that it was difficult to reconcile their results with an impact origin for this crater, because they could find no compelling arguments for an impact origin and suggested that their gravity data favoured the original explanation of Wagner (1922), that the crater was a true 'cryptovolcano.' They did, however, state that errors in their assumptions could arise from not correctly estimating the sediment-country rock density contrast, the breccia-country rock density contrast, or from misplacing the lower boundary of the hypothetical breccia lens. Nevertheless, they concluded that the possible range in the morphological characteristics of impact craters was much wider than previously known and that the variables affecting hypervelocity impact events were not fully understood. Fudali et al. (1973), like Milton and Naeser

(1971), stressed that, in the absence of impact diagnostic features, only drilling of the crater could reveal unequivocal evidence for the origin of the Saltpan crater. With the drilling of the core in the centre of the crater in 1988, all the hypothetical parameters used by Fudali et al. (1973), became known parameters.

2.3 CHRONOLOGY

Geochronological studies on the Bushveld Complex commenced more than thirty years ago when the first age determinations were made by Nicolaysen et al. (1958) and Schreiner (1958). Numerous ages have been determined for the Bushveld granite which include Pb-Pb ages of 2052±48 Ma, and 2063±30 Ma (Walraven et al., 1982). More recently, Walraven et al. (1987) obtained an U-Pb zircon age on the granites relevant to this study, namely the Nebo granites, of 1980+48 -43 Ma. This was interpreted by them as a minimum age for the Nebo Granite. They attribute the discrepancy between the age obtained and the approximate 2050 Ma limit on the Bushveld granites to be a consequence of disturbances of the U-Pb isotope systematics of the Nebo Granite zircons. The most recent crystallization age determined for the Nebo granites is 2054.4±1.8 Ma (Walraven and Hattingh, 1993). For this age determination on zircons from the granite they used the Pb-evaporation technique. Their studies support the interpretation that other dates obtained prior to this study, which are lower than 2054 Ma, reflect disturbance of the respective isotope systems used for the dating. The ages (1980-2054 Ma), however, represent the possible range of ages for the formation of the Nebo Granite, which forms the target rocks of the study area.

As in the case of the granite, a number of dates have been obtained for constituents of the Pienaars River Alkaline Complex, which forms an integral part of the study area. Dates of 1290±180 Ma to 1330±80 Ma were determined for a swarm of dykes related to the Pilanesberg Complex, and possibly to the Pienaars River Alkaline Complex, by Schreiner and Van Niekerk (1958) and Van Niekerk (1962). Oosthuysen and Burger (1964) reported an age of 1420±70 Ma for a Leeuwfontein (Figure 3.2) sample. [All original dates have been re-calculated to the new decay constants recommended by Steiger and Jäger (1977).] More recently, Harmer (1985) carried out whole-rock Rb-Sr

isotopic analyses on eight samples from various localities in the Pienaars River Alkaline Complex. The results indicate that this complex was emplaced over a protracted time period between circa 1430 Ma and 1300 Ma ago.

Milton and Nasser (1971) presented fission track ages for zircon and apatite crystals in the crater carbonatites of 1.9 and 0.6 Ga, respectively. Partridge et al. (1990) and Reimold et al. (1991) reported a K-Ar age of 1.36 Ga for biotites from a lamprophyre sample from the inner crater rim. As was observed by these authors, such ages are clearly incompatible with the youthful morphology of the crater. Furthermore, the fact that fragmental granite breccia overlies Mesozoic Karoo grits along sections of the crater rim, also suggest a relatively young post-Karoo age (less than 160 Ma) for the cratering event (SACS, 1980).

Partridge et al. (1993) noticed broad sedimentary cycles in the [illegible]ts, which corresponded with major phases in the evolution of the crater lake. Superimposed were cyclical patterns of accumulation reflecting environmental changes on millennial to seasonal timescales. These authors carried out ^{14}C age determinations on algal debris from the upper 20 metres of the core sediments. The results obtained indicated a mean sedimentation rate of about 1 metre/2000 years. This accumulation rate indicates an age of approximately 200 000 years for the lowermost crater-fill sediments.

Storzer et al. (1993) recovered glass fragments from granitic breccia of the core. Several hundred of these sub-millimetre-sized glass fragments were studied for fission tracks. The results of their studies gave an age of 220±52 ka, which is in excellent agreement with the extrapolated ^{14}C age (Partridge et al., 1993) for the accumulation of the crater sediments and with the youthful morphological appearance and good preservation state of the crater. Despite this well-established age dichotomy for the cratering event and volcanic intrusives, the proponents of the 'cryptovolcanic' hypothesis continued to emphasise the improbable coincidence of an impact event into an alkaline-volcanic area.

2.4 DRILLCORE RESULTS

Prior to the detailed mapping, mineralogical, and chronological studies of 1992-1993 (this

work; Reimold et al., 1992), no unequivocal evidence for an impact origin of the Pretoria Saltpan crater was available, and this hypothesis was based entirely on morphological observations (such as the circularity of the structure and the raised rim). The alleged local association to volcanic rocks was still widely regarded to favour a volcanic (i.e., cryptovolcanic) origin.

Several shallow boreholes had been sunk into the crater sediments prior to 1972. The Pratley Manufacturing and Engineering Company sunk a borehole to 172 metres using a rotary drill. Core recovery was poor allowing for no firm conclusions on the origin of this structure. A more detailed investigation of the Pretoria Saltpan crater began in 1988, when a borehole was sunk to a depth of 200 metres near the centre of the structure through the crater fill into the subcrater basement. This second attempt was made under the direction of T.C. Partridge, using a combination of tube-sampling and rotary drilling techniques. The two main arguments for this project were a) that the crater sediments, undisturbed since formation of the crater, presented a unique source of palaeoclimatic and palaeoenvironmental information for the mid-latitudes of the Southern Hemisphere, completely unrivalled by any other site in the Southern Hemisphere, and b) that only drilling could provide conclusive evidence of the processes that led to the formation of the structure (cf. also Milton and Naeser, 1971, and Fudali et al., 1973). This research project utilised a multi-disciplinary approach in order to allow full coverage of all aspects concerning cratering-related processes, as well as post-cratering sedimentation, biological aspects, and paleoenvironmental studies.

The stratigraphic column (after Reimold et al., 1992) for the drillcore obtained is shown in Figure 2.1: approximately 90 m of crater sediments, including several thin debris flow units, are underlain by a 53 m thick unit of unconsolidated fragmental breccia consisting of granitic "sand" intercalated with fractured granite boulders. The sand contains a small amount of diatomite, siltstone and shale of probable Karoo age (these lithologies would represent the upper thin veneer, on top of the Bushveld granite, of the pre-cratering target stratigraphy). Kerr et al. (1993) have classified the upper 15 metre (90 to 105 metre depth) as a "transported, terrigenous gravel and sand". This they attribute to sub-angular and rounded grains present in this layer. However, Kerr et al. (1993) have

observed that the mineralogical composition of this section is essentially the same as that of the underlying 40 metres, and contains an abundance of clear to brownish glass fragments. Their description of this 15 metre layer suggests a cratering-throw-back origin rather than their interpretation of transported sediments. Below this breccia strongly fractured and locally brecciated Bushveld granite was intersected. A discrepancy exists concerning the lower limit of the 'breccia' layer, that is, the boundary separating the fall-back breccia and the autochthonous fragmented granite. Partridge et al. (1990) placed this boundary at 151 metres, whereas Reimold et al. (1991) placed it at 143 metres (see Chapter 5 for an interpretation of the subsurface structure using gravity modelling). Nevertheless, the amount of coherent granite steadily increases to a depth of 200 m, where solid basement was reached and drilling was suspended.

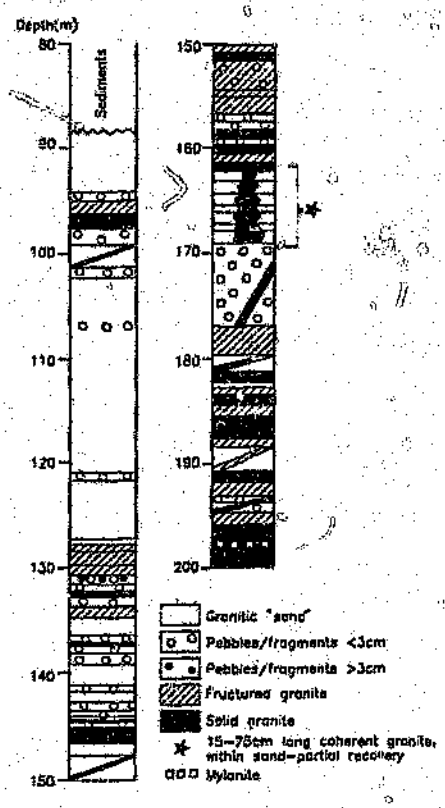

Figure 2.1 Results of the 1988/1989 drillcore (from Reimold et al., 1992).

Until mid-1990 only the bottom part of the drill core (fractured and coherent basement) as well as selected granite samples from the crater rim had been studied and no evidence for impact-diagnostic shock deformation was found (Partridge et al., 1990). However, as soon as the sandy breccia at intermediate depths was studied petrographically, not only were a large number of shock metamorphosed quartz and feldspar grains observed, but also abundant glass and melt fragments were noted (Reimold et al., 1991, 1992). Thus in 1991, the first definite evidence, in the form of bona-fide (impact diagnostic) shock metamorphism, for the origin of the Pretoria Saltpan crater by meteorite impact was presented. In addition, glass and melt fragments, often containing abundant sulphide spherules, were discovered. Instrumental neutron activation analysis was used to confirm the presence of a small meteoritic component in these glass and melt fragments.

Consequently the breccia layer was classified as an unconsolidated equivalent of "suevitic" breccia (defined as a fragmental breccia with a melt component: Hörz, 1965), known from many confirmed impact structures (Reimold et al., 1991, 1992; Reimold and Koeberl, 1992).

The fact that no shock metamorphic effects were detected from granite rim and crater floor would not be in conflict with an impact origin. Other impact structures of similar size do not display shock effects in rim or basement rocks either - obviously the impact of relatively small projectiles does not release sufficient energy (Dence, 1968). However, in the course of the recent detailed mapping, a number of breccia occurrences and breccia float specimens were collected from the rim and from the crater floor, respectively, some of which contain quartz grains with shock deformation (see below, Chapter 6).

Not a trace of volcanic rock was observed in the drillcore. Both the drilling results and geophysical data (Chapter 5) reject the possibility that the structure could be located above a volcanic vent.

CHAPTER 3 REGIONAL GEOLOGY

3.1 GENERAL GEOLOGY

An area of approximately 200 square kilometres surrounding the Pretoria Saltpan was mapped. The area covered by the shuttle photograph (Figure 3.1) coincides approximately with the regional geological map produced (see insert in the back pocket).

Figure 3.1 Shuttle photograph (STS 273990; courtesy Lunar and Planetary Institute, Houston) of the Pretoria Saltpan crater and its environs (north is at the top). The black circular feature in the centre of the crater is the crater lake. The ejecta blanket extends for about one crater diameter around the crater. The south-north flowing "Soutpan" stream flows just to the east of the ejecta blanket.

The entire study area is set predominantly in Nebo Granite, which is the main granite type of the Bushveld Complex and includes the Veekraal granite, the Sekhukhune granite, the Steelpoort Park granite and granites in the Potgietersrus and Villa Nora areas (Coertze et al., 1978), and is shown as the Lebowa Granite Suite in Figure 1.2. The mapped area is located only about 10 kilometres from the margin of the Pienaars River Alkaline Complex (Figure 3.2 shows the distribution of members of this Complex). Various rock types from this complex were used as a comparison to intrusives found in the mapped area (see section on petrography, Chapter 6). Granite outcrop is generally discontinuous. The largest coherent outcrop area observed covers a 20x20 metre area. Large parts of the country-side are covered by coarse sands and grits derived from weathering of the underlying Nebo granite. Other areas are covered by Karoo or by alluvium (mostly sand) - see regional map insert in the back pocket. The near-surface regional structure that existed at the time of impact and which has not changed significantly since then consists of minor faults (see regional map insert in the back pocket), a sub-horizontal joint set, and three sets of sub-vertical joint sets (discussed in more detail later in this chapter).

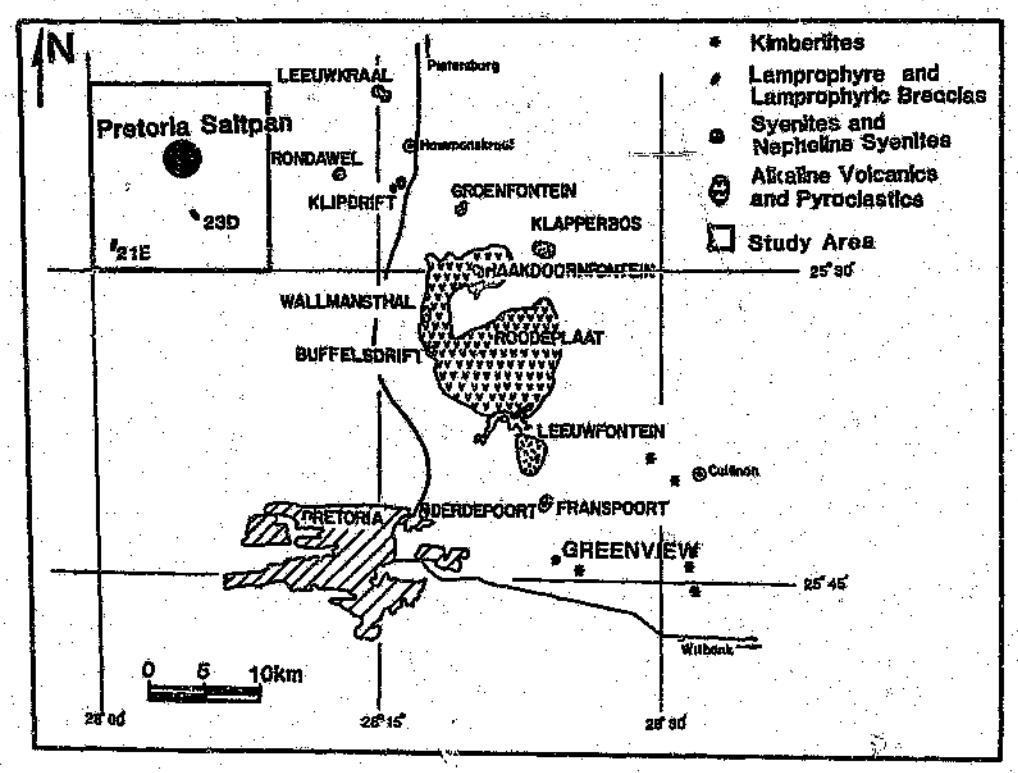

Figure 3.2 Location of the Pretoria Saltpan and mapped surroundings with respect to members of the Pienaars River Alkaline Complex (modified after Harmer, 1985).

Intrusives

Numerous small intrusives were observed to cross-cut the granite at various localities in the mapped area (see regional map insert in the back pocket). These intrusives are lamprophyric or trachytic in composition, and it will be shown that they have very similar mineralogical and chemical compositions compared to the intrusives occurring at the crater site. For a comparison of the mineralogy and chemistry of the crater rim samples and samples from the crater environs, refer to Chapters 6 and 7, respectively. Two lamprophyric outcrops, which have been reasonably preserved and are well exposed, will serve as examples of intrusives occurring in the crater environs.

The first of these intrusives (Sample 21-E) occurs approximately 9 kilometres to the southwest of the crater and is exposed in a pipe-line trench. It intrudes weathered granite in the form of a sub-vertical dyke which feeds a crude sill-like feature (Figure 3.3). At the same locality other smaller outcrops in the form of veins less than 20 centimetres wide or stringers of the same material were observed. Figure 3.4 is of such an intrusive, and shows a very sharp contact with the granite. The lamprophyre is slightly finer-grained and appears to be more fractured at the contacts. Most lamprophyre at this locality is extremely altered and is typically replaced by iron-oxide. Figure 3.5 shows another example of a lamprophyre vein with sharp contacts to the granite country rock.

The second occurrence of a well-preserved lamprophyric dyke (Sample 23-D) is located approximately 5 kilometres to the southeast of the crater (see regional map). This dyke (Figure 3.6) is only 5 centimetres wide, but is well preserved and unaltered. This lamprophyre is finer-grained than the other lamprophyre samples discussed previously, most likely as a result of its lesser width. Lamprophyric and trachytic dykes occur at most reasonably sized (i.e., at least 5x5 metres) granite outcrops, indicating that alkaline and mafic intrusive activity is pervasive throughout the mapped area and not restricted to the crater site, which was previously believed to be the case.

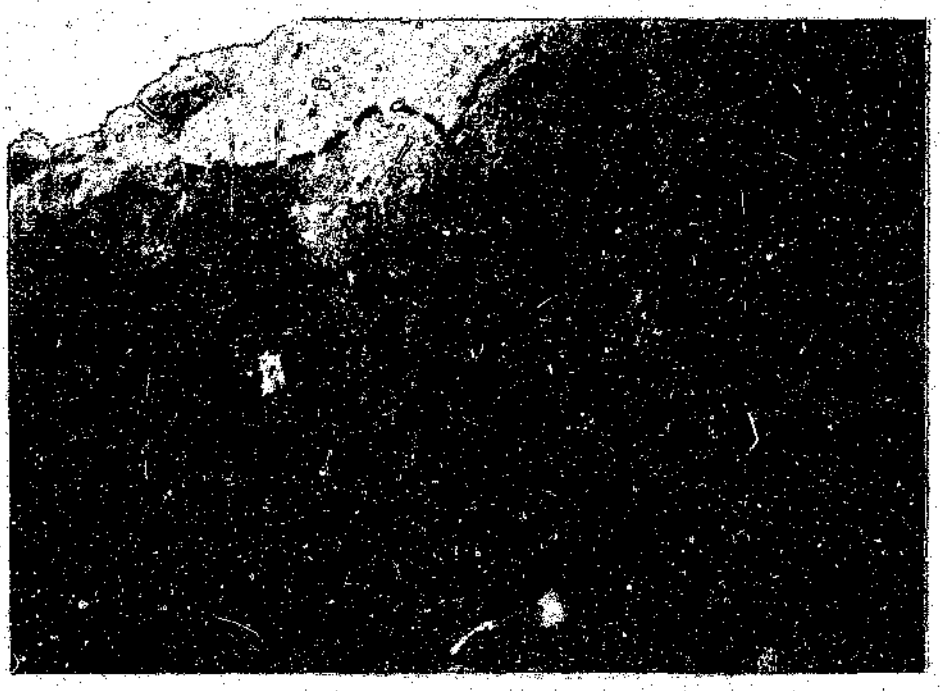

Figure 3.3 Lamprophyre dyke with a crude sill-like feature found in the crater environs (Sample 21-E: see regional map insert for location).

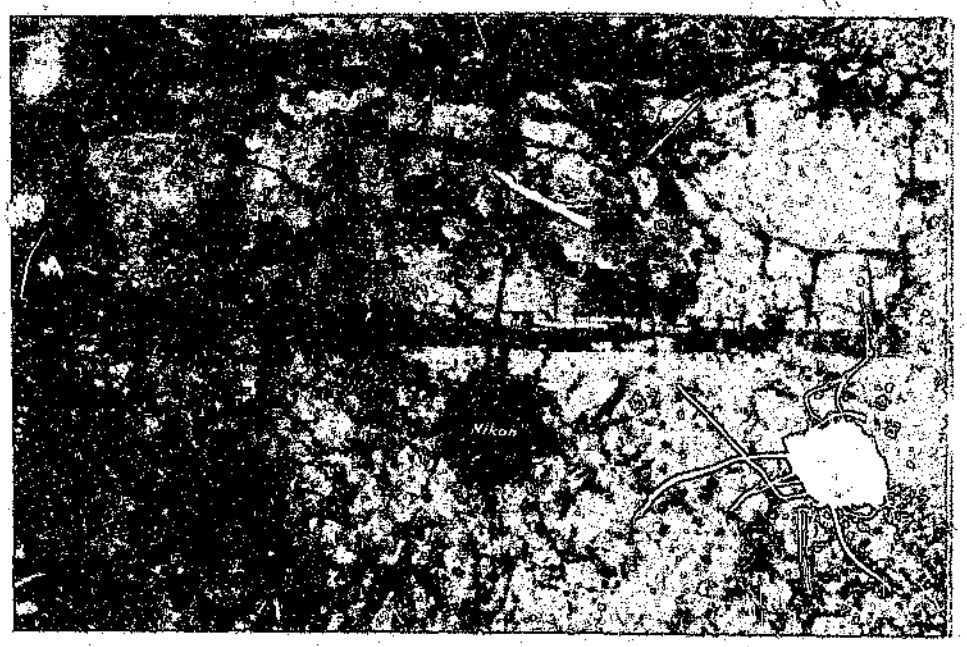

Figure 3.4 Granite (at bottom)-lamprophyre contact relationship from the same locality as Sample 21-E (see regional map insert for locality).

Figure 3.5 Typical appearance of altered lamprophyre. The dark colour on the weathered surface is the result of iron staining. The lower part of the outcrop is the granitic country rock.

Xenoliths

Two types of xenoliths were observed in the granite in the mapped region. First, a finer grained granite having the same mineralogy as the Nebo granite (Figure 3.7), and second, an albitic gneiss (Figure 3.8), the composition of which is discussed in the section on mineralogy (Chapter 6). Both types of xenoliths have a sub-rounded form, probably due to reworking or marginal melting and loss of material to the younger host granite during emplacement. The origin of these two xenolith types was not considered, as they clearly are unrelated to the other intrusives encountered in the mapped area.

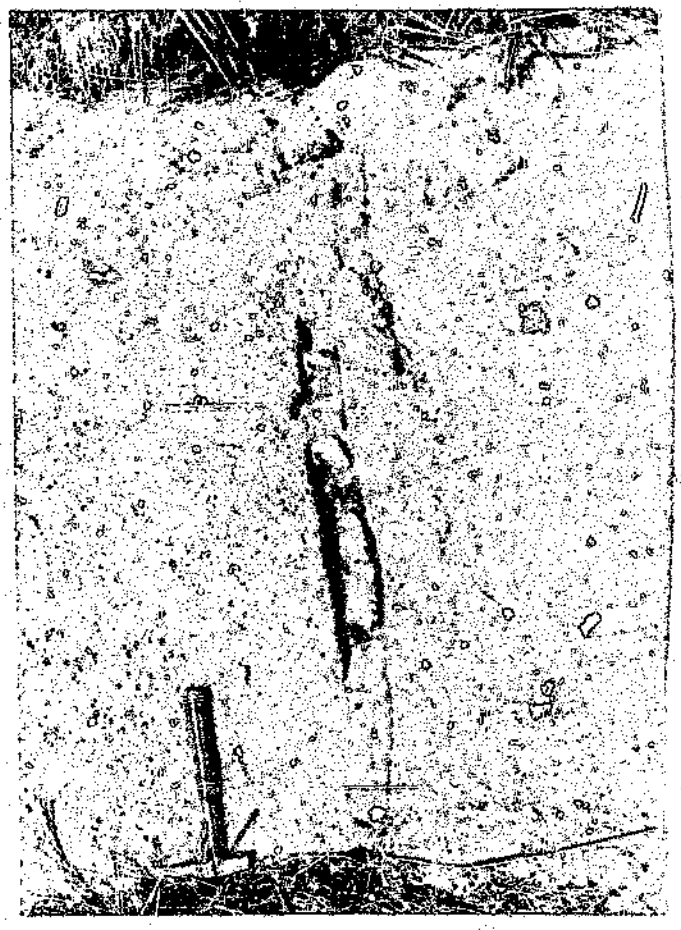

Figure 3.6 Thin, well preserved lamprophyre dyke (Sample 23-D: see regional map for locality). Note that this dyke has right-lateral strike-slip displacement.

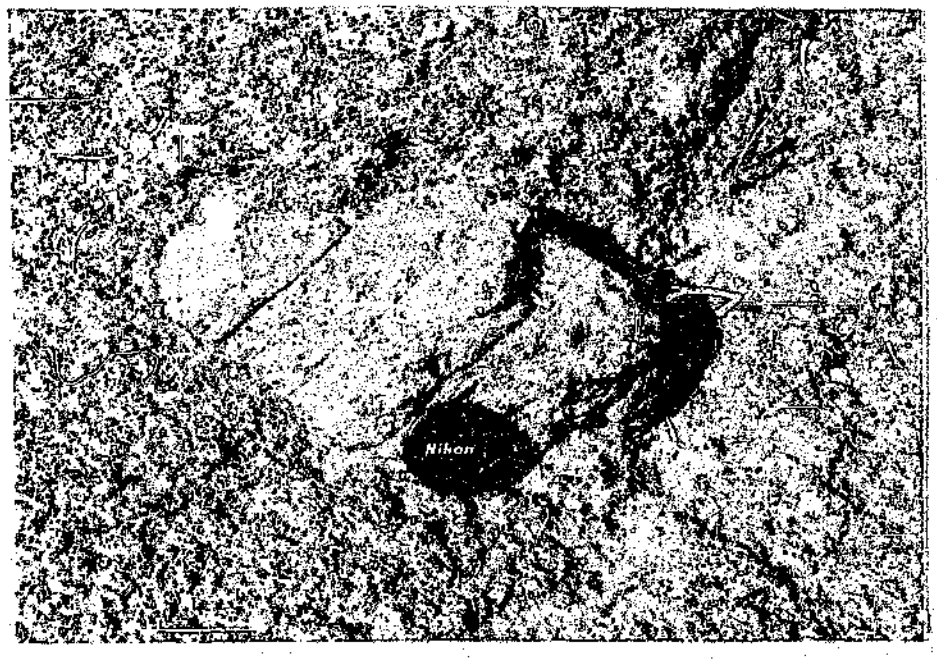

Figure 3.7 Fine grained granite xenolith, occasionally observed in the Nebo granite.

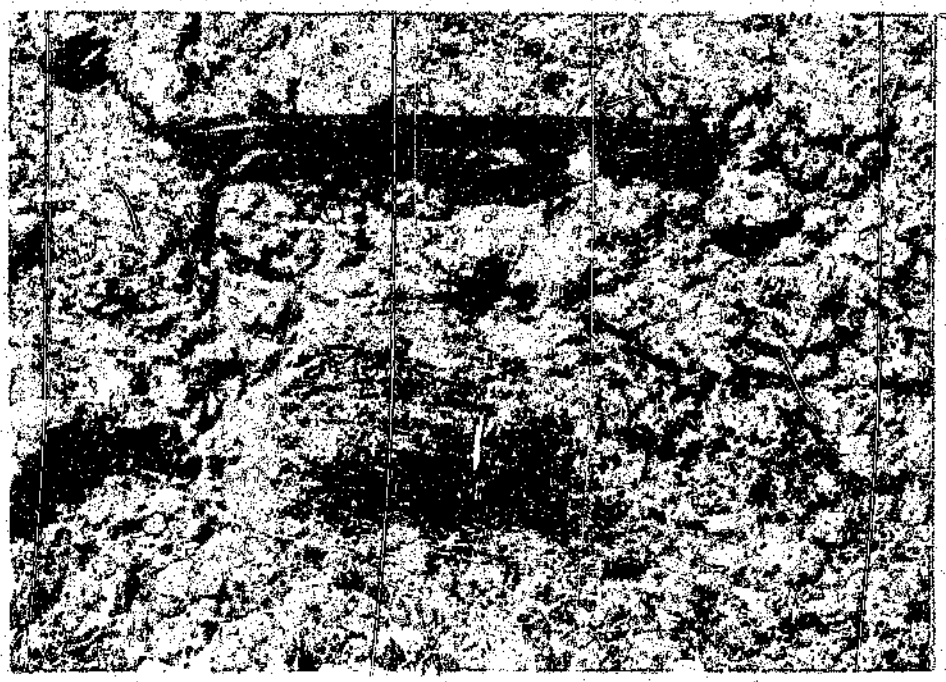

Figure 3.8 Albitic gneiss xenolith observed at one locality (approximately 3 kilometres to the south of the crater) in the Nebo granite.

Veining

Quartz veining in the granite occurs at various localities in the mapped area. Nowhere is it seen to cut the Karoo sediments. Other veins (1 to 5 centimetres in width) of granitic composition, and which appear to be the result of remobilized quartz and feldspar due to shearing (evidenced by the alignment of particles along the strike of the feature), are found at a number of localities. Figure 3.9 shows such a vein which was located approximately 3 kilometres to the west of the crater. These linear features are usually continuous for a distance of about 5 metres. They appear to be unrelated to the cratering event, as they often occur some distance from the crater. They also have no preferred orientation with respect to the crater (i.e., radial or concentric) and rather appear to be part of, or a result of, the regional deformation.

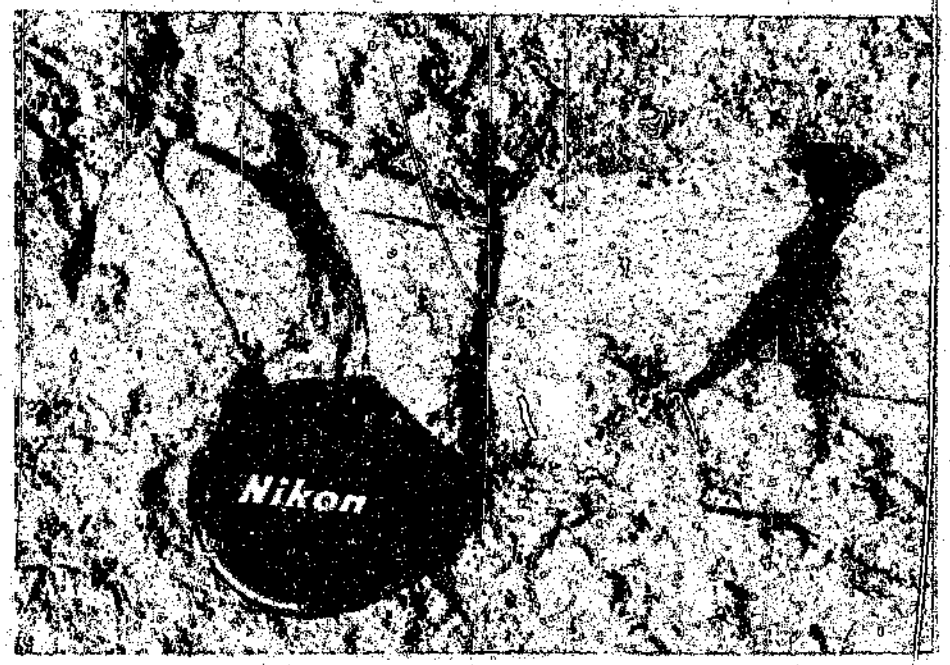

Figure 3.9 Remobilized quartz and feldspar in a shear zone, encountered in the Nebo Granite at a locality 3.5 kilometres to the south of the crater.

Karoo sediments

Various Karoo sediment types may be found at different localities (see regional map insert) within the mapped area. These include the abundant grits, also exposed at the crater, a sandstone variety, a paraconglomerate and a shale. The Karoo sediments are exposed along denuded areas such as non-perennial stream beds and vehicle-eroded secondary roads. The grits vary in thickness from a few centimetres to approximately 1.5 metres. They are comprised predominantly of granite-derived material as evidenced by the clast types (mostly sub-rounded quartz grains). The Karoo grits lie unconformably on the Nebo granites (Figure 3.10). This figure also exhibits the typical occurrence of these grits. The granitic surface on which the grits lie is undulating and represents a hiatus during which erosional processes could act on what appears to have been for some time a stable surface. The granite is more weathered at this surface, indicated by the preservation of smaller granitic fragments which represent the initial stages in the breakdown of the original granite surface. In general the Karoo sediments are not as altered as those encountered at the crater site. This has been attributed to the fact that

rock at the crater site has been fractured and brecciated to a greater extent allowing infiltration of surface water, which would enhance the natural weathering process. Sometimes the grits are unaltered, but normally they form tabular masses of ferruginous lateritic grit. The grits may show crude stratification or horizontal bands a few centimetres in width. The grits are composed of subangular to rounded grains of quartz having an average diameter of 3 millimetres. Stratification and, to some extent, grading of the grits is well-exposed in the eastern section of the mapped area in river beds (Figure 3.11).

Figure 3.10 Typical occurrence of Karoo grits unconformably overlying the Nebo granite. The hammer has been placed on the contact.

Figure 3.12 shows a poorly sorted, polymict paraconglomerate which was only observed in the eastern section of the mapped area. The clasts consist of various sandstones, jasper, and vein quartz, and may be as large as 5 centimetres in diameter.

Figure 3.11 Grading and stratification present in the Karoo grits.

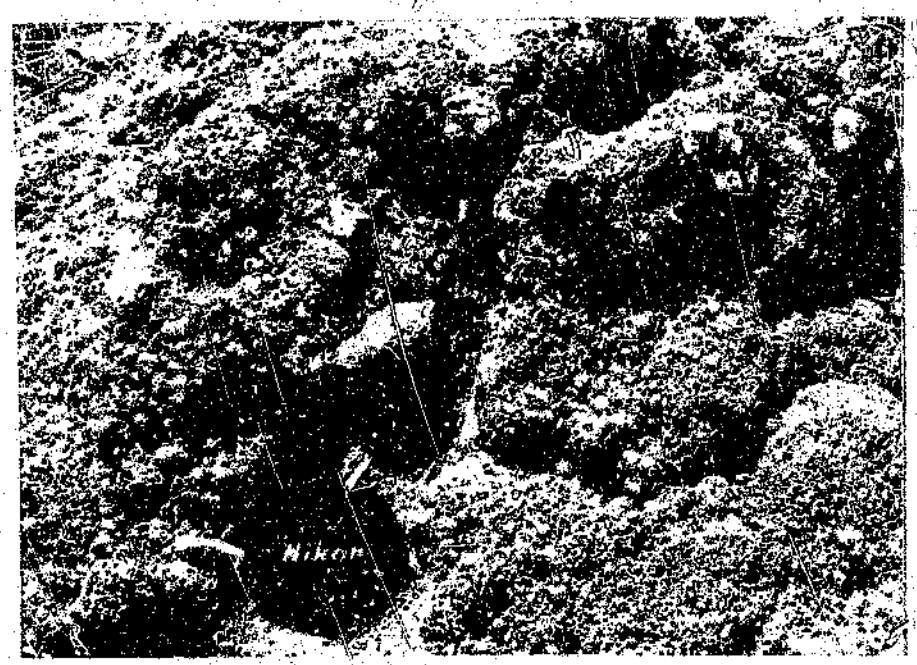

Figure 3.12 Paraconglomerate belonging to the Karoo sediment suite, as encountered in the study area.

In the southern section of the mapped area a similar, but much coarser-grained paraconglomerate was observed with clasts as large as 25 centimetres in diameter (Figure 3.13). The clasts at this locality are poorly sorted and may be angular to rounded. The fact that the sediments are noticeably coarser-grained, more poorly sorted and more angular in the south all point to a southern source area for the Karoo sediments encountered in the mapped area. Other sediments found in the same area include a planar cross-bedded, medium-grained sandstone interbedded with grits and a massive shale. To the northwest of the crate, a boulder of grits interbedded with sandstone contained a thin (2 millimetres wide) carbon seam. The origin of this boulder is unknown, as it was found in a stream bed, but presumably forms part of the Karoo sediments. The Karoo sediments are known to be rich in coal in many parts of the country.

Figure 3.13 Paraconglomerate encountered in the southern portion of the study area. The large clasts imply a proximal source area.

Recognition of small crater form

A second, smaller, circular depression about 400 meters in diameter situated 3.5 kilometres to the southeast of the Pretoria Saltpan crater is suggestive of a twin crater. Figure 3.14 shows this feature in relation to the position of the Pretoria Saltpan crater.

Figure 3.14 The location of the small crater form in relation to the position of the Pretoria Saltpan crater (Orthophoto Numbers: 2528 AC 17 and 18; Government Printers, Pretoria).

An aerial view of this crater form (Figure 3.15) shows the perfect circularity of the structure. The feature is approximately 3 meters deep, measured from rim "crest" to floor, and except for low-lying, scattered Karoo sediment occurrences, no outcrop is present. This outcrop may be seen on a contour map in Figure 5.11. Figure 3.16 shows the lack of relief at this site, which is more readily recognised by the change in vegetation. Larger trees are not able to grow in the mud-filled centre which is only vegetated by various grasses and isolated small shrubs. As this site had never been investigated before, various geophysical surveys were conducted.

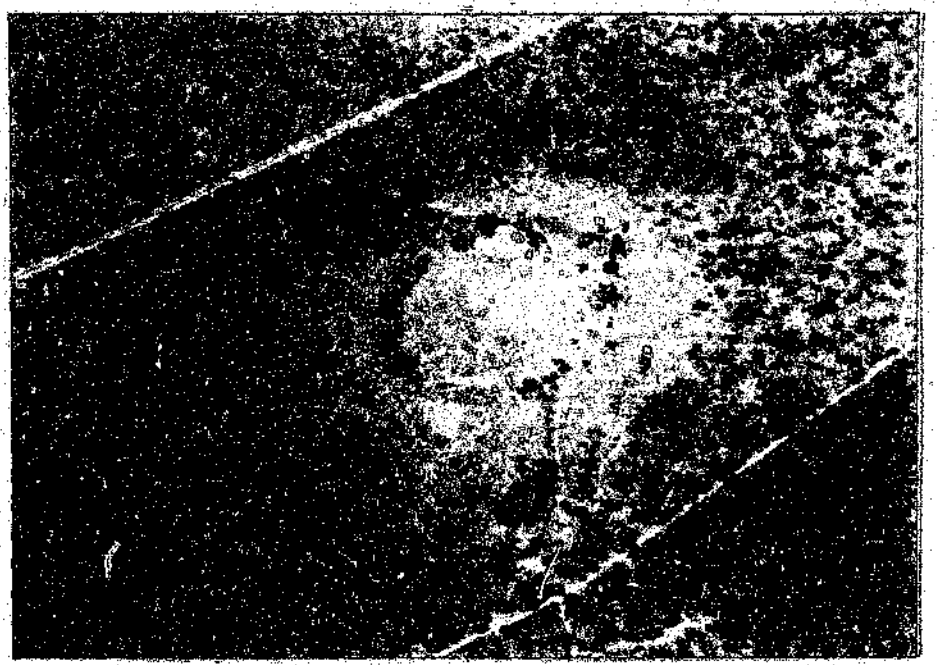

Figure 3.15 Aerial view of small circular ~~crater~~ form to the southeast of the main crater (diameter A-A' is approximately 400 metres).

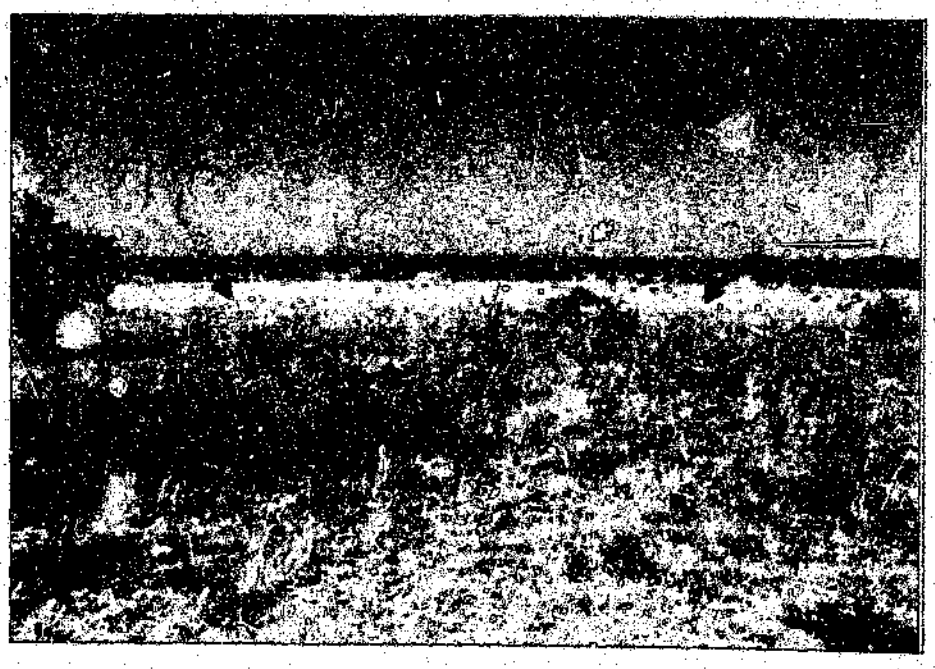

Figure 3.16 View of the small crater form towards the south. Note the small changes in relief towards the far rim and the change in vegetation at the contact (see arrows) between the central muds and the Karoo Grits of the rim zone.

Dyke feature

A large east-west trending dyke feature approximately 3 kilometres to the north of the main crater was noted on the 1:50,000 regional aero-magnetic map. No outcrop of this highly magnetic feature was found. The results of the magnetic survey carried out over this feature, their interpretation and implications will be dealt with in Chapter 5.

3.2 STRUCTURE

Jointing

The interpretation of the regional joint and fracture pattern is based on the structural analysis of various exposures in nine different areas (shown in Figure 3.19), each individual area totalling a few km^2, within an area of 200 km^2 surrounding the Pretoria Saltpan crater. A comparison of the fracture pattern within the crater rim exposures to that of the uninfluenced crystalline basement of the wider environs gives an indication to what extent the impact affected the target rocks. Criteria which allowed for a reliable comparison of the crater to the surrounding area include: the same rock types, similar pre-impact structures and an identical tectonic history after the impact event.

On the exposed rock surfaces, in the form of typical granite-dome-type outcrops exposed in river beds, the joints commonly exhibit narrow, closed, parallel, and widely-spaced fracture surfaces (Figure 3.17). The jointing is especially well-exposed in erosionally-stripped non-perennial river beds. Only the strike orientations of such joints could be taken, as often no clearly defined surfaces are present on this type of outcrop that would allow dip measurements. Other outcrops associated with steeper topography, such as river gulley walls, may exhibit joint sets, on which both a strike and a dip could be measured. These outcrops, however, are not common in the mapped area and therefore only joint strike analysis could be performed with the available information.

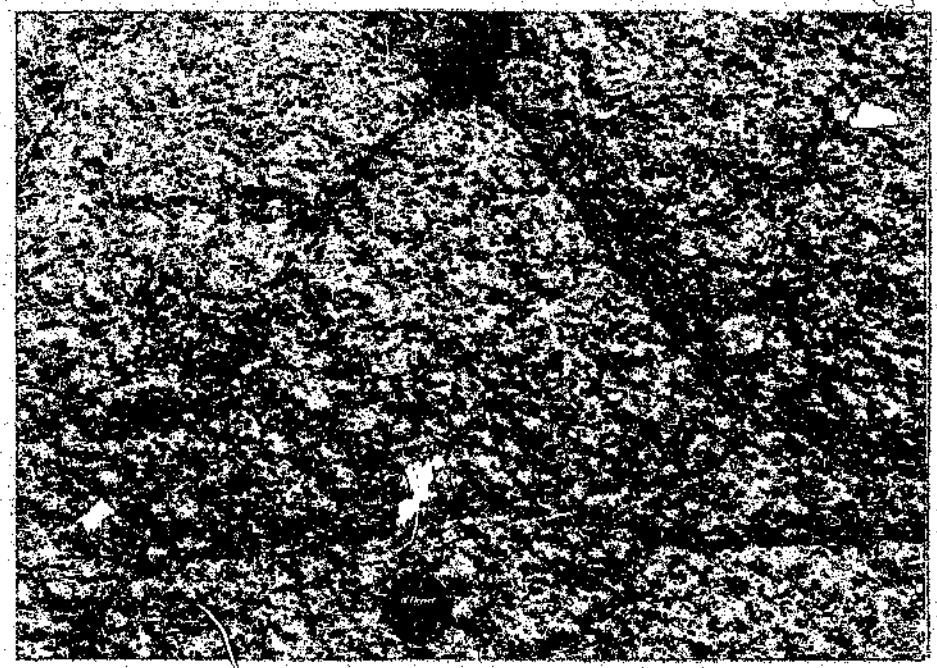

Figure 3.17 Typical granite outcrop suitable for joint orientation analysis.

No displacement of adjacent sides of joints was observed, although joint and fault displacement is not easily determined in what was often intensely weathered granite. The widths between fracture surfaces are generally microscopic, but could be up to a few millimetres in more weathered areas. The drainage system of the study area is controlled to some extent by the regional structure, in particular the joint pattern. Some non-perennial streams have resulted from the intense weathering and erosion of joint fractures, to such an extent that the original joint fractures now dictate and form the river paths, which may form channels up to several metres across. Figure 3.18, photographed approximately 2 km to the south of the crater, shows such a river, whose course is entirely controlled by the joint pattern, in particular the northeast-southwest joint-set.

Figure 3.18 River paths are strongly influenced by joint orientations at certain points along their paths.

In addition to the vertical jointing already discussed, an important joint set occurs at most outcrops in the region in a horizontal to sub-horizontal orientation. These joints are most probably the result of uplift and denudation of the region, resulting in the release of stored elastic stress in the essentially solid rock. These extensional or stress-release joints are particularly useful in determining dips in the granite at the crater site, as elsewhere in the mapped area they are mostly horizontal, indicative of the pre-impact conditions (see also Feuchtwanger, 1973).

The patterns of the regional joint and fracture orientations measured at the various localities (indicated by numbers on the regional map) are shown in Figure 3.19. It should

be noted that these joint orientation diagrams show a few differently orientated joint systems. It is impossible to try to explain the origin of every joint set at the available outcrops, as each locality exhibits a unique joint pattern and hence a unique structural domain, possibly as a result of small differences in tectonism throughout the mapped area. Instead, the overall joint pattern of the mapped area was determined by combining all joint measurements, which resulted in a typical joint pattern with three prominent joint orientations (Figure 3.20).

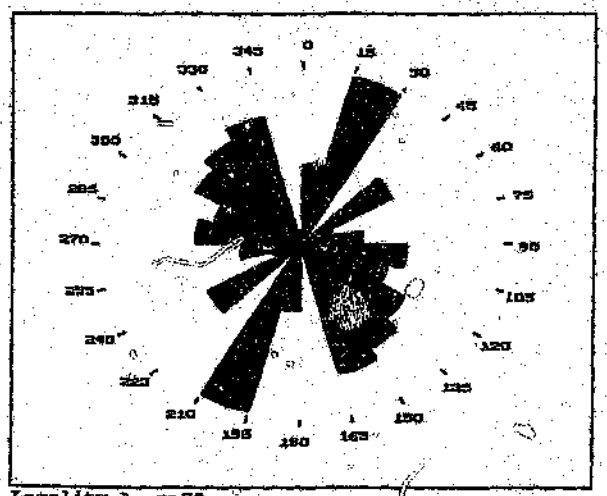

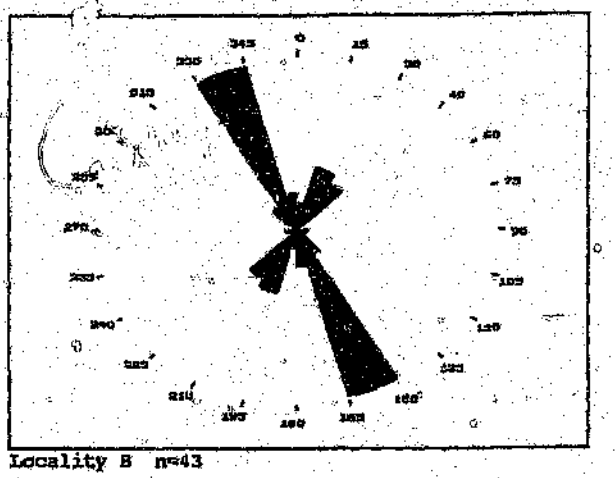

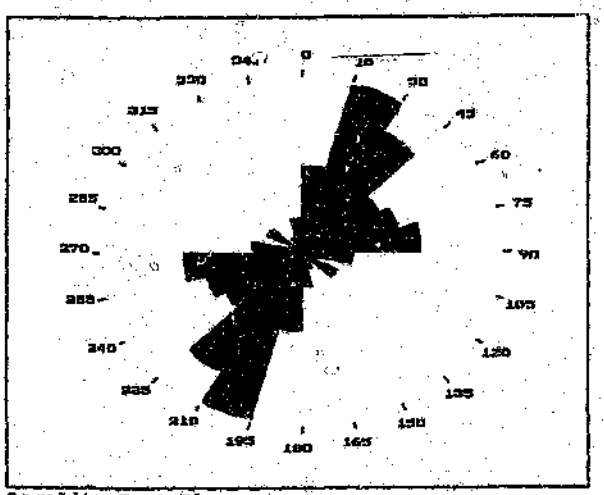

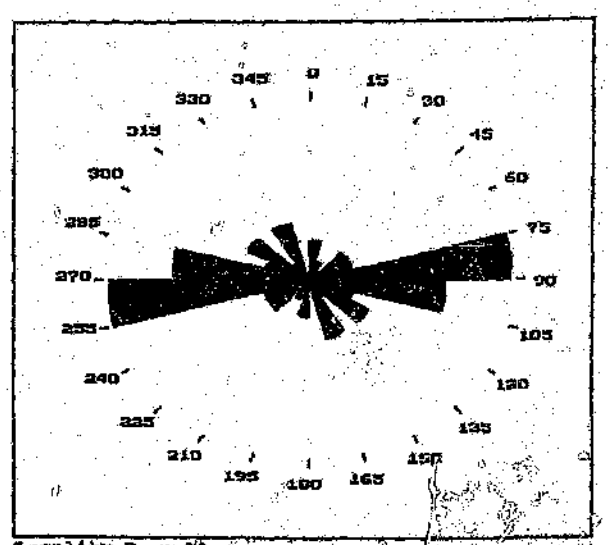

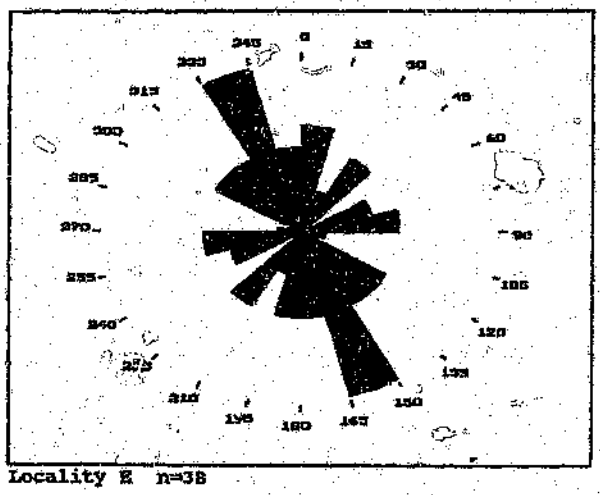

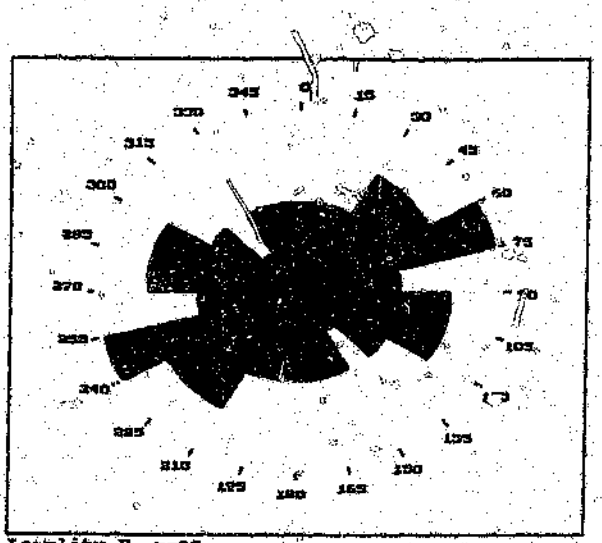

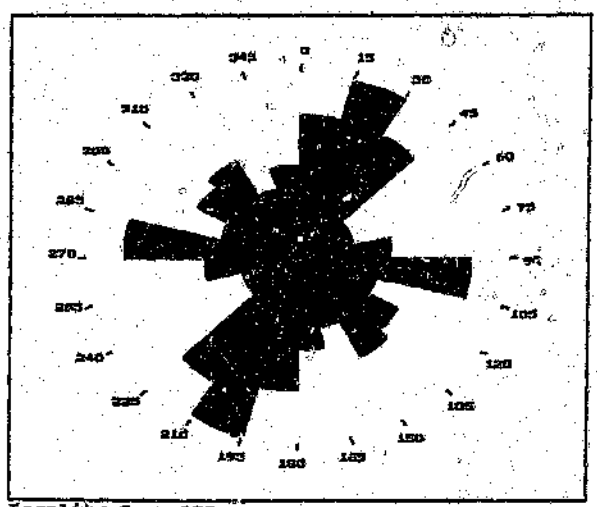

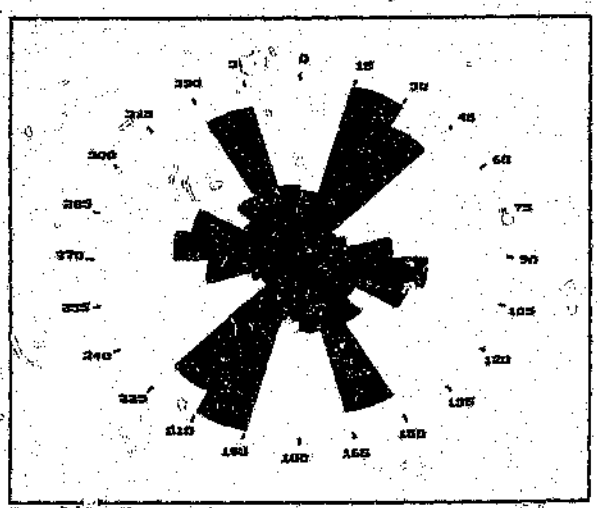

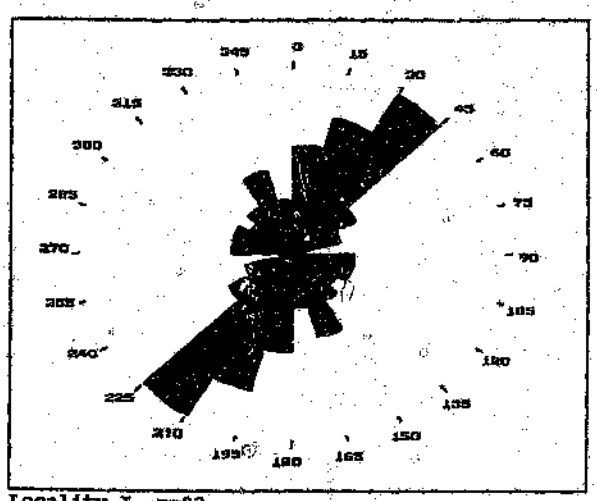

Figure 3.19 Joint patterns measured at nine different localities in the study area (for localities see regional map insert). Number of measurements denoted by n.

From Figure 3.20 it is evident that the most prominent joint direction in the Bushveld granite in the environs of the Pretoria Saltpan crater is approximately north-northeast to south-southwest. A second system, which is slightly less developed, is approximately north-northwest to south-southeast, and a third, and least developed of the three systems, is oriented east-west. The average spacings between the joints could not be estimated accurately, because they varied from tens of centimetres to a few metres.

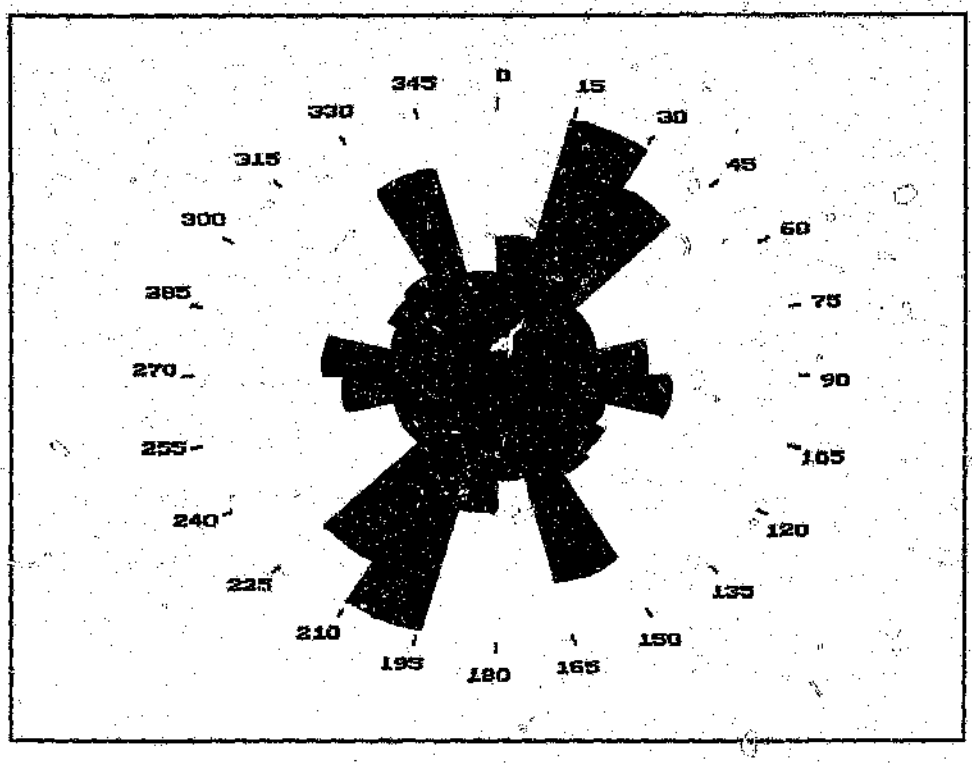

Figure 3.20 Joint pattern for the entire crater environs, obtained by combining all joint orientations measured in the study area (n=690).

Joints, faults, or planes of weakness in the target rock have been shown to play a role in affecting the final crater form (Melosh, 1989). However, due to the complex nature of the regional joint patterns encountered in this region, no attempt has been made at correlating joint patterns and crater shape.

Lineaments

Regional lineaments were studied on aerial photographs (see regional map insert) and are probably continuous extensions of the joints observed on a smaller scale. They are therefore interpreted as master joints rather than major faults (which, however, cannot be completely excluded). The reason for this deduction is that the rose diagram representing the overall strike anomalies of the regional joint sets can generally be matched to most of the lineaments which were observed on a macro-scale using aerial photographic methods. The orientations of joints and fractures in the crystalline basement outside the crater do not exhibit a strong homogeneous and characteristic pattern, such as that found around the Rochechouart impact structure (Bischoff and Oskierski, 1987). This may be attributed to the fact that close to the crater no outcrop is present and instead is covered by a thick layer of granite-derived sands.

Some lineaments may represent regional faulting. This could not be verified, as no surface expression of faulting is present on the flat, thickly soil-covered surfaces where these photolineaments were noted. If this is the case, the regional faulting trends would be subparallel to the prominent joint sets. An important observation, however, is that an agreement between the joint strikes and the photolineations can be observed in the mapped area.

Faulting may be observed on an outcrop scale in the granite. This small-scale faulting is generally truncated at the granite-grit boundary indicating that this faulting pre-dates the Karoo sediments. Displacement of the order of a few centimetres was noted on some of these faults, but they are believed to have little significance in the interpretation of the regional lineaments which were noted on the aerial photographs.

As a result of the regional joint and fracture (lineament) analysis, it can be stated that the arrangement of the joint systems in the entire area outside the impact structure originated from normal tectonic processes and was apparently not affected by the impacting event. This does not apply to the crater rim joint systems discussed in the following chapter.

CHAPTER 4 CRATER GEOLOGY

4.1 GENERAL GEOLOGY AND CRATER MORPHOLOGY

Although terrestrial impact craters often exhibit structural peculiarities which are not predicted by any model (Bischoff and Oskierski, 1988), studies of the surface geology of a crater is an important prerequisite for the reconstruction of crater development. The Pretoria Saltpan is a bowl-shaped depression forming a gigantic amphitheatral depression with a maximum rim elevation of 119m above the present crater floor and 60m above the surrounding plains. It occurs wholly within the homogeneous granitic rocks of the Bushveld Igneous Complex. The rim is made up of mounds and ridges separated by saddle-shaped gaps (see Figure 1.1).

The inner slopes of the crater are markedly steeper than the outer slopes with gradients up to 36° and becoming more gentle down slope. It was found that four slope types, differentiated by gradient, can be distinguished on the inner crater rim. These four types have been shown to have distinctive sedimentary characteristics (Brandt, 1991). The lowermost slope, which is essentially level, is composed of a soft, sticky mud. The next two slopes, referred to as the lower and middle slopes, with average gradients of 8° and 16°, respectively, are composed of sand (granite detritus) and rare granite boulders. The upper slope consists of a thin layer of weathered granite and many loose fragmented granite boulders, as well as some boulders that apparently are in situ.

On the outside, the crater rim initially falls steeply and then gradually changes slope to the level of the relatively flat surrounding countryside. This outer slope consists largely of alluvial detritus and varies in length, but is on average 500 metres long. The exact limit of the ejecta blanket (visible on aerial photographs in the form of a 500 metre wide zone) is obscured by the denudation and erosion of the rim and probably some reworking of the debris ejected from the crater. In 1991 trenching at two sites (150 and 800 metres directly north of the northern rim) was carried out to determine the nature of the deposits outside the crater rim. Both trenches were approximately two metres

deep and revealed the following (Reimold, pers. comm.): the trench further away from the rim (800 metres north of the rim) consisted of typical weathered granite down to a depth of 1.7 metres, after which 0.3 metres of solid granite was encountered. This profile exhibited no evidence of ejected granite breccia. The closer trench (150 metres north of the rim) consisted of an upper 1.8 metres of crudely stratified, coarse-grained, immature sediment (angular as the distance from the rim crest is not sufficient to round fragments). From 1.8 metres to the limit (two metres) of the trench a poorly sorted ejecta deposit containing angular fragments, up to approximately ten centimetres in diameter, was observed. Much of the original ejecta blanket has been removed by erosion and is characterised by large blocks of granite in certain places on the rim and hummocky topography for several hundred meters beyond it. The blocks are usually largest on the rim, presumably because their ejection velocity was lowest. Outcrops of seemingly undisturbed granite blocks may be found in the north on this gradually descending slope. Some of these outcrops, due to their elevation with respect to the surrounding area, appear to be the in-place uplift of the pre-impact ground, as a consequence of deformation related to the cratering event. Strong horizontal compressive forces push outwards from the crater centre as it grows, fracturing the rock and squeezing it upwards (Melosh, 1989).

A broad, shallow (up to 2.85 metres deep - Ashton and Schoeman, 1983) saline lake, which contracts and expands with seasonal precipitation, overlies a thick succession of lake sediments in the central area of the crater. The lake is also fed by two springs issuing from the crater floor where drill cores were extracted for research purposes. The drill cores intersected a sandy aquifer, the suevitic breccia between 90 and 152 metres depth (Partridge et al., 1993), and as the level of the crater floor lies below the water table, the water continuously flows from these holes. Prior to the drilling, the crater was occupied by a shallow seasonal pool.

The pre-impact conditions were undoubtedly similar to those seen in the surrounding countryside at present, that is, a broad expanse of generally flat terrain consisting of a crystalline basement overlain by a horizontal to sub-horizontal veneer of sedimentary rocks of the Karoo Sequence. The drainage system in the study area consists mostly of

non-perennial streams with an overall flow direction from south to north. The drainage pattern of the "Soutpan stream", which winds around the crater on it's eastern side, suggests that if this minor drainage system existed at the time of impact, the impact event may have resulted in a new flow path which is at present to the east of the original path. Ample field evidence, however, suggests that the pre-impact surface was essentially flat at the time of impact. Although uniform, isotropic, and homogeneous geological material is scarce or non-existent, the slight undulations on this surface and minor structures observed in the crater environs should have had a minimal effect on the cratering processes. Also, due to a lack of evidence and due to complex regional joint patterns, as mentioned in Chapter 3, no conclusions have been drawn on the possible effects of jointing on the cratering processes, morphology, and structure, such as those from Meteor Crater, Arizona (Shoemaker, 1960). Shoemaker noticed that the regional jointing controlled the shape of the crater, which is somewhat squarish in outline; the diagonals of the square coincide with the trend of the two main sets of joints.

Intrusives

Small basic and alkaline intrusives are present on the rim. They are particularly abundant on the northern rim, with a few occurrences elsewhere. The crater map insert (in the back pocket) shows the occurrences of intrusive and the other structural features discussed in this chapter. The intrusives include lamprophyre, constituting most of the intrusives, trachyte, phonolite and carbonatite. Most of these rock types occur in the form of veins or dykes and possibly sills in loose granite boulders, and very few of the intrusives studied are believed to be in situ. Even those which were assumed to be in situ may be part of a large reoriented granite block, which was moved in the cratering event. Lamprophyre outcrops, which are best preserved and show the best field relationships, are typically fractured and extend over distances which rarely exceed 1 metre in length. Figure 4.1 represents a typical lamprophyre outcrop on the northern crater rim, and Figure 4.2 shows a particularly well preserved segment of lamprophyre dyke, which, as in the case of the regional geology, shows a very sharp cross-cutting relationship with the granite.

Figure 4.1 Typical lamprophyre occurrence on the northern crater rim.

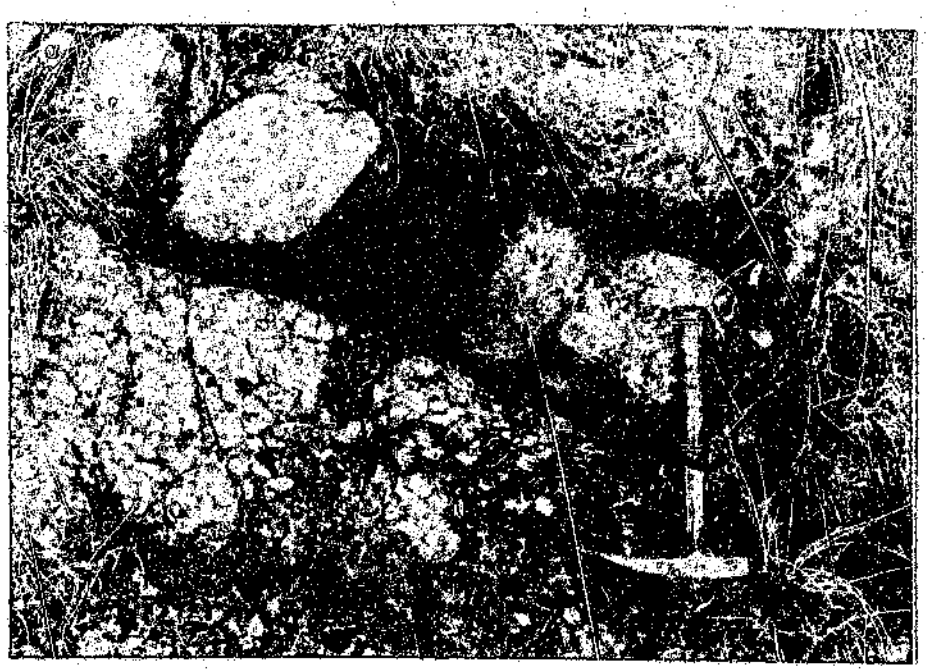

Figure 4.2 Segment of a well preserved lamprophyre dyke showing the cross-cutting relationship with the host granite.

Carbonatite occurs at two sites: the first site on the inner and lower southwestern rim of the crater was already described before (e.g., Wagner, 1922). Here carbonatite occurs as large tabular masses. It is not possible to determine whether these blocks are in situ or not. Figure 4.3 shows this carbonatite which is cut by secondary quartz and calcite veins, and which has incorporated into it numerous, often well-defined angular schist fragments, the origin of which has not been determined. It has been suggested (e.g., Wagner, 1922) that the schist was incorporated into the carbonatite prior to intrusion, and that it originally formed part of a pre-Bushveld stratigraphic horizon (such as a Transvaal Supergroup shale). No granite-carbonatite relationship can be determined at this occurrence.

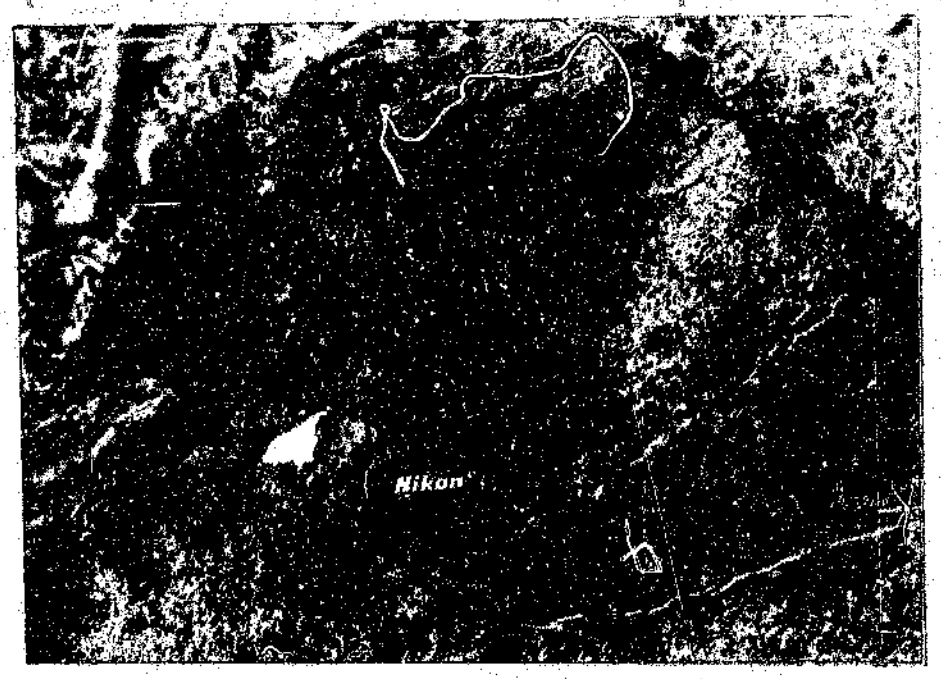

Figure 4.3 Carbonatite occurrence on the lower, inner southwestern rim (Sample 95), with numerous, well-defined schist fragments.

The second occurrence, located on the lower western slopes of the crater (Figure 4.4) exhibits a sharp granite-carbonatite contact. This outcrop, which now is partly altered to a fine-grained yellow clay, can be chemically related to the first outcrop and shows a similar mineralogy in some less altered parts of the sample. In this case, however, the

carbonatite contains angular granitic fragments of varied orientations, indicating a violent emplacement of the carbonatite at this locality.

Figure 4.4 Granite-carbonatite relationship (Sample 107).

The various dykes were previously thought to have a radial or peripheral disposition with respect to the crater centre (Feuchtwanger, 1973). Detailed mapping and plotting of the dyke orientations with respect to the centre of the crater, however, revealed that most of the intrusives have no preferred orientation with respect to the crater centre. Figure 4.5 shows a detailed, planetabled map of a particularly well preserved trachyte dyke or dykes outcropping on the northern rim at the well-used "crater view-site". It is evident from this map that these dykes or sills have been faulted both radially and concentrically by a post-intrusive event.

It should also be noted that the various granite blocks containing the trachytic intrusives have many different orientations, implying that fairly complex faulting took place in this upper portion of the rim. Figure 4.6 is a sketch of what is believed to have resulted in the complex structure observed at this site and at other localities on the inner rim. The

trachyte at this particular location is extremely altered, as seen in Figure 4.7, and was only recognized as such by its chemical composition.

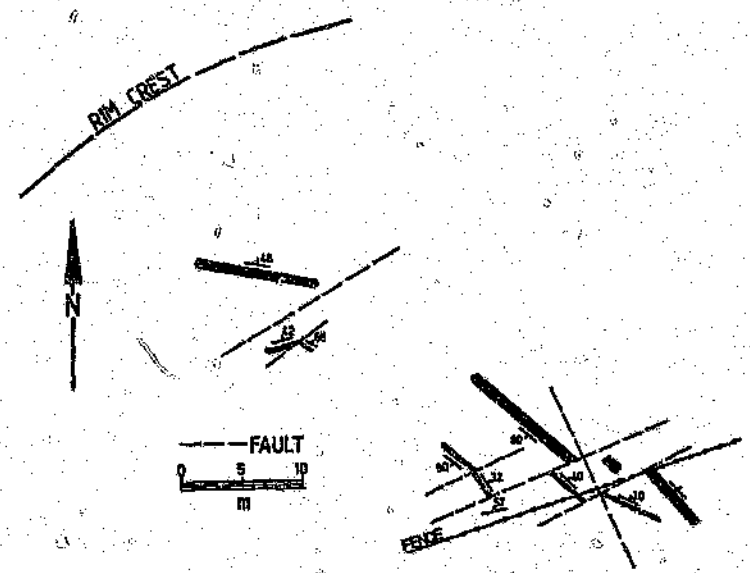

Figure 4.5 Detailed planetabled map of a radially and concentrically faulted trachyte dyke. The small numbers indicate the dip measured for each fragment of the dyke.

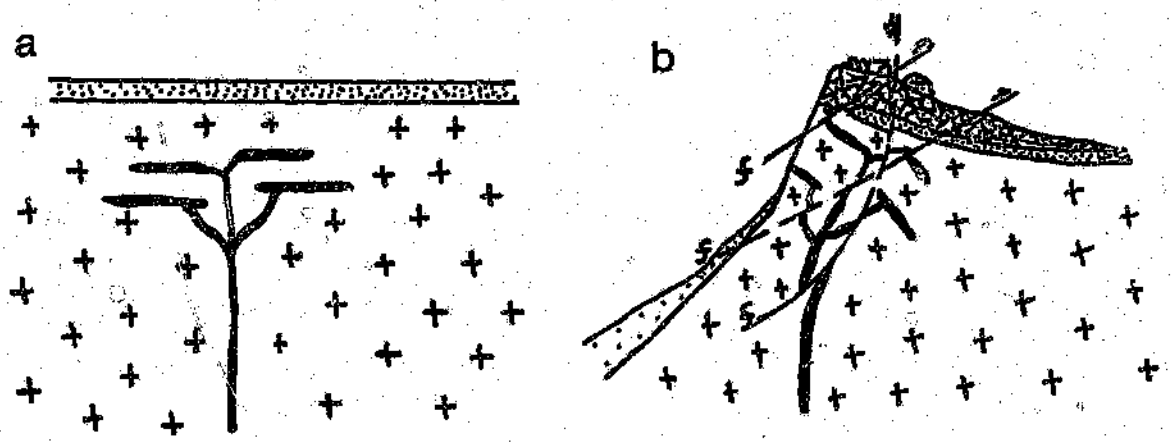

Figure 4.6 Sketch of (a) Pre-impact conditions, and (b) Post-impact structures resulting from the cratering event: the upper portion of the rim is believed to have been thrust outwards resulting in outward-dipping rotated blocks; superimposed on these thrust faults are normal modification, or post-impact structures. Dykes and sills within the original granite would be faulted into numerous orientations as shown in the figure.

Figure 4.7 Highly altered trachyte dyke (Sample 24: a typical north-rim sample).

Karoo sediments

The Karoo grits do not completely encircle the crater, having over considerable stretches either been removed by denudation or having not been present at all at certain localities around the rim. The latter situation would be due to the pre-impact distribution of these sediments. Wagner (1922) noted that the basal portion of the breccia on the rim contains small fragments of the same type as the underlying Karoo grits. The highly laterized nature of the grits, which have been buried by the ejecta breccia, indicates that they most probably were exposed to surface weathering prior to their burial. The fragmental rim breccia is well preserved in the crater rim section, particularly in the southern sectors of the rim, which are exposed by the two artificial cuttings, and will be dealt with in the following section.

4.2 STRUCTURE OF THE RIM

The secondary road leading to the crater centre from the southeast (see crater map insert in back pocket) provides the best section through the crater rim. The section shows, in descending order: granitic throwout breccia, ferruginized Karoo grits and reddish, deformed granite. The granitic throwout breccia (Figure 4.8) consists of poorly sorted angular clasts which range in size from a microscopic scale to greater than a metre in diameter. The contact between the breccia and the grits must represent the level of the original surface at the time of the cratering event.

Figure 4.8 Throwout granite breccia at the top of the crater rim section, southeast rim sector.

Deformation in the crystalline rim is not as clear as that encountered in other impact craters with well defined stratigraphy. However, sets of tight, closely spaced, originally horizontal sheeting joints were particularly useful in determining the deformation experienced by the target rocks due to the cratering event. This joint set, which parallels

the Karoo sediments in the crater environs (see Figure 4.9), is most probably the result of stress release or extension due to removal of overburden. In addition to this joint set, compressional shear has given rise to the development of a fracture cleavage which is partitioned into zones which apparently experienced greater strain or represent less competent layering (Figure 4.10). Fracture cleavage is defined as a non-penetrative foliation consisting of persistent, closely-spaced fractures which may be found in igneous rocks (McClay, 1987). This fracture cleavage is common in the lower portion of the crater wall, where strain was imparted mainly along horizontal directions, and hence parallel to the sheeted joints discussed above.

Figure 4.9 Horizontal joint set observed in the granite in the crater environs.

Figure 4.10 Fracture cleavage partitioned into zones of greater strain or less competent layering.

The structure in the crater walls consists mainly of faults, fractures and local brecciation in the granite, which may be moderately folded and uplifted. The intensity of deformation increases upwards towards the top of the crater wall, where the granite may be vertical to overturned and is generally broken into blocks. Faulting associated with the outward and upward displacement of the granite includes thrust, normal and reverse faulting. Some high-angle faults may be related to joint orientations - other faults occur at a variety of attitudes to the jointing. Low-angle jointing plane faults are common with a pronounced horizontal component. Thrust paths which point radially outwards, determined by thrust movement of blocks, are a major aspect of the tectonic style in the crater rim.

Lower crater wall

Low in the crater rim, the granite generally dips gently inwards (Figure 4.11c). It has been suggested (e.g., Fudali et al., 1973) that the inward dip of the lower portion of the rim is the result of tilting and subsidence of a large coherent segment of the original rim,

as a result of an explosive volcanic event. Rather, this downwarped strata appears to be the result of movement along closely-spaced, discrete shear surfaces. A cleavage, which can locally be seen in section (such as that seen in Figure 4.10), also aids with the determination of the dip of the granite, which parallels and enhances the once horizontal sheeting joints seen in the environs. Most probably the sheeting joints originally formed due to extension resulting from the removal of overburden on the sub-horizontal pre-impact surface, whereas the cleavage appears to be a fracture cleavage resulting from the impact event. The granite exhibits poor foliation in the crater wall and is rarely seen in the lower crater rim due to poor exposure. In a few areas of the lower crater wall some granitic blocks are seen to dip gently outwards. This is only representative of isolated areas, where the otherwise inward-dipping granite has been disrupted to a greater extent.

A deep trench in the southwestern crater wall, that was previously referred to as "Mauss' Cutting" (Wagner, 1922), shows that in the lower crater section the granite dips inwards instead of dipping at a steep angle outwards. This clearly represents a reversal in the direction of the average dip encountered at the rim, as for example observed on the well-preserved crater access road section (Figure 4.11). As a result of weathering and erosional processes the surface along Mauss' Cutting does not exhibit the original state of this rim section and offers no extra information on the structure of the crater to that which could be obtained from the road cutting section.

Mid-crater wall

The mid-section of the rim, that is the section between the lower, inward-dipping granite and the upper, outward-dipping granite, is assumed to consist of an anticline, which is locally displaced along some inward-dipping faults, very similar to those described from the Odessa crater (Shoemaker and Eggleton, 1961), as well as outward-dipping faults. This anticline is clearly exhibited in the mid-section of the road cutting which leads into the crater (Figures 4.11 and 4.12). The amplitude of the anticline is approximately two metres and the fold axis is concentric about the centre of the crater. According to Gault et al. (1968), folds like this one result from initial outward motion, that is the granite is first driven outwards in a horizontal direction and then deflected upwards towards the surface.

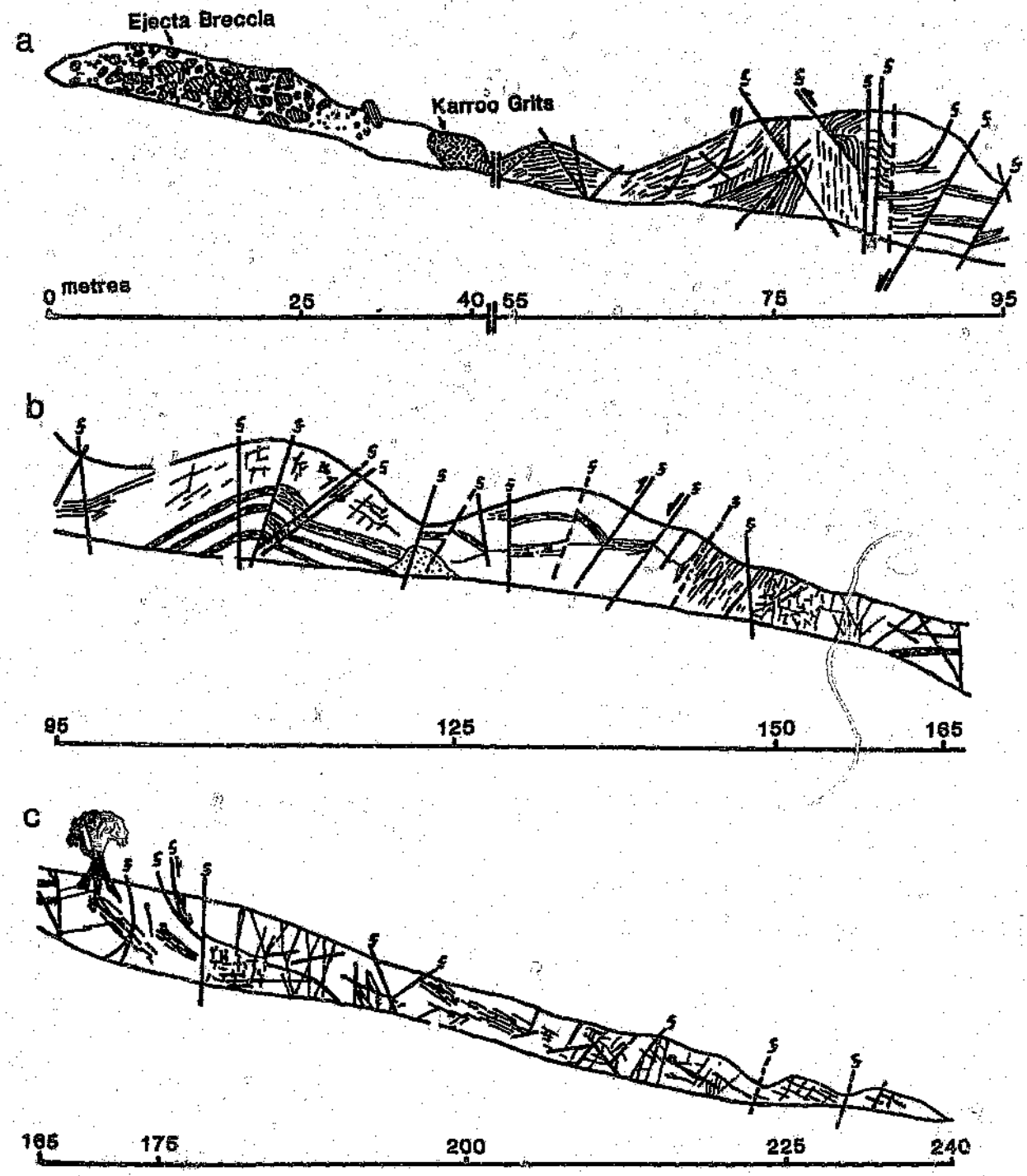

Figure 4.11 Section of the crater rim along the access road from the southeast into the crater: (a) upper crater wall showing ejecta breccia overlying Karoo grits, which overlies steeply outward-dipping granite, (b) mid-crater wall exhibiting an anticline, and (c) lower crater wall with generally shallow, inward-dipping granite.

Figure 4.12 Anticline in the mid-crater wall of the crater rim section.

Milton and Naeser (1971) noted parting planes in the two artificial cuts through the crater wall, which were deformed by an abundance of folds and thrust faults on a scale of decimeters. They suggested that these were the result of strong shear or compressive stresses (as are the structures in Figure 4.11b). Milton and Naeser (1971) noted that, to their knowledge, features such as these have never been noted at a maar, and that the resemblance of features such as these to those in the walls of known meteorite craters is striking.

Upper crater wall

Closer to the top of the rim the granite dips outwards at varying degrees, indicating that the rim granite has been upwarped. It is not overturned anywhere along the rim to the same extent as that encountered at Meteor Crater, Arizona (Shoemaker, 1960). Granite fragments, identified as throwout debris, are, however, stacked in an inverted stratigraphic sequence (granite breccia overlying younger Karoo sediments) at various localities along the rim (see Figure 4.8). The inverted stratigraphy is not always present,

because collapse of upper rim sections in smaller craters frequently carries the rim cover downwards into the crater cavity (Melosh, 1989). Proceeding downward, the steeply dipping granite blocks are bounded by two rather poorly defined parallel and steep faults (Figure 4.11a). The granite on either side of these faults is highly weathered and intensely fractured. These two faults represent a transitional zone, above which the dips of the granite are increased and almost vertical. Below these two faults, the deformation is slightly more ductile resulting in folding of the mid-section of the rim and less steeply outward-dipping granite at the inner margin of the fault. The upper, steepened granite and the Karoo sediments overlain by the ejecta breccia are also broken by a number of small, nearly vertical, radial faults, which have caused the numerous depressions seen along the rim crest. These near-vertical faults display a scissor-type displacement in the southern section of the rim. This type of displacement was also noted by Shoemaker and Eggleton (1961) at Meteor Crater. Figure 4.11a shows the complex faulting and structure of the upper crater wall.

A few normal faults, concentric to the rim and well known from other larger terrestrial impact structures such as Clearwater, Manicougan, and Siljan (Bischoff and Oskierski, 1987), as well as craters of similar dimensions (e.g., Meteor Crater, Shoemaker 1960) are exposed in the upper parts of the crater wall in the northwestern and southeastern sectors of the crater. Figure 4.13 shows such a normal fault on the upper section of the southern rim. The relative displacement of the lower block is towards the crater centre. Wall failure normally takes place during the modification stage by inward and downward gliding of rock slabs along listric faults resulting in the rotation of the gliding blocks into outwardly inclined positions (Bischoff and Oskierski, 1988). The first map of the crater by Wagner (1922) exhibits a ring fault, which was attributed to subsidence following a volcanic explosion. As little or no information on impact crater structure was available at that time, an impact origin was disregarded. Thus, what Wagner interpreted as a subsidence ring fault, is most likely what has been interpreted by the author as normal faulting of the modification stage, as described above. A few blocks on the upper rim appear to have rotated around a vertical axis in addition to the processes discussed above. The amount of rotation was usually difficult to determine, but was in the range of 10 to 50 degrees. This sort of deformation was noted by the author at Meteor Crater

(see Chapter 9 for a comparison to Meteor Crater), too.

Figure 4.13 Normal fault on the upper southern rim formed during the modification stage. The crater centre is to the left and the left-hand block has moved downwards and was rotated clockwise.

Fault breccia is not common, but is well preserved in one locality, on the crest of the eastern rim, in the form of a radial breccia dyke (see section 4.3). One or two concentric fractures were interpreted as inward-dipping thrust faults, although this is purely speculation, as the true sense of displacement could not be determined accurately.

In general, the development of thrusts and other fault types appears to be related to strain movements or stress released during the crater formation. It is interesting to note

that the walls of maars and diatremes are characteristically cleanly truncated, whereas on impact shock is propagated through the rock and produces deformation at a distance, resulting in the walls of an impact crater being intensively and pervasively deformed (Milton and Naeser, 1971; Melosh, 1989), such as that seen in the Saltpan crater rim section (Figure 4.11).

Jointing

The jointing patterns of the crater rim are markedly different to those observed in the surrounding regional geology. No attempt was made to show the actual physical traces of joints on the crater map, as they were generally far too numerous and much too short to portray at reasonable map scales. Instead, the orientations of the dominant systematic sets of joints are portrayed through a series of rose diagrams, each representing a certain area of the crater rim. This was achieved by carrying out a detailed structural analysis of several exposures inside the crater and on the rim. These analyses provided a better insight into the fracturing which resulted from the impact event.

The joint patterns obtained are shown in Figure 4.14 which exhibits an orthogonal radial and concentric joint pattern. The joint plane attitudes are, however, inconsistent and vary from approximately 40° to vertical. They are generally very steep with an average dip of about 70°. The fracture planes are frequently inclined towards the crater centre. These inward-dipping planes would have allowed block movement, associated with both normal and thrust faults encountered within the crater rim. It should be noted that not all fractures encountered conform to the typical radial and concentric pattern obtained for the joint sets.

An explanation for the origin of some of these joint sets could be that granite blocks were displaced or faulted along radial and concentric fracture planes, and that distinguishing faults from the joints at times may be an impossible task. Due to the lack of fault-defining features many fractures may either be joints or glide planes. However, the impact triggered the formation of radial and concentric fractures in the target rocks in addition to the existing fractures or joints, as would be expected. In general, where the original rim of the crater is preserved, an increase in jointing, along with the deformation

and re-orientation of pre-existing joint planes, can be related to strain accompanying crater formation. In view of the regional fracture analysis, it can be stated that the arrangement of the main joint and fault planes outside of the impact structure originated mostly from normal tectonic processes and not as a consequence of the impact event.

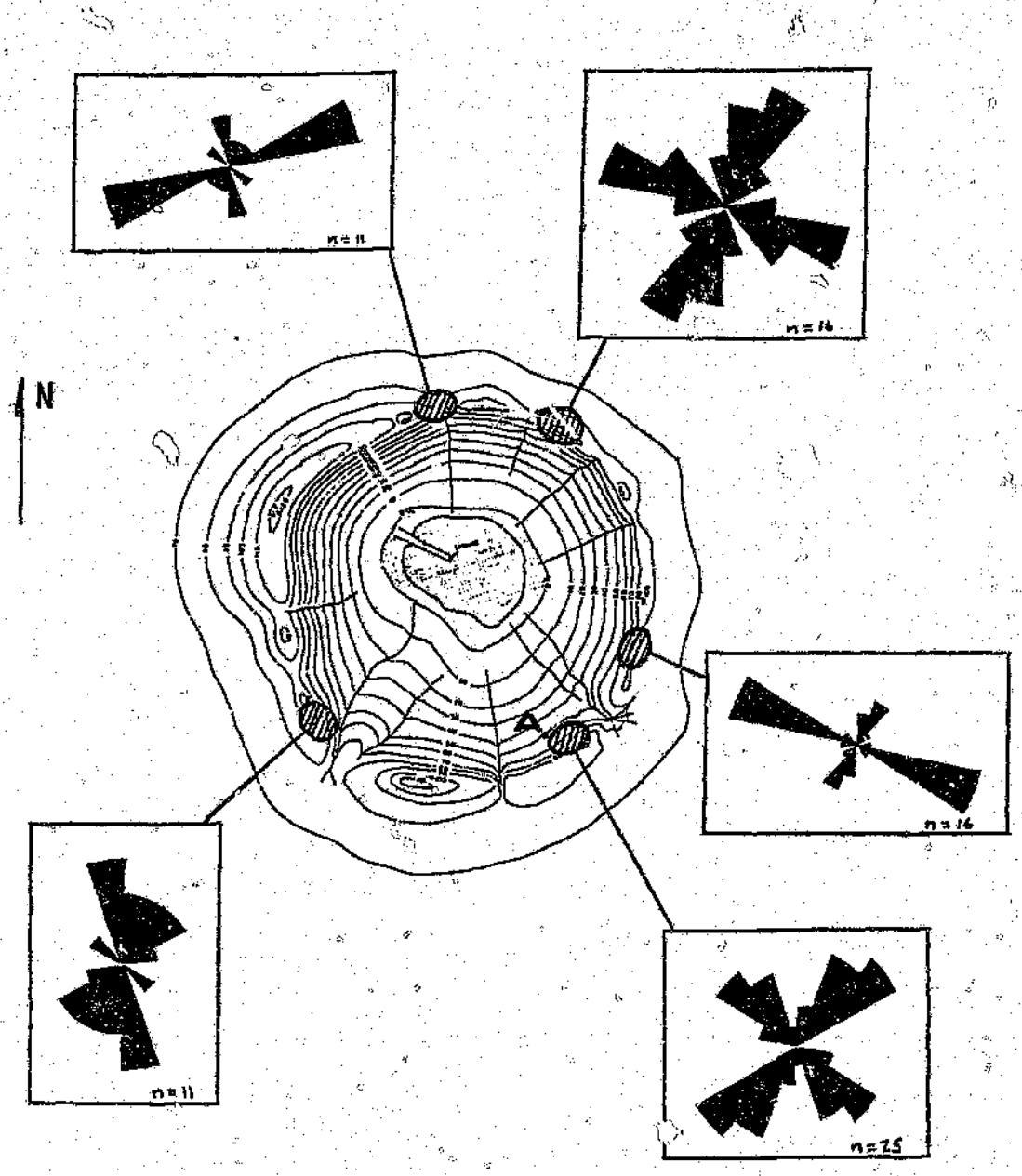

Figure 4.14 Joint orientations taken at selected sites on the crater rim (after Brandt, 1991).

Aerial photography interpretation

Aerial photographs revealed the presence of fractures surrounding the crater. These fractures are generally radial, with one or two occurring circumferentially, and all occur within a few hundred meters of the rim (see regional map insert). These features were not observed in the field due to the extensive ejecta blanket cover, and therefore no further information regarding displacement and hence fracture (or fault) type was possible.

4.3 BRECCIA DYKES

Fragments of granitic breccia were found at numerous localities on the inner slopes of the crater, with the exception of two outcrops of autochthonous breccia, the locations of which may be seen in Figure 6.34 (page 109). In general, the breccia dykes or fragments of such dykes show sharp contacts with the country rock, extend for several metres, and may be terminated by the border of an outcrop or granite-derived sands. The first outcrop, in the form of a sub-vertical, radial breccia dyke, occurs on the upper portion of the eastern rim (Figure 4.15). This dyke consists of granitic fragments which are crudely aligned with the orientation of the dyke. The matrix consists of a fine-grained matrix having a composition similar to that of the host granite.

The second outcrop shows a similar matrix, but larger granitic clasts than in the previous sample are also crudely aligned (Figure 4.16). This occurrence (Sample 77: see figure 6.33 for location) was observed in the lower portion of the southern rim in a large tabular granite block. Although this block appears to be in situ, it may have originated further upslope. These two outcrops, as well as numerous fragments of similar breccia, were observed only within the crater rim and are all believed to be a direct result of the cratering event, as they were not found anywhere else in the studied area.

Figure 4.15 Sub-vertical radial breccia dyke (Sample 72: for locality see Figure 6.33).

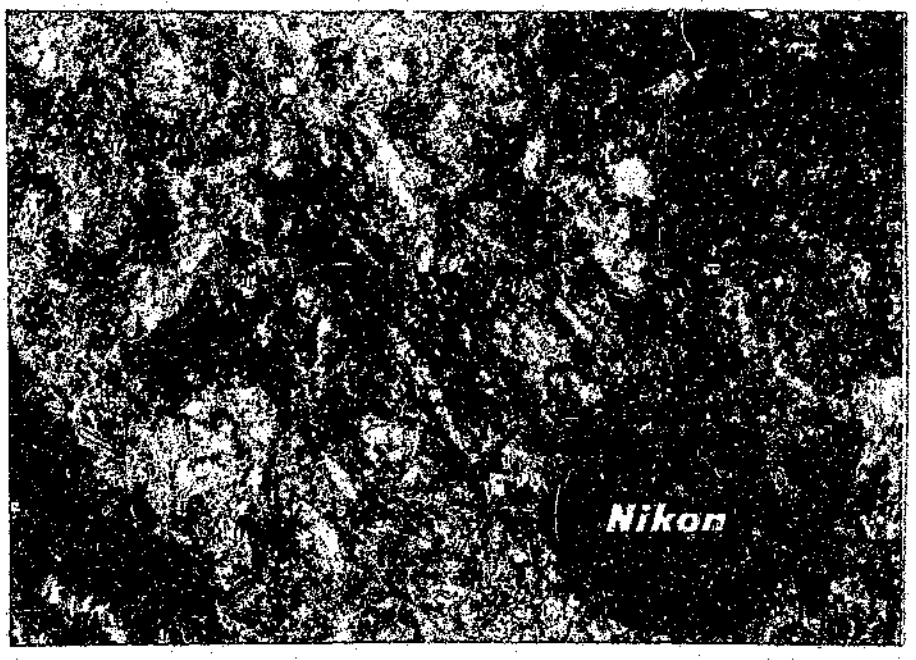

Figure 4.16 Massive tabular granite breccia found on the southern lower, inner slopes.

4.4 THE DRILLCORE

Compressional shock waves that pass across discontinuities such as joints, will be reflected, in part, as tensional waves, or will move on as weak secondary rarefraction waves (Short, 1970). Such shock waves can cause rock to break up in place, moving fragmented material over short distances. These mechanically ruptured and possibly ejected fragments eventually make up allochthonous impact breccias. Below the crater base, however, the rock units are subject to decaying shock intensities and give rise to what is known as autobrecciated fragments (Short, 1970). It is this lower portion of the core, below the crater-fill breccia, which shows many continuous unrotated blocks or clasts separated only by fracture surfaces, that were analyzed for variations in fracture orientations. Although no significant results were obtained from the joint analysis of the core, Figure 4.17 shows the trend of fracture orientations with respect to the vertical, plotted against depth. From the figure it is evident that the fractures are steeper at greater depths.

One possible explanation for these observations is that at greater depths the rock experiences less compressive stress. It is therefore less deformed at greater depths and displays joint orientations at these depths, which more closely resemble the typical regional joint orientations, which are usually subvertical.

The diversity of the fracture orientations seen in the core probably indicates that the impact triggered the formation of various sets of randomly oriented new fractures in the target rock in addition to already existing fractures of largely subvertical attitude. Subhorizontal jointing is believed to be found only at or near the surface, the effect of which is evidenced at shallower depths in Figure 4.17.

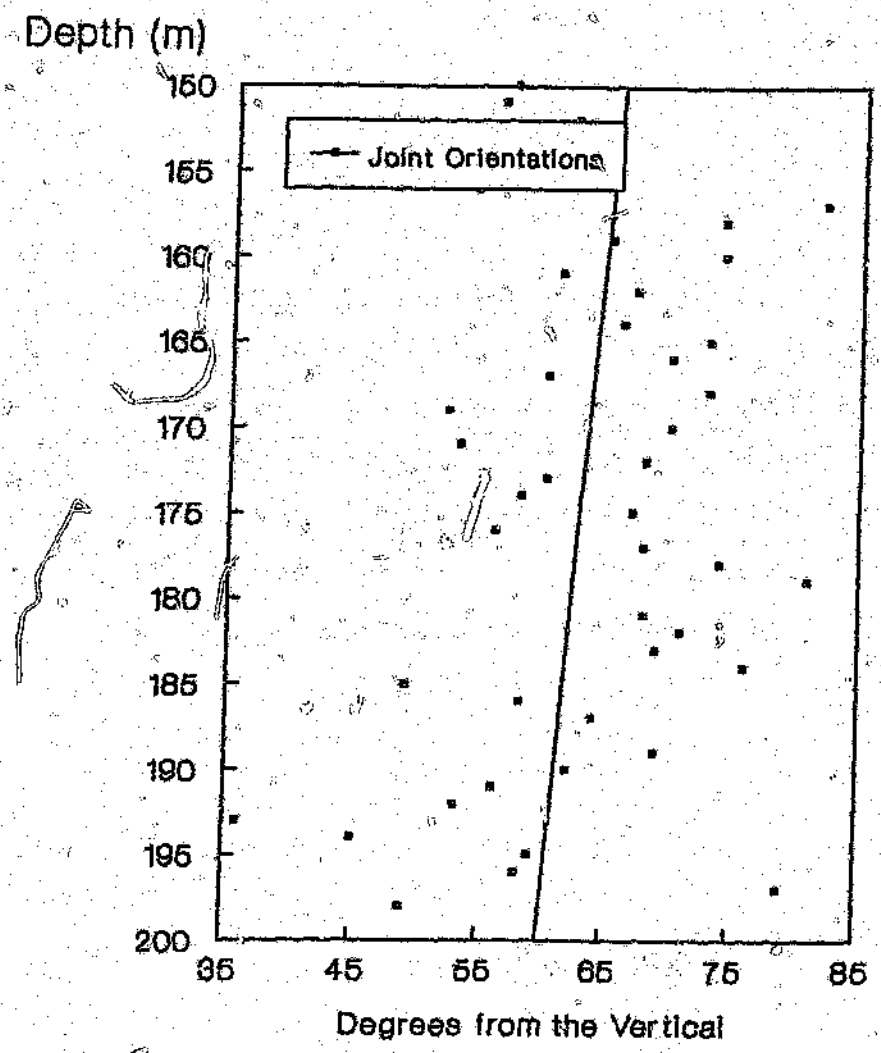

Figure 4.17 Fracture orientations (with respect to the vertical) versus depth. Each point represents approximately 7 joint measurements. The total number of measurements used in this study was 332.

CHAPTER 5 GEOPHYSICAL RESULTS

5.1 MAIN CRATER

Geophysics is an important tool for the initial recognition and study of terrestrial impact craters, many of which, particularly large and old ones, are buried by sediments accumulated at post-impact times or are deeply eroded. The geophysical methods employed at the Pretoria Saltpan crater and to other features in the crater environs included gravity, magnetic, seismic, electrical and ground-probing radar techniques. The results correspond to the typical geophysical signature of small impact structures. As gravity can be directly related to impact-induced density changes (Pilkington and Grieve, 1992), more emphasis was placed on the gravity method.

Gravity results

According to Pilkington and Grieve (1992), a circular gravity low is the most common and conspicuous geophysical signature over a simple bowl-shaped crater. The primary controls on anomaly amplitude are the depths of the low-density breccia zone and the nature of sediments occupying the central zone of the crater, and their density contrasts with the surrounding target lithologies (Pilkington and Grieve, 1992). A gravity model can easily be obtained using available morphometric and other parameters, such as layer thicknesses and densities, which may be available, especially where drilling was carried out.

Only one geophysical study was carried out previously on the Pretoria Saltpan crater. The results of a gravity reconnaissance study by Fudali et al. (1973) failed to support an impact origin, as at that time they could find no compelling arguments for an impact origin, and their gravity data appeared to differ from what they expected for an impact crater of the dimensions of the Pretoria Saltpan. That is, their results did not produce a symmetrical, smooth gravity signature that would be expected for a simple bowl-shaped impact crater. Their findings, however, did not provide unequivocal evidence in favour of an internal origin either, as they could find no signs of any high pressure phases, such

as garnet, which are often associated with kimberlites. They also noticed that the Saltpan is an isolated feature in a region that has been stable at least since the Permian, implying that, if it were of endogenic origin, it was a unique volcanic occurrence in the region. Fudali et al. (1973) concluded that the crater had been generated by a gas-charged intrusion of kimberlite or carbonatite. Despite the new information provided by the drill-core and the more recent results obtained concerning the impact origin of the crater, it was deemed necessary to carry out a more detailed gravity survey in order to obtain a) three-dimensional information about the crater shape and fill, and b) to further investigate the relationship between volcanic intrusives and the crater structure. A gravity profile of higher resolution was obtained, modelling of which would rely on less assumptions than Fudali et al.'s (1973) work.

The positions of the gravity lines for this study and that of Fudali et al. (1973) are shown in Figure 5.1. Thirty-three gravity stations were located along traverse (a) in an almost perfectly straight line across the crater interior. This traverse was extended for approximately 300 meters across the crater rims to the north and to the south.

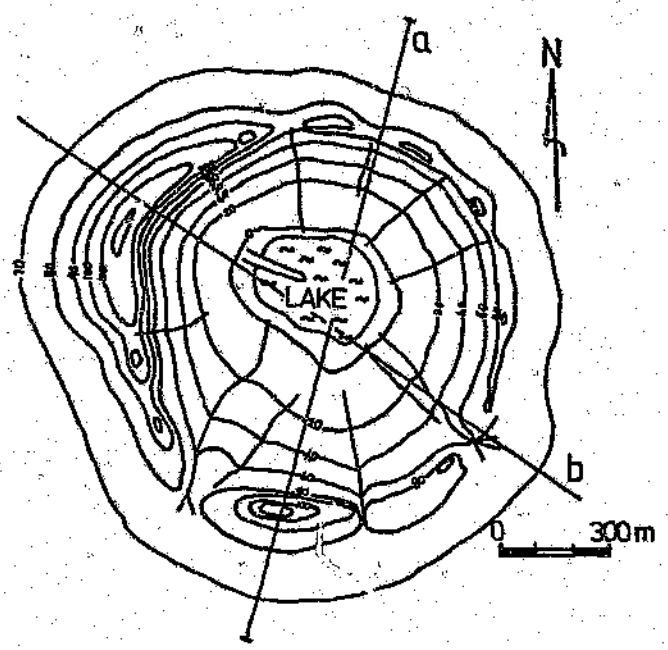

Figure 5.1 Position of gravity profile of this study (a) and that measured by Fudali et al. (1973), (b).

Both the gravity and elevation profiles (Figure 5.2) were measured relative to an arbitrary base station near the crater floor. Station elevations were determined using a level, and gravity readings were taken using a La Coste and Romberg Gravimeter with a sensitivity of 0.01 mgal. Raw gravity data were corrected for instrument drift, elevation, latitude and effects of the severe topographic differences (hilly crater rim versus flat crater floor) encountered. The terrain corrections were made using a Hammer overlay chart, up to zone G, constructed to the same scale as a 1:2500 topographic map of the crater.

The gravity profile is smooth, except for one or two small anomalies on the crater rims, which are probably caused by difficulties in determining accurate terrain correction values. No other reasons, besides data collection and data corrections, could be determined, that may have given rise to the crater rim anomalies. A strong, centred, negative, residual Bouguer anomaly (Figure 5.2b), which reaches a minimum of about -3.2 mgal with respect to the regional field, was obtained. A slight regional gravity trend is present, which corresponds to the gravity trend discussed by Fudali et al. (1973). This regional trend is insignificant with respect to the anomaly measured over the crater interior and was removed for the modelling.

It is most likely, from the knowledge of the crater fill stratigraphy obtained from the borehole (Chapter 2), that the low density lake sediments and the underlying breccias are the cause of the observed local negative anomaly. The density of the relatively undisturbed granite was taken to be 2.67 g/cm^3. Density measurements on various granite samples confirmed this estimate.

The low density sediments which represent the crater fill are believed to be the primary contributor to the observed residual anomaly. The sediments consist of mud, below which is a zone of essentially fractured granite with interbedded granitic sands. The bulk densities of the constituents of the crater sediments (0 to 90 metres) are the only densities which were not physically determined. However, various densities for the muds and interbedded muds and sands were applied in a best-fit model density calculation for the sediments. The densities determined depended on their relative proximity to the

original crater walls, that is, greater densities were assigned to sediment bodies closer to the crater wall as they have a higher sand content. This is due to erosional processes associated with the steep inner slopes of the crater, and the fact that the muds are the final and most distal product of erosion (Brandt, 1991). The densities of granitic breccia ("sands") and fractured granite taken from the drill-core were determined to be 1.30 and 2.61 g/cm^3, respectively. Using this information together with available thicknesses and densities obtained from the core, average densities for each 10 metre interval of the 90 metre to 200 metre depth profile could be determined. The zone of granitic breccia below the muds was found to contribute only slightly to the anomaly.

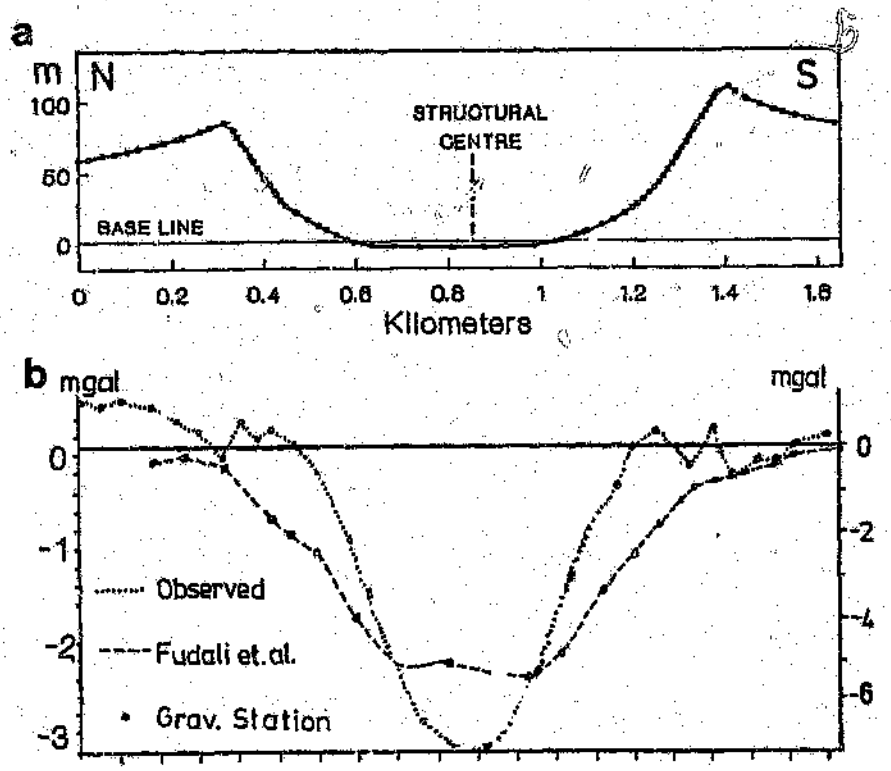

Figure 5.2 a) North-south elevation profile across the Pretoria Saltpan crater.
b) Gravity profiles from this study and from Fudali et al. (1973). Note: right hand mgal scale is for the Fudali et al. profile only.

Thus relatively well-constrained density and layer thickness values were used in constructing the gravity model shown in Figure 5.3b. Modelling was carried out using a computer program (GRAV2DC version 4.6) written by Mr G.R.J. Cooper of the

Department of Geophysics, University of the Witwatersrand. The subsurface configuration was approximated using a number of slabs with various cross-sectional shapes. The cross-section of the bodies obtained in the model yielded strike lengths (not shown in the figure) which decrease from the centre of the model (crater) outwards, in order to simulate the circular geometry of the composite body in plan view. The various densities used for each slab are tabulated in Figure 5.3b. The size of the negative anomaly plus the known densities may be used to infer the physical dimensions of the crater fill. Unlike Fudali et al.'s interpretation of 1973, the data presented here are compatible with the anatomy of a small bowl-shaped impact crater. The Pretoria Saltpan crater results are in excellent agreement with results obtained by Fudali (1979) for the poorly exposed Wolf Creek Crater, Australia, of similar dimensions (0.875 kilometres) and age (<0.3 ka).

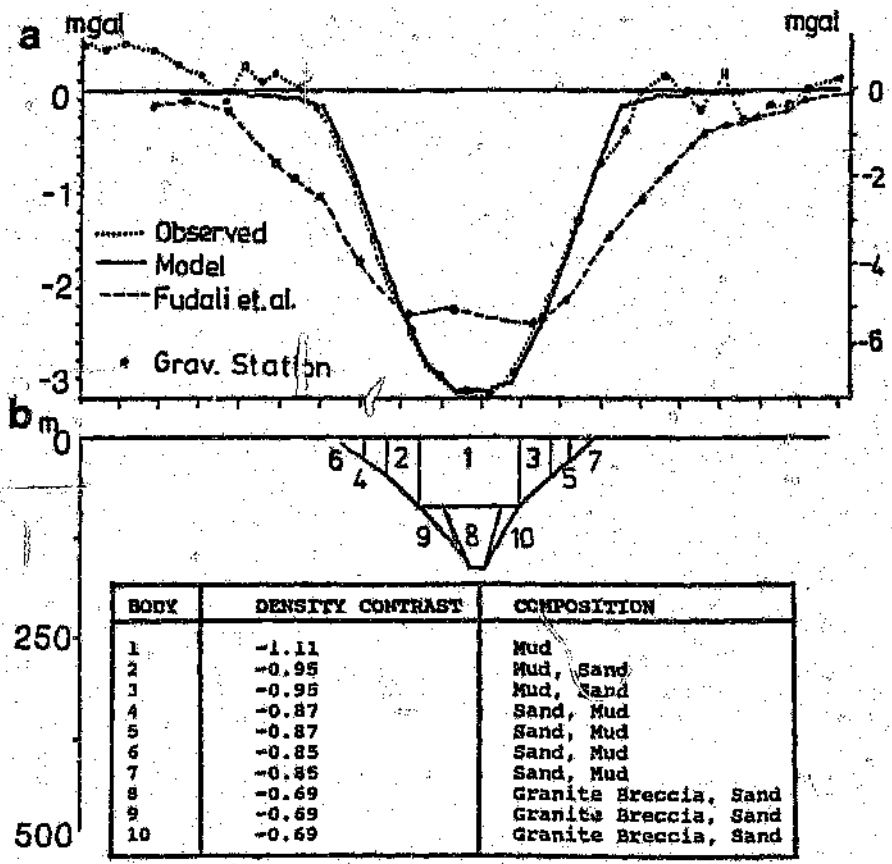

BODY	DENSITY CONTRAST	COMPOSITION
1	-1.11	Mud
2	-0.95	Mud, Sand
3	-0.95	Mud, Sand
4	-0.87	Sand, Mud
5	-0.87	Sand, Mud
6	-0.85	Sand, Mud
7	-0.85	Sand, Mud
8	-0.69	Granite Breccia, Sand
9	-0.69	Granite Breccia, Sand
10	-0.69	Granite Breccia, Sand

Figure 5.3 a) Gravity profiles (this study and Fudali et al., 1973). Note: right hand mgal scale is for the Fudali et al. profile only. b) Gravity model obtained using the best fit model curve in Figure 5.3(a). Density contrasts of the bodies used in the model are all relative to the density of the granitic country rock (2.67 g/cm^3) and are given in g/cm^3.

Magnetic results

According to Pilkington and Grieve (1992), magnetic anomalies associated with impact craters are generally more complex than the gravity signature, because of the much greater variation in the magnetic properties of rocks. The character of the magnetic anomaly and crater morphology can not be directly correlated, as is the case for gravity data, but a broad correlation between anomaly form and crater size may exist (Pilkington and Grieve, 1992). These authors also observed that impact sites may be marked by the absence of significant changes in the observed magnetic field. Target rocks may acquire a shock remnant magnetization, in addition to demagnetization, in the direction of the Earth's magnetic field at the time of impact. The intensity of this shock remnant magnetization is proportional to the ambient field strength (Pohl et al., 1975). Furthermore, following impact, elevated residual temperatures and hydrothermal alteration may produce new magnetic phases leading to the acquisition of a chemical remnant magnetization in the direction of the ambient field. It is evident that a number of processes may be responsible for changes in the observed magnetic field, which may therefore vary from one impact site to the other.

The magnetic survey across the Pretoria Saltpan crater was carried out along three parallel profiles, separated from each other by 175 metres (Figure 5.4). The central traverse coincided with the gravity and topographic profiles (Figure 5.2), in a roughly north-south direction. Measurements were obtained at 20 metre intervals and each traverse extended 1 kilometre beyond the crater rim, resulting in three profiles each a little longer than 3 kilometres. Three profiles were needed to determine any lateral (east-west) variation that may exist in addition to a detailed north-south profile.

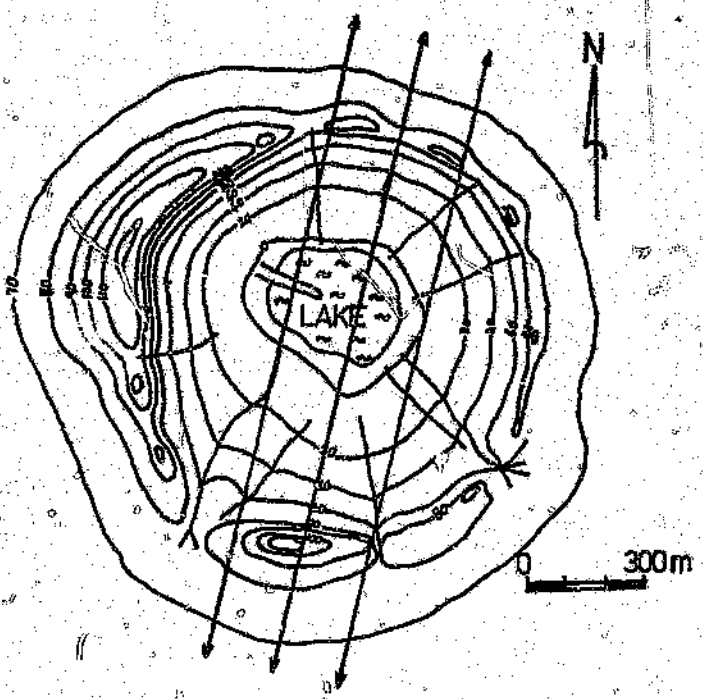

Figure 5.4 Position of the three magnetic profiles across the Pretoria Saltpan crater. Note: all profiles extend one kilometre beyond the rim crest.

In all three cases (Figure 5.5), the magnetic data obtained exhibits the known regional trend (also shown in Figure 5.5). This trend is expressed as limited east-west variation, but with a significant (110 nT) gradient from north to south. The only significant changes to this otherwise straight regional trend are local anomalies on the northern, inner slopes of the rim which coincide with the positions of lamprophyric dyke outcrops or boulders. The other smaller anomalies near the lake and at the southern portion of the survey are caused by scrap metal, fences and a cattle enclosure. These observations rule out the possibility that a magnetic volcanic pipe exists anywhere near the crater centre below the crater sediments.

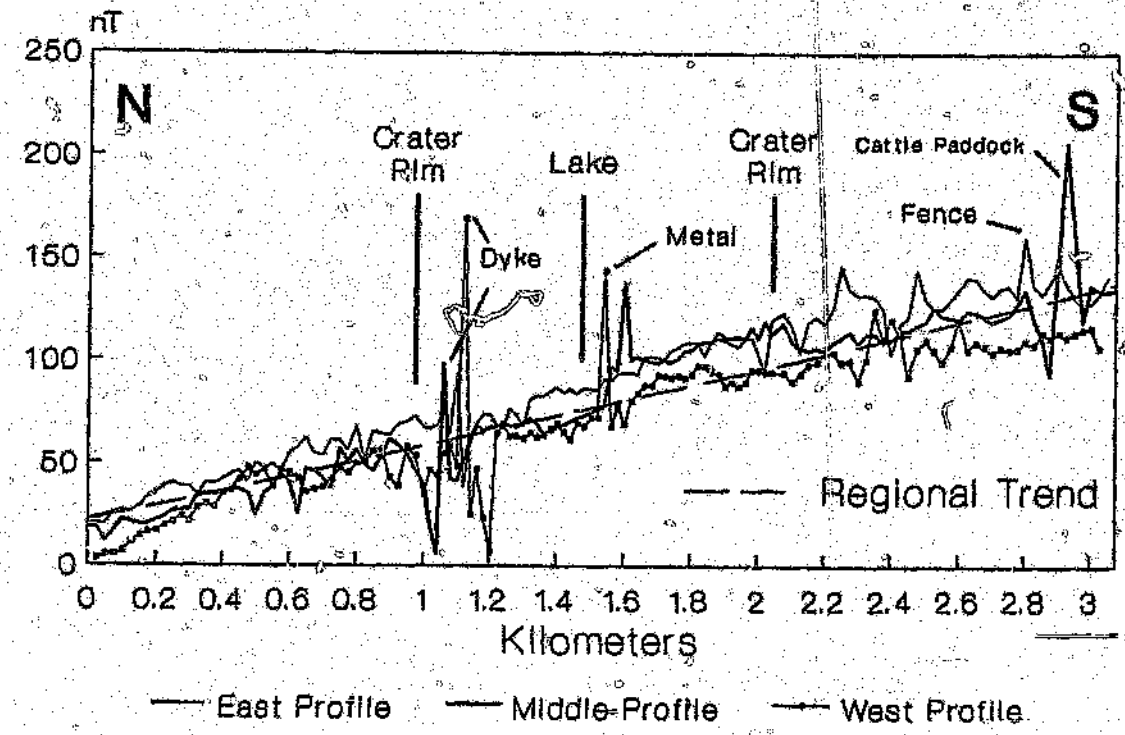

Figure 5.5 North-south profiles of the three magnetic surveys.

It was noted that the regional trend on the 1:50,000 aeromagnetic map (Figure 5.6 shows part of this map) curved slightly northwards in the vicinity of the crater site. Removing the regional component resulted in a slightly off-centre and almost circular residual magnetic signature (Figure 5.7). The total amplitude of this residual anomaly is only 50 nT, which is not very significant with respect to changes in the regional field at this site. This residual anomaly is thought to have been generated either by the cratering event or produced by terrain gradients which would in effect change the flight level resulting in subtle changes in the observed magnetic field.

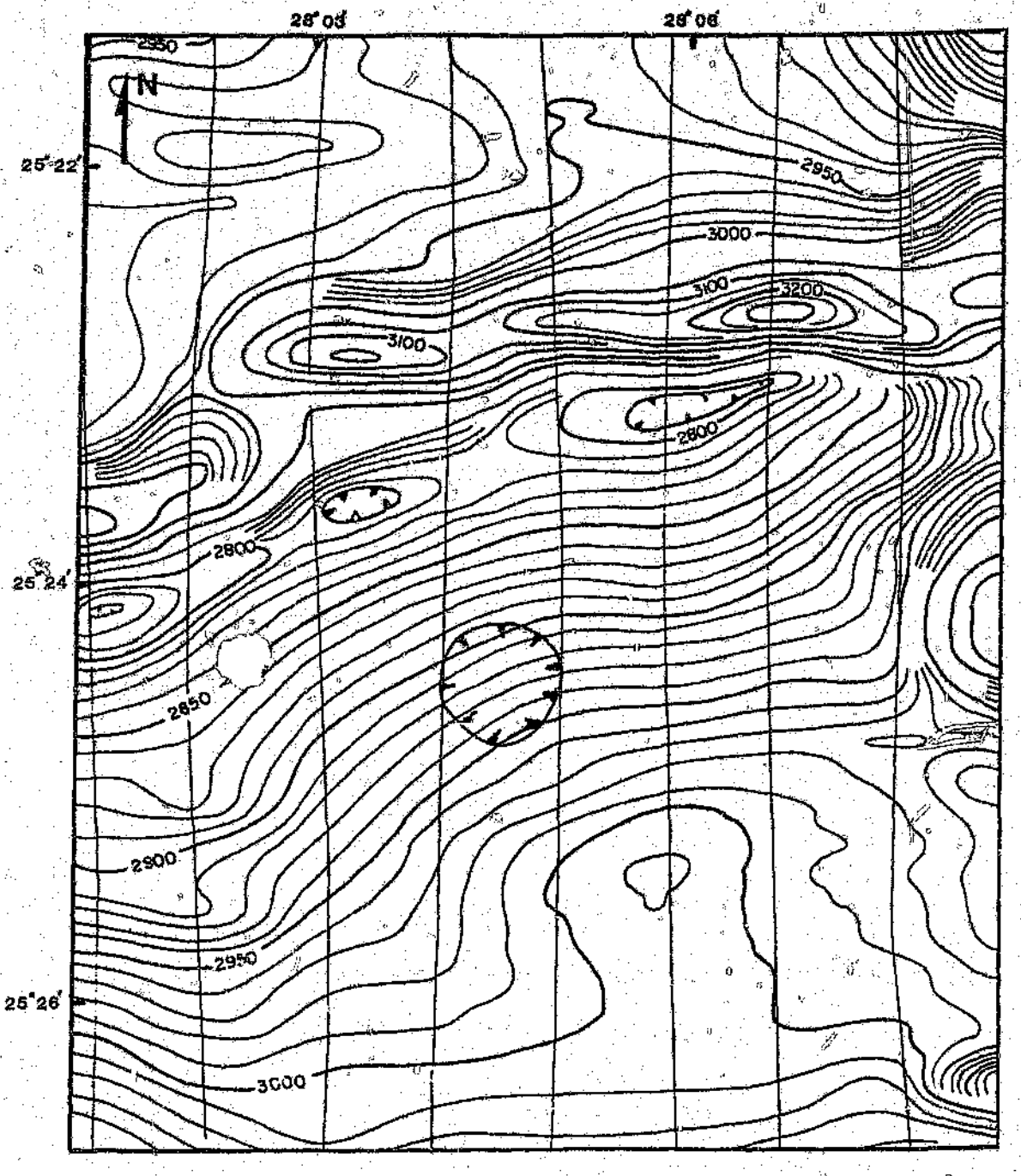

Figure 5.6 Aeromagnetic map of the crater and its environs. The crater is the central near-circular feature (diameter: 1.13 kilometres). Part of map 2528 AC, published by the Geological Survey of South Africa.

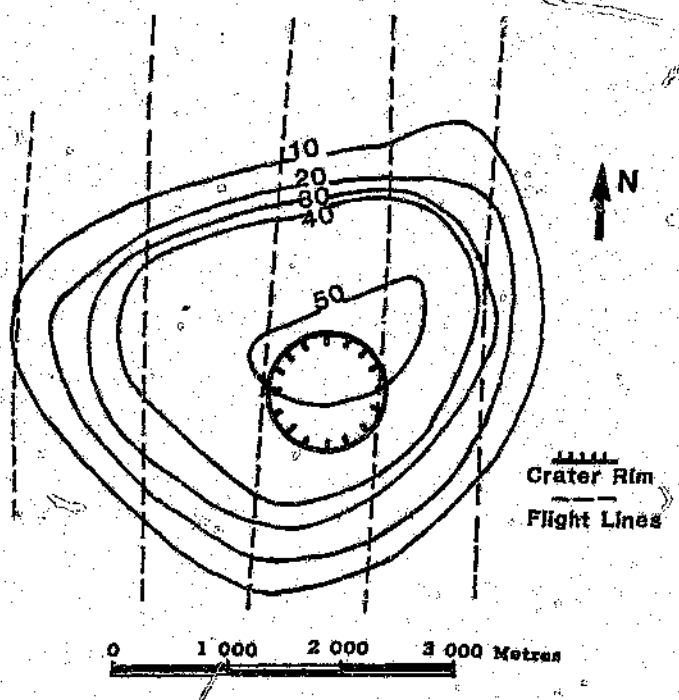

Figure 5.7 Residual magnetic signature after removal of the regional component.

5.2 POSSIBLE SATELLITE CRATER

In the complete absence of any exposure in this mud-covered depression, it was thought that geophysical techniques would perhaps yield information on the interior stratigraphy of this possible "twin" or "satellite" crater to the Pretoria Saltpan crater.

Gravity results

Twenty-four gravity stations were located along two traverses, perpendicular to each other, in north-south and east-west directions across the depression. Each gravity traverse was approximately 500 meters in length. Both the gravity and the corresponding topographic profiles were measured relative to an arbitrary base station located near the centre of the feature. Elevation data were obtained and corrections were applied as discussed above for the experiments on the main crater. Terrain corrections, however, were not necessary at this site, as the maximum elevation gradient was determined at 3 metres only.

A very slight, positive gravity anomaly (Figure 5.8) was observed over the depression. A positive gravity signature is contrary to what would be expected of an impact crater. Trenching near the centre of the feature revealed a calcrete layer at 0.76 metres. The slight gravity high could theoretically be a result of some dense (2.5 g/cm^3) sedimentary fill overlying fractured crater floor and rim. These gravity signatures, however, are thought to represent most probably a regional gravity effect rather than a lithological contrast of some sort. The regional gravity trend observed at the main crater is not observed at this site (most likely due to the fact that these gravity traverses were much shorter than that of the main crater).

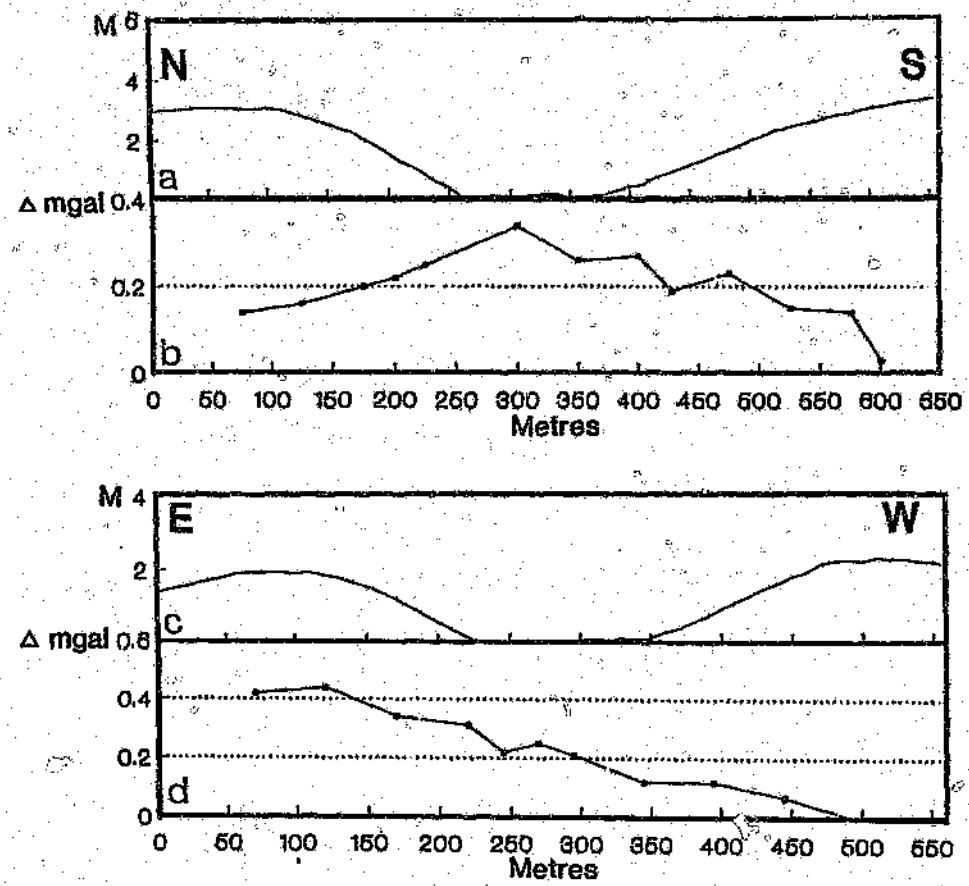

Figure 5.8 **(a)** North-south elevation profile of the possible satellite crater. **(b)** North-south gravity signature of the possible satellite crater. **(c)** East-west elevation profile of the possible satellite crater. **(d)** East-west gravity signature of the possible satellite crater.

Magnetic results

A magnetic survey was conducted along the same north-south and east-west lines used

for the gravity survey. The station spacing was 5 metres. As in the case of the gravity, the magnetic signature (Figure 5.9) only represents the regional magnetic trend. The presence of this trend was confirmed by information obtained from the 1:50,000 aeromagnetic map. The signatures, however, do exclude the possibility of the existence of a magnetic volcanic, for example kimberlite, pipe which may have been thought to exist below this circular feature.

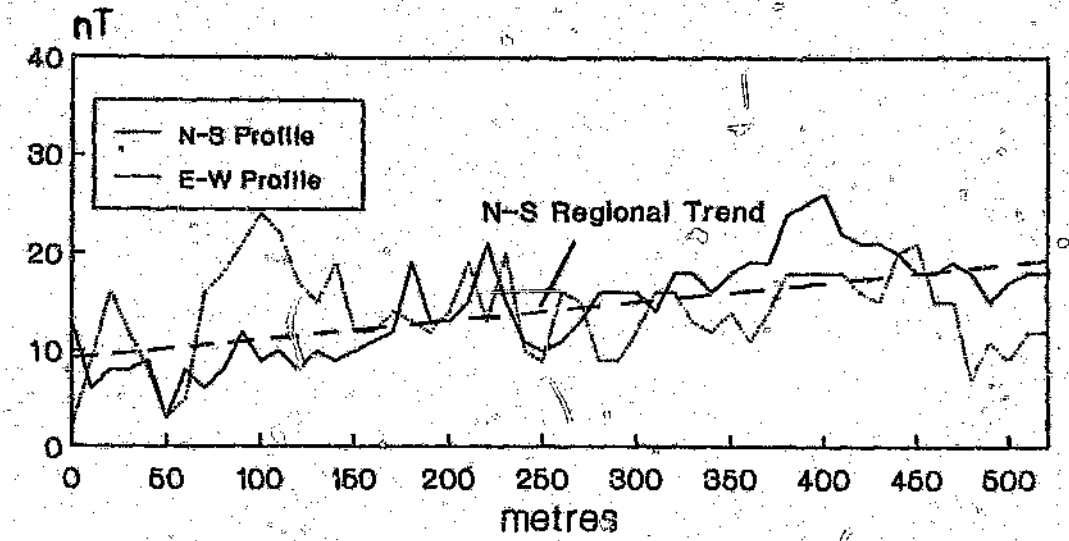

Figure 5.9 Results of the magnetic survey for the possible satellite crater.

Seismic results

Seismic surveys may provide a detailed image of the subsurface structure of impact craters. Changes of seismic velocities will occur as the result of discontinuities, for example, lithological breaks and voids.

Three separate refraction seismic experiments were conducted at a series of sites with increasing distance (28 m, 130 m, 263 m) from the centre of the structure, as indicated in Figure 5.10. The energy for these experiments was obtained using a large mallet.

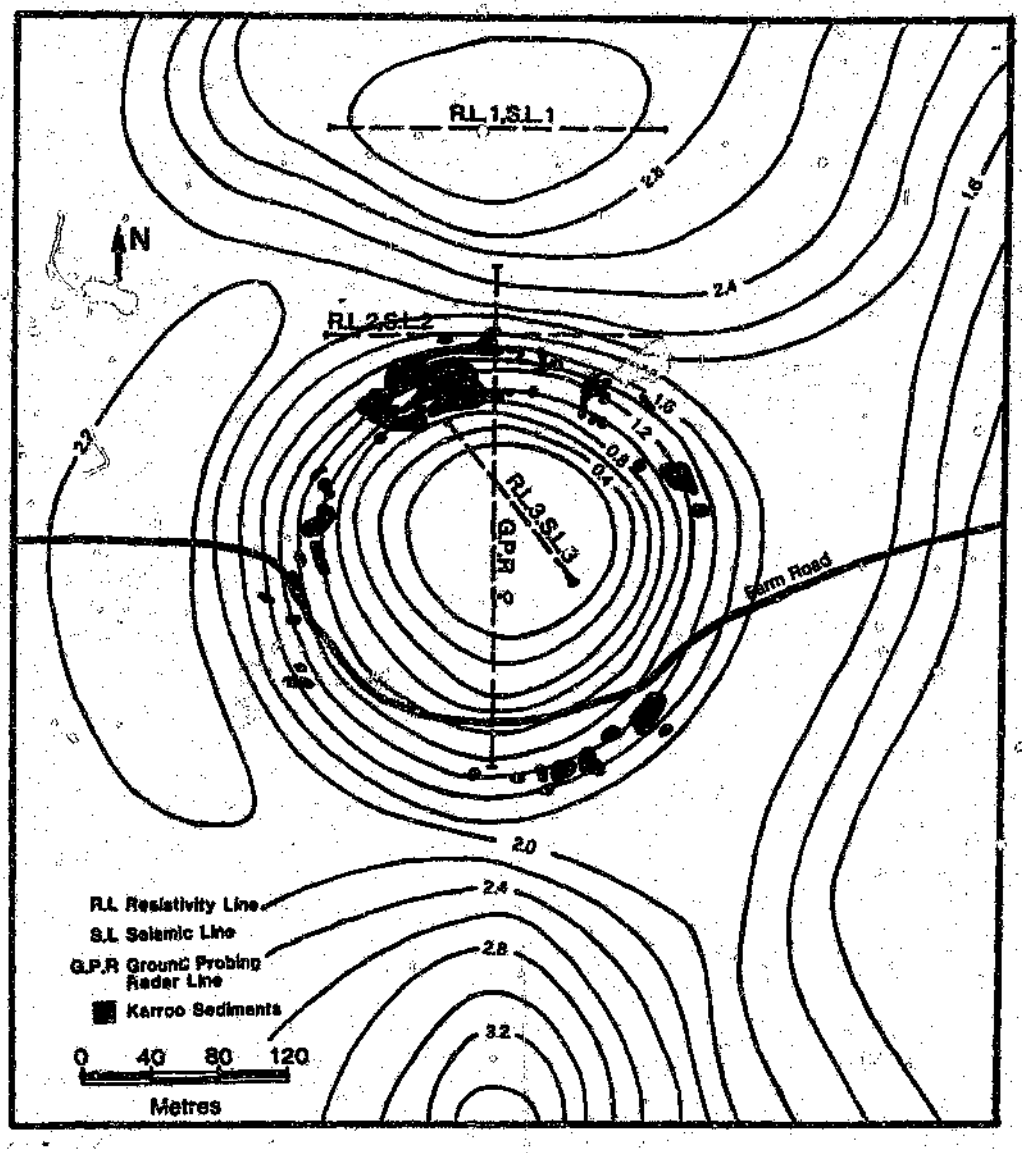

Figure 5.10 Contour map of the possible satellite feature with the position of geophysical survey lines.

A summary of the results is shown in Figure 5.11b, with inferred boundaries for regimes of different velocities between the three survey sites. The lateral distribution of the velocities indicates a central low velocity region, as one would expect for an impact crater. The outer low velocity zone, however, is more pronounced and extends deeper than the inner zone with respect to the high velocity central zone. According to Pilkington and Grieve (1992), the fractured zone at Barringer (Meteor) Crater in

Arizona extends up to one crater diameter beyond the crater rim, as evidenced by velocities that increase radially away from the structure. In the case of this small structure, however, the effects of fracturing cannot be distinguished from jointing which may also lead to density and hence velocity changes. Thus the outer zone may have lower velocities as a result of deep weathering (due to jointing) or as a result of intense fracturing perhaps related to a cratering event.

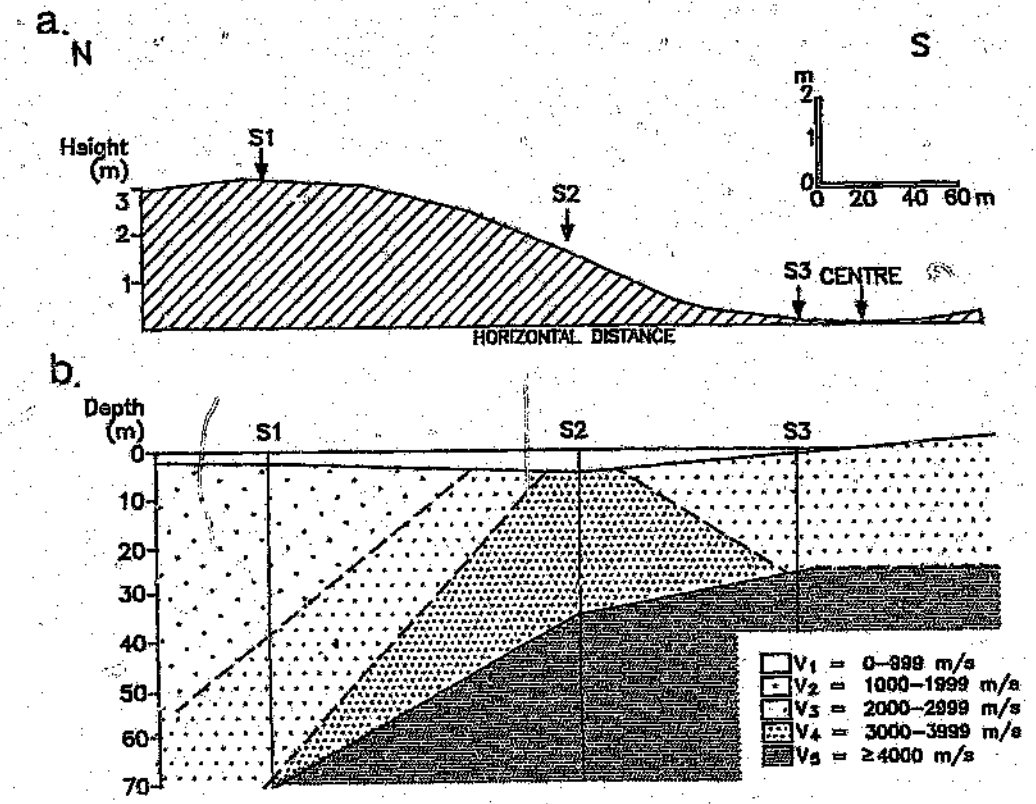

Figure 5.11 (a) Elevation profile of the possible satellite crater from the north to the crater centre (refers to the positions of the various refraction soundings S1-S3). (b) Interpretation of the sub-surface velocities, using the results of the three seismic surveys. Note that the horizontal distances for both diagrams are coincident.

Resistivity results

As the conductivity of rocks is heavily dependent on their water content, brecciation and

fracturing typically found at an impact structure would be expected to cause large changes in the electrical properties of the target lithologies (Pilkington and Grieve, 1992). Three separate resistivity soundings were conducted using a Schlumberger array at the same sites used for the seismic surveys (for the locations of these sites see Figure 5.10). A summary of the results is shown in Figure 5.12, with resistivity contrast boundaries inferred between the survey sites. The low resistivities seen at the centre are typical of crater-fill muds, however the generally low resistivities seen at the outermost survey are most likely the result of either fracturing or jointing. Comparing the resistivity (Figure 5.12) and the seismic (Figure 5.11) results shows some similarities, that is, a high velocity and high resistivity zone at the centre of the structure. These two parameters decrease with increasing distance from the centre.

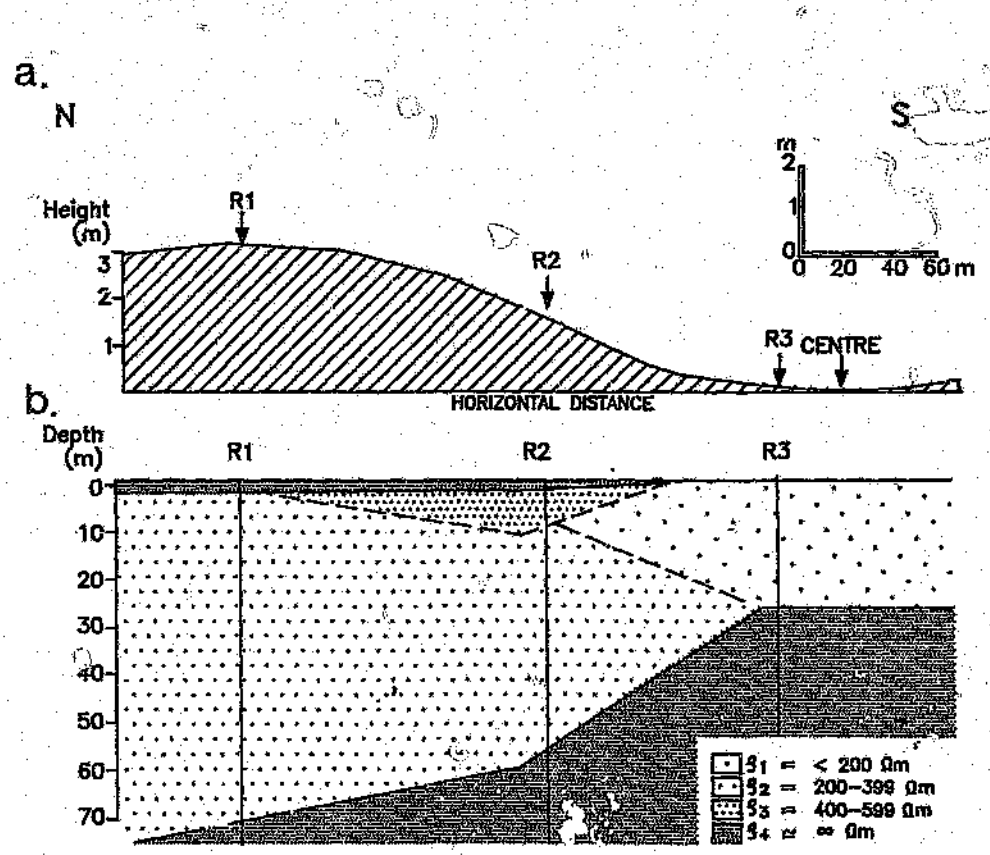

Figure 5.12 (a) Elevation profile of the possible satellite crater from the north to the centre (refers to the positions of the various resistivity soundings). (b) Interpretation of the sub-surface resistivity, using the results of the three resistivity soundings. Note that the horizontal distances for both diagrams are coincident.

Ground-probing radar results

This relatively new geophysical tool (Pilon et al., 1991) operates on the same principles as conventional radar. A short pulse of electromagnetic energy is emitted by a transmitter antenna and then reflected off an electrical boundary. The reflected signal is received by a second antenna. The two-way travel time for this process is measured and the depth to the reflector can be determined, if the propagation velocity of the material is known (Davis and Annan, 1989). This propagation velocity can be determined by conducting a simple, common midpoint reflection survey.

A single north-south ground-probing radar transect, which passed through the centre of the structure was conducted. The position of the 300 metre transect is shown in Figure 5.10. A Pulse EKKO IV ground-probing radar system was deployed, using a frequency of 50 MHz, an antenna separation of 4 meters and a step interval between sampling points of 0.5 metres. These experimental conditions optimized the depth of penetration for the sub-surface properties detected in the common mid-point reflection survey. Under ideal, dry conditions the depth of penetration might have been as much as 100 metres, as was achieved in a similar study at Meteor Crater (Pilon et al., 1991).

The survey conducted across the feature was, on the whole unsuccessful, as a very wet upper conductive mud unit prevented depth penetration of the signal. As the reflections are caused by dielectric contrasts in the subsurface materials (Davis and Annan, 1989), the shallow conductive layer produced the obvious set of prominent horizontal reflections seen in the centre portion of the profile of Figure 5.13. At the edges of the section (the only dry ground in the section) the reflections dip in a direction that indicates an outward dip of the subsurface at an appropriate position of the rim of the feature. Thus, the dipping reflections may represent the outer section of the raised rim at approximately 125 metres from the centre of the structure on the northern and southern portions of the section. The identification of these reflectors is subjective, as confident interpretation requires supplemental ground truth constraints which are not yet available.

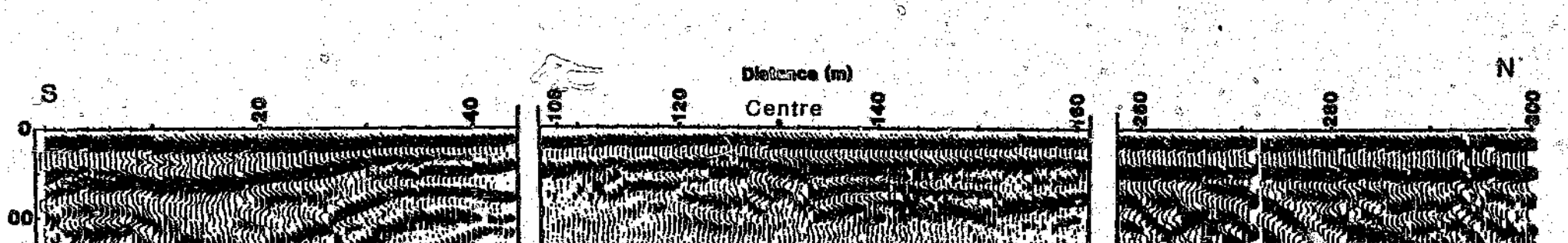

Figure 5.13 Results of the ground-probing radar survey conducted over the possible satellite crater. The crater centre is at approximately 150 metres and 1ns ≈ 0.1 metres.

5.3 DYKE FEATURE NORTH OF THE CRATER

As previously mentioned (Chapter 3), a large east-west trending feature, approximately 3 kilometers to the north of the Pretoria Saltpan crater, was recognised on the 1: 50,000 aeromagnetic map (refer to Figure 5.6). No outcrop of this positive dyke-like anomaly was found. A ground magnetic survey was conducted to obtain a magnetic signature of higher resolution than that of the 1:50,000 aeromagnetic map. The results are shown in Figure 5.14. The 1.7 kilometre magnetic survey was conducted just off the main road (see regional map insert for location) with readings taken at 20 metre intervals. Using the half maximum width method (Henderson and Zeitz, 1948), the width of this feature was calculated to be approximately 300 metres. Using two separate methods, namely, the horizontal slope distance method (Vacquier et al., 1951) and Peters' "P" method (Peters, 1949), two depths below surface of 166 metres and 140 metres, respectively, were obtained. This result explains the lack of outcrop and surface expression of the geophysically recognised feature.

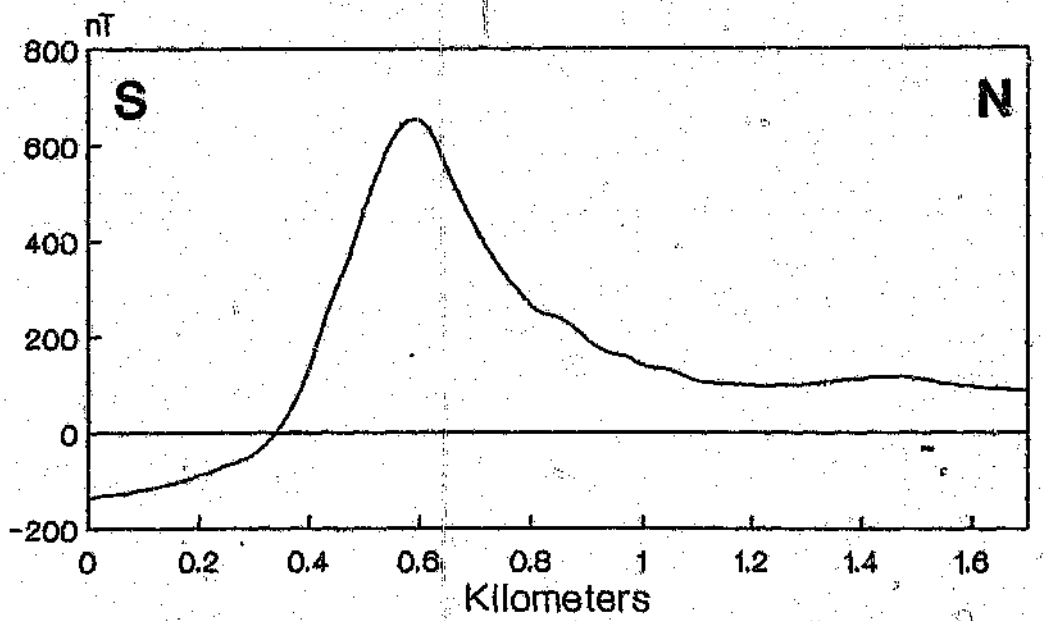

Figure 5.14 Magnetic anomaly obtained over the large magnetic dyke feature to the north of the Pretoria Saltpan crater.

The existence of a large magnetic dyke (the only magnetic rock type encountered in the study area was lamprophyre) to the north of the crater may well aid in the interpretation of the regional magmatic history, evidence of which is found at the crater site (cf. Chapter 4). If this feature is a lamprophyric dyke or some other alkaline intrusive, it may be directly related to those intrusives found on the inner northern crater rim, the presence of which was used in the past as argument against an impact origin.

6.1 BASEMENT ROCKS

All the localities of samples collected within the confines of the crater, which will be referred to in the following chapters, are shown in Figure 6.1. The locations of samples collected from the crater environs, which are discussed in the following chapters and used for comparisons to the crater samples, may be seen on the regional map insert.

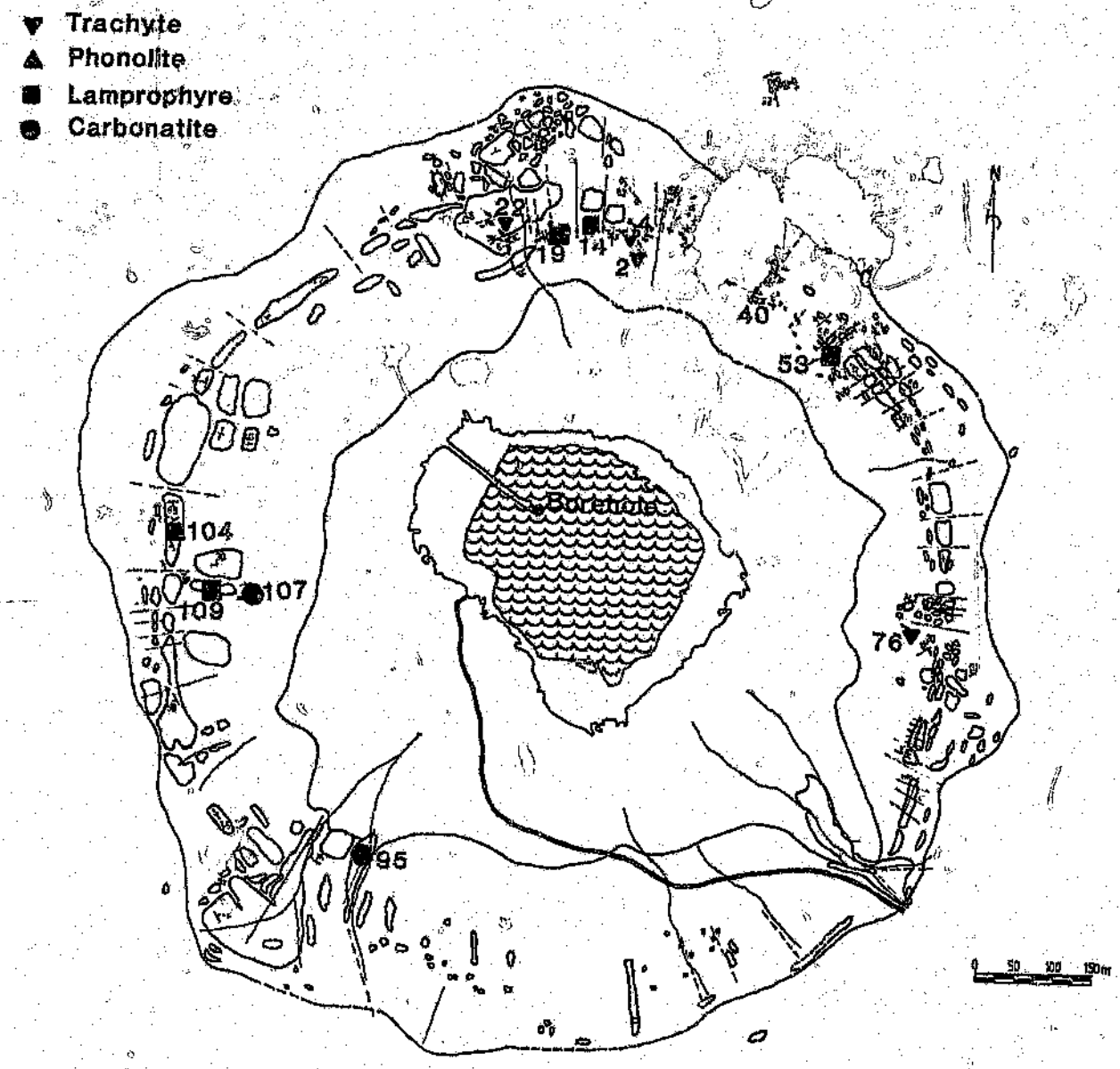

Figure 6.1 Map with sampling sites (and numbers) of samples studied petrographically.

Granite

Granite is the most common rock type in the mapped area and occupies the areas of higher elevation on the inner and outer rims of the crater. In hand specimen the fresh, unaltered granite appears as a coarse-grained, pink rock. The largest grains of pink or light brown feldspar are anhedral and are interlocked with large quartz grains. Minor amounts of hornblende and biotite constitute the mafic mineral content. Hornblende and biotite are rarely found together in the same thin section, or even in several samples from the same sample site. Accessory minerals are magnetite, apatite, zircon and rutile, besides traces of secondary chlorite and calcite (Wagner, 1922). According to Wagner (1922), three feldspar varieties are present, namely orthoclase, albite-oligoclase, and oligoclase, all of which may show some alteration in thin section (see section on altered granite below). Perthitic intergrowth is a common feature between these feldspars. Plagioclase forms small homogeneous grains, often with rectangular or square outlines.

Altered granite

Highly altered granite, common to the study area and particularly abundant in parts of the crater rim, is recognised by its typical white to greyish colour. This colour can be attributed to the products of altered feldspar, primarily kaolinite. The deep weathering evident on parts of the crater rim appears to be the result of meteoric waters permeating into the granite along fractures and joint planes. The near-vertical fractures common to the rim allow easy access for surface precipitation. The granite weathers into large rounded boulders or into smaller angular, crumbly fagments of feldspar and quartz. The muds occupying the bottom of the crater are partly the final products of the decomposed granite (Wagner, 1922). The soft white kaolinite alteration product appears in thin section as a fine-grained, "speckled" mineral with high birefringence.

Micro-granitic pods/xenoliths

These light-grey to pink rocks are comprised of the same components as the granite, i.e., quartz, orthoclase, biotite, hornblende, and some plagioclase. They are medium to fine-grained rocks and have a hypidiomorphic-granular texture. Although they have a texture and composition similar to that of the typical Nebo granites, they are markedly finer-grained. Pods of this fine-grained granite occur as rounded xenoliths (up to 30

centimetres in diameter) in the granite, exhibiting fairly sharp contacts. They are not found at all outcrops in the mapped area, but are quite common along the western crater rim. Figure 6.2 shows a typical thin section impression of such a sample. Other samples of this variety were found to have a lower mafic component and hence a lighter, pinkish colour. These samples are composed predominantly of quartz and orthoclase, with minor magnetite and very little biotite. One such sample was found on the western crater rim as small (30 x 20 centimetre), sub-rounded patches within the Bushveld Granite.

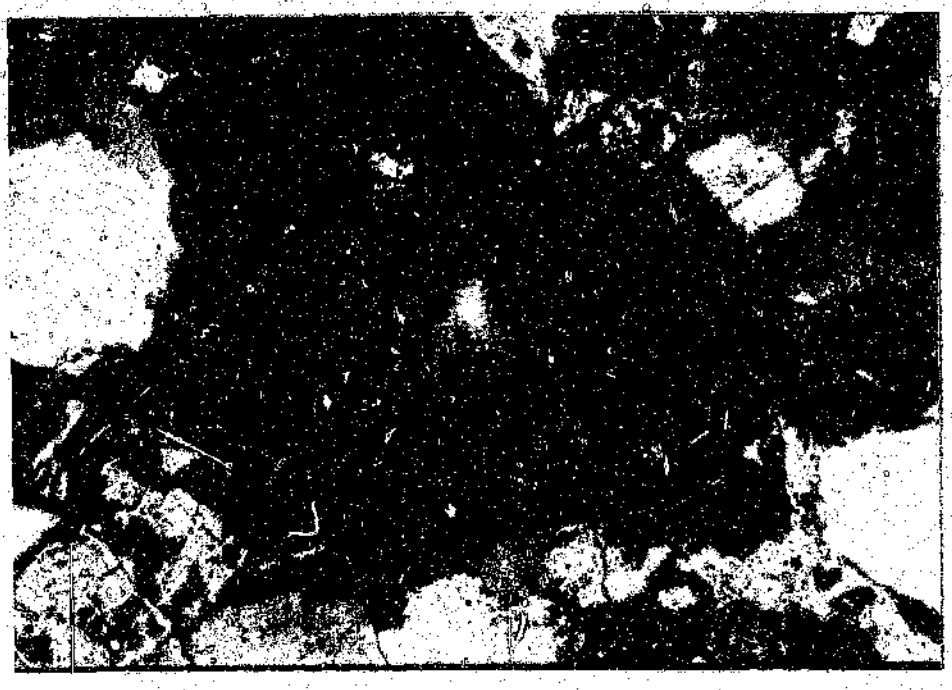

Figure 6.2 Thin section of a micro-granite xenolith. The texture and composition is similar to the Nebo granites, but it is markedly finer-grained (crossed polarized light; field of view: 2.3x3.4 mm).

Albitic gneiss

Xenoliths of this rock type were found approximately 3 kilometres to the south of the crater in a large granite outcrop (refer to Figure 3.8). This rock type is composed of phlogopite, plagioclase, and microperthite (intergrowth of K-rich feldspar in Na-rich feldspar). The plagioclase was identified as pure albite with the aid of X-ray diffraction methods. Tourmaline and quartz are present in minor amounts. This grey rock has a

texture which is medium-grained granoblastic. Crude, discontinuous gneissose bands are typical for this rock type and are generally a few millimeters wide (Figure 6.3). The bands are characterised by an accumulation of well-aligned biotite flakes. Poorly developed schistocity, such as that seen in this sample, is representative of low grade metamorphism. These metamorphosed xenoliths appear to be of a granitic (orthogneiss) rather than a sedimentary (paragneiss) origin, as they appear to have a primary igneous texture.

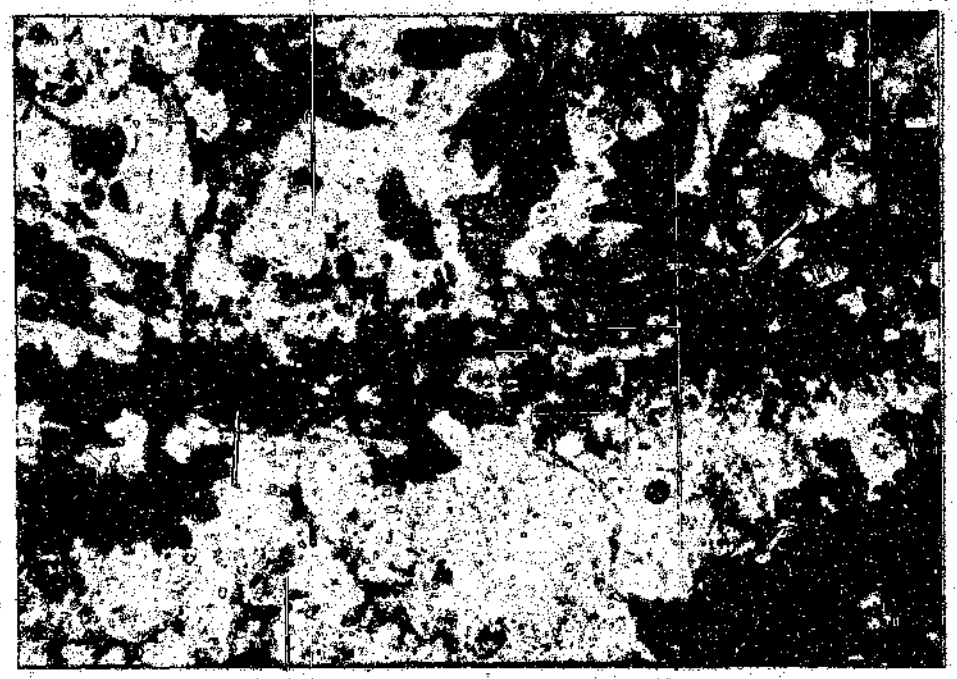

Figure 6.3 A gneissose band in an albitic gneiss xenolith (plain polarized light; field of view: 2.3x3,4 mm).

6.2 INTRUSIVES

6.2.1 TRACHYTE

These greenish-brown to pink rocks typically consist of sanidine, microcline, plagioclase, nepheline, biotite, and aegerine phenocrysts set in a fine-grained matrix of these minerals. Variations in texture, composition and combinations of minerals constituting

the phenocrysts will be discussed using individual samples as examples. The groundmass exhibits a typical trachytic texture: instead of showing a single universal alignment direction for the phenocrysts, there are numerous domains, each with its own preferred direction or pattern of feldspar laths. Quartz (occasionally a secondary mineral), calcite (secondary), and zircon constitute minor minerals in the matrix. The overall texture is markedly porphyritic due to the presence of subhedral phenocrysts set in the groundmass of small elongate feldspar microlites.

Sample 2

In this sample (Figure 6.4), found on the northern crater rim, the groundmass-forming feldspar laths occur as spherulites. These radial patterns represent devitrification of the original glassy groundmass, probably around small microcrysts. The phenocrysts of subhedral nepheline and euhedral aegerine are intensely altered and often replaced with a secondary carbonate material.

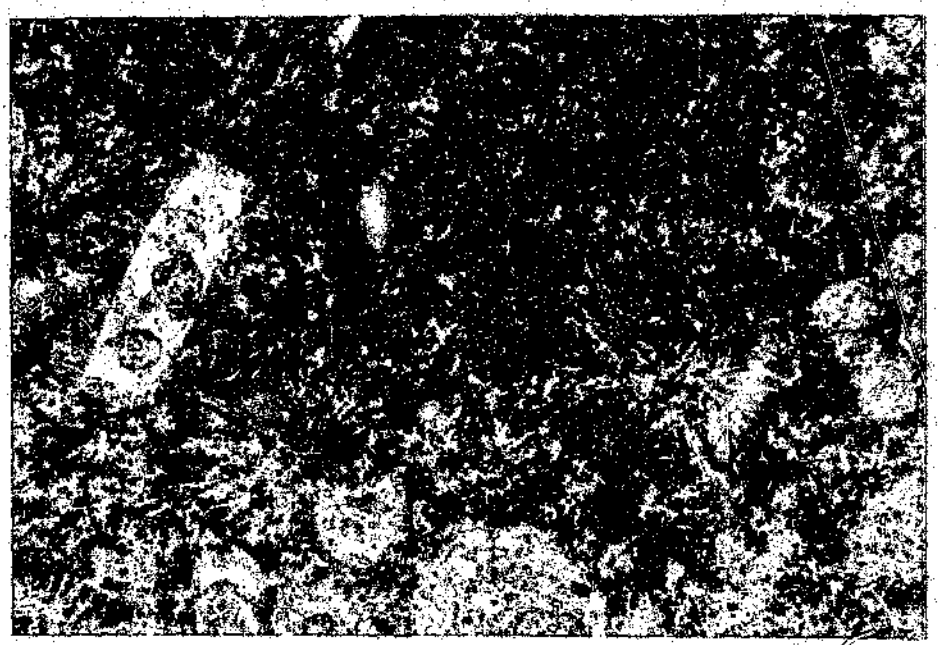

Figure 6.4 Thin section of a trachyte in which the groundmass exhibits a radial devitrification pattern (Plain polarized light; field of view: 1.5x2.2 mm).

Sample 76

This fairly altered sample exhibits a groundmass which has been replaced by late-stage iron oxides, primarily hematite or goethite, recognised by the typical red staining. Calcite is present as a secondary mineral, where remobilization processes have precipitated fine-grained calcite in voids, with recrystallized plagioclase at times forming the rim of these cavities.

Sample 22

This sample, which is petrographically recognised as a trachyte specimen, only by its phenocrysts and devitrified spherulitic matrix (which was later confirmed by its chemical composition, cf. Chapter 7), has a groundmass predominantly composed of kaolinite. Locally the original radial texture of the groundmass is still preserved in the altered matrix. Although it is significantly kaolinized, some fresh biotite phenocrysts may be found (Figure 6.5). Biotite does not occur as phenocrysts in all trachyte samples, but where it is present, it represents the most common phenocryst type. Secondary hematite or goethite has precipitated along fractures and in voids, and secondary sphene, which now is altered to leucoxene, can be found as a by-product of the alteration of biotite to chlorite. Minor quartz may be found and is assumed to be of secondary origin, as altered phenocrysts of nepheline are present, too.

Sample 21-I(2)

This sample was collected approximately 9 kilometres to the southwest of the crater, where it intruded into a well-exposed granite outcrop (see regional map insert for location). Many opaque, Fe-rich areas (Figure 6.6), and the fine-grained matrix are indicative of a high degree of alteration and an original, fine-grained texture of this rock. The groundmass is believed to consist mainly of altered fine-grained potassic feldspar and a clinopyroxene. In hand specimen this altered rock is a yellow, earthy, easily disintegrating mass. This rock was also identified as trachyte by chemical analysis. The main alteration product in this specimen is montmorillonite.

Figure 6.5 Altered trachyte (Sample 22) with relatively fresh biotite phenocrysts (cross-polarized light; field of view: 2.3x3.4 mm).

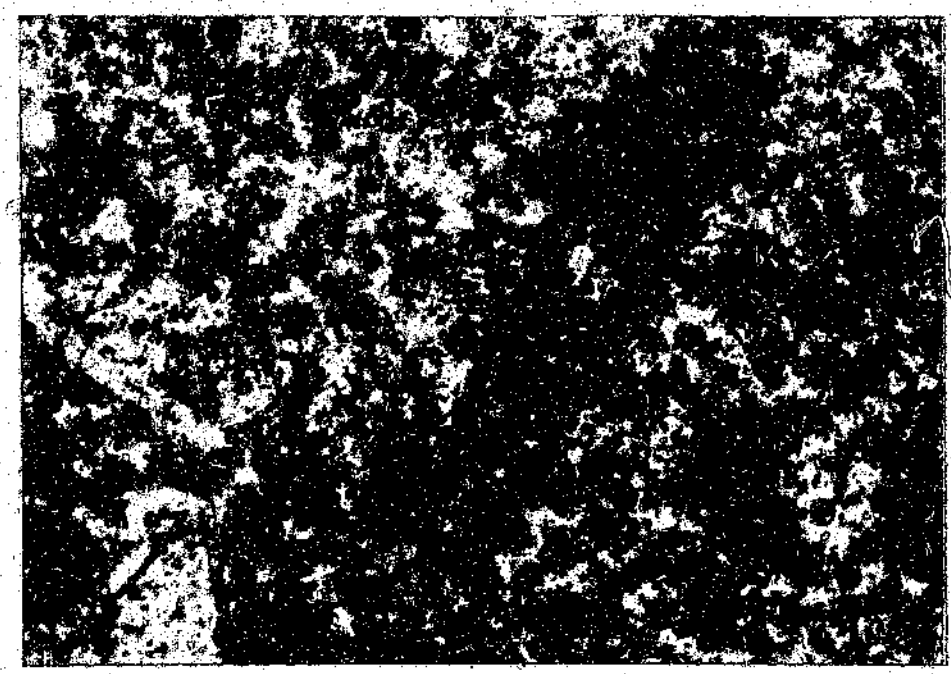

Figure 6.6 Highly altered trachyte sample (plain polarized light; field of view: 1.2x1.7 mm).

Sample 4 (granite-trachyte contact specimen)

The only trachyte-granite contacts found are sharp, with some granite brecciation and assimilation. Figure 6.7 shows such a contact of a crater rim trachyte. Relics of what appears to be biotite in the trachyte show alignment parallel to the trachyte-granite contact.The trachyte in this sample is extremely altered and replaced by iron-oxides, but still shows the contact relationships well.

Figure 6.7 Granite-trachyte contact. The granite, which has been brecciated, is the lighter material on the right-hand side of the photomicrograph (cross polarized light; field of view: 2.7x3.4 mm).

6.2.2 PHONOLITE

This fine-grained rock (Sample 40) consists chiefly of potassic feldspar (microcline), and albitic plagioclase laths. Texturally this specimen is similar to trachyte, and is only

differentiated from the trachytes by its chemical composition (Chapter 7). Only this one sample, taken from an outcrop on the northeastern rim, was found on the inner slopes of the crater rim. The groundmass consists of numerous domains, each having its own pattern of feldspar laths. Spherulitic aggregates are abundant (Figure 6.8). This dark, pinkish rock with light green and darker (brown to black) domains shows a typical porphyritic texture with anhedral phenocrysts of nepheline, aegirine, and biotite. The darker pink zones within the groundmass probably represent the original extremely fine-grained devitrified or glassy material. Alteration and replacement of the phenocrysts with an opaque mineral (unidentified) is quite common.

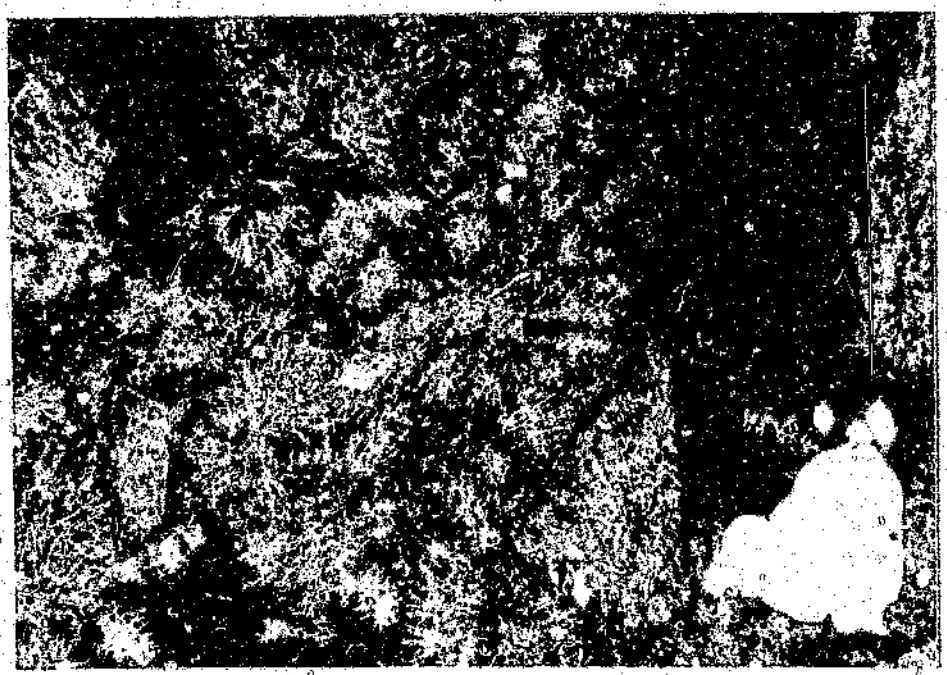

Figure 6.8 Thin section area of phonolite (Sample 40). The green phenocrysts are aegirine, and the white phenocryst (bottom right) is nepheline set in a spherulitic, predominantly feldspar matrix (plain polarized light; field of view: 2.3x3.4 mm).

6.2.3 LAMPROPHYRE

The lamprophyre of the study area is characterized by euhedral ferro-magnesian phenocrysts, usually diopside, set in a fine-grained groundmass containing the same minerals with feldspar or feldspathoids (nepheline). The most common mineral in these dark green to black (melanocratic) rocks is diopside, constituting more than 50 percent of the rock. Figure 6.9 represents a typical lamprophyre from the crater rim. It shows clinopyroxene which forms euhedral, fine-grained, acicular (needle-like) phenocrysts (which may be zoned), together with subhedral titanomagnetite and biotite phenocrysts. Although the clinopyroxene is generally fine-grained, some phenocrysts may reach 2 to 3 millimetres in length.

Figure 6.9 Typical lamprophyre (Sample 53) from the crater rim (cross polarized light; field of view: 1.8x2.7 mm).

Orthoclase is present in minor amounts and occurs only in the aphanitic or micro-

granular groundmass. Other minerals, which may be found, include titanoaugite (identified by its purple pleochroism; Heinrich, 1965), carbonate material (see Figure 6.10), and sphene. Magnetite, the reason for the high susceptibility of these rocks, is abundant in the groundmass and may be found incorporated into the pyroxene phenocrysts. Magnetite appears primary in some cases, but is also found as a secondary mineral. Some ocelli or segregations of carbonate material are microscopically apparent. They may enclose some magnetite or pyroxene, rarely have well-defined margins and usually grade into their host (Figure 6.11). The sample shown in this figure (Sample 41) consists almost entirely of carbonate and chlorite.

Not all the lamprophyre samples collected display all these features, and, as in the case of the trachytes, several varieties were noted from one sample and locality to the next. The following examples show some of the common variations seen in this rock type.

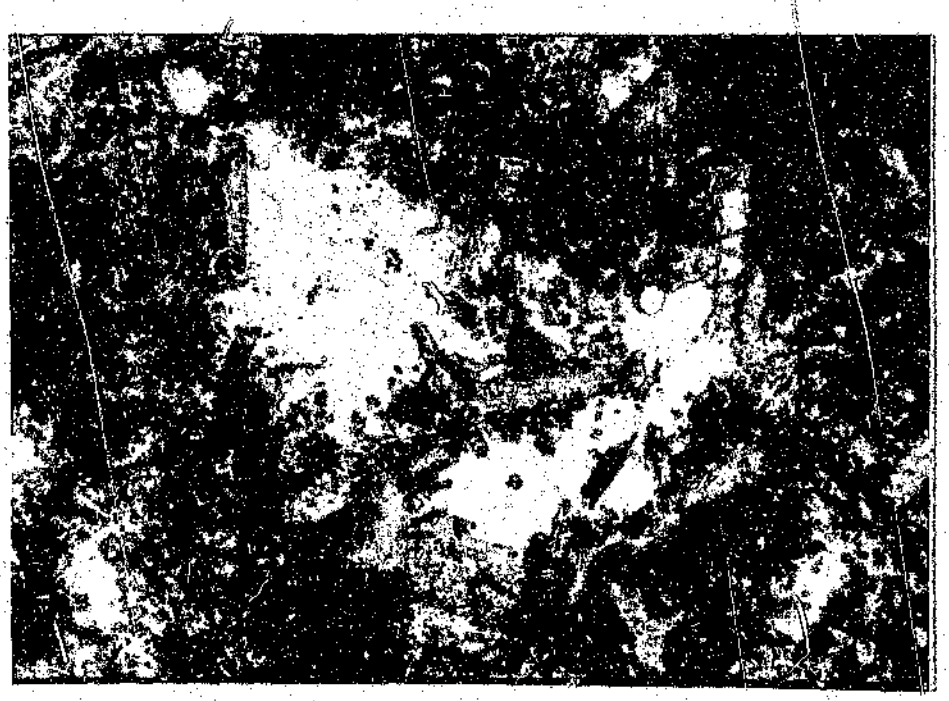

Figure 6.10 Secondary carbonate (white mineral) in a groundmass containing abundant magnetite, in a lamprophyre (Sample 53) (plain polarized light; field of view: 1.5x2.2 mm).

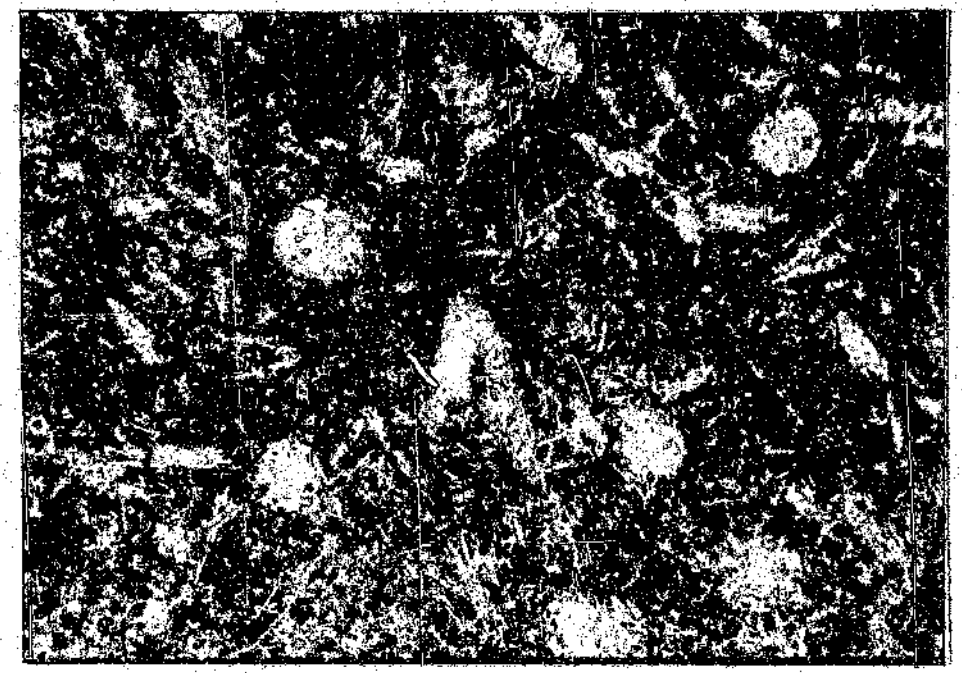

Figure 6.11 Carbonate ocelli in a highly altered lamprophyre (Sample 41) (plain polarized light; field of view: 3.4x2.3 mm).

Sample 19

This crater rim sample exhibits abundant subhedral biotite associated with magnetite. Such an amount of biotite (Figure 6.12) is not seen in all lamprophyre samples. Normally this mineral is part of the finer-grained groundmass. Plagioclase is more common than orthoclase in the groundmass, and secondary calcite forms approximately 20 percent of this sample, which is a higher percentage than that seen in other lamprophyre samples. The green mineral is chlorite, as alteration product of biotite.

Sample 109

This crater rim sample (Figure 6.13) exhibits the typical glomeroporphyritic texture (a porphyritic texture in which groups of crystals are scattered throughout a finer-grained groundmass) seen in most of the lamprophyres. In this case the clinopyroxene crystals grow in coarse, radiating clusters. Fine-grained subhedral magnetite is predominantly found in the matrix, but occasionally is overgrown by clinopyroxene.

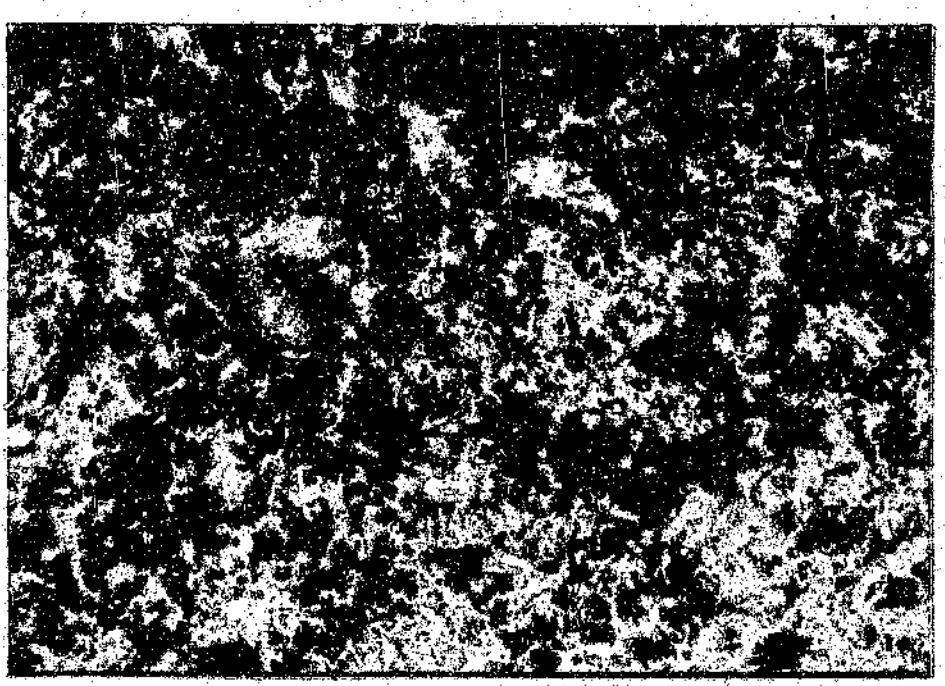

Figure 6.12 Lamprophyre section (Sample 19) showing the association of biotite and magnetite (plain polarized light; field of view: 1.5x2.2 mm).

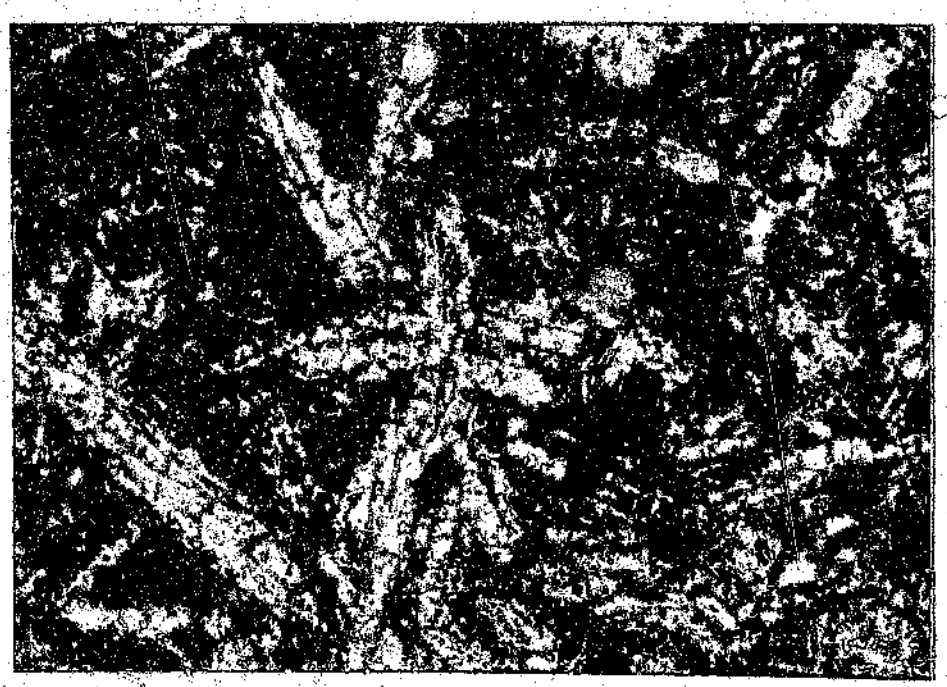

Figure 6.13 Typical glomeroporphyritic texture of lamprophyre sample 109 (plain polarized light; field of view: 1.5x2.2 mm).

Sample 23-D

This sample was collected from a well preserved vertical dyke cross-cutting a granite outcrop approximately 5 kilometres to the southeast of the cater (see regional map insert for location). The diopsidic pyroxene forms phenocrysts, that are smaller than in other samples. Calcite ocelli (segregations) are abundant in the very fine-grained matrix (Figure 6.14). It should be noted that this sample, collected some distance from the Saltpan crater, has a close resemblance to some of the crater rim samples (e.g., Sample 41, cf. Figure 6.11).

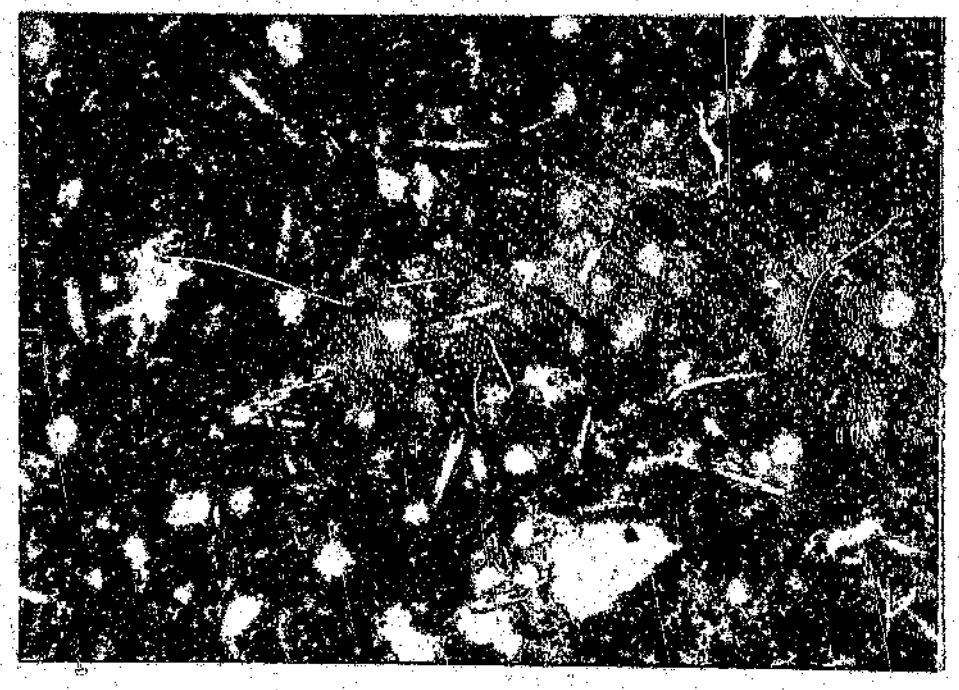

Figure 6.14 Fine-grained lamprophyre (Sample 23-D) from the crater environs (plain polarized light; field of view: 2.3x3.4 mm).

Sample 21-I(3)

This sample was collected some 9 kilometres to the southwest of the crater. It is very friable, as it is more intensely altered than other samples. It was identified as a lamprophyre by its mineralogy and texture, which are similar to those in the other lamprophyre samples (e.g., Sample 53, cf. Figure 6.9). No calcite was found in this sample. The chemical composition also indicates a depletion in CaO. Figure 6.15 shows

an altered clinopyroxene phenocryst which is characteristically - for weathered samples decorated by magnetite. The magnetite in this sample appears to be an alteration product after clinopyroxene. The groundmass consists of fine-grained orthoclase, microcline, plagioclase, magnetite, and clinopyroxene.

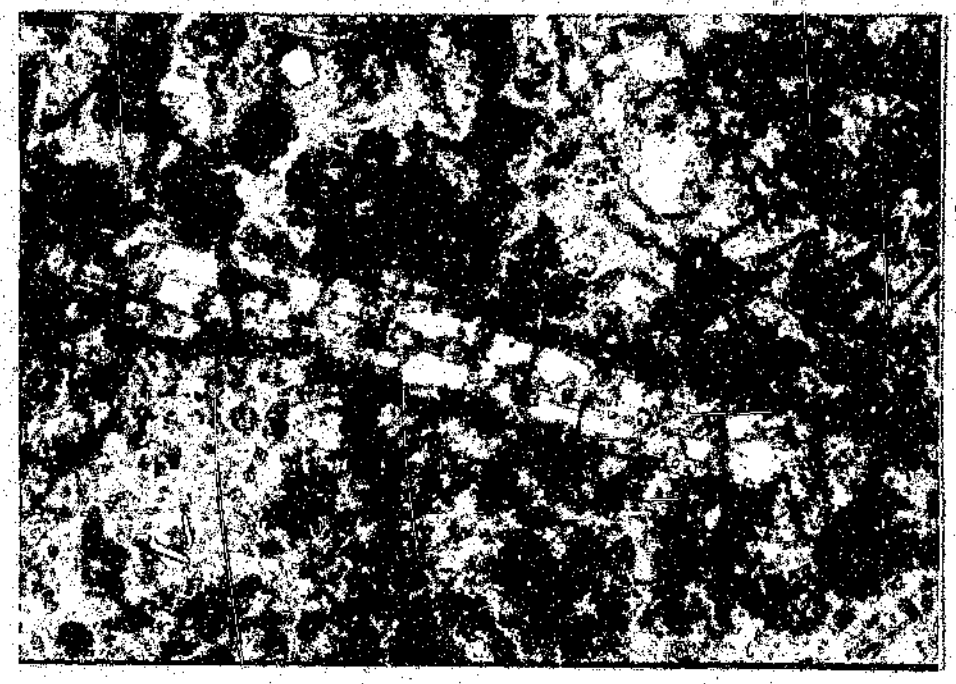

Figure 6.15 Altered lamprophyre (Sample 21-I(3)) from the crater environs with magnetite surrounding a corroded pyroxene phenocryst (plain polarized light; field of view: 1.5x2.2 mm).

Sample 21-E

This sample (Figure 6.16) was collected close to the locality of the previous sample, about 9 kilometres to the southwest of the crater, and is used in comparison to the crater rim samples. The similarity in texture and mineralogy between this sample and some of the rim samples is particularly striking (compare Figures 6.9 and 6.13). Clinopyroxene phenocrysts and groundmass grains are acicular.

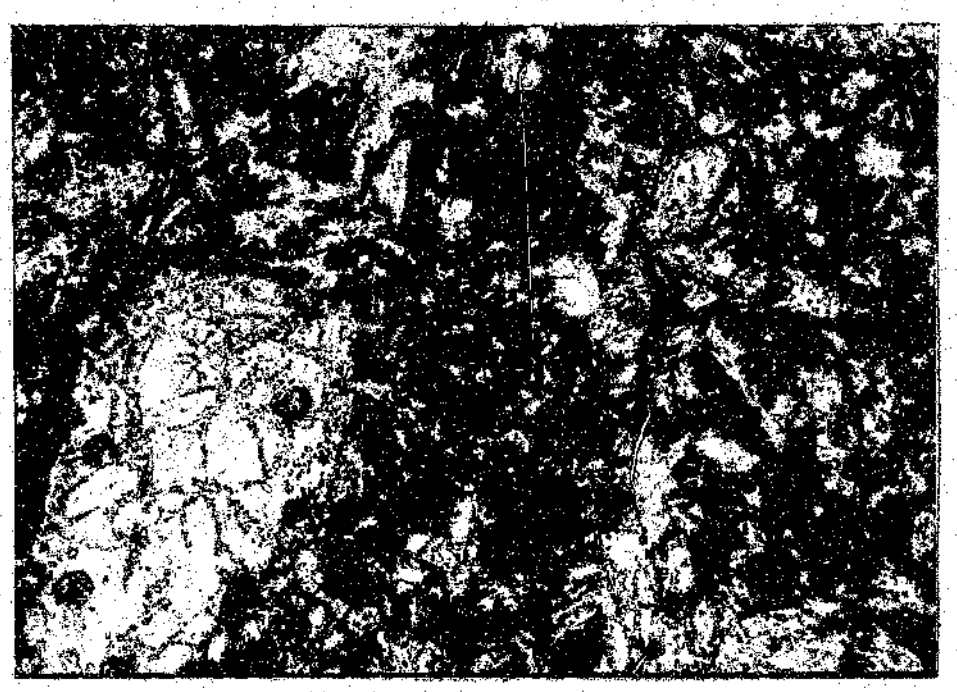

Figure 6.16 Lamprophyre (Sample 21-E) from the crater environs showing a similar texture and mineralogy to the crater rim samples, e.g., Sample 53, Figure 6.9. The large white phenocrysts are clinopyroxene. Other minerals present include magnetite (black mineral), biotite (brown mineral) and feldspar in the groundmass (plain polarized light; field of view: 1.5x2.2 mm).

6.2.4 CARBONATITE

The definition of a true carbonatite is based on both the composition and genesis. Carbonatite must have a granular texture consisting of primary carbonate minerals (calcite, dolomite or other rock forming carbonates) that have to comprise at least 50 volume-percent of the rock, and it must exhibit the primary features of a volcanic or intrusive rock (Verwoerd, 1967).

The light grey to pinkish, fine-grained carbonate rocks found at the crater are composed of approximately 80 volume-percent carbonate material which includes calcite, dolomite and ankerite in descending order of abundance. The carbonate material does not exhibit

an allotriomorphic texture (anhedral igneous texture). Instead, the matrix consists of an altered, fine-grained mosaic of carbonate material with disseminated subidiomorphic titanomagnetite and accessory pyrite, chlorite, apatite, muscovite, and quartz. Chlorite forms the most abundant phenocryst type believed to be an alteration product of primary mica. This texture is clearly represented in Figure 6.17. Fragments or xenoliths of a dark green chlorite schist are scattered throughout the carbonate matrix. Figure 6.17 shows some of these chlorite schist clasts, as well as the finer chlorite in the groundmass. The chlorite schist xenoliths form positive features on the weathered rock surface. Their origin is still uncertain, but presumably they represent a pre-Bushveld lithology.

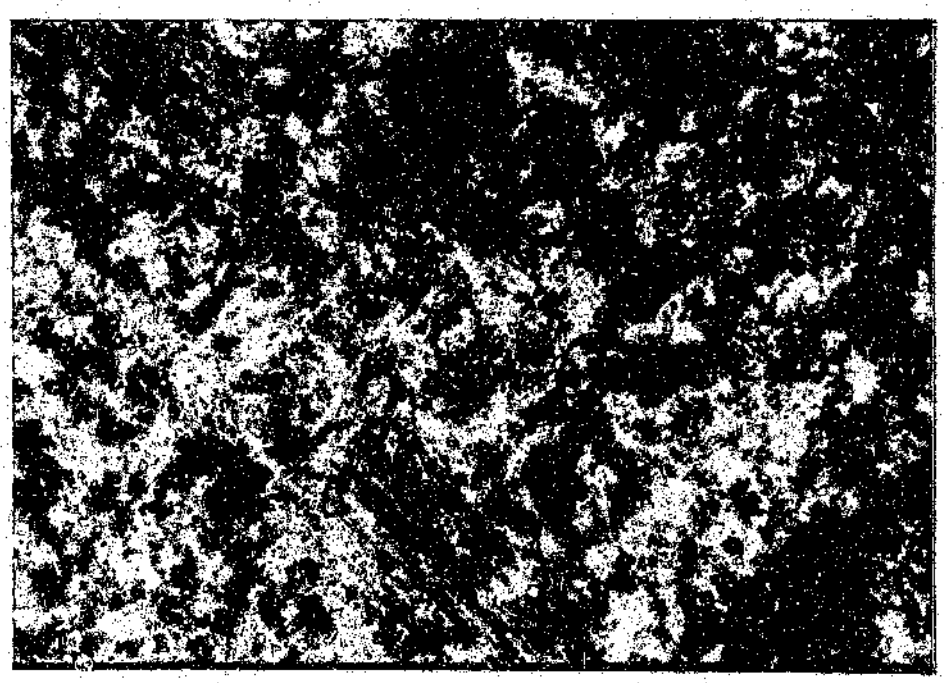

Figure 6.17 Thin section of a carbonatite (Sample 95) which shows the mosaic texture and the chlorite schist fragments (cross polarized light; field of view: 2.3x3.4 mm).

At one locality on the western rim a carbonatite dyke (approximately 20 centimetres wide, Figure 4.4) contains subangular Bushveld granite xenoliths up to a few centimetres in diameter. These granitic xenoliths were probably incorporated into the dyke from the granitic wall rock by a stoping process. Some carbonatite specimens were found to

contain secondary oxide stringers which were identified as specularite. Remobilized, secondary calcite forms veinlets which cross-cut the primary texture. Figure 6.18 shows secondary silica which has formed in voids in Sample 95. This mineral is probably tridymite. Tridymite is an orthorhombic mineral (SiO_2) which usually contains variable amounts of Al, K and Ca (Heinrich, 1965). The crystals are tabular and euhedral, and form elongate lath-like cross sections. The photomicrograph (Figure 6.18) shows the typical parallel extinction and fan-shaped habit of tridymite. According to Heinrich (1965), these lath-like crystals can exhibit wedge-shaped twins as shown in Figure 6.18. Only two occurrences of this carbonatite were encountered within the crater rim (see crater map insert).

Figure 6.18 Secondary tridymite within cavities in carbonatite sample 95 (cross polarized light; field of view: 2.3x3.4 mm).

6.2.5 THE PIENAARS RIVER ALKALINE COMPLEX

Various samples from the Pienaars River Alkaline Complex (Figure 3.2), in particular from the Roodeplaat Complex, were collected to compare with the alkaline rocks from

the crater and the immediate crater environs. The available Roodeplaat rock suite is quite extensive, consisting of 11 different samples, many of which are different rock types. Some of the rock types are mineralogically similar to those found in the mapped area (the crater and its environs). Figure 6.19, a simple geological map of the Roodeplaat Complex, shows the localities where all the studied samples were collected.

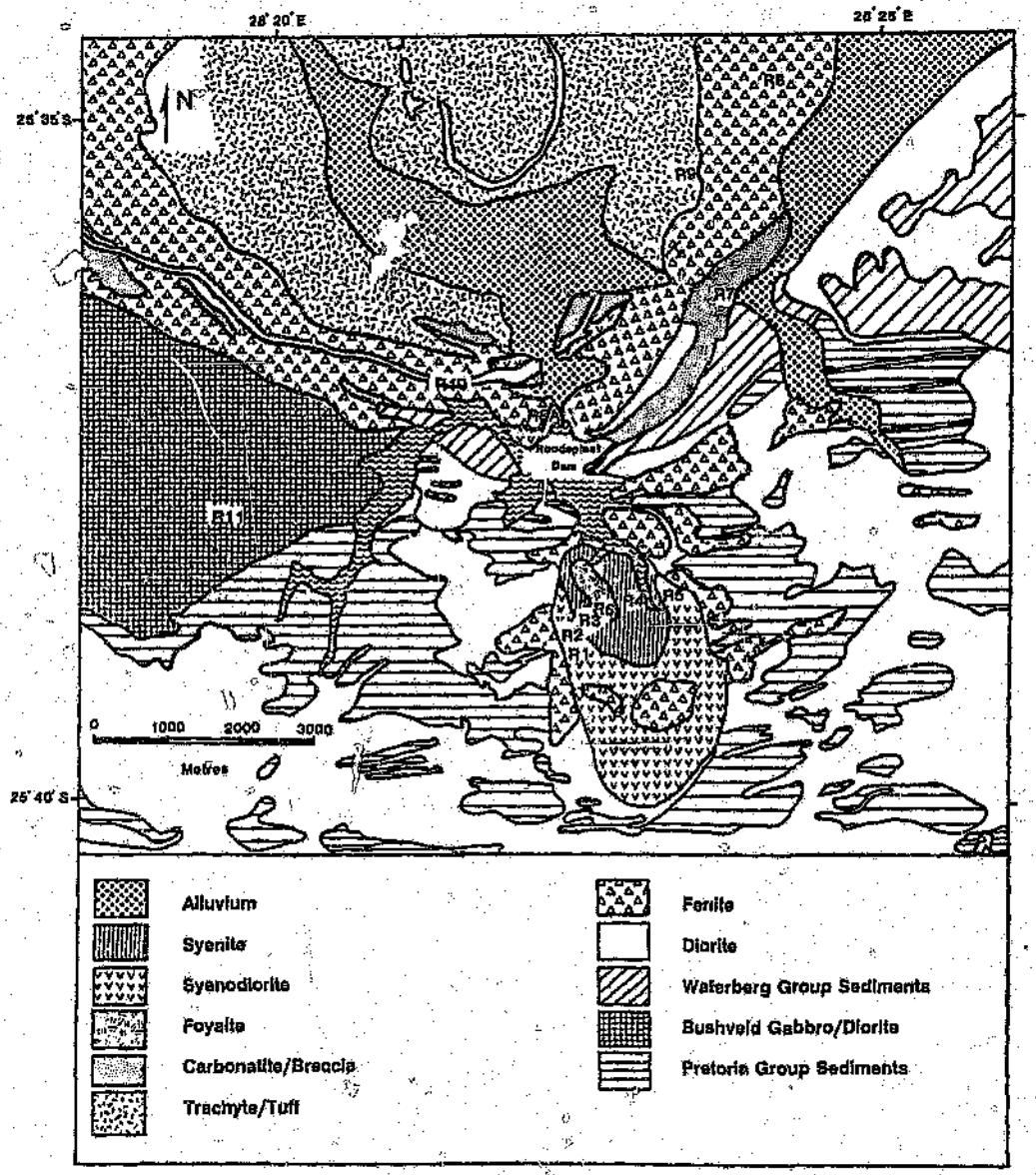

Figure 6.19 Simplified geological map of the Roodeplaat Complex (part of Geological Survey map 2528 CB) showing sampling sites for the studied samples (R1-R11).

Roodeplaat diorite dyke (Sample R1)

This medium-grained rock intrudes the syenodiorite and exhibits a granular texture. Plagioclase is the major phase and forms euhedral crystals with remnant twinning (Figure 6.20). The average plagioclase composition is approximately An_{40} determined by CIPW normative calculations using major element XRF results. The subhedral to anhedral green amphibole forms prismatic, strongly pleochroic crystals which are mostly formed interstitially between plagioclase. Some quartz and K-feldspar is present. The plagioclase is fairly clouded as the result of alteration (sericitisation). Twinning occurs in a few actinolite crystals. An opaque phase, identified as magnetite, forms a minor constituent.

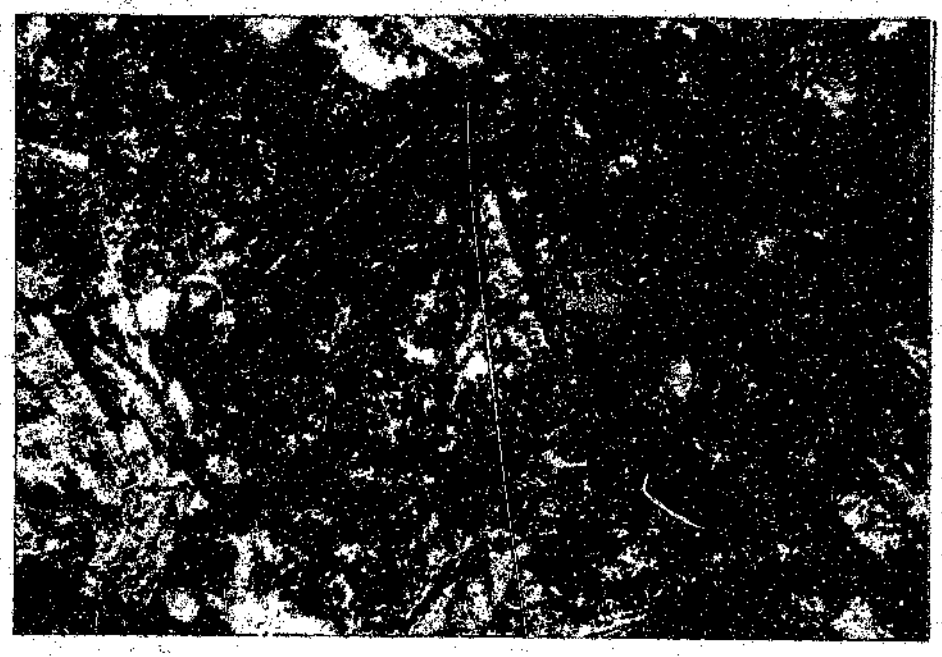

Figure 6.20 Thin section of a Roodeplaat diorite dyke, Sample R1 (cross polarized light; field of view: 2.3x3.4 mm).

Roodeplaat granodiorite (Sample R2)

This medium-grained rock consists essentially of quartz and plagioclase, which is accompanied by minor amounts of alkali feldspar and some hornblende (actinolite) (Figure 6.21) and quartz. An opaque phase, probably magnetite, is also present. The

feldspar may be subhedral to euhedral, forming acicular crystals, whereas the hornblende is anhedral. The often clouded (due to alteration) plagioclase exhibits remnant twinning which aids in distinguishing it from the potassic feldspar. Chlorite is present as an alteration product after hornblende.

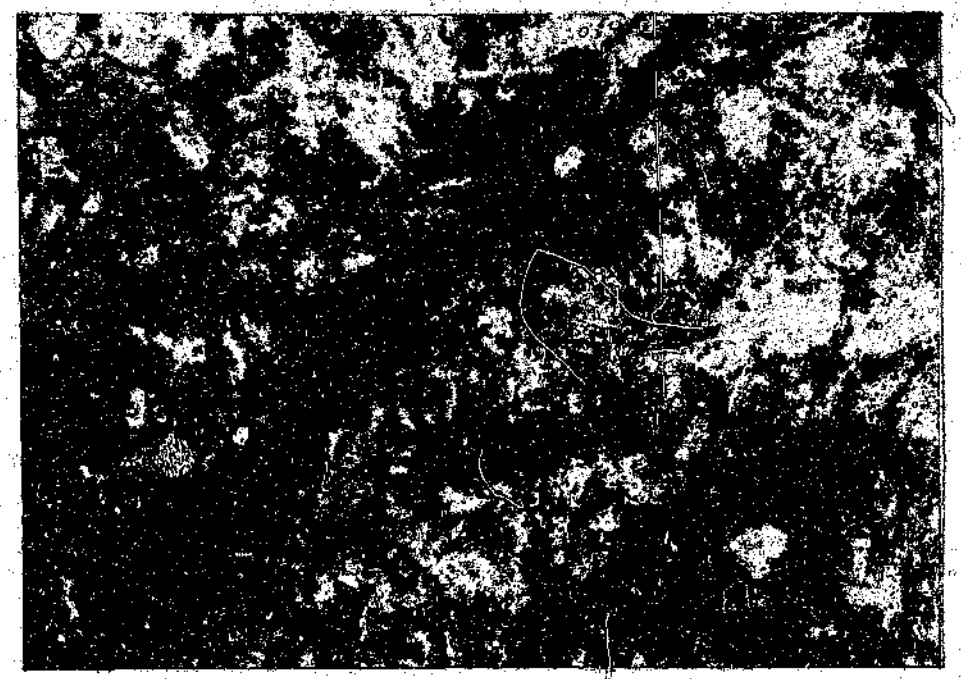

Figure 6.21 Thin section of a Roodeplaat granodiorite, Sample R2 (plain polarized light; field of view: 2.3x3.4 mm).

Roodeplaat peralkaline syenite (Sample R3)

This light-coloured, coarse-grained rock consists chiefly of alkali feldspar and albitic plagioclase. The feldspars are generally subhedral and commonly tabular. Anhedral biotite, clinopyroxene, hornblende and quartz are present in small amounts (Figure 6.22). The biotite is a deep green-brown variety and is generally associated with hornblende. The clinopyroxene is a pale lilac-blue augite showing strong pleochroism. Accessory magnetite, forming euhedral cubic crystals, most commonly occurs within the augite, biotite and hornblende. Apatite is present in minor amounts.

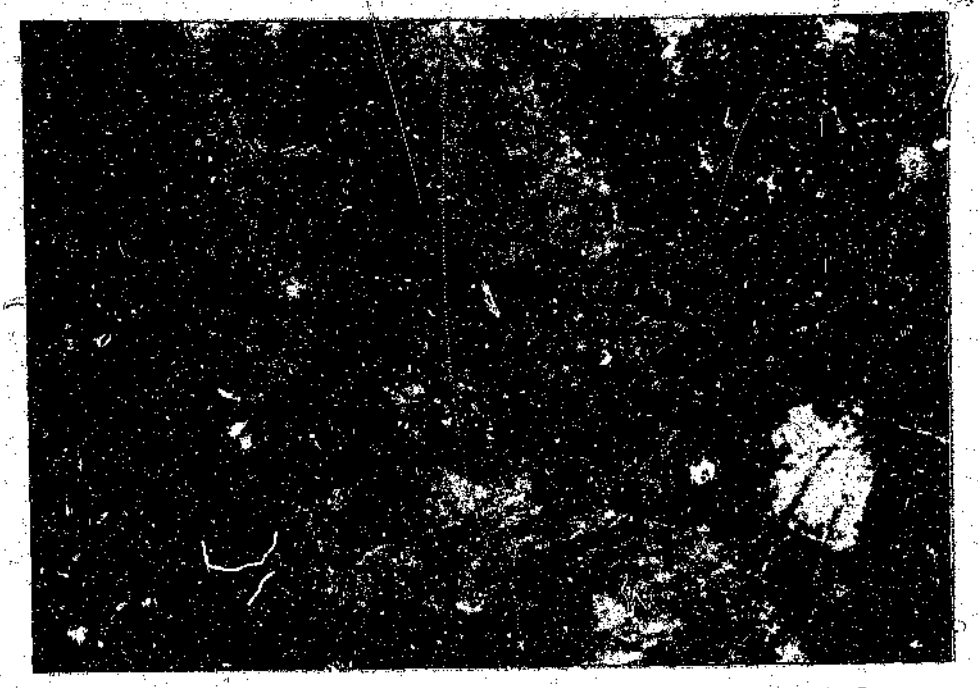

Figure 6.22 Thin section of a Roodeplaat peralkaline syenite, Sample R3 (cross polarized light; field of view: 1.8x2.7 mm).

Roodeplaat fine-grained peralkaline syenite nodule (Sample R5)

This sample occurs as finer-grained, darker (melanocratic) nodules (too small to be shown in Figure 6.19) within the peralkaline syenite (Sample R3: previous description). The mineralogy (Figure 6.23) is very similar to that of sample R3, and it should be noted that the chemical composition of these two rock types are almost identical. These nodules are phanerocrystalline, that is all crystals of the principal minerals can be distinguished by the unaided eye. They are, however, strongly heterogranular, with the identifiable phenocrysts occurring in a finer-grained groundmass of the same minerals. The subhedral to anhedral phenocryst and groundmass crystals of biotite, clinopyroxene, hornblende, quartz and an opaque phase (magnetite) are poikilitically enclosed by altered alkali feldspar and altered plagioclase. The large phenocrysts of plagioclase are commonly tabular. Minor zircon and apatite are present.

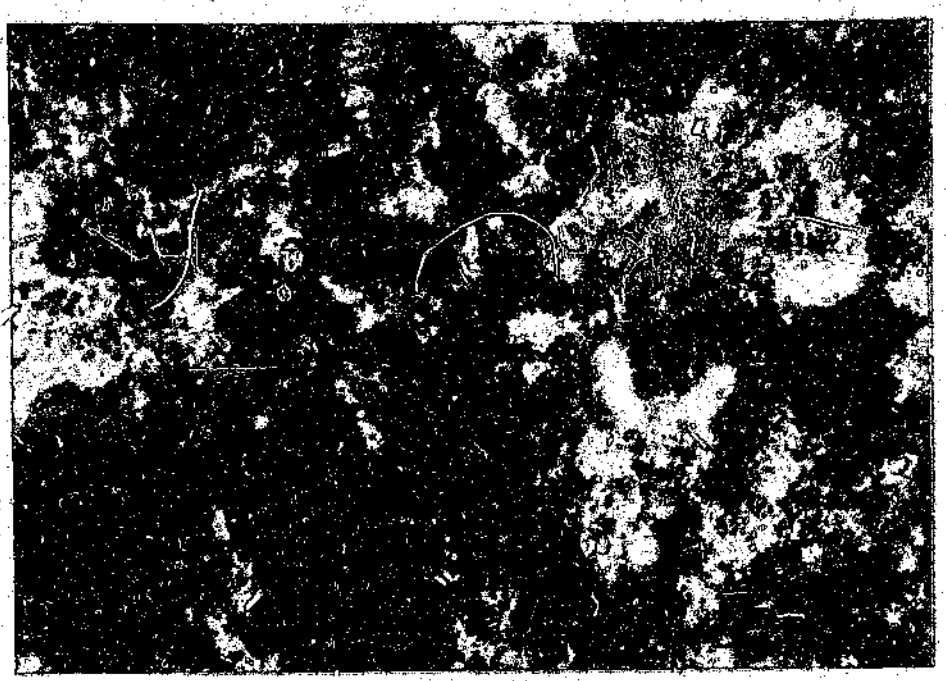

Figure 6.23 Thin section of a fine-grained peralkaline syenite nodule, Sample R5, occurring within Sample R3 (plain polarized light; field of view: 0.8x1.1 mm).

Roodeplaat perthitic syenite (Sample R4)

This reddish rock, which in hand specimen is speckled with dark green-black, light green, and some purple colour, is characterised by a porphyritic texture. Red feldspar phenocrysts comprise more than 80 volume-percent of the rock (Figure 6.24). As this rock is highly altered (see multi-colouring in figure), the normative mineralogical composition of the feldspar was determined from a chemical analysis. The tabular feldspar phenocrysts are antiperthites, in which the potassium-rich phase forms the exsolution lamellae and the sodium-rich phase the host crystal. These feldspar crystals may reach 3 centimetres in length. The other, less abundant, minerals are chlorite, epidote, fluorite, and an opaque phase, which is most probably hematite. Chlorite and epidote are the alteration products of the original ferro-magnesian minerals,which were most likely hornblende and clinopyroxene. Epidote shows the characteristic bright interference colours and complex zoning under high magnification and crossed polars. This rock, which should compositionally be a syenite, does not plot in the syenite field

(Chapter 7), as the perthites were most probably formed by hydrothermal replacement of K-feldspar through the introduction of albite or oligoclase, resulting in the low potassic content.

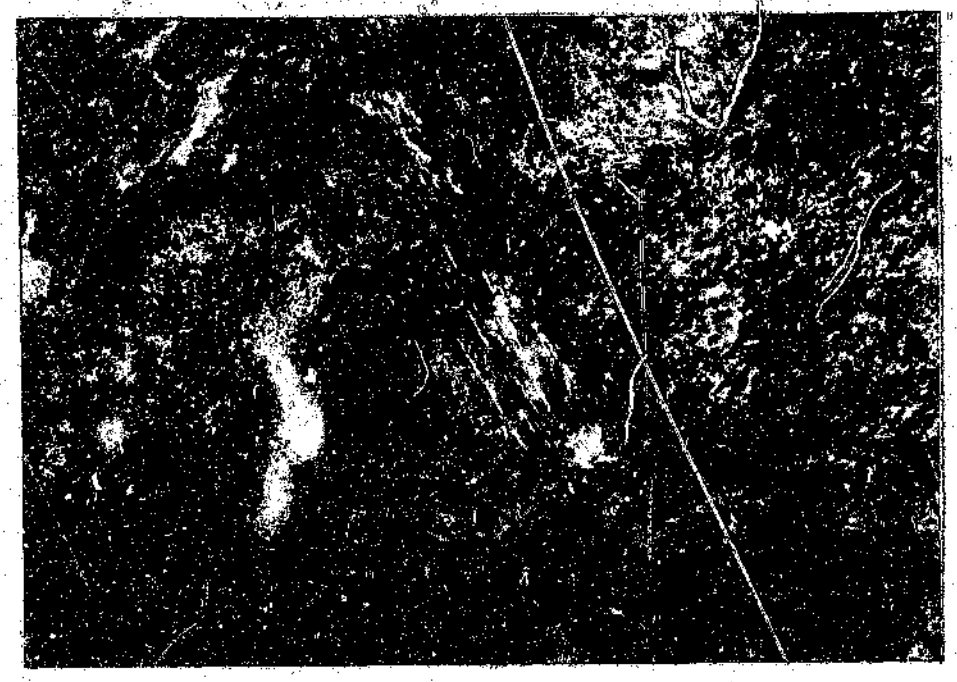

Figure 6.24 Thin section of a Roodeplaat perthitic syenite (Sample R4, cross polarized light; field of view: 2.3x3.4 mm); showing tabular feldspar phenocrysts, chlorite and epidote.

Roodeplaat fine-grained feldspathoid syenite (Sample R6)

This maroon-brown, fine-grained rock type is comprised predominantly of subhedral elongate K-feldspar and albite phenocrysts set in a groundmass of similar mineralogical composition, but with some chlorite, hornblende, mica, pyroxene (aegirine), and nepheline (Figure 6.25). As the groundmass is not quite aphanitic, this rock has not been classified as phonolite. Although the groundmass appears relatively altered, it is indeed holocrystalline. No glass or devitrification textures, such as those seen in sample 40 (phonolite) from the Pretoria Saltpan crater rim, were recognised. An opaque phase of unknown composition is also present.

Figure 6.25 Thin section of a Roodeplaat fine-grained feldspathoid syenite, Sample R6 (cross polarized light; field of view: 0.9x1.4 mm).

Roodeplaat carbonate breccia (Sample R7)

This heterogranular carbonate-rich rock displays a variety of clasts, of different size and degrees of alteration, set in a fine-grained groundmass. The clasts are generally sub- or well-rounded. The dominant clast type is chlorite-rich and may be accompanied by plagioclase and carbonate material or be replaced by secondary quartz (Figure 6.26). A single clast of angular quartz fragments cemented by an iron oxide indicates that this breccia took up some silica during the stoping process. The calcite crystals are euhedral, indicating a primary origin. However, this cannot be stated with absolute certainty, as intense alteration and hydrothermal activity have taken place. A few clasts texturally of obvious igneous origin, are present. They were not identified, but are believed to have originally been from a deep-seated lithology and were merely incorporated into this rock by stoping processes. Another phase is present, in which calcite and quartz occur together, indicating that both these minerals have been remobilized. Secondary iron oxide has resulted in an almost opaque groundmass in some parts and severe staining in

others. Otherwise the groundmass consists of carbonate and minor quartz.

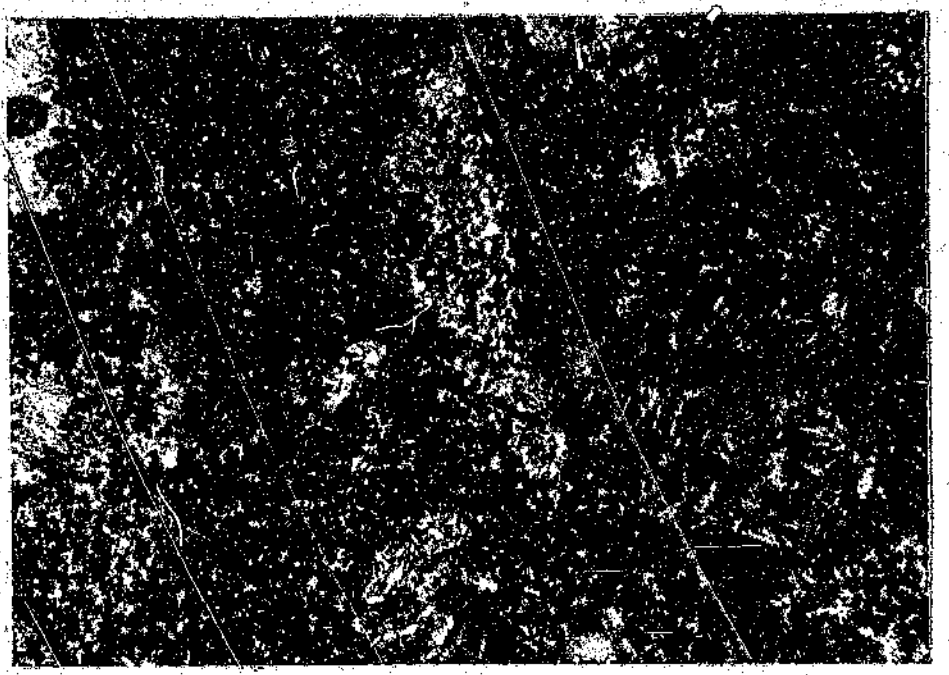

Figure 6.26 Thin section of a Roodeplaat carbonate breccia, Sample R7, with chlorite-rich clasts and one igneous (brown) clast. The matrix consists of carbonate minerals, chlorite and secondary quartz (cross polarized light; field of view: 2.3x3.4 mm).

Roodeplaat fenite (Sample R8)

This red, aphanitic rock consists almost entirely of K-feldspar, probably as a result of metasomatism. A fenite is a metasomatic altered rock and is commonly found surrounding a carbonatite (Verwoerd, 1967) (Figure 6.19 shows this). Spherulites, intergrowths of needles of K-feldspar and quartz, radiate from common nuclei (Figure 6.27). These features abut onto each other. Some red iron oxide staining has filled cavities and results in an overall red tinge of the sample. Alkali exchanges are believed to have occurred between crystallizing magma and the surrounding country rock. This would be possible only by means of migrating hydrothermal fluids. No evidence is present that could assist in identification of the original rock type with any certainty.

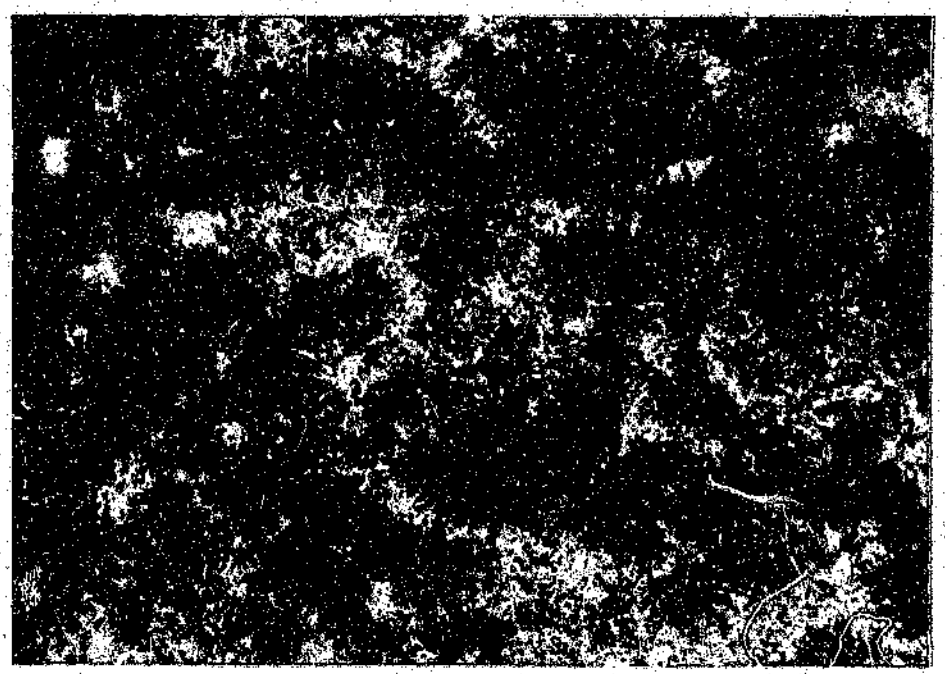

Figure 6.27 Thin section of a Roodeplaat fenite, Sample R8 (plain polarized light; field of view: 2.3x3.4 mm).

Roodeplaat feldspathoidal microsyenite (Sample R8A)

This fine-grained, pink-maroon rock is speckled with light green and dark maroon phenocrysts. The red, highly altered, tabular feldspar phenocrysts (original composition assumed to be that of sanidine from the bulk chemical composition and typical twinning) are scattered throughout the fine-grained maroon and white groundmass. Figure 6.28 shows the texture of this rock. Biotite occurs in minor amounts as phenocrysts. Chlorite and epidote form alteration products after the original ferro-magnesian minerals which include a green amphibole and a pyroxene. These minerals, together with a sericitized sanidine, form the light green phenocrysts. The fine-grained groundmass contains all these minerals, but includes an isotropic feldspathoid mineral which was identified as nosean, as well as (perhaps) some sodalite (available identification methods did not allow the distinction of these two minerals). An accessory yellow, anhedral, isotropic mineral, thought to be allanite, is also present in the groundmass. The feldspar forms coarse radial glomeroporphyritic textures within the groundmass, along which intense alteration, and secondary iron staining has occurred.

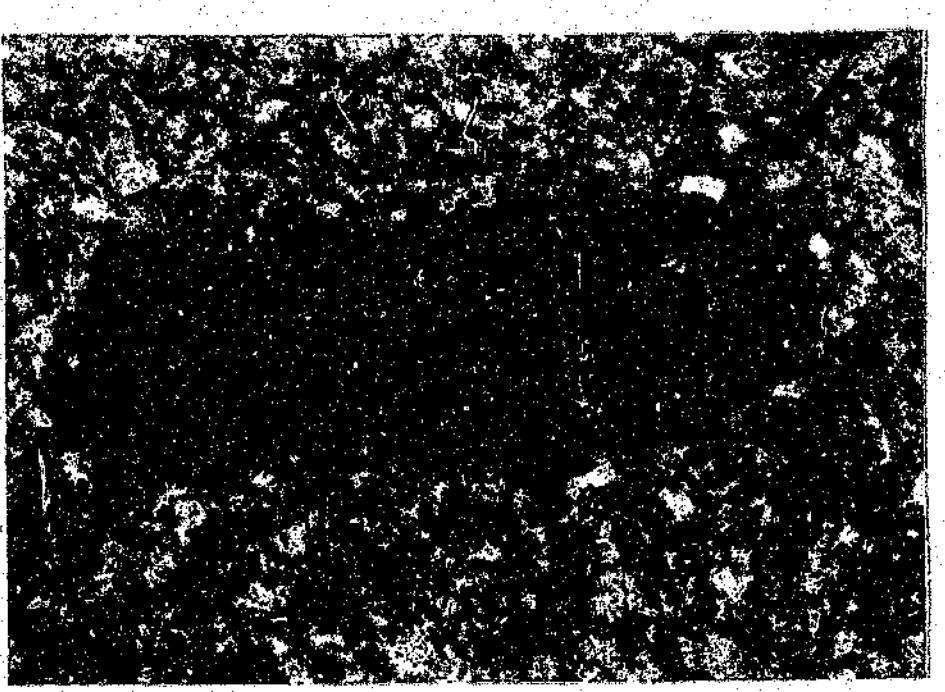

Figure 6.28 Thin section of a Roodeplaat feldspathoidal microsyenite showing a large feldspar phenocryst in a fine-grained groundmass, Sample R8A (cross polarized light; field of view: 2.3x3.4 mm).

Roodeplaat carbonate "lamprophyre" (Sample R9)

This black rock is mottled with dark green and white zones (Figure 6.29), and cut by white carbonate veinlets. It is intensely altered, so that the original fabric and mineralogy are only preserved in some places. The two most abundant minerals, which form both phenocrysts and a significant proportion of the groundmass, are chlorite and calcite, (Figure 6.29), besides some other carbonate phases. Pyroxene remnants are easily identified by the original cleavage (Figure 6.30). A secondary iron oxide is present, which has replaced various pyroxene grains. The groundmass is speckled with this opaque phase which constitutes approximately 25 volume-percent of the matrix. The groundmass appears to contain laths of what may have originally been feldspar. However, the exact composition is undeterminable using normal optical methods. The texture is similar to that seen in lamprophyre samples from the Pretoria Saltpan, and it is therefore assumed that the original rock type was a lamprophyre. As discussed in Chapter 7, the chemical composition is strikingly similar to that of the lamprophyre samples obtained at the Pretoria Saltpan.

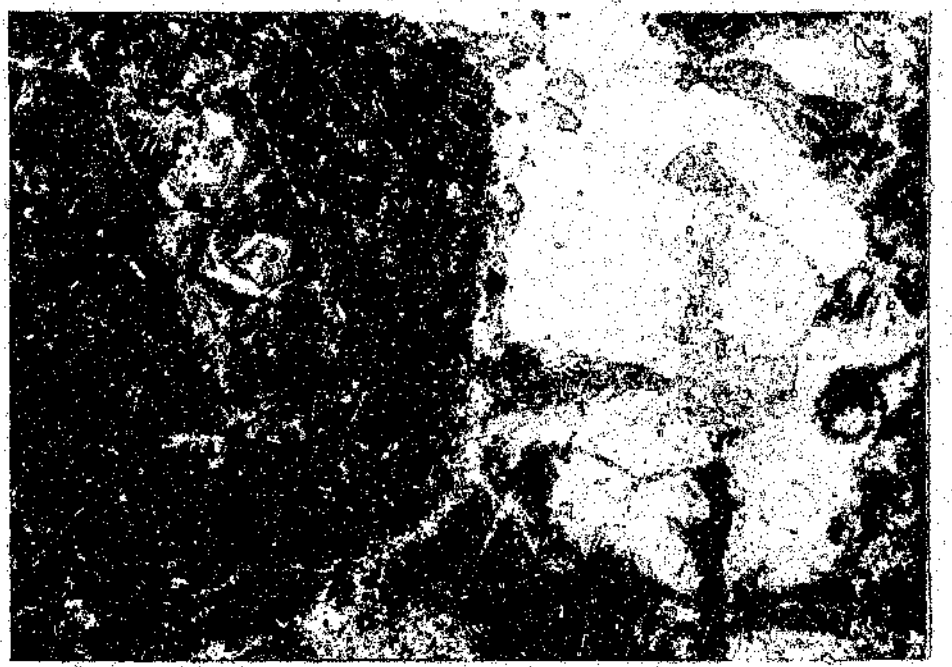

Figure 6.29 Thin section of a Roodeplaat carbonate "lamprophyre," with a dark groundmass, a thoroughly altered phenocryst, and a carbonate-chlorite assemblage (Sample R9) (cross polarized light; field of view: 2.3x3.4 mm).

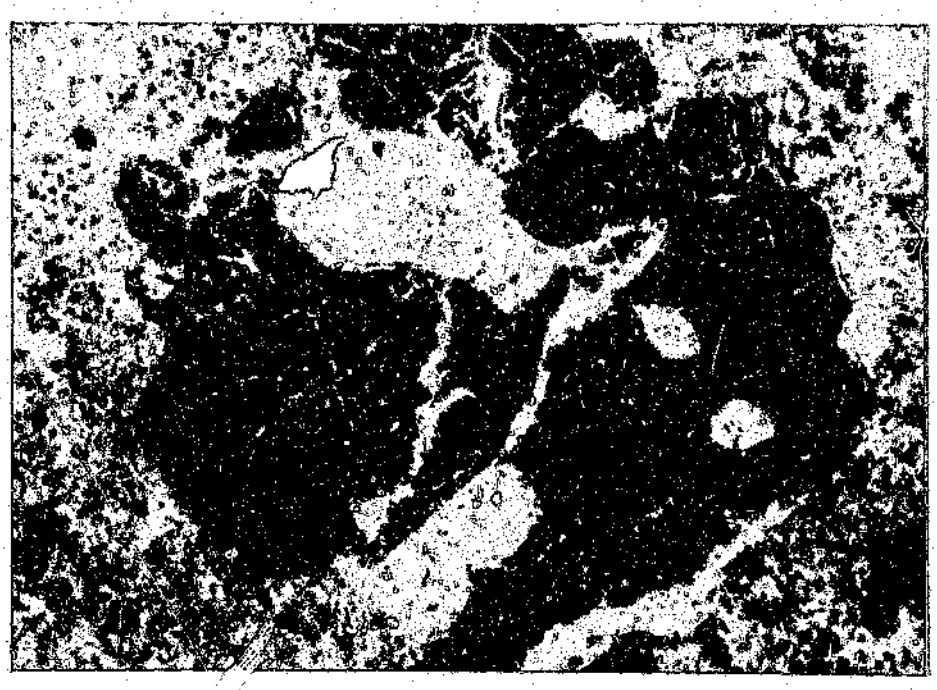

Figure 6.30 Pyroxene remnant identifiable by its original cleavage, Sample R9 (plain polarized light; field of view: 2.3x3.4 mm).

Roodeplaat basalt (Sample R10)

This fine-grained, dark grey-green rock exhibits a subophitic texture of euhedral plagioclase crystals that are cemented by anhedral crystals of pyroxene (titaniferous augite). Secondary quartz and an iron oxide form accessory minerals. Some chlorite is present as an alteration product of clinopyroxene, and epidote as an alteration product of plagioclase (see Figure 6.31). This rock type was classified as a basalt by its appearance, its chemical composition, mineralogy and texture.

Figure 6.31 Thin section of a Roodeplaat basalt, Sample R10 (cross polarized light; field of view: 1.5x2.2 mm)

Roodeplaat gabbro (Sample R11)

This coarse-grained rock is essentially composed of calcic plagioclase and augite. Other minerals present are orthopyroxene, hornblende, chlorite, possibly some biotite, and minor amounts of quartz. The feldspar grains in this granular, subophitic rock are more or less equant and anhedral, and twinning is developed in the anhedral, ophitic augite (Figure 6.32). The most common of the accessory constituents is an opaque mineral,

most probably ilmenite, which is also present in the exsolution lamellae of some pyroxene crystals.

Figure 6.32 Thin section of a Roodeplaat gabbro, Sample R11 (cross polarized light; field of view. 2.3x3.4 mm).

Klipdrift syenite

This medium-grained syenite occurs about 3 kilometres to the south-southwest of Hammanskraal on the farm Klipdrift (see map: Figure 3.2). This lithology has a subophitic texture of strongly-zoned, euhedral alkali feldspar prisms poikilitically intergrown with aegerine diopside (Harmer, 1985) and soda amphibole (riebeckite) clusters. Interstitial quartz and an opaque phase are present in small amounts.

Leeuwkraal phonolite

These phonolites outcrop 5 kilometres to the north-northwest of Hammanskraal and are composed of alkali-feldspar, clinopyroxene and nepheline phenocrysts set in a groundmass of the same minerals plus amphibole. Sphene, some fine-grained feldspar,

nepheline and an opaque phase are present in the groundmass. Only one sample was analyzed. However, according to Harmer (1985), different samples from the same outcrop contain various amounts of alkali feldspar, and the clinopyroxenes have an aegirine-augite to aegirine-diopside composition.

6.3 KAROO SEDIMENTARY ROCKS

This group of rocks, described by other authors (Wagner, 1922; Feuchtwanger, 1973) as "Karroo Grits", includes shale, sandstone and even some carbonaceous material. These sedimentary rock types, however, do not occur in close proximity to the crater, but may be found in the wider region. The most common occurrence of the dark grey-brown Karoo rocks is a coarse grit-like rock (Figure 6.33), composed almost entirely of angular quartz grains cemented by a hydrated iron oxide. It is often strongly laterized and is most probably a residual deposit formed under a previous, more humid climatic condition.

Figure 6.33 Thin section of a typical "Karroo Grit" sediment, common to the study area (cross polarized light; field of view: 1.8x2.7 mm).

6.4 CRATER BRECCIAS AND SHOCK METAMORPHISM

Breccias are a prominent feature of impact structures (e.g., Dence, 1968). In addition to the extensive deposits of loose allochthonous breccias found on the upper portion of the rim and the large volume of predominantly monomict autochthonous and allochthonous granitic breccias of the upper crater floor (evidence of which is in the drill-core), other breccia types are also present in the Saltpan crater. Various monomict autochthonous breccias occur both in situ on the crater rim and as numerous loose boulders within the confines of the crater. Several breccia fragments consist of granitic cataclasite with matrix particles up to several millimetres in size. The presence of breccias alone, however, is not unequivocal evidence which could permit the recognition of an impact origin (Grieve and Pesonen, 1992). However, where shock metamorphic effects occur within breccias, they have to be designated as being of impact origin.

Within 400 meters of the edge of the 3.8-kilometre-diameter Brent Crater in Canada the country rocks are fractured, locally brecciated and hydrothermally altered, but they exhibit no microscopic evidence of shock metamorphism (Dence, 1968). The significantly smaller Pretoria Saltpan crater was therefore not expected to show widespread shock metamorphic effects in the rim rocks. However, in total contrast to this expectation shock metamorphism was found in various breccia samples from the crater rim. The dynamic origin of this deformation is not doutful, as impact-characteristic shock effects such as planar elements and partial isotropism were discovered. The original distribution and exact occurrence of many of the breccia samples is not known, largely because of the scarcity of breccia outcrops.

Examination of at least one thin section from each of the rim-breccia samples was made under the petrographic microscope. Microprobe analyses were carried out to determine the composition of the matrix material of various samples. Figure 6.34 shows the locations of the breccia samples from the crater confinement.

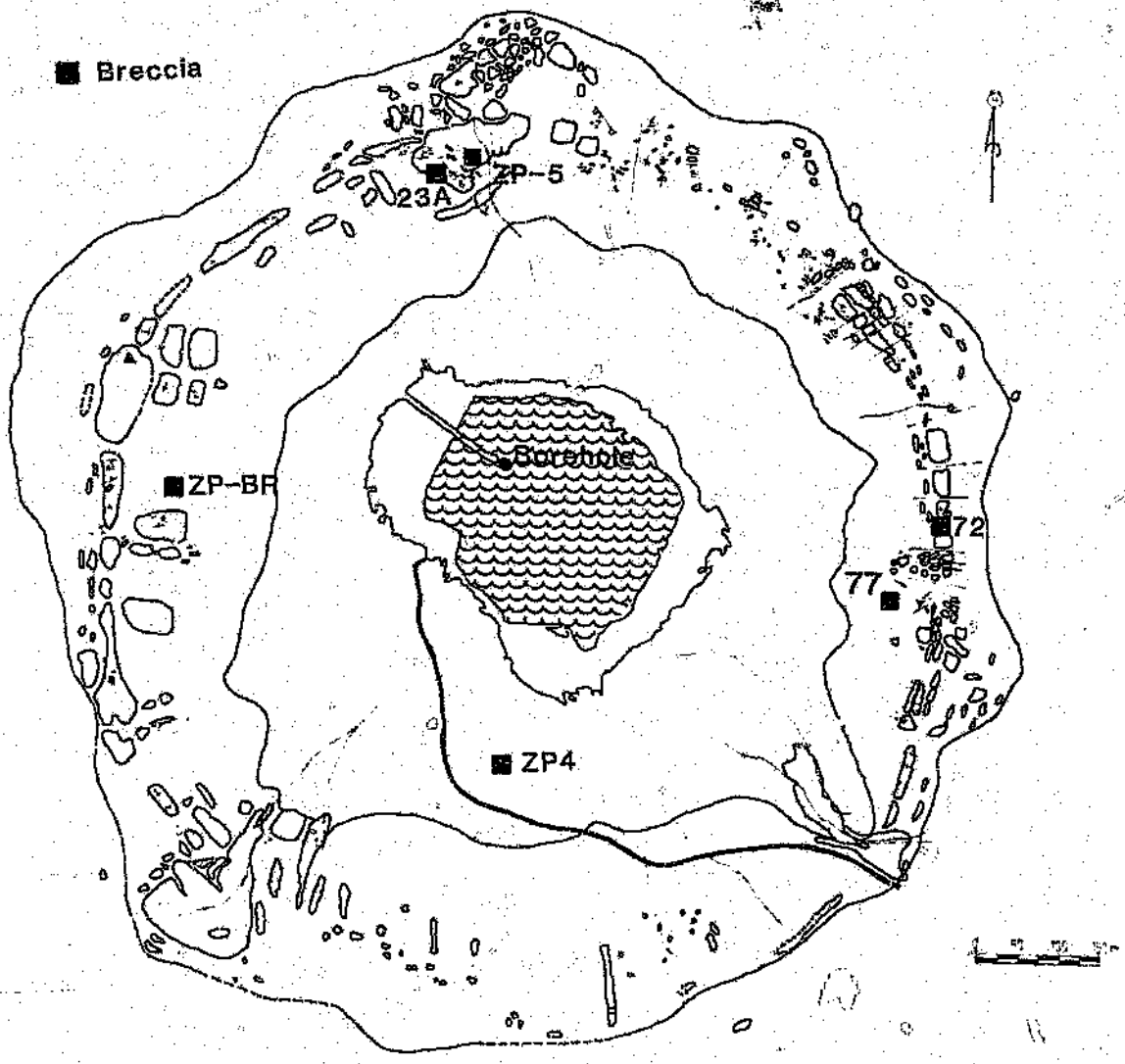

Figure 6.34 Locations of all breccia samples found at the crater site in this study.

Breccia dyke (Sample 72)

This autochthonous monomict granitic breccia occurs in situ as a radial, sub-vertical, ten centimetre wide breccia dyke (see Figure 4.15) on the upper portion of the eastern rim (Figure 6.34). This outcrop extends radially for approximately three metres. It consists of granite-derived fragments which are between 1 millimetre and 2 centimetres long and are enclosed in a much finer matrix of the same minerals (Figure 6.35). Banding or

alignment of the clasts is evident and may be a result of flow or shearing. Many of the fragments appear to be sheared and otherwise fractured under brittle conditions. The alignment of the clasts, and to some extent of the matrix minerals, may be a result of a process termed autobrecciation. According to Short (1970), this process is a result of shock waves moving through a rupture zone. They may be strong enough to initiate slip movements along a pre-existing fault or joint-bounded blocks, which can result in fragmentation and granulation of rock masses leading to the formation of breccias similar to those in fault zones. The main stress is of a shearing nature, evident from the extention and crude alignment of elongate particles (Figure 6.35). No evidence of melting or vesiculation can be seen in this sample.

Figure 6.35 Autochthonous monomict breccia occurring as a radial, sub-vertical breccia dyke. Note the crude alignment of clasts which are parallel to the strike of the dyke (cross polarized light; field of view: 2.7x3.4 mm).

Cataclasite (Sample series ZP-BR)

This sample, occuring as a lose boulder, was found on the lower western slope of the crater interior. Breccias of this type are comprised entirely of a single lithotype, that is

granite fragments which have not moved relative to each other except for small displacements and rotations over distances less than the fragment dimensions. The granite clasts are set in a very fine-grained matrix, with grain sizes on the order of a few microns, and which appear black in hand-specimen (Figure 6.36). Figure 6.37 represents a typical section which shows various degrees of alteration within the matrix and to some extent alteration of the clast boundaries.

Cataclasite (Sample ZP-4)

This breccia sample is of exactly the same type as that previously discussed, with the exception that it is less altered than the previous sample. Figure 6.38 shows a part of ZP-4 which is less altered than typically encountered. Many boulders of this breccia type were encountered on the inner slopes of the crater rim. The granite clasts are angular to sub-angular and vary from less than 1 millimetre to a few centimetres. The original matrix composition is believed to have been granitic. The brown alteration (Figure 6.38) is a result of secondary iron oxide.

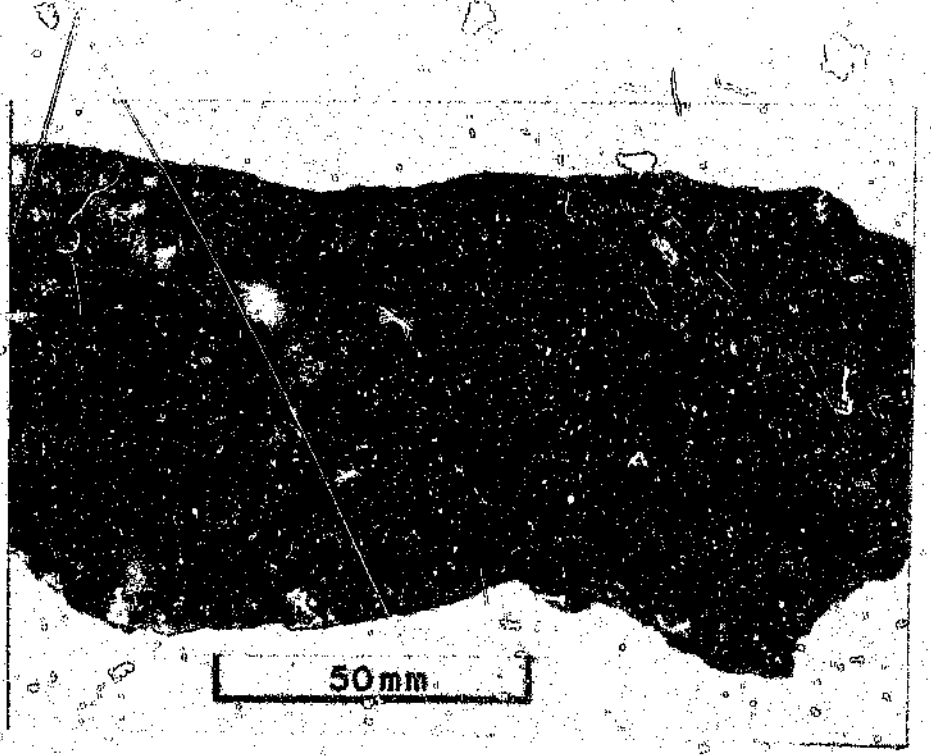

Figure 6.36 Altered cataclasite breccia (Sample ZP-BR)

Figure 6.37 Typical section of a cataclasite showing various degrees of alteration (plain polarized light; field of view: 1.5x2.2 mm).

Figure 6.38 Section of a relatively fresh cataclasite (Sample ZP-4; plain polarized light; field of view: 1.2x1.7 mm).

Quartz micro-veining cuts both the clasts and the matrix, indicating a secondary origin for these veins. Sample ZP-BR-A (Figure 6.39) exhibits a common feature of these breccias. The angular clasts or fragments are lath- or wedge-shaped and generally parallel the larger clast boundaries indicating an overall compressive stress perpendicular to the long axes of these clasts.

Figure 6.39 Common parallel form of clasts indicative of stress conditions, Sample ZP-BR-A (plain polarized light; field of view: 2.2x1.5 mm).

Numerous fractures were encountered in clasts of these samples. One such fracture was an iron-oxide-filled staggered fracture shown in Figure 6.40. The iron-oxide cement may be replaced by yet a later-stage cement, namely quartz which exhibits a combination of a competitive crystal growth fabric and a blocky cement fabric. The quartz cement is undoubtedly the last stage of alteration evidenced by the quartz veinlets cutting through the iron-oxide cement.

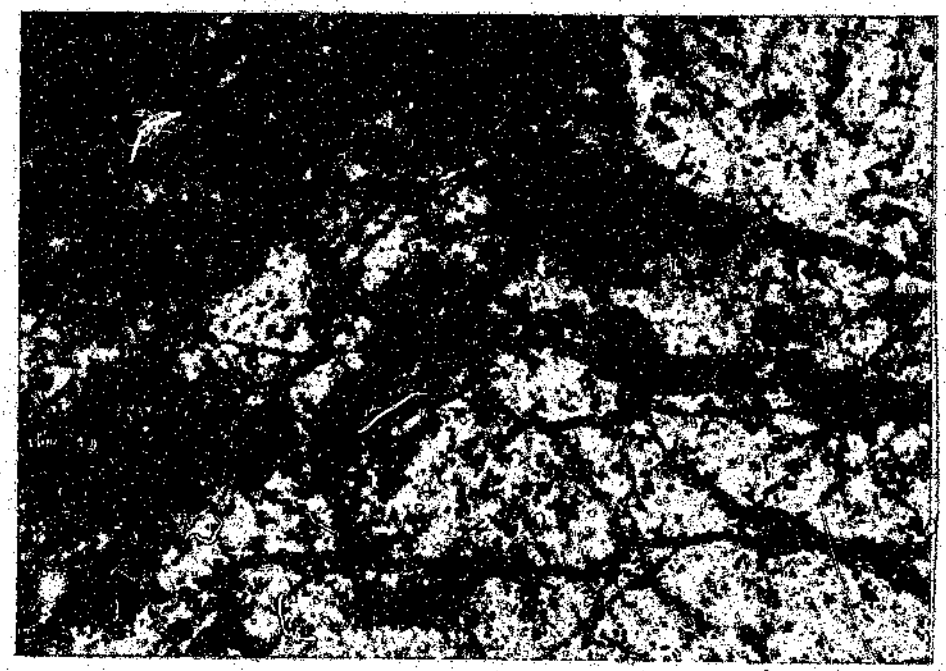

Figure 6.40 Staggered fractures occurring in Sample ZP-BR (plain polarized light; field of view: 1.5x2.2 mm), filled with iron oxide.

No clasts that could be related to a lithology other than the host lithology were observed. Thus the green-brown to black matrix which binds the fragments together was assumed to be derived from the parent material. Microprobe analysis of several matrices, however, revealed a different situation. Rather than having a granitic composition, these matrices have silica-depleted, iron-enriched compositions (Table 6.1). This is attributed to hydrothermal overprinting by Fe(Mn)-rich fluids in addition to some alteration of the pre-existing clast material. The iron-rich matrix, besides being comprised of an iron-rich phase, also contains fine grains of quartz and altered feldspar. In addition, sample ZP-BR exhibits a high Mg content. No reasonable explanation for this has been found, however, the matrix may contain some chlorite, which was not noticed in thin section. The low totals that the three samples show are a result of high loss on ignition (LOI) values and have been attributed to water-bearing phases, thought to be present in the altered matrices.

	i) Sample ZP-BR	ii) Sample SP-72	iii) Sample SP-23A
SiO_2	25.75	12.08	21.47
TiO_2	0.13	2.46	10.49
Al_2O_3	18.18	3.95	10.69
FeO	39.86	68.67	36.97
MnO	0.01	0.04	1.26
MgO	5.95	0.10	2.99
CaO	0.11	0.02	0.03
Na_2O	0.01	0.06	0.05
K_2O	0.05	3.23	2.40
Cr_2O_3	0.06	-	0.01
NiO	0.01	0.02	0.07
Total	90.12	90.63	86.43

Table 6.1 Microprobe results of: i) Cataclasite matrix
ii) Breccia dyke matrix
iii) Matrix of breccia at granite-trachyte contact.

Shock metamorphic effects were noticed in many clasts in breccia sample ZP-BR, in two different forms: kinked fractures (Figures 6.41, 6.42) and planar deformation features (PDFs-Grieve et al., 1990). Quartz shows the largest variety of distinctive responses to shock over a wide range of shock pressures. Feldspar shows less diversity, while micas and other minerals are even more restricted in resolving shock metamorphic grades (e.g., Dence, 1968). Kink-banding is the most frequently observed shock effect in sheet silicates and other layered crystal structures, such as graphite, although they may occur in shocked

quartz and feldspar, too (Bunch, 1968). Kink bands are a result of plastic deformation (Stöffler, 1972), and in biotite are formed by dynamic pressures between 1 and about 45 GPa (Hörz and Ahrens, 1969; Schneider, 1971). Kink-banded fractures such as those in Figures 6.40 and 6.41 are representative examples of kink-banding seen in quartz grains in this breccia type.

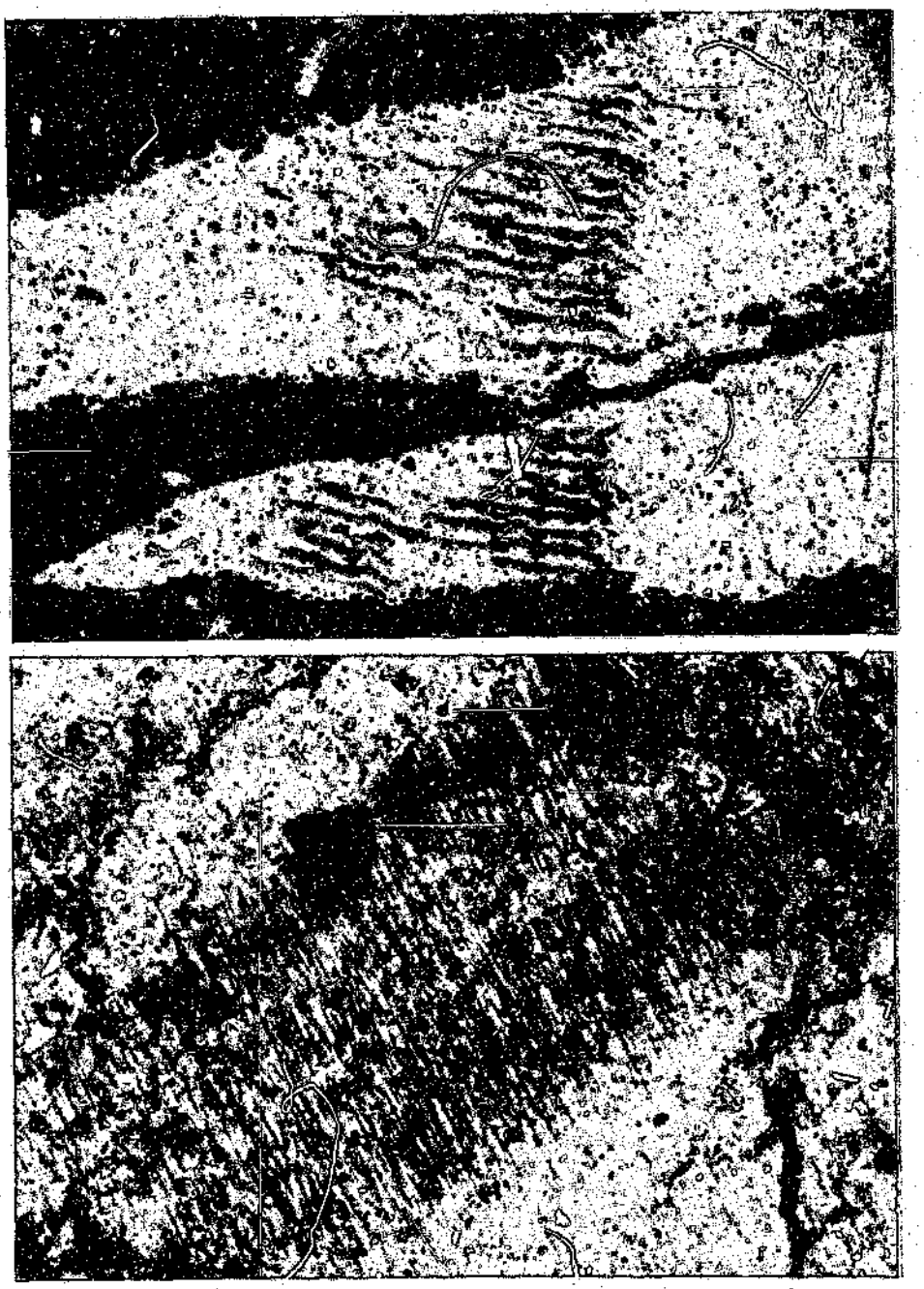

Figures 6.41, 6.42 Kinked fractures occurring in breccia sample ZP-BR (plain polarized light; field of view: 0.49x0.72 mm for both photo-micrographs).

As kink-banding is a widespread deformation effect in rock-forming minerals, frequently produced under normal tectonic deformation conditions, that is by natural static deformation, it is not a diagnostic indicator of dynamic (shock) deformation, unless it is associated with other unequivocal shock effects. Planar deformation features (Grieve et al., 1990; Alexopoulus et al., 1988) occur as a single set or multiple sets of parallel optical discontinuities. Figure 6.43 shows typical planar deformation features, predominantly in the form of parallel fluid inclusion trails, encountered in quartz grains in breccia sample ZP-BR. Also note the parallel fractures in the crystal that appear very similar to those observed in experimentally (at about 29 GPa) deformed quartz (Reimold and Hörz, 1986).

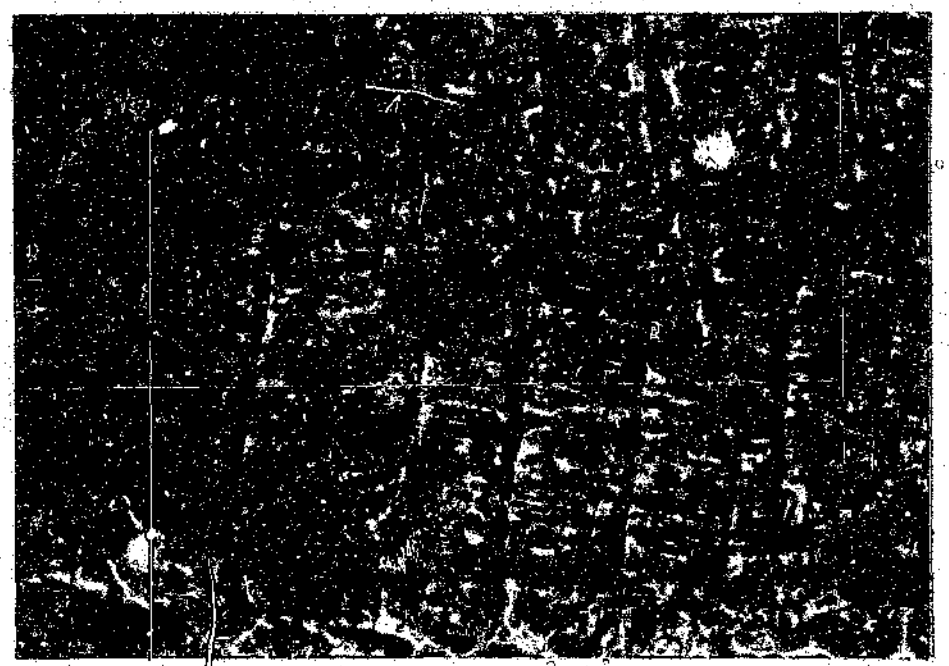

Figure 6.43 Planar deformation features (see arrow) and fractures typically occurring in shocked quartz grains in cataclasite of the Pretoria Saltpan crater in Sample ZP-BR (plain polarized light; field of view: 0.15x0.22 mm).

Reimold et al. (1987) proposed the following definition to distinguish pseudotachylite from cataclastic or mylonitic breccias : "Pseudotachylite is a fragment-laden breccia with either aphanitic or crystalline melt matrix, whereas mylonites/ultramylonites are still

considered clastic (yet frequently recrystallised) breccias". They also suggested that pseudotachylite occurring in impact structures may be distinguished from impact melt breccias by the complete lack of shock deformed clasts, and by the typical angular shape of the small clasts. Although many of the clasts encountered in the studied breccias are angular, shock metamorphic effects were identified in numerous clasts. Due to the altered state of the matrix it was not possible to identify the original nature of the matrix, that is whether it was originally aphanitic (pseudotachylite-like) or fine-grained clastic. Considering the above classification and the presence of the shock metamorphic effects, these samples have been termed cataclasites, and are regarded as *autochthonous monomict fragmental impact breccia*. Another example of this sample type is ZP-5 (see Figure 6.34 for location), again containing quartz grains with PDFs (Figure 6.44).

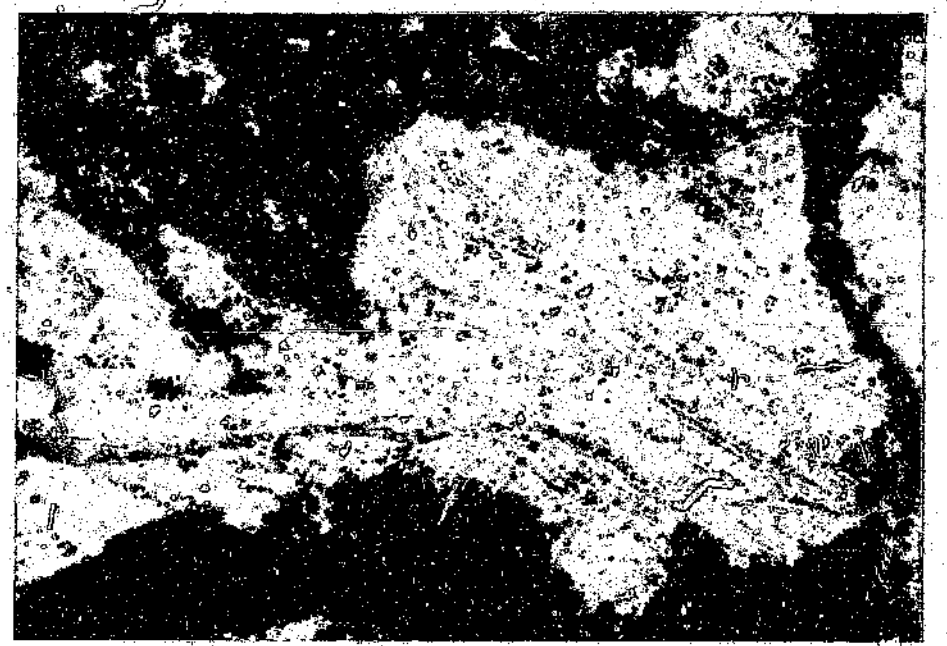

Figure 6.44 Breccia (Sample ZP-5) exhibiting planar deformation features in a quartz grain (cross polarized light; field of view: 2.3x3.4 mm).

Breccias which have a similar altered appearance in thin section to the samples discussed in the above section may also be found in contact with veins of altered trachyte. However, these vein-related breccias do not contain any shock-related deformation

effects. They are therefore believed to have resulted from the rapid emplacement of the volcanic veins.

Dyke-contact breccia (Sample SP-23A)

This breccia specimen was found at a trachyte-granite contact on the northern crater rim (see Figure 6.34) and is most likely the result of the trachyte intrusion rather than the cratering event. The trachyte at this contact is totally altered and microprobe results (Table 6.1) indicate iron enrichment at the contact. Figure 6.45 shows the granitic breccia fragments at the contact, which are enclosed by an iron-rich secondary opaque phase. The granite breccia clasts may be totally or partially altered, evidenced by the very fine-grained clay-mineral particles that are always in contact with the granite breccia fragments. These particles constitute approximately 50 volume-percent of the matrix near the trachyte-granite contact; the other 50 percent being the totally altered or replaced iron-rich opaque phase.

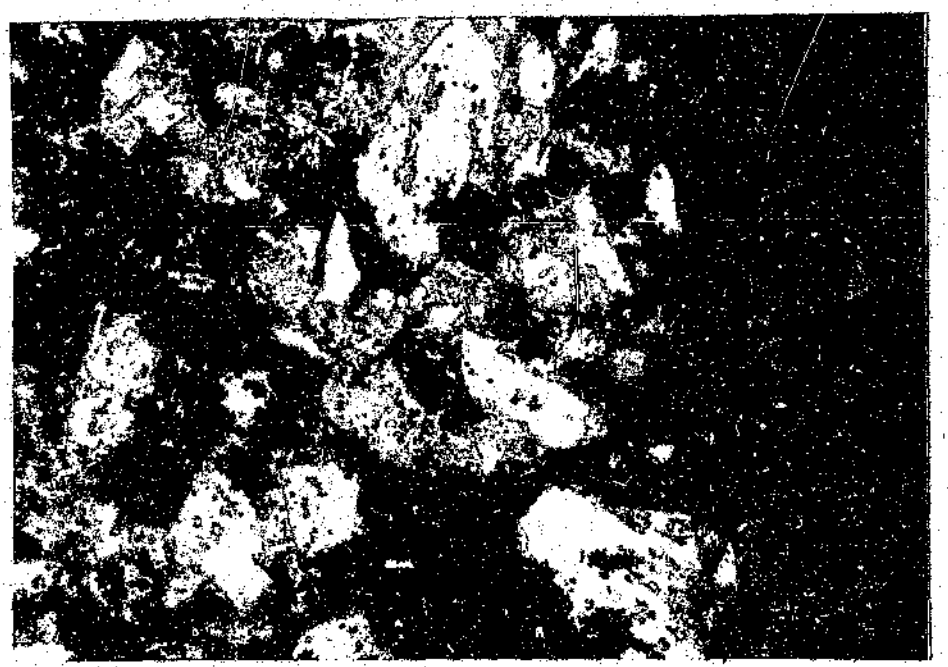

Figure 6.45 Trachyte-granite contact breccia (Sample 23-A). The trachyte is the darkened area to the right and has been totally replaced by a secondary iron-rich phase at this point. Some of this alteration may be seen in the granite near the contact (plain polarized light; field of view: 1.5x2.2 mm).

Cataclastic shear zone breccia (Sample SP-U)

This sample was taken from a location (granite outcrop) approximately 3 kilometres to the south of the crater (see also Chapter 3, Figure 3.9, which refers to this locality). This breccia, on thin section scale, appears similar to the impact-produced breccias discussed previously: sub-angular clasts, mainly quartz and some altered feldspar, are contained in an opaque iron-rich matrix (Figures 6.46). In general, the clasts are less angular than those of the impact-produced breccias, and the black iron-rich matrix is not seen to cut through the clasts as is quite common in the latter case. Most of the feldspar in this breccia is altered to clay minerals, indicative of a high degree of alteration, possibly due to fault-related hydrothermal activity. Secondary quartz, having a blocky cement texture, is present in this altered feldspar.

Figure 6.46 Shear zone breccia (Sample SP-U) from the crater environs (cf. text for description and Chapter 3 for the geological setting). The yellow area at the left margin is predominantly altered feldspar with light patches of secondary quartz (plain polarized light; field of view: 1.5x2.2 mm).

Shock metamorphic effects in the drill-core

Reimold et al. (1991, 1992) prepared 31 grain mounts from the granitic sands between depths of 90 and 146 metres. These sections revealed the presence of multiple sets of bona fide planar deformation features (abbreviated PDFs - Grieve et al., 1990) in quartz, alkali feldspar and plagioclase grains, and of diaplectic quartz glass, as well as fragments of brownish or clear glasses. Many quartz or feldspar grains were partially or completely isotropized. They also noted up to 2 centimetre large melt breccia fragments, with glassy matrix and angular granite-derived mineral fragments. Accordingly the sands were classified (Reimold et al., 1992) as an unconsolidated equivalent of *suevitic* impact breccia, such as that described from the Ries crater by Stöffler et al. (1977). Sulphide (FeS_2) spherules up to 300 microns in diameter, but usually smaller than 40 microns, occur frequently in the melt and glass fragments and also form a general constituent of the fine fraction of the breccia (Reimold et al., 1991, 1992). They found several spherules which consist of an outer shell of pyrite around an inclusion of silicate in droplet form, probably representing impact glass. These shock deformation effects represent the complete range of shock metamorphic pressures from about 15 to 45 GPa, and, according to Reimold et al. (1992), are unequivocal proof for the origin of the Pretoria Saltpan crater by meteorite impact.

For this study, grain mounts were prepared from the granitic sands of the core between depths of 90 and 146 metres. Polished thin sections were cut and examined under the optical microscope and with a universal stage. Standard universal stage procedures were employed to obtain the orientation of planar deformation features with respect to the optical orientation of the host grains. It was estimated that the measurements are accurate to within 5°, as the deformation of these grains makes accurate orientation of the optical c-axis difficult. Indexing of planar deformation features was done in stereographic projections in a Wulff net. The angles of poles of the planar deformation features to the c-axis of the host grains were thus determined. Statistics of these angles are shown in Figure 6.51.

In thin section many quartz grains display planar deformation features that are characteristic of shock metamorphism (Alexopoulos et al., 1988; Grieve et al., 1990).

Typical planar deformation features from Saltpan samples are shown in Figures 6.47 and 6.48. The deformation planes are crystallographically controlled, and often occur in orientations that are diagnostic for shock deformation (e.g. various papers in French and Short, 1968). A maximum of four intersecting sets of PDFs per grain were observed, although one or two orientations per grain were more common. Orientations of PDFs were determined in 22 grains, of which 15 had one, four had two, two had three, and one had four orientations.

Other shock produced features such as the presence of glass spherules (Figure 6.49) and diaplectic glass (Figures 6.50a and 6.50b) were also confirmed in this study. According to Stöffler (1972), Reimold and Hörz (1986), and others, diaplectic quartz glass is produced in the shock pressure range from ca. 30 to 45 GPa and the shock temperature must be lower than the melting point or at least the glass transition temperature. At higher temperatures, implicating higher shock pressures, shock fusion takes place and glasses quenched from a liquid will be formed (Stöffler, 1972).

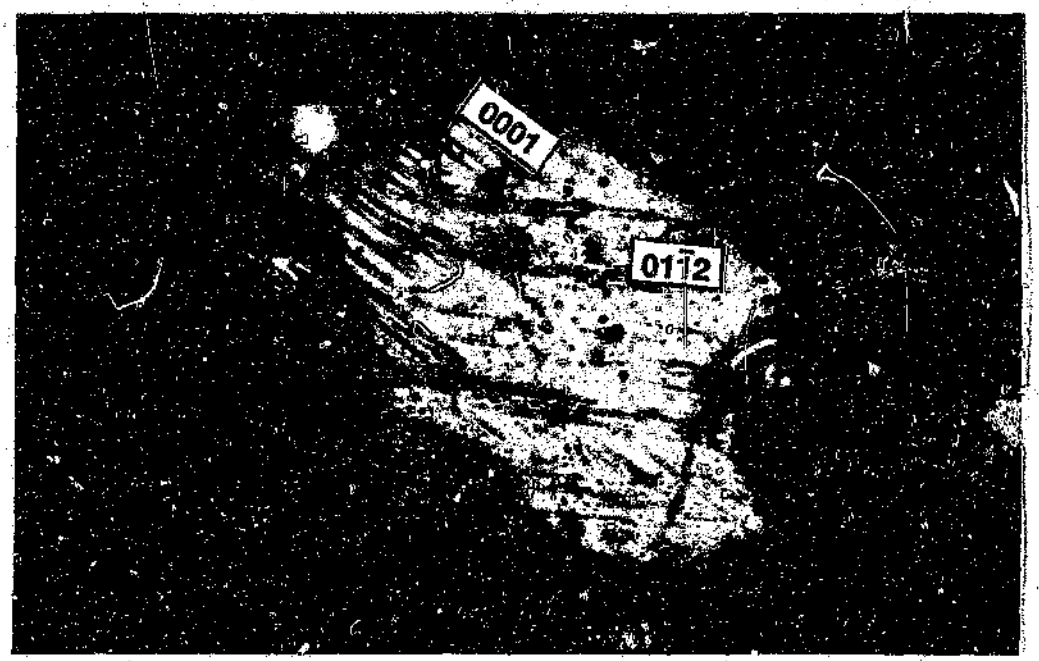

Figure 6.47 Photomicrograph of planar deformation features in a quartz grain from 122 metres depth (crossed polarized light; field of view: 0.24x0.36 mm).

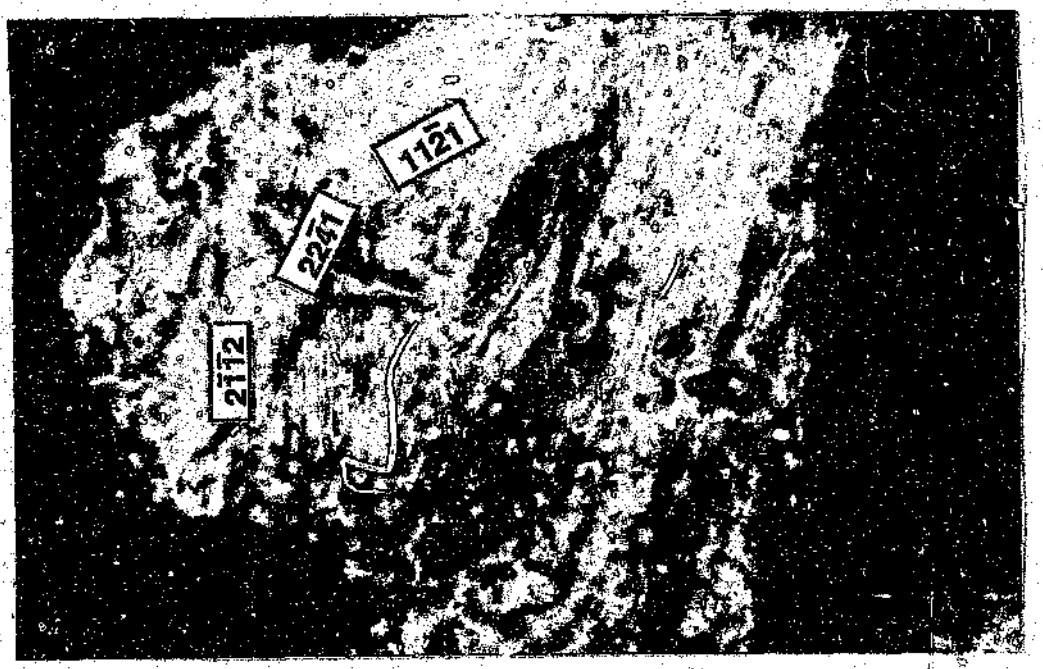

Figure 6.48 Another photomicrograph of planar deformation features in shocked quartz from 122 metres depth (crossed polarized light; field of view: 0.24x0.36 mm).

Figure 6.49 Photomicrograph of a glass spherule (plane polarized light; field of view: 0.49x0.72 mm).

Figure 6.50 Photomicrograph of a diaplectic quartz grain (central grain) in **a)** plane polarized light and **b)** crossed polarized light, showing the typical isotropism in crossed polarized light (field of view: 0.75x1.12 mm).

The frequency diagram of the angles between 30° and 85° (Figure 6.51) indicates predominance of PDFs parallel to (01$\bar{1}$3), (10$\bar{1}$2), (01$\bar{1}$1), (10$\bar{1}$1), (11$\bar{2}$1), (22$\bar{4}$1), and (51$\bar{6}$1). Angles parallel to (0001) and (10$\bar{1}$3), however, were rarely observed. With the exception of these two angles the general characteristics of the obtained histogram (Figure 6.51) are similar to results obtained from a number of other impact craters (e.g. Robertson et al., 1968; Bunch, 1968). According to Robertson et al. (1968), the presence of planar deformation features parallel to (10$\bar{1}$2) is indicative of a higher level of quartz deformation. Figure 6.52 shows results obtained for PDF orientations determined in quartz grains from the Saltpan suevite by W.U. Reimold (unpubl. data). His samples were derived from the same section of core and from similar individual depths sampled for this study. Clearly these results are similar to those obtained in this study, that is, similar maxima were obtained, and the overall shapes of the graphs are comparable.

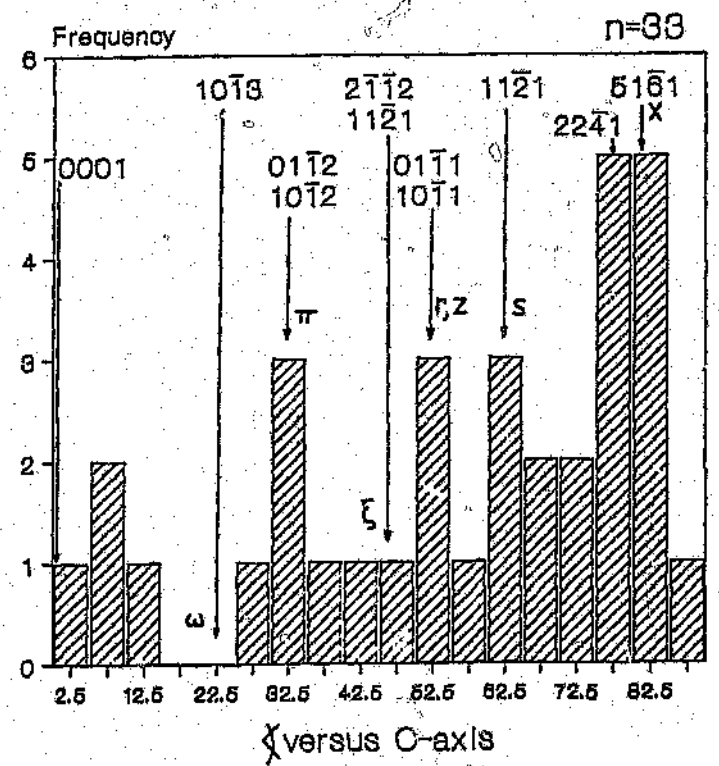

Figure 6.51 Frequency diagram for the angle between the c-axis of the host quartz crystals and the normals to the orientations of planar deformation features.

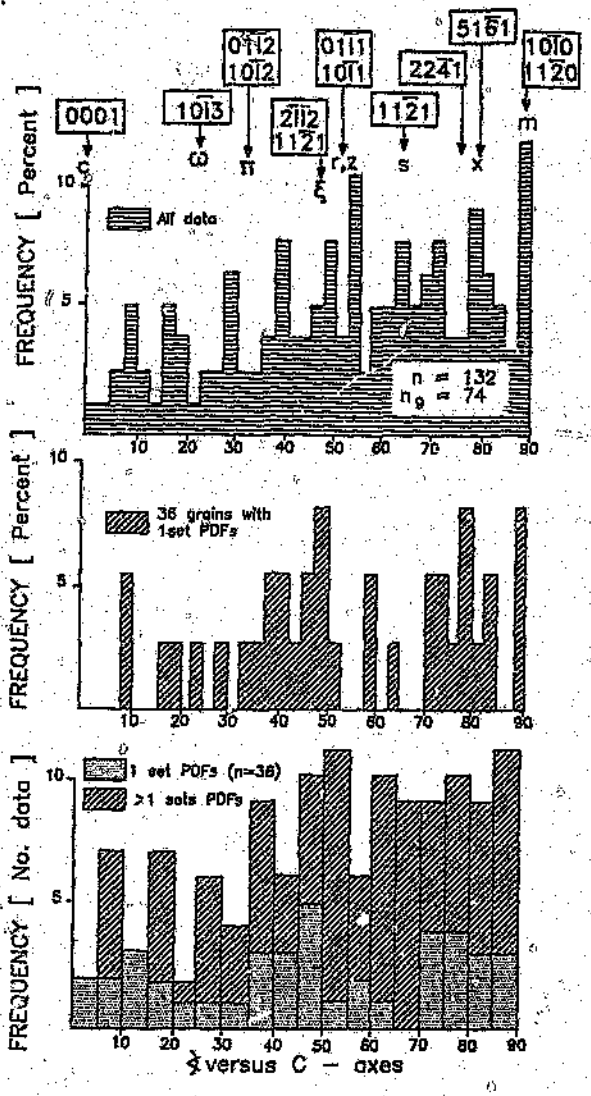

Figure 6.52 Frequency diagram for the angles between the c-axes of host quartz and the normals to planar deformation features (courtesy of W.U. Reimold).

7.1 X-RAY FLUORESCENCE DATA

The chemical compositions of the country rock varieties, as well as of the various basic and alkaline intrusives within the crater and from the crater environs, were determined. In some cases this was necessary to determine the correct rock types, particularly of altered samples. These data were further needed to determine whether the intrusives from within the crater are related to the intrusives of the crater environs and to the Pienaars River Alkaline Complex.

Method

Major element concentrations were determined by X-ray fluorescence techniques in the Geology Department, University of the Witwatersrand. Samples were crushed and milled to a fine powder. Approximately 2 grams of powder were weighed into a silica crucible and heated to 1000°C for six hours. The sample was reweighed to calculate the loss on ignition (LOI). Approximately 0.28 grams of baked powder were mixed with $NaNO_3$ and Spectroflux 105 (lithium tetraborate, lithium carbonate and lanthanum oxide). This mixture was melted to make fusion discs after the method of Norrish and Hutton (1969). Samples were analyzed on a Phillips PW X-ray fluorescence spectrometer. Major and minor element oxides were determined from the concentrations. The results are tabulated in Appendix A. Total iron contents are expressed as Fe_2O_3. Carbon and water contents of selected samples were determined by means of a Leco RC-412 multi-phase carbon determinator. These results are also tabulated in Appendix A. Accuracy limits, as determined by standard replicate analysis are for Fe_2O_3: 0.05%; TiO_2: 0.02%; MnO: 0.03%; K_2O: 0.08%; P_2O_5: 0.05%; SiO_2: 0.5%; MgO: 0.5%; Na_2O: 0.3%; Al_2O_3: 0.3%; CaO: 0.1%.

Approximately 4 grams of the same powder used for the preparation of the fusion discs was used to press powder briquettes using boric acid as a base. The briquettes were analyzed on the same X-ray fluorescence spectrometer used for the determination of

major element concentrations. Concentrations of the trace elements Rb, Sr, Y, Zr, Nb, V, Cr, Co, Ni, Cu, Zn and Ba were determined, and the data obtained are given in Appendix C. Accuracy limits for the trace elements as determined by standard replicate analysis are for Rb: 2 ppm; Sr: 2 ppm; Y: 1 ppm; Zr: 1 ppm; Nb: 1 ppm; V: 3 ppm; Cr: 2 ppm; Co: 2 ppm; Ni: 5 ppm; Cu: 2 ppm; Zn: 1 ppm; Ba: 3 ppm.

7.1.1 MAJOR ELEMENT RESULTS

The major element classification of the rock types from the study area was achieved using selected oxide ternary plots in conjunction with plots of CIPW normative data. The CIPW normative calculations were done on a 3803 IBM mainframe computer using a programme written by Prof. T. S. McCarthy and Mr. D. G. Jeffery at the University of the Witwatersrand. The major element results, as well as the trace element results (to be dealt with in a following section), were considered when chemically classifying these samples according to rock types. The sample material available for analysis was often of a highly weathered nature. High Fe_2O_3/FeO ratios, high H_2O and high CO_2 (Appendix A) contents revealed the degrees of weathering. This effected the results to some extent; however, most of the 39 samples analyzed gave reasonable results as shown by the Totals in Appendix A.

Oxide ternary diagrams

Two different ternary diagrams, Fe_2O_3-MgO-Al_2O_3 and K_2O-CaO-Na_2O, are shown in Figures 7.1a and 7.1b, respectively. These figures represent the total variability of the samples collected from the crater and its environs. Three selected samples from the Pienaars River Alkaline Complex (specifically the Koodeplaat Complex), which are petrologically similar to the crater samples, are also included in these two figures. Petrographic descriptions of these three samples (R6-fine grained feldspathoid syenite/foyaite; R8A-feldspathoidal microsyenite and R9-carbonate "lamprophyre") are given in Chapter 6.

In both figures the different rock types exhibit various compositions, with trachyte

showing the greatest variation. This has been attributed to the highly variable degrees of alteration of particularly the trachyte sample group. The fields for less weathered lamprophyre, carbonatite, granite, and granite breccia show considerably less variation. Figure 7.1a, the Fe_2O_3-MgO-Al_2O_3 plot, exhibits a characteristic of the granite breccias, which was noted during petrographic analysis: they are all enriched in iron with respect to the original granitic composition. Figure 7.1b, the K_2O-CaO-Na_2O plot, shows similar results to those of Figure 7.1a, with the exception of one point which falls outside its field, namely lamprophyre sample 21-I(3). This is again believed to be the result of alteration.

Lamprophyre samples were plotted on the total alkali-silica (TAS) diagram after Le Bas et al. (1986). Figure 7.2 shows that the alkaline lamprophyres typically plot in the foidite and tephrite/basanite fields (Rock, 1991). In this diagram, several data for samples from the Greenview lamprophyric vent (McNerney et al., 1992) are also represented. This body is part of the Pienaars River Alkaline Complex and occurs approximately 12 kilometres to the south of the Roodeplaat Complex (Figure 3.2). The Greenview lamprophyre data show significantly more scatter than the lamprophyres from this study, but a definite similarity with regard to total alkali-silica contents exists for samples from these two studies. Although some samples, including sample 21-I(3) from the crater environs, plot into the trachybasalt field, these data, as suggested by McNerney et al. (1992), may reflect secondary enrichment in SiO_2. This type of enrichment was also noted in altered trachyte samples, which will be shown in the following section dealing with CIPW-normative diagrams. A further correlation between the different studies may be seen in the CaO versus MgO plot for the same sample suite (Figure 7.3). These samples all have similar compositions to the alkaline lamprophyre field defined by Rock (1991), which has CaO at 10 wt% (average) and MgO at 4 to 10 wt%.

Although the Pienaars River Alkaline Complex samples do not always coincide exactly with the fields obtained for the crater samples and those from the crater environs, they appear to be quite similar, indicating possibly a common source or genetic relationship for all the studied samples and the Pienaars River Alkaline Complex.

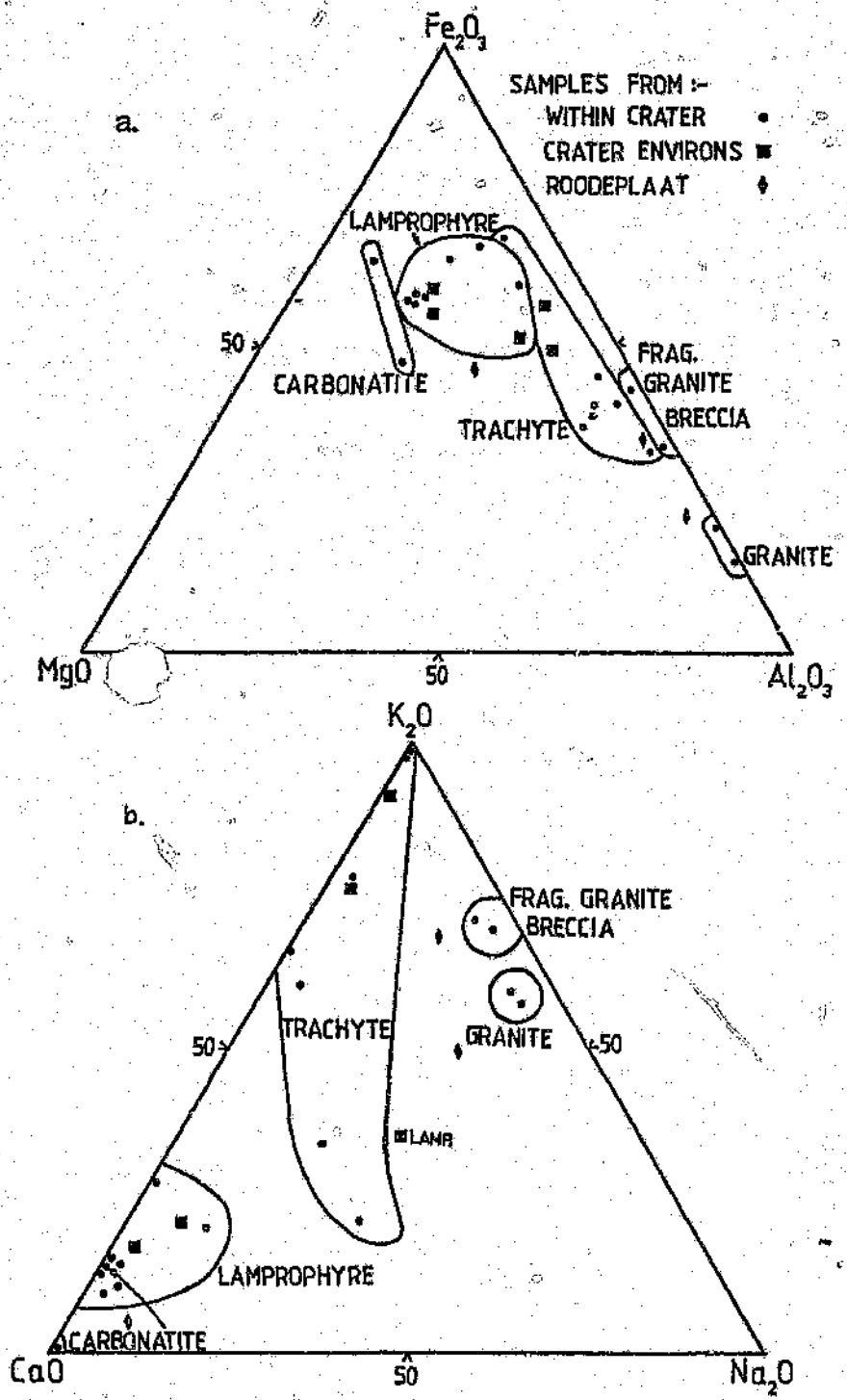

Figure 7.1 Ternary diagrams: (a) (Fe_2O_3-MgO-Al_2O_3) and (b) (K_2O-CaO-Na_2O), representing the major element compositions of all samples analysed from the Pretoria Saltpan crater, with selected samples from the Roodeplaat Complex.

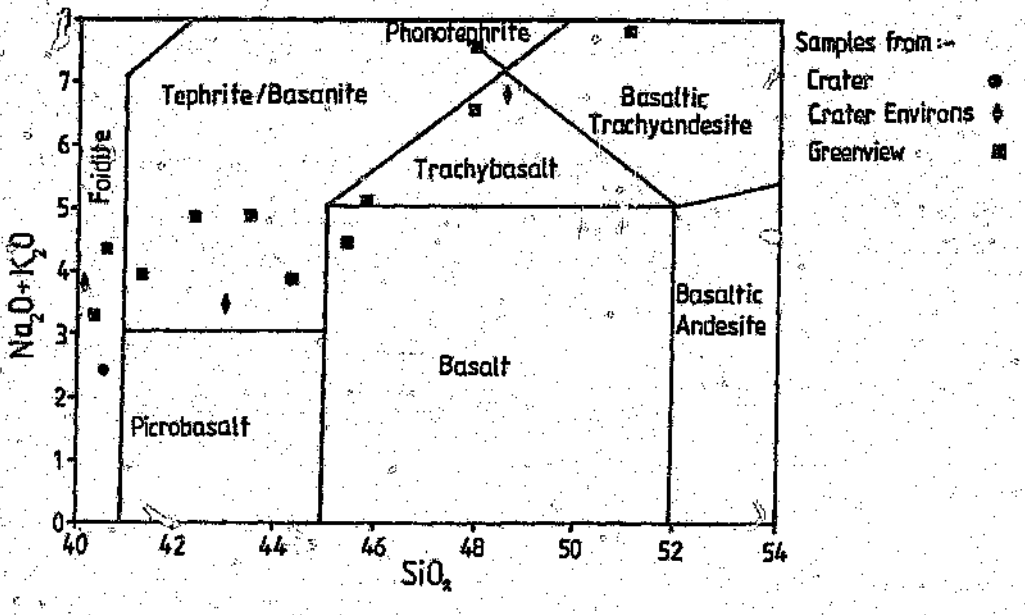

Figure 7.2 Total alkali-silica (TAS) diagram after Le Bas et al. (1986). Note that the alkaline lamprophyres typically plot in the foidite and tephrite/basanite fields (Rock, 1991). Greenview data were taken from a study of the Greenview lamprophyric breccia vent (McNerney et al., 1992), which forms part of the Pienaars River Alkaline Complex.

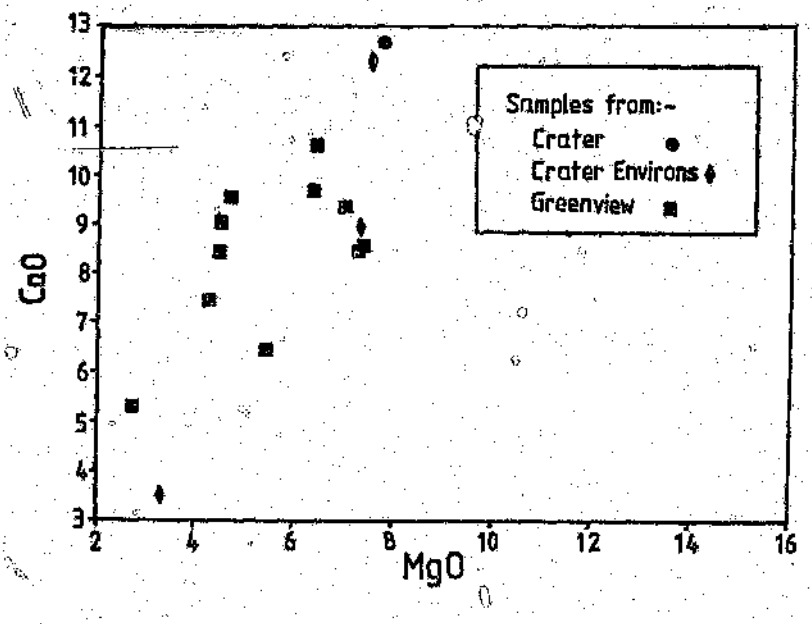

Figure 7.3 CaO versus MgO plot of the Greenview data (McNerney et al., 1992) and data from this study.

CIPW-normative diagrams

Figures 7.4a and 7.4b show CIPW-normative plots for the analysed samples, again in comparison to Roodeplaat and Greenview data. Five chemically different fields can be recognised, that is, trachyte, lamprophyre, carbonatite, granite and granite breccia fields. Optical mineralogy confirmed that the mineralogy predicted by the CIPW-normative plot was correct.

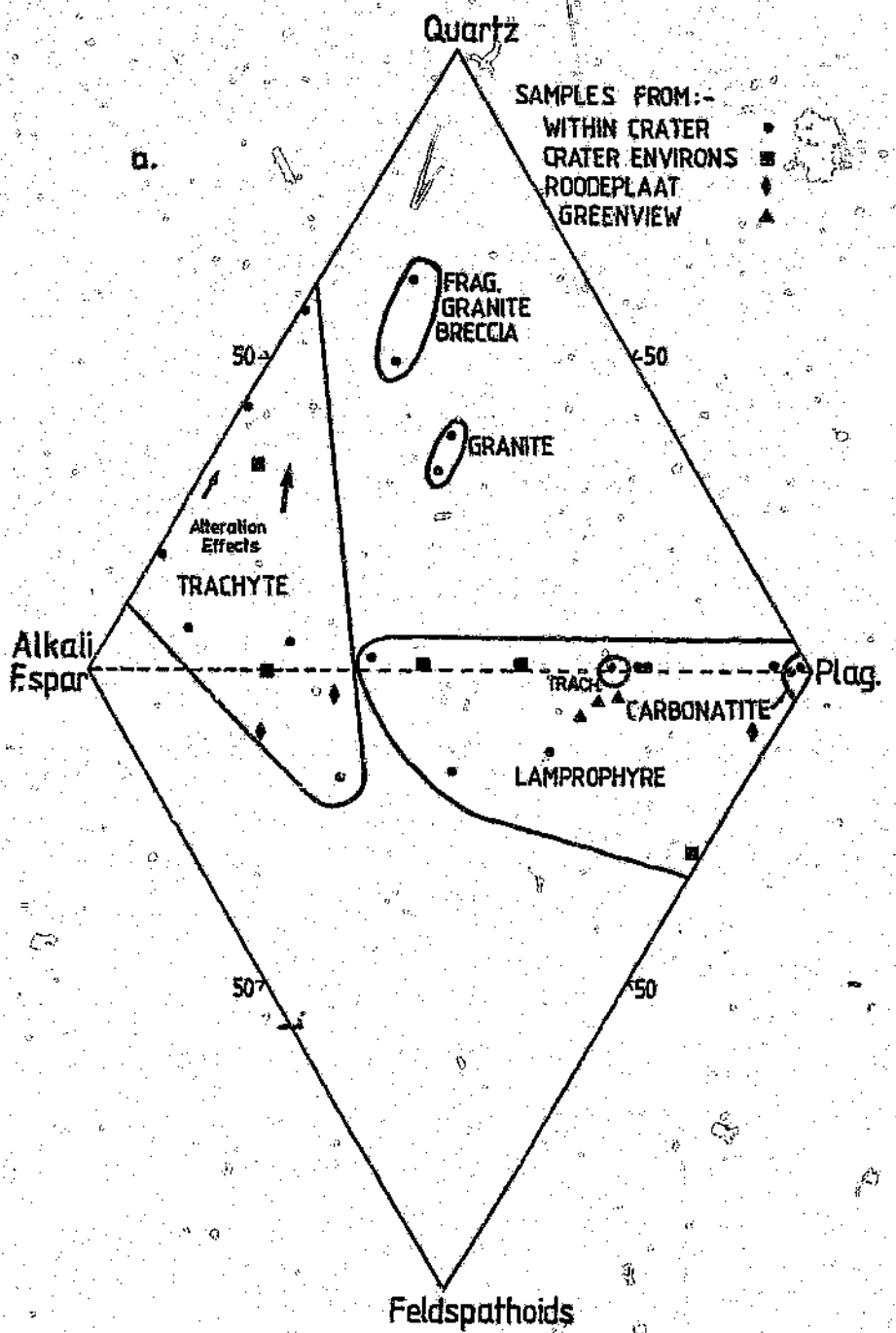

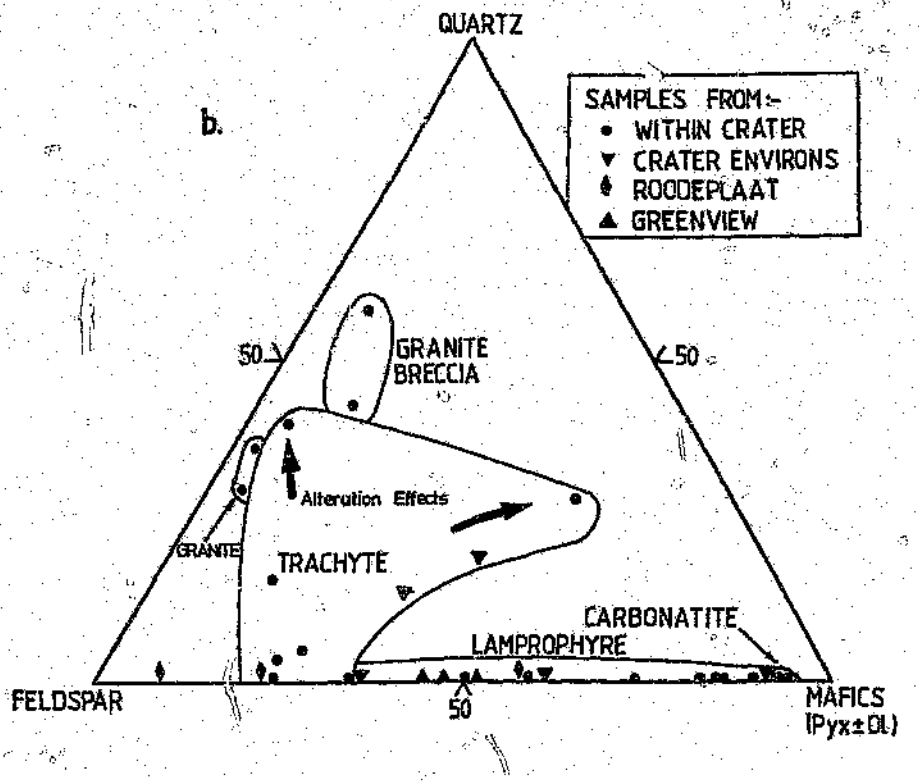

Figure 7.4 CIPW-normative mineralogy of different lithologies from the Pretoria Saltpan crater and environs, together with selected Roodeplaat and Greenview (McNerney et al., 1992) samples: (a) normative quartz-plagioclase-orthoclase-feldspathoid abundances; (b) normative quartz-feldspar-pyroxene (±olivine) abundances.

Both figures show that the granite breccias are more quartz-normative than the original unaltered granite. This result is indicative of an increase in silica due to remobilization and concentration of silica along fracture planes and in voids which were produced during brecciation. Trachyte, showing the largest scatter and the greatest variation in alteration degrees of all the rock types analysed, exhibits an increase in silica, and hence quartz content with increasing alteration. This is seen in both Figures 7.4a and 7.4b. The apparent availability of silica may be attributed to the abundance of quartz-rich granite which comprises the country rock and in all cases the host rock to breccia. Thus the same fluids which are responsible for the alteration of trachyte and granite were SiO_2-enriched.

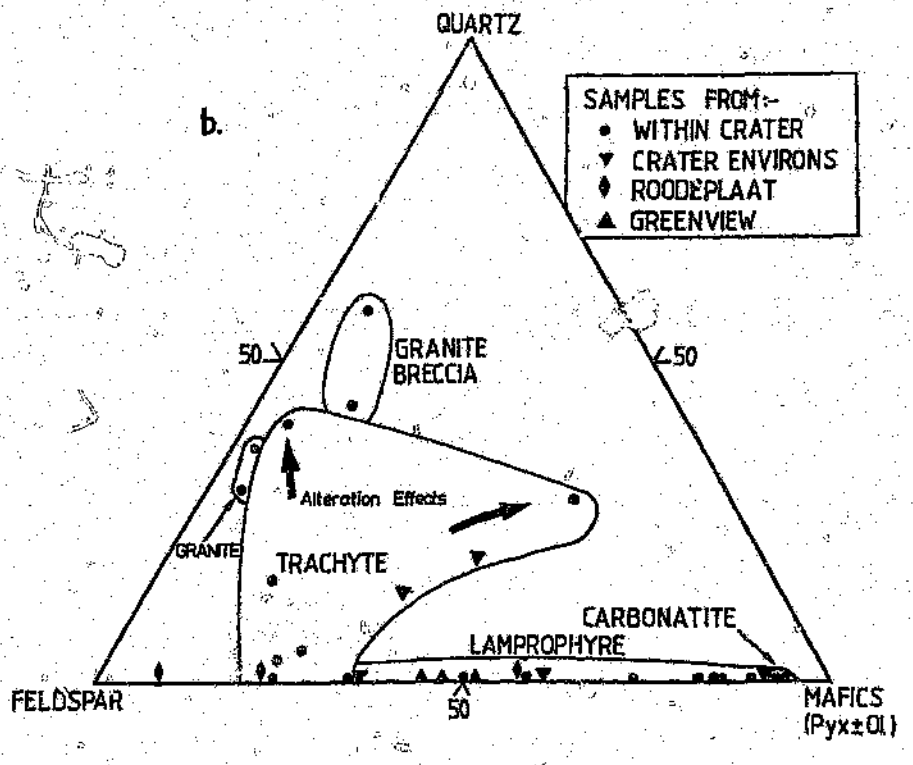

Figure 7.4 CIPW-normative mineralogy of different lithologies from the Pretoria Saltpan crater and environs, together with selected Roodeplaat and Greenview (McNerney et al., 1992) samples: **(a)** normative quartz-plagioclase-orthoclase-feldspathoid abundances; **(b)** normative quartz-feldspar-pyroxene (±olivine) abundances.

Both figures show that the granite breccias are more quartz-normative than the original unaltered granite. This result is indicative of an increase in silica due to remobilization and concentration of silica along fracture planes and in voids which were produced during brecciation. Trachyte, showing the largest scatter and the greatest variation in alteration degrees of all the rock types analysed, exhibits an increase in silica, and hence quartz content with increasing alteration. This is seen in both Figures 7.4a and 7.4b. The apparent availability of silica may be attributed to the abundance of quartz-rich granite which comprises the country rock and in all cases the host rock to breccia. Thus the same fluids which are responsible for the alteration of trachyte and granite were SiO_2-enriched.

The lamprophyres are typically silica-deficient and show varying feldspar/mafic ratios (Figure 7.4b) and varying plagioclase/potassic feldspar ratios (Figure 7.4a). The carbonatites apparently are rich in mafic minerals, however, this does not represent the true mineralogical composition and is rather a consequence of the low feldspar and quartz abundances.

7.1.2 TRACE ELEMENT RESULTS

Trace elements in lamprophyre samples

The range of trace elements for lamprophyre samples collected within the crater is shown in Figure 7.5. Superimposed on this range are the trace element patterns of selected samples from the crater environs, as well as a strongly altered Pienaars River Alkaline Complex sample (R9), which is thought, on petrographic grounds, to have originally been a lamprophyre. Also on this range are typical trace element abundances of Greenview lamprophyre samples after McNerney et al. (1992).

This diagram reflects the similarity of the distribution patterns of the crater samples and the samples from the crater environs and from the Pienaars River Alkaline Complex, with the exception of only a few aberrant data points. These results are strongly suggestive of a common source for the crater rim lamprophyres and the lamprophyre samples of the surrounding terrain, when compared against the total possible variation in lamprophyres studied by Rock (1991) from different sources. The variations seen in the crater sample range, for example for Sr, may be attributed to alteration processes or minor variations within the parent magma body.

Trace elements in trachyte samples

The range of trace element abundances for the crater trachyte samples is shown in Figure 7.6. Data for two samples from the crater environs and two samples from the Pienaars River Alkaline Complex are superimposed on this range. As in the case of the lamprophyres, the distribution patterns of all these samples are quite similar.

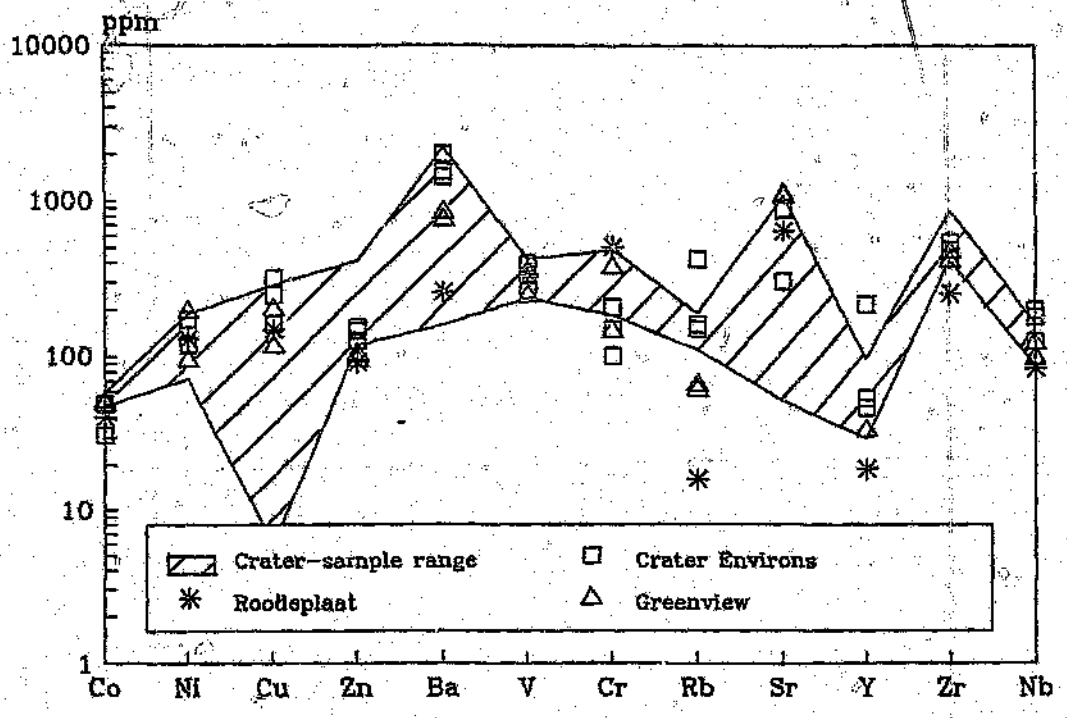

Figure 7.5 Trace element contents of selected lamprophyre samples, superimposed on the range of crater rim lamprophyre samples.

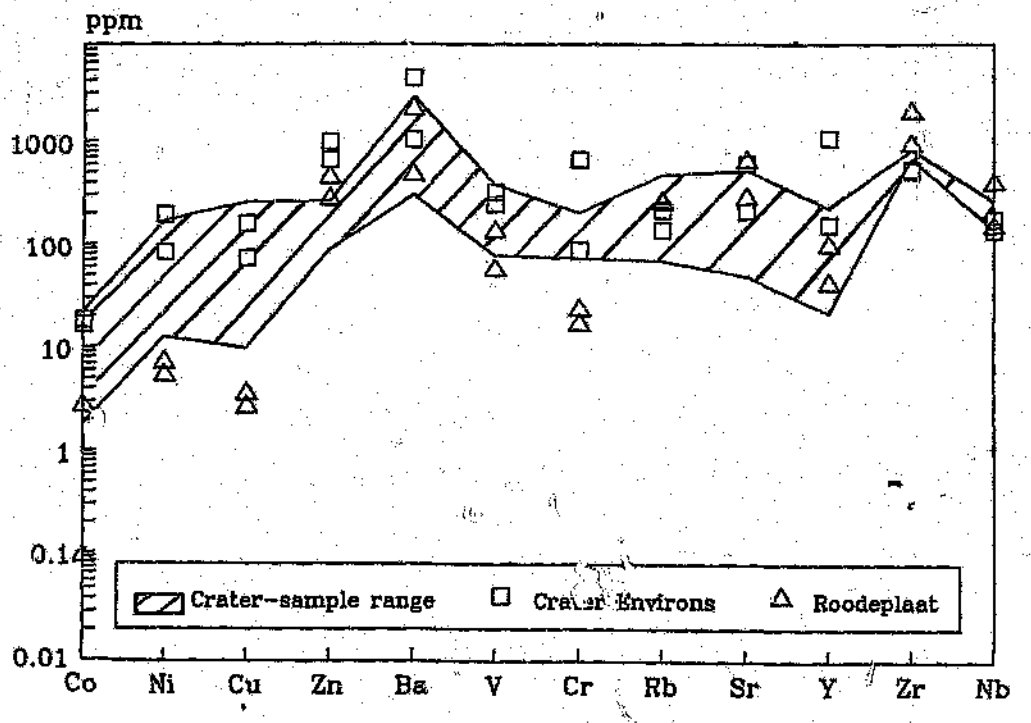

Figure 7.6 Trachyte trace elements of selected samples superimposed on a range of crater rim trachyte samples.

Trace elements in carbonatite samples

Only two carbonatites from the crater itself were analysed. Carbonatites were not found in the crater environs, most likely due to a lack of outcrop in this entire region. Also, carbonatites are very susceptible to surface weathering and would not be expected to form prominent outcrop. Thus no trace element data from any regional carbonatites could be compared to those of the crater carbonatites. The trace element variation for the two carbonatites is shown in Figure 7.7. The basic trend of trace elements is similar for these two samples, but no attempt should be made at diagnosing the differences in the results for the two samples, as one carbonatite sample is significantly more altered (Sample 107) than the other.

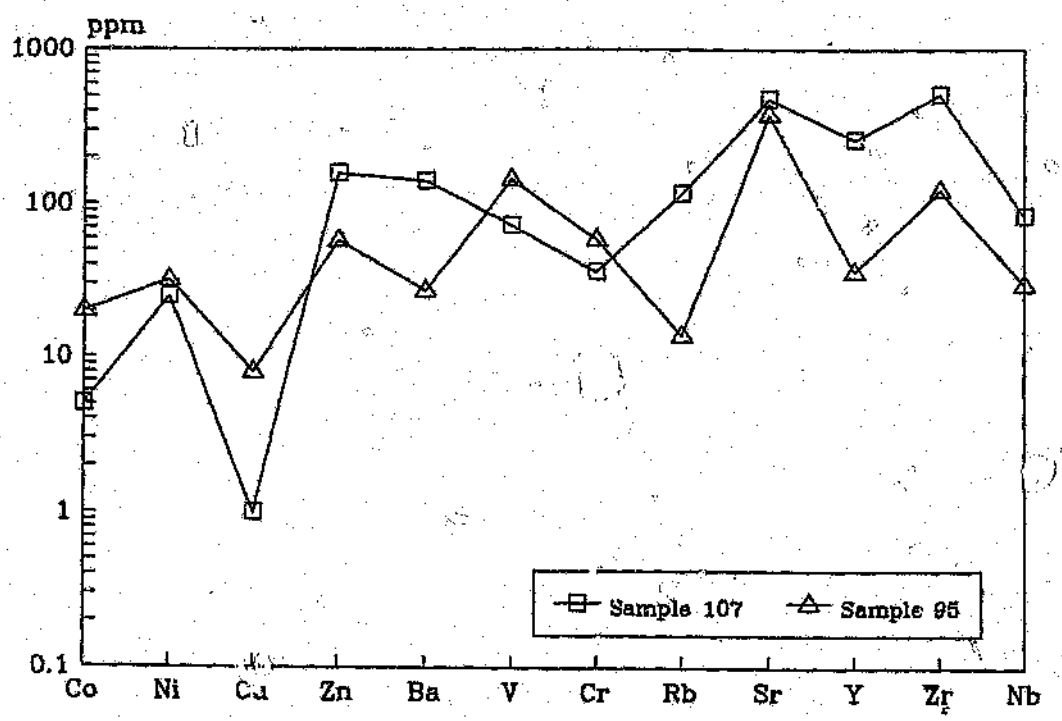

Figure 7.7 Plot of trace elements for the two crater rim carbonatites.

7.1.3 ELECTRON MICROPROBE RESULTS

Pyroxene compositions of selected unaltered lamprophyre samples collected within the

crater and in the crater environs were determined by electron microprobe analysis. The data were obtained with a Camebax 355 Microprobe (at 15 kV acceleration voltage and a current of 14nA on brass) at the Rand Afrikaans University, Johannesburg. The results are tabulated in Appendix B. Only the lamprophyres contained fresh, unaltered pyroxenes, so that this study had to be restricted to this rock type. Figure 7.8 shows compositions of pyroxenes from lamprophyre samples found both within the crater and in the surrounding country-side. Each point represents an average of five analyses, usually taken from 2 to 3 pyroxene crystals in each sample. It was found that the pyroxenes used for this study were fairly homogeneous and not zoned. Figure 7.8 shows a good similarity of compositions for all the pyroxenes analyzed. It should be noted that Wallace (1979) obtained very similar results for the rocks from the Saltpan crater that he called augitites, which are believed to be equivalent to the lamprophyres of this study.

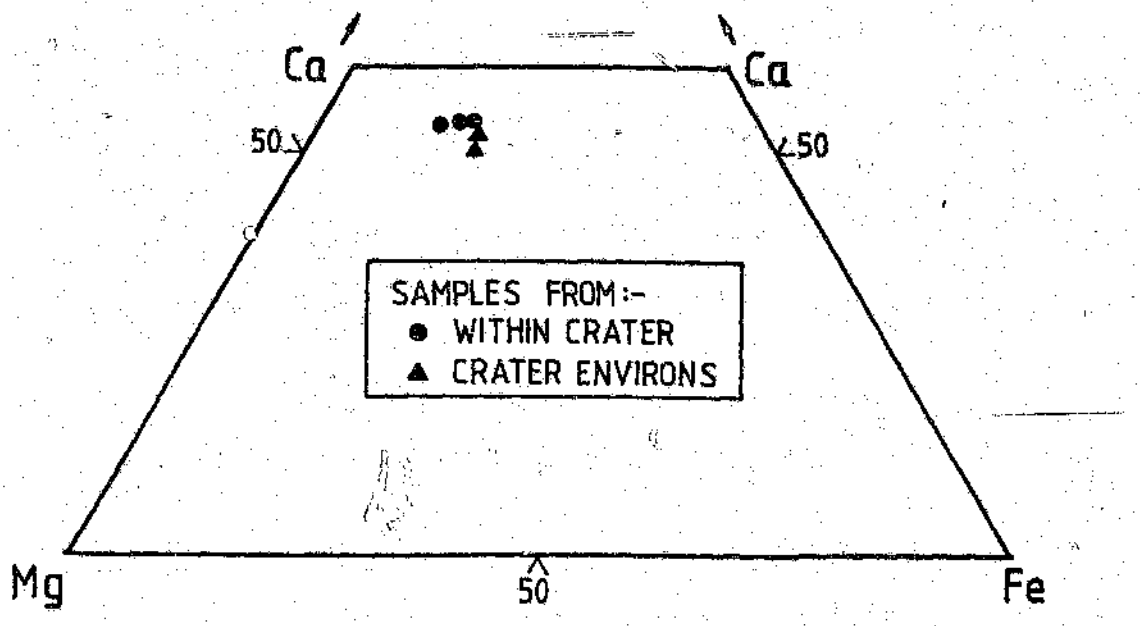

Figure 7.8 Pyroxene compositions of lamprophyre samples from the Pretoria Saltpan crater and its environs.

These results further support the assumption that all the lamprophyre samples collected from within and from the region outside the crater have a common source. The trachytes were generally very altered, but the microprobe results did confirm that the pyroxenes, identified in the trachytes using optical methods, were in fact of an aegirine-augite

composition.

7.2 RESULTS OF INSTRUMENTAL NEUTRON ACTIVATION ANALYSIS

Selected samples from the crater and its environs were analyzed by instrumental neutron activation analysis following the technique described by Koeberl et al. (1987) and Koeberl (1993). The results are presented in Appendix D. These analyses were kindly provided by Prof. C. Koeberl, Institute of Geochemistry, University of Vienna. The samples used in this analysis were chosen as they were extremely altered, and positive identification using other methods, such as major element chemistry and petrographical analysis was unsatisfactory. Many of the results (Appendix D) are therefore probably not typical (but probably approximate) values for well preserved and unaltered samples of these rock types. Differences in abundances for crater rim and crater environ samples may be attributed to this. The results obtained by INAA (Appendix D) frequently confirm the results obtained by X-ray fluorescence techniques (Appendix C), as is shown, for example, by the Sr values of Sample 95 (379 ppm using XRF, and 387 ppm using INAA techniques).

7.2.1 RARE EARTH ELEMENT DATA

Figures 7.9a through 7.9c present C1-normalized rare earth element patterns for (a) lamprophyres from the crater rim, the crater environs, an average alkaline lamprophyre, and an average ultramafic lamprophyre (Rock, 1991); (b) trachytes from the crater rim and a Roodeplaat feldspathoidal microsyenite; (c) two crater rim carbonatites superimposed on a range of typical carbonatite values (Cullers and Graf, 1984). The Roodeplaat sample was included for comparison, as the major element abundances and the mineralogical compositions are similar to those of the trachytes from the study area.

The three figures show three distinct rare earth element patterns. The crater rim lamprophyres (Figure 7.9a) have strikingly similar abundances for most elements, when compared to the two average lamprophyre patterns (Rock, 1991), and to the patterns of samples from the crater environs. As the analyzed samples were all weathered to various

degrees, some of the discrepancies between individual patterns may well be attributed to this. As in the case of other elements, the rare earth element abundances may indicate a common source for the crater rim lamprophyres and the lamprophyres from the crater environs.

The two crater rim trachytes (Figure 7.9b), which are also extremely altered, have very similar light rare earth element (LREE) abundances, but deviate from each other from Gd onwards. Sample SP-22, the more weathered of the two, is more enriched in heavy rare earth elements (HREE). The Roodeplaat sample (R8A) has a very similar pattern to sample SP-76 (the less weathered crater rim sample), but is relatively strongly enriched in La and Ce.

The two crater rim carbonatites (Figure 7.9c) exhibit similar patterns, but sample SP-107 (the weathered sample) is enriched by several orders of magnitude throughout the spectrum of REEs. Superimposed on this figure is a typical range of REE contents found in carbonatites that contain no Ce anomalies (Cullers and Graf, 1984). The crater rim carbonatites do not match this field; this may be attributed to the fact that carbonatites have the highest REE contents of any rock type and in the light of total variability observed, individual samples may well lie outside this field (Cullers and Graf, 1984).

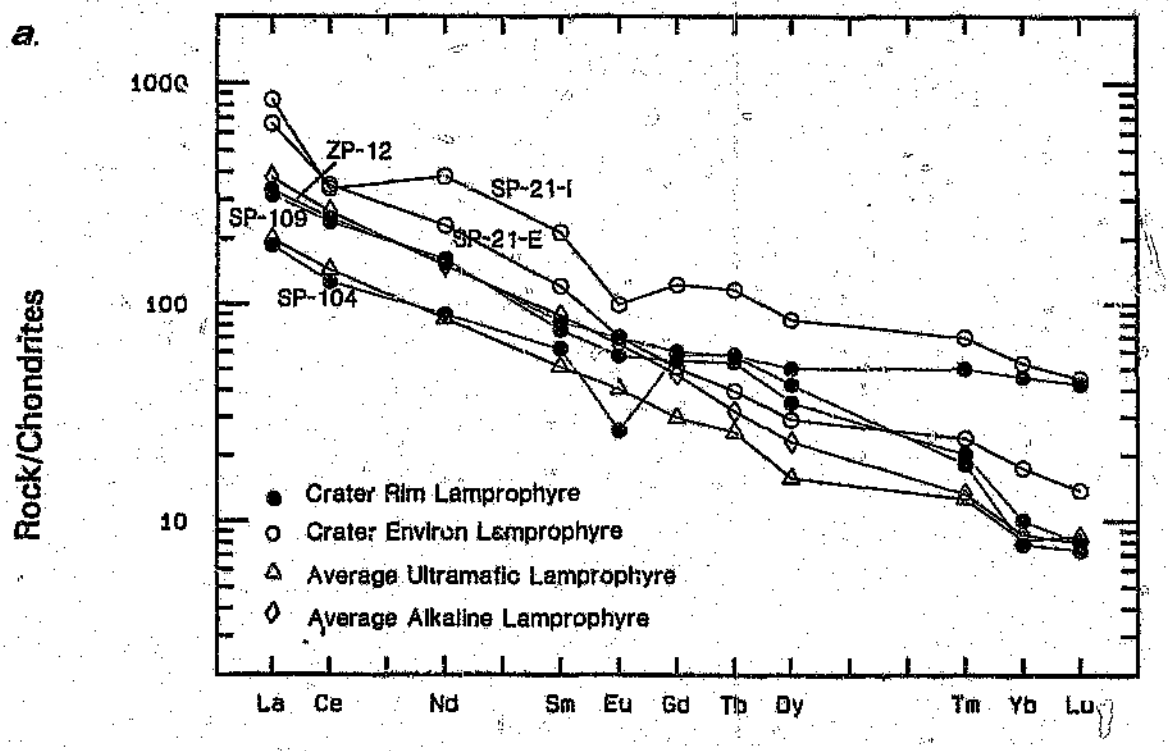

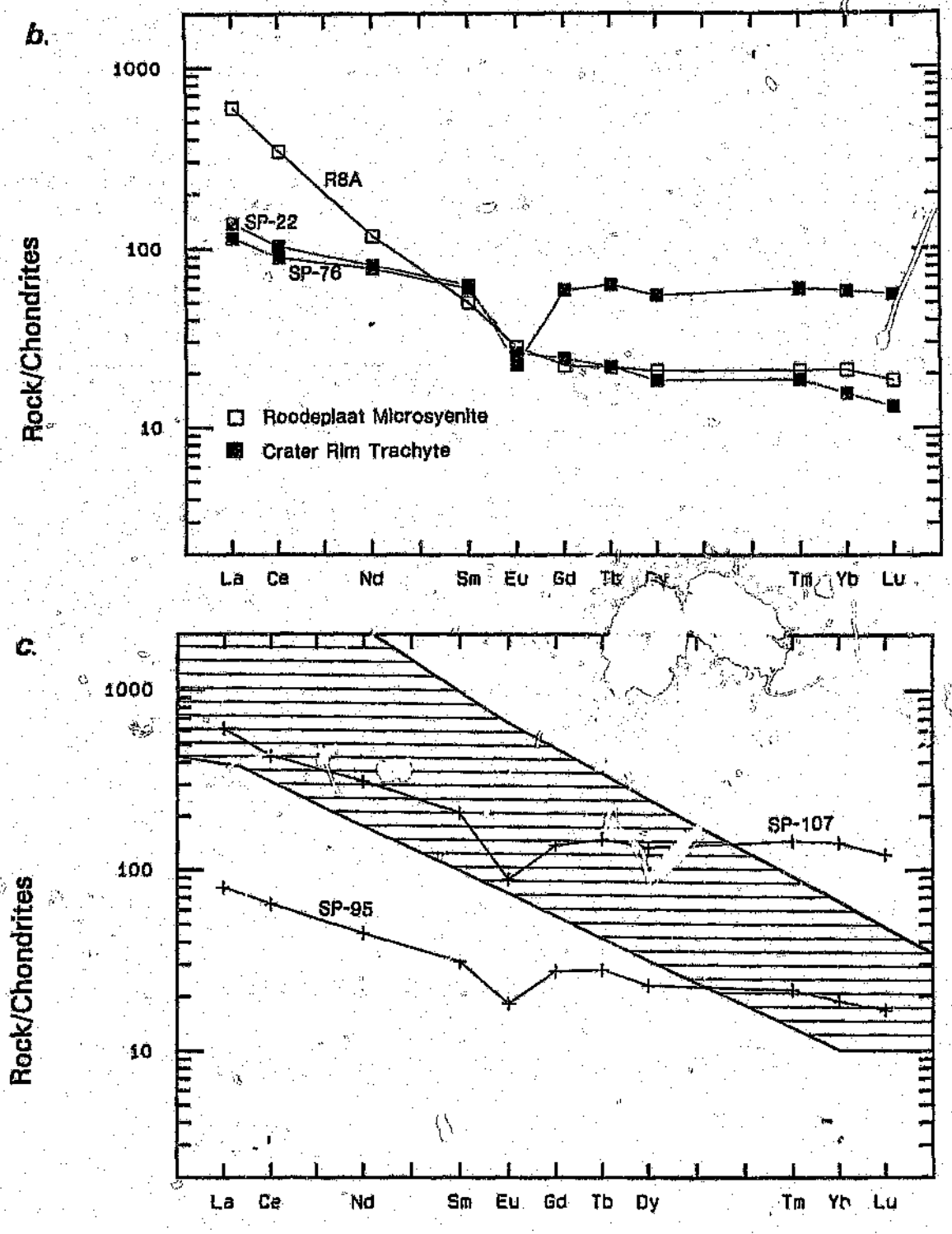

Figure 7.9 C1-normalized REE abundances for (a) lamprophyres, (b) trachytes, and (c) carbonatites (shaded area represents a typical range of REE contents found in carbonatites that contain no Ce anomalies (Cullers and Graf, 1984)). Normalization factors used for all three figures are after Nakamura (1974).

7.2.2 OTHER LITHOPHILE AND SIDEROPHILE ELEMENT DATA

Distribution patterns for selected lithophile elements in the analyzed lamprophyre, trachyte, and carbonatite samples are presented in Figures 7.10a-c, respectively. Each diagram reflects some degree of homogeneity of element abundances within each rock type. Figure 7.10a shows the similarity of element abundances (with the exception of a few elements) in the crater rim lamprophyres and corresponding samples from the crater environs. This particular result again suggests that the lamprophyres from the crater rim are likely to be part of a more regional magmatic event.

Trace element abundances were determined for bulk breccia and glass fragments from the drill-core by Koeberl et al. (1994a). Enrichments of Cr, Co, Ni, and Ir (values as high as 290 ppm, 625 ppm, 1200 ppm, 100 ppb respectively; compare values obtained for volcanic intrusives: Appendix D) were determined for glasses or sulphide spherules, and somewhat lower abundances for the bulk breccias. These enrichments were attributed to a meteoritic contribution, but previous mixing relationships (Reimold and Koeberl, 1992) could not explain simultaneous enrichments observed in Mg and Fe. Koeberl et al. (1994a) have explained these abundances by a chondritic contribution rather than from an iron meteorite which would not account for the enrichments in Mg and Cr. The lower Cr, Co, Ni, and Ir values of the alkaline and ultra-mafic intrusives from this study, against the values cited by Reimold and Koeberl (1992), clearly favours a meteoritic contribution rather than an intrusive contribution.

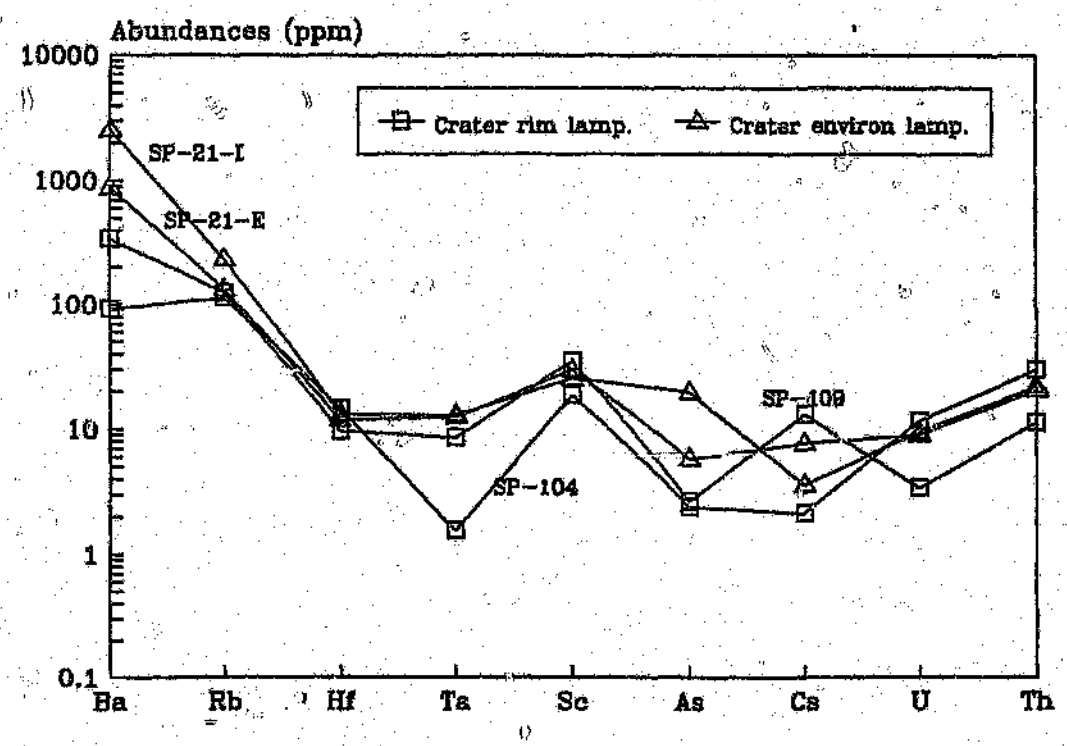

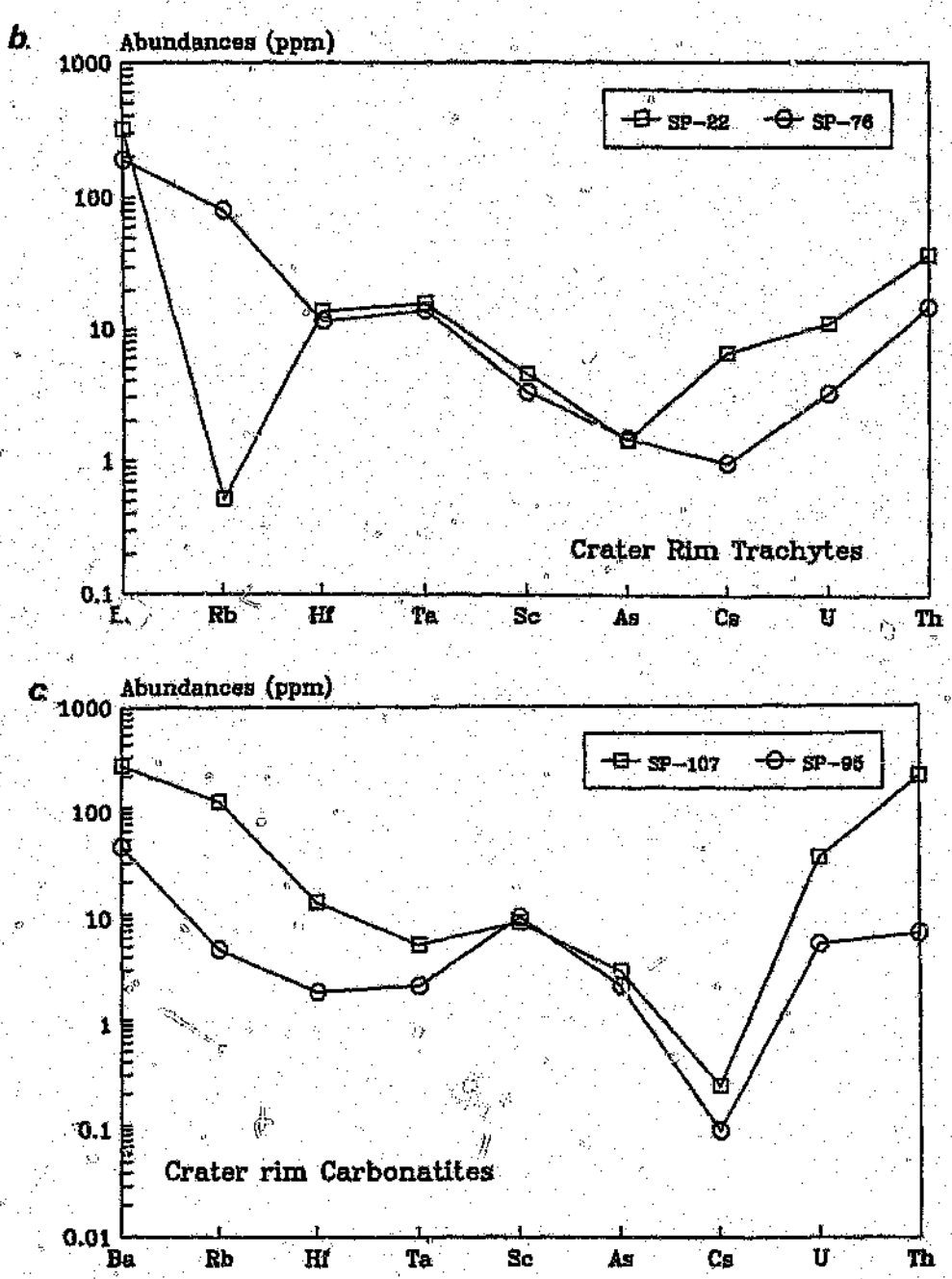

Figure 7.10 Abundances of selected lithophile elements, as determined by Instrumental Neutron Activation Analysis, in (a) lamprophyres, (b) trachytes, and (c) carbonatites.

Rb-Sr dating was carried out on the phonolite sample from the crater rim, one lamprophyre sample from the crater environs, and a peralkaline syenite from the Roodeplaat Complex, as only limited chronological data was available for this rock suite. In addition to obtaining a reliable age for the rocks, a comparative study involving the three areas, that is, the crater, the crater environs, and the Roodeplaat Complex, could possibly relate these rocks, which have been shown to be mineralogically and chemically similar (Chapters 6 and 7), chronologically too.

Summary of previous chronological data relevant for this study

Many chronological data have been obtained in the past for samples from the Pienaars River Alkaline Complex, which forms an integral part of the study region. Some of these results are summarized in Table 8.1, together with the ages previously determined for various intrusives from the crater rim. From these results it is evident that all intrusives from the crater and the Pienaars River Alkaline Complex were intruded around the same period and may all be part of the same igneous event at about 1.3 Ga ago. The exception to this age are the fission track data obtained by Milton and Naeser (1971) for a crater carbonatite (see Table 8.1 for their results). They showed that fission tracks in zircon may be erased in a period of days at 600°C, the approximate crystallisation temperature of carbonatite (Wyllie, 1966), but suffer no loss in geological time at temperatures below about 350°C. Tracks in apatite would be erased in a few seconds at 600°C and would show some loss in 100 Ma at temperatures as low as 75°C, indicating that the zircon date should be that of crystallisation of the carbonatite magma. The apatite date was interpreted by Milton and Naeser (1971) as presumably reflecting the time when uplift and/or erosion brought the carbonatite to within a few kilometres of the surface.

Two different studies yielded good chronological data for the Saltpan cratering event (Table 8.2). Partridge et al. (1993) carried out ^{14}C age determinations on algal debris from the upper 20 metres of the core sediments. The results obtained indicated a mean sedimentation rate of about 1 metre/2000 years and an age of approximately 200 ka for

the lowermost crater-fill sediments. A very similar age of 220±52 ka was obtained by Storzer et al. (1993), who studied glass fragments, recovered from the core, for fission tracks. These relatively young ages for the cratering event (Table 8.2) are in excellent agreement with the preserved state of the crater. Clearly the crater age is quite different from that of the alkaline and ultramafic intrusives in the general region. Nevertheless, there are still sceptics that relate the Saltpan cratering event to the igneous activity that occurred in the region around the crater.

Rock Unit/Sample	Age in Ma	Type of Determination	Source
Pilanesberg Complex	1250±60	K-Ar, biotite	Snelling (1963)
Leeuwfontein	1420±70	U-Pb, zircon	Oosthyzen & Burger (1964)
Crater Carbonatite	600±90, 1900±400	Fission Track, apatite Fission track, zircon	Milton and Naeser (1971)
8 Pienaars River Alkaline Complex Samples	1300-1430	Rb-Sr, zircon	Harmer (1985)
Crater Lamprophyre	1360	K-Ar, biotite	Partridge et al. (1990)
Crater Lamprophyre	1459±22	Rb-Sr, biotite	Walraven, (unpubl): see Appendix B.

Table 8.1 Age data on alkaline volcanic rocks from the crater and the Pienaars River Alkaline Complex.

Sample	Age in Thousands of Years	Type of Determination	Source
Drill core sediments	±200	^{14}C and sedimentation rate extrapolation	Partridge et al., (1993)
Glass fragments from drill core	220±52	Fission track	Storzer et al., (1993)

Table 8.2 Age data for the cratering event

Rb-Sr Dating: this study

As only limited chronological data obtained on intrusives from the immediate crater area are available, it was found that additional dating of intrusives from the crater and of previously unstudied samples from the crater environs would provide further information on the ages of intrusives from the entire study area, and could perhaps settle the remaining argument about the relationship between the cratering event and the igneous events. Consequently, a number of specimens from the crater area and environs were dated by the Rb-Sr isotope method (e.g., Faure, 1977).

Analytical Procedures

Chronological analysis was carried out in the Isotope Research Unit of the Bernard Price Institute for Geophysical Research at the University of the Witwatersrand. The analytical methods used for this study are essentially those described by Smith et al. (1985) and Brown et al. (1989). The samples, comprising a crater rim trachyte, a lamprophyre from the crater environs, and a Roodeplaat peralkaline syenite were crushed and sieved to obtain 250-500 and 100-250 micron size fractions. The sieved fractions were cleaned in analytical grade alcohol and distilled water. Biotite, hornblende, plagioclase and clinopyroxene separates were prepared by handpicking, in order to obtain the most suitable and least weathered material for isotopic analysis. Impurities in 9 mineral separates and 3 whole rock samples were removed first by leaching in 1N HCl and then by handsorting under a binocular microscope. Separates ranging in weight from 5 milligrams to 100 milligrams were dissolved in a purified combined HF and HNO_3 solution after addition of ^{84}Sr and ^{87}Rb spike tracer solutions. The teflon beakers containing the samples were covered and heated on hot plates for 2 to 3 days. The cover slips were then removed allowing the remaining acid to dry. The dried samples were re-dissolved in 6N HCl to insure complete dissolution of samples and mixing between sample and tracer. The samples were dried and then taken into either a purified 2.15N or a 2.59N HCl solution. These solutions were passed through ion exchange columns filled with 50W-X8 Dowex resin to separate Rb and Sr fractions. Two total method blanks were measured, the results of which never exceeded a few nanograms for Rb (< 0.5 ng) or Sr (< 8.5 ng). These contributions are insignificant with respect to Rb and Sr

concentrations in these samples (Table 8.3) and therefore blank corrections were not applied.

A single-collector Micromass 30 mass spectrometer and a multiple collector VG354 mass spectrometer were used to analyze Rb and Sr isotopic concentrations, respectively. Uncertainty estimates are 0.6, 1.5, 1.6 and 0.02 relative percent on Rb concentrations, Sr concentrations, $^{87}Rb/^{86}Sr$ ratios and $^{87}Sr/^{86}Sr$ ratios, respectively (Smith et al., 1985). The $^{87}Sr/^{86}Sr$ ratios were normalized to $^{88}Sr/^{86}Sr = 8.375$. The average $^{87}Sr/^{86}Sr$ ratio determined for the E&A standard is 0.70800 ± 4 (1σ standard deviation for 81 analyses since 1989), and for the SRM987 standard it is 0.71022 ± 3 (1σ standard deviation for 59 analyses since 1988). Accuracy for concentration determinations has been monitored by periodic analysis of feldspar standard SRM607. Also, tracer solution calibrations have been monitored with in-house gravimetric standards. The processing and regression of the Rb-Sr isotopic data was carried out using the "GEODATE" version 2.2 package developed by Egglington and Harmer (1991), applying the decay constant of $1.42 \times 10^{-11} y^{-1}$.

Results

Table 8.3 shows the Rb and Sr concentrations, as well as the $^{87}Rb/^{86}Sr$ and $^{87}Sr/^{86}Sr$ ratios obtained for all analyzed samples. The data are presented in Figures 8.1 and 8.2. All three rock types were altered to some extent. This is evident from the scatter of points at the lower end of the data spread (see Figure 8.2), indicating some degree of open system behaviour for Sr. Using all these points together does not yield an isochron. Therefore, in order to get a reasonable lower constraint and hence a better chance to obtain an isochron, various combinations of these samples were tried in data regression. Considering the data closest to the intercept, inclusion of a pyroxene (Cpx-9), a plagioclase (Plag-6) and two hornblende (Hld-4 and Hld-5) data could be used to constrain the lower end of a possible isochron. The other lower end data, that is, those of the three whole rock samples (WR-R3, WR-40, WR-21-E) had to be excluded, as their inclusion did not result in isochron definition. This is attributed to the fact that the rocks are fairly altered. The initial ratio of 0.7026 is controlled by the clinopyroxene (Cpx-9) and the hornblende (Hld-4), and is similar to values for megacrysts in the 1180 Ma Premier kimberlite (Smith, 1983). According to Smith (1983) these rocks are of direct

mantle derivation, apparently from a source similar to that of the Pretoria area kimberlites.

Sample No. and type	Rb (ppm)	Sr (ppm)	$^{87}Rb/^{86}Sr$	$^{87}Sr/^{86}Sr$
1 Biotite: Roodeplaat syenite (R3)	406.9886	50.090	24.5950	1.1709
2 Biotite: Roodeplaat syenite (R3)	477.6769	44.010	33.3320	1.3376
3 Biotite: Roodeplaat syenite (R3)	485.6158	42.973	34.3360	1.2220
4 Hornblende: Roodeplaat syenite (R3)	14.9996	129.955	0.3341	0.7087
5 Hornblende: Roodeplaat syenite (R3)	9.5308	179.495	0.1535	0.7068
6 Plagioclase Roodeplaat syenite (R3)	23.4435	2264.743	0.0299	0.7045
7 Biotite: crater phonolite (40)	320.3680	35.150	27.6940	1.2229
8 Biotite: crater phonolite (40)	308.1291	38.654	24.0720	1.1557
9 Clinopyroxene: crater environ lamprophyre (21-E)	2.7023	235.697	0.0332	0.7034
R3 Whole-Rock: Roodeplaat syenite	73.0064	1592.010	0.1328	0.7065
40 Whole-Rock: crater phonolite	215.2740	679.535	0.9180	0.7258
21-E Whole-Rock: crater environ lamprophyre	142.0993	837.791	0.4908	0.7112

Table 8.3 Rb and Sr concentrations and isotopic ratios for samples analyzed in this study.

One biotite sample (3-Bio: see Figure 8.1), which was separated from 2-Bio by hand-shaking the paper it was placed on, was noticed to contain small fragments of chlorite which had broken off from the edges of the biotite, and was therefore excluded from all regressions. It was not expected to give reasonable results; however, due to the lack of other mineral separates available, it was included in the analysis on the off-chance that it would produce acceptable results. Other isochron ages were obtained using other lower end data combinations and four biotite data (that is, excluding the biotite Bio-3 values), and these results are listed in Table 8.4.

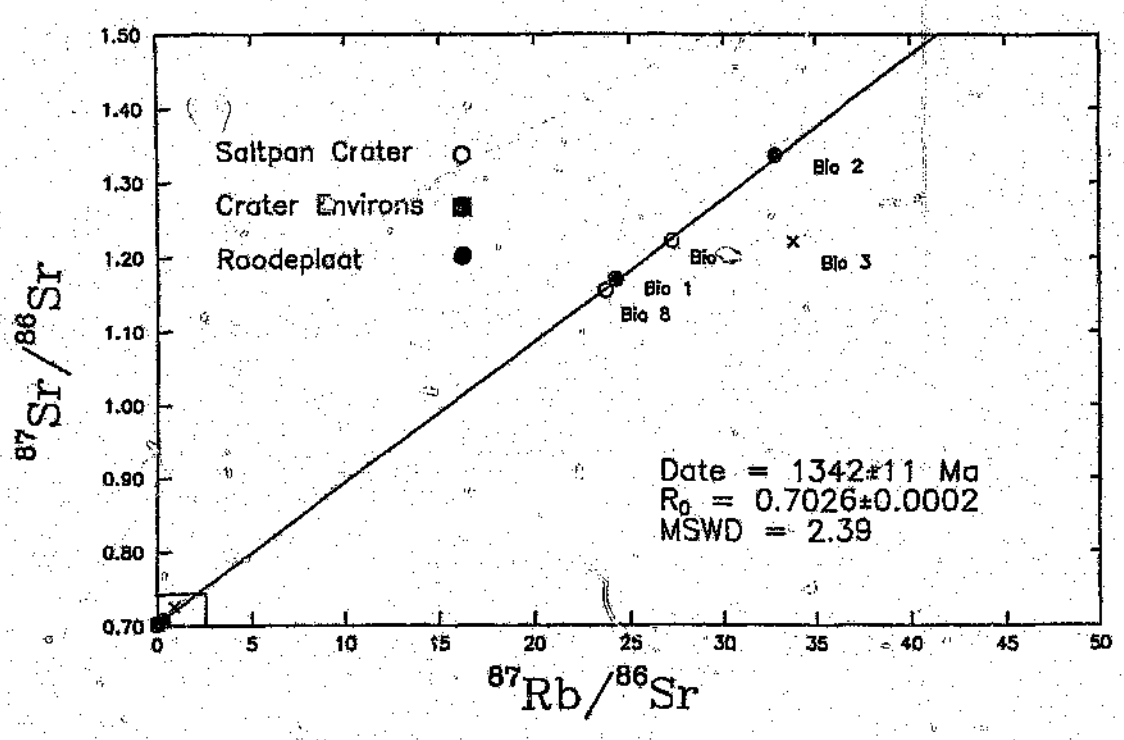

Figure 8.1 Isochron diagram for studied samples using Cpx 9 and Hld 4 as the lower limit constraints. Crosses indicate samples excluded for the calculation of these results. This combination gives the best fit isochron age.

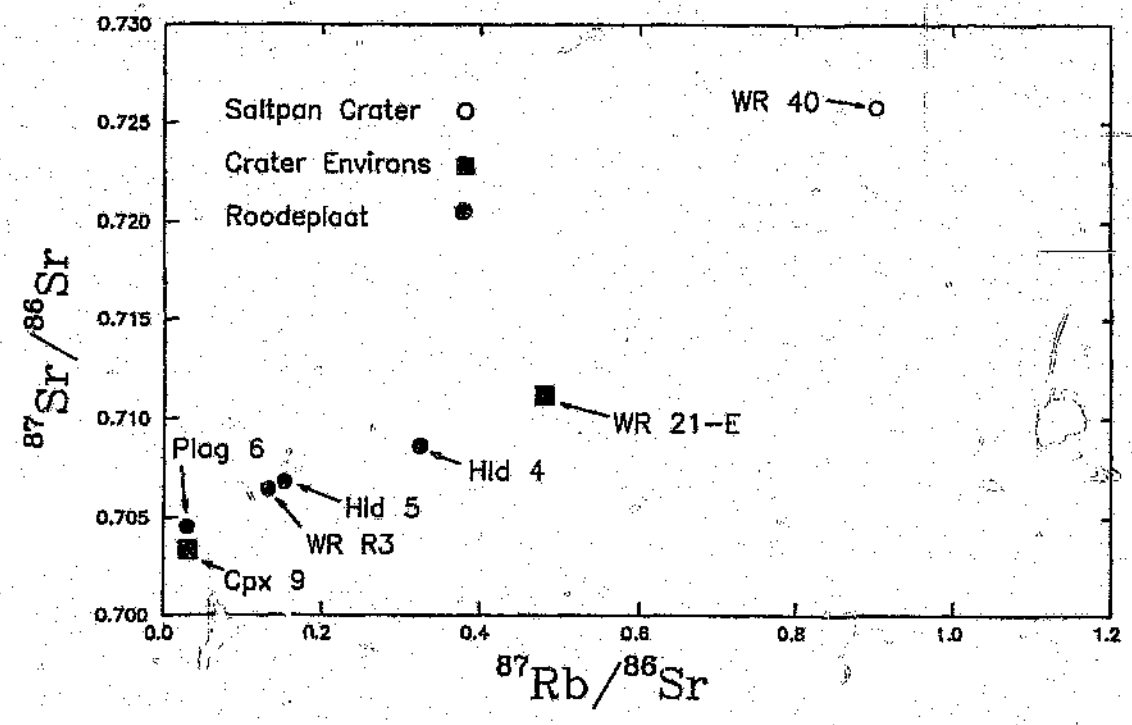

Figure 8.2 Diagram of the "lower end" values, combinations of which were used to calculate isochron ages (cf. text). Scatter is attributed to alteration.

Samples/separates used for Isochron Calculations	Resulting Age	Initial Ratio (R_0)	MSWD
Hld-5 (and four biotites)	1340±11 Ma	0.7040±2	0.941
Cpx-9 (and four biotites)	1343±11 Ma	0.7028±2	0.907
Plag-6 (and four biotites)	1340±11 Ma	0.7040±2	0.942
Hld-4 (and four biotites)	1344±11 Ma	0.7024±2	0.895
Hld-5, Plag 6 (and four biotites)	1339±11 Ma	0.7040±1	0.738

Table 8.4 Isochron results for calculations with different sample combinations. Errors are 1σ, and errors on initial ratios refer to the last digit of the R_0 value.

From these results it is obvious that, although there is a certain scatter in the data (Figure 8.2), different combinations of data result in isochrons yielding very similar ages and errors. Figure 8.1 shows an isochron representing the best fit calculation, using a hornblende (Hld 4 from the Roodeplaat syenite) and the clinopyroxene (Cpx 9 from a crater environ lamprophyre) data to constrain the lower limits. This isochron shows the perfect alignment of biotites from the crater rim sample and the Roodeplaat sample. Biotite model ages were calculated using initial ratios R_0 of 0.7024 - 0.7040, constrained by the intercepts of the isochron calculations (Table 8.4). The biotite model ages obtained are:

for Bio-1: Roodeplaat biotite- 1320 Ma
Bio-2: Roodeplaat biotite- 1321 Ma
Bio-3: Altered Roodeplaat biotite- 1056 Ma
Bio-7: Crater rim phonolite biotite- 1303 Ma
Bio-8: Crater rim phonolite biotite- 1305 Ma

These model ages, with the exception of that for altered biotite Bio-3, all correlate reasonably well with the isochron age of 1342±11 Ma (Figure 8.1).

All the above Rb-Sr age data, with the exception of one age (1056 Ma) obtained for an altered sample, be it biotite model ages or various isochron ages, all fall into the range between 1300 Ma and 1350 Ma. These ages apply to both the crater rim sample, a lamprophyre from outside of the crater and a Roodeplaat sample. These ages also agree well with the results obtained in previous chronological studies, as summarized in Table 8.1. In conclusion, these results support the argument that the intrusives of the entire region are more or less coeval and have no association with the cratering event at ca. 200 ka ago.

CHAPTER 9 DISCUSSION

In 1988 a borehole was drilled to obtain the necessary information for the establishment of the true origin of the crater and to document and study the accumulated, undisturbed crater sediments for palaeoenvironmental changes since the formation of the crater (Scott, 1988; Partridge et al., 1993). Thus the drillcore allowed for a good vertical control of the crater fill, whereas the crater itself had only been studied superficially (Feuchtwanger, 1973) before the drillcore became available.

As the origin of the Pretoria Saltpan crater has been a matter of controversy for the last century, much research has been carried out on this structure. The fortuitous coincidence of the spatial occurrence of the crater with mafic and alkaline intrusives has been the main argument against the impact interpretation. The areas outside of the rim and the possibility of occurrences of mafic and alkaline rocks both in the wider region and within the crater have been disregarded in previous work. The objectives of this study attempt to resolve any existing controversies therefore may be summarized as follows:

1) A geochronological analysis was required to improve the understanding of the occurrences of the various intrusives.

2) Trace element analysis was required to reveal which rock types contributed to the high siderophile element abundances detected in the crater fill breccias, and to understand any relationships the intrusives from the crater site may have with the rocks from the crater environs and the Pienaars River Alkaline Complex.

3) Detailed mapping of the crater rim and its environs, together with comparative petrographic and chemical studies on samples from the crater and its environs was required to investigate the possibility of an association of the basic and alkaline intrusives with the cratering event. A detailed structural analysis would contribute to a better understanding of the cratering processes and allows to compare an impact structure in a crystalline target to the well studied Meteor Crater, Arizona, which was formed in sedimentary target rocks.

4) With the aid of the stratigraphy provided by the drill-core, better modelling of geophysical data was possible. A gravity survey of higher resolution than that of Fudali

et al. (1973) was carried out and should lead to a better understanding of the subsurface structure and the crater-fill configuration. In addition, a first magnetic survey has also been carried out over the Saltpan crater.

5) A second, smaller depression to the southeast of the main crater, which was not recognised before and may represent a twin or satellite crater, was investigated geophysically using magnetic, gravity, seismic and resistivity methods.

Regional geology

Mineralogical and chemical results indicate that the alkaline and ultramafic intrusives found at the crater site, which were previously used as an argument in support of a volcanic origin for the crater, are found in the crater environs as well. These rock types are also related to each other with regard to their respective ages (1.2-1.4 Ga) and were found to be much older than the crater itself. The Pretoria Saltpan crater is situated only about 10 kilometres from the presently known margin of the Pienaars River Alkaline Complex. This Complex occupies an extensive area in which recurring plutonic and volcanic mafic and alkaline igneous activity took place, with no less than 20 intrusive plugs, pipe swarms and volcanic occurrences known within a radius of 80 kilometres (e.g., Fudali et al., 1973; Harmer, 1985). However, all of these features pre-date the Permian. No Karoo volcanics were encountered in the mapped region, which therefore indicates that the entire region has been geologically inactive since the alkaline volcanic activity at about 1300 Ma ago. The crater formed at 220±52 ka ago in a long before geologically inert terrane. The regional joint and fracture system in the entire area outside of the impact structure originated from normal tectonic processes and was not affected by the cratering event.

Crater geology

The well exposed rim shows intense deformation of originally horizontally jointed rocks. The recognised deformation features are typical structures of simple bowl-shaped impact structures: closer to the crater floor, the rim granite dips gently inwards and there is evidence for shallow inward-dipping, closely spaced shear surfaces. Towards the rim crest the granite dips gently outwards to varying degrees, which is indicative of upwarping. Ejecta debris (granitic fragmental breccia) is found in an inverted stratigraphic sequence

(older granitic breccia overlies younger Karoo Grits) at various localities along the rim. The rim is disrupted by concentric thrust faults and radial fractures. The mid-section of the rim consists of an anticline, which is locally displaced along some inward-dipping faults. A few concentric inward-dipping normal faults are superimposed on the structures of the upper rim. These are thought to have been formed during the modification stage towards the end of the cratering stage. All these structures, or combination of these structures, are well known from other terrestrial simple bowl-shaped impact structures, in particular Meteor Crater, Arizona and the Odessa crater, Texas. According to Shoemaker (1960), no crater of demonstrated volcanic origin, particularly the maar type crater with which Meteor Crater, as well as the Pretoria Saltpan crater, have been compared (e.g., Milton and Naeser, 1971), has a structure or arrangement of debris in the rim comparable to that observed at small impact structures such as Meteor Crater and the Pretoria Saltpan.

Detailed mapping has revealed that most of the intrusives on the crater rim have no preferred orientation, contrary to the proposal by Feuchtwanger (1973). Instead, many dykes and sills have been faulted both radially and concentrically by a post-intrusive event, undoubtedly by the impact event. The jointing patterns of the crater rim and close environs are markedly different from those observed in the surrounding region, and exhibit a well-defined radial and concentric pattern, which can be related to strain deformation, caused by the upward and outward movement of material when the shock wave and the reflected rarefraction waves reached their limits (Shoemaker, 1960) during the cratering event.

Comparison to other meteorite craters

The Pretoria Saltpan Crater exhibits a structure similar to that of the Odessa crater. The features common to both the Pretoria Saltpan crater and the Odessa crater are: a) steeply outward-dipping rock and throwout (ejected) fragmental breccia on the upper rim, b) a faulted anticline in the mid-rim and c) inward-dipping structures on the lower rim. Figure 9.1a shows the structures of the Odessa crater and 9.1b the structure of Meteor Crater (compare Figure 4.11: section of the Pretoria Saltpan crater rim). Figure 9.2 (cf. Figures 9.1a and 9.1b) is a schematic cross-section of the Pretoria Saltpan crater

based on the structural studies and on the drill-core stratigraphy, modified after Reimold et al. (1992) and Partridge et al. (1993). Figure 9.2 shows that the structures in the rim of the Saltpan crater (listed above) have similarities to the structures of both Odessa and Meteor Craters.

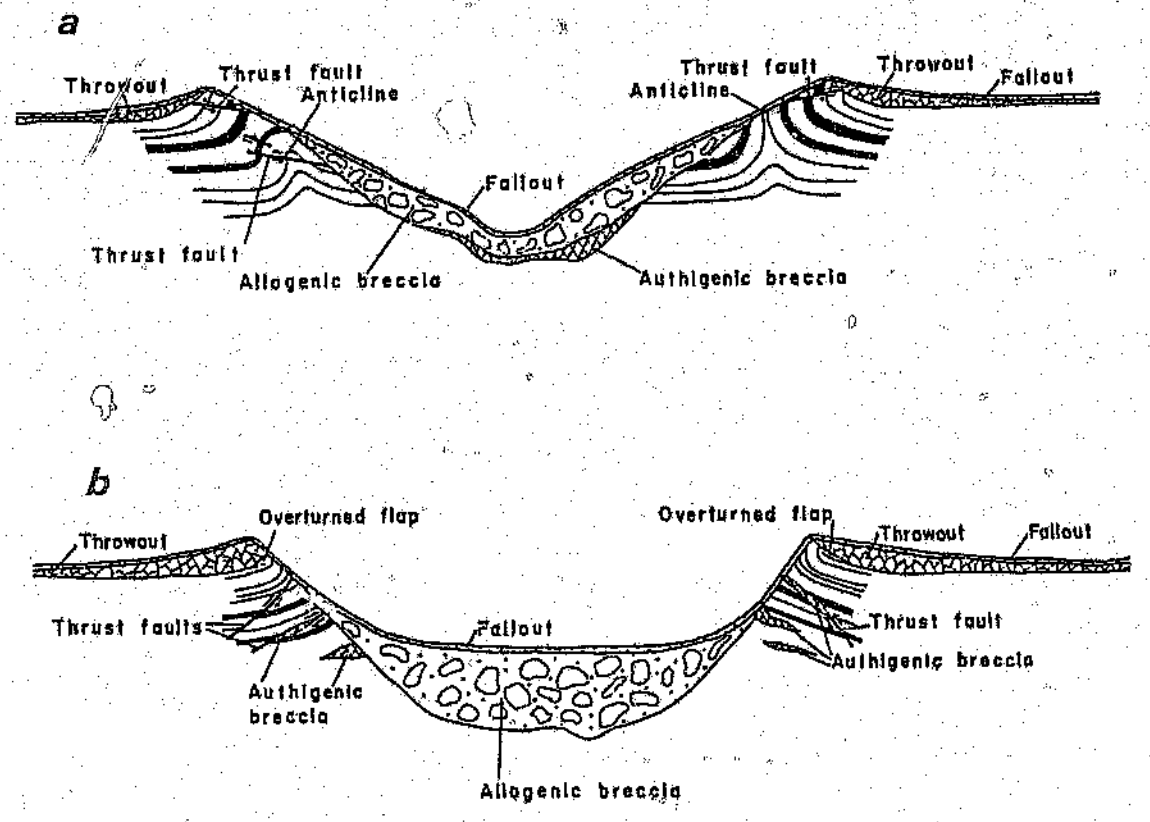

Figure 9.1 Schematic cross sections illustrating the structure of **(a)** Odessa crater and **(b)** Meteor Crater (after Shoemaker and Eggleton, 1961).

The Pretoria Saltpan crater exhibits many of the deformation structures observed at Meteor Crater (Figure 9.1b), and has a strikingly similar topographic appearance to this crater (compare Figures 9.3 and 9.4). The rim of Meteor Crater is at present 47 metres (originally 67 metres (Melosh, 1989)) above the surrounding plain (Figure 9.3; compare with Figure 9.4), with an original depth below the plain of about 150 metres (Melosh, 1989). These values are very similar to those for the Pretoria Saltpan, of 60 metres (maximum present height) and 149 metres, respectively.

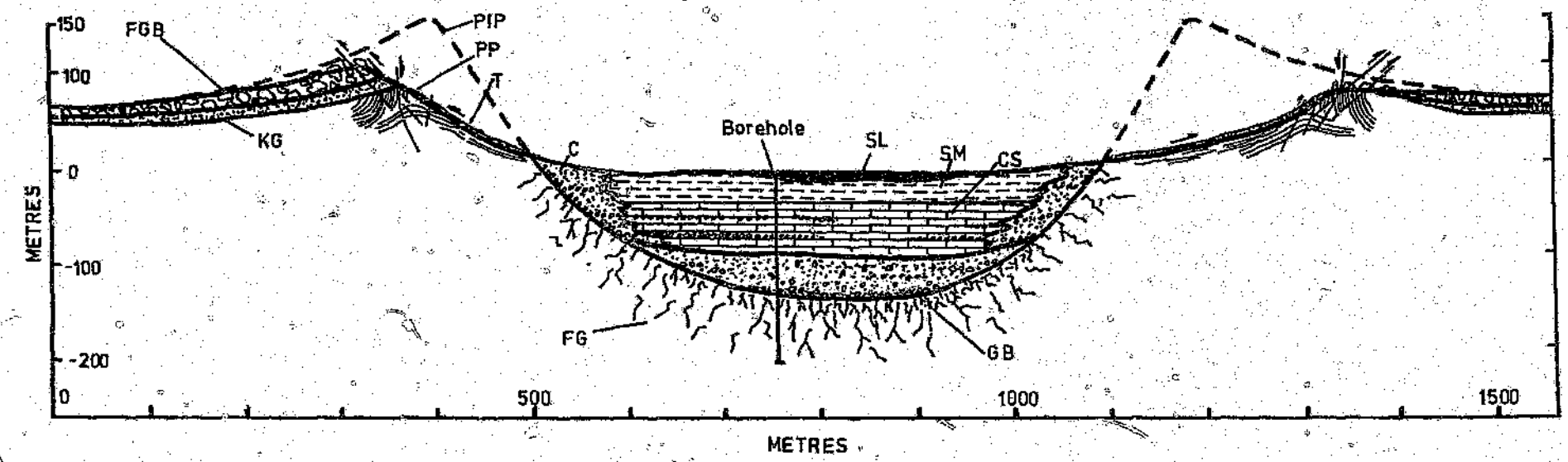

Figure 9.2 Schematic cross-section of the Pretoria Saltpan crater based on the drill-core stratigraphy (Reimold et al., 1992; Partridge et al., 1993) and the structure of the rim (this study). C=colluvium, CS=carbonate rich sediments, FG=fractured granite, FGB=fragmental granite breccia (allochthonous), KG=Karoo grits, MGB=monomict (cataclastic) granite breccia (autochthonous), PIP=inferred post-impact profile, PP=present profile, SL=saline lake, SM=saline muds, T=talus.

Figure 9.3 View of the uptilted northern rim of Meteor Crater, as seen from a distance of approximately 1.5 kilometres. The rim-to-rim diameter of Meteor Crater is 1.2 kilometres.

Figure 9.4 View of the Pretoria Saltpan crater rim from the south. Note the similarity in morphology to that of Meteor Crater (Figure 9.3).

Joints, faults, or planes of weakness in the target rock have affected the final shape of Meteor Crater. Seen in plan view, the crater is more square than circular, with small tear faults at each "corner" of the rim (Melosh, 1989). This square shape of the crater has been attributed to two orthogonal sets of vertical joints traversing the sedimentary rocks in which the crater was formed. These joint sets cut approximately diagonally across the crater's square shape (Shoemaker, 1963). As discussed in Chapter 4, the joint sets in the region of the Pretoria Saltpan are more complex (three prominent joint sets were determined for the crater region, and each locality may exhibit a unique joint pattern). Apparently these did not play a significant role in determining the final shape of the crater. This could well be the result of different target lithologies, as Meteor Crater seems to be the only documented case, where jointing has played an important role in final crater shape.

Considering the fact that the age of Meteor Crater is approximately one quarter of that of the Pretoria Saltpan structure, the overall morphology of Meteor Crater is extremely similar to that of the Saltpan crater (Figures 9.3 and 9.4); that is, the Saltpan crater is almost as well preserved as Meteor Crater. Figure 9.5 shows one of the largest ejecta blocks at Meteor Crater. Blocks of these dimensions were not observed at the Pretoria Saltpan crater, but may have existed prior to erosion and denudation of the crater rim. Ejecta blocks with dimensions of a few metres, however, are observed on the eastern rim (Figure 9.6) and also occur on the northern rim as partly buried massive granite outcrops.

Figure 9.7 exhibits the steepened upper portion of the rim at Meteor Crater, which is very similar to that of the Pretoria Saltpan crater (where it is not clearly visible due to the vegetation cover). Figure 9.8 exhibits the radial faulting present at Meteor Crater, which is typical of impact structures. At the Pretoria Saltpan crater the presence of such faults has given rise to the undulating topography of the rim and the erosional gullies. The radial and upward displacement seen in Figure 9.8 was not observed to this extent at the Pretoria Saltpan crater, probably as a consequence of the vegetation cover and the more poorly preserved outcrop.

Figure 9.5 One of the largest ejecta blocks on the rim of Meteor Crater. This block is about 6 metres high.

Figure 9.6 One of the largest ejecta blocks on the eastern rim of the Saltpan crater. This block is about 3.5 metres high.

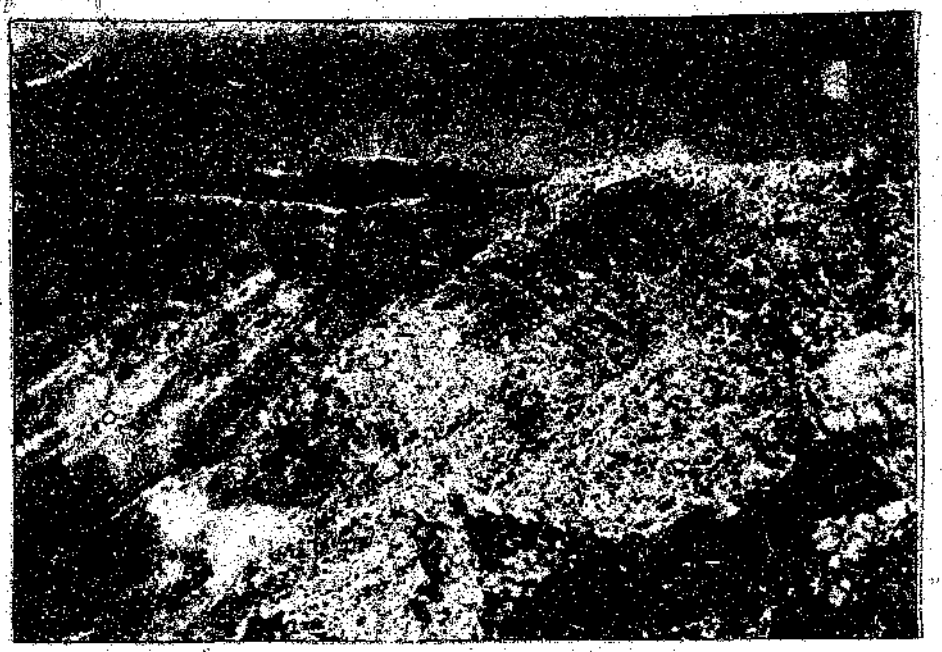

Figure 9.7 Upturned strata at the upper rim at Meteor Crater, which may be observed on the upper rim of the Pretoria Saltpan crater, too. In the background the San Franciscan volcanic peaks, some 80 kilometres to the west of Meteor Crater, are visible.

Figure 9.8 Typical impact-induced radial faulting in the upper rim of Meteor Crater. Note the radial and upward displacement at this locality.

Figure 9.7 Upturned strata at the upper rim at Meteor Crater, which may be observed on the upper rim of the Pretoria Saltpan crater, too. In the background the San Franciscan volcanic peaks, some 80 kilometres to the west of Meteor Crater, are visible.

Figure 9.8 Typical impact-induced radial faulting in the upper rim of Meteor Crater. Note the radial and upward displacement at this locality.

Many blocks which have been uptilted and rotated by almost 90° were observed, particularly on the upper portion of the rim, at Meteor Crater (Figure 9.9 shows such a block). Reorientation of granite blocks to this extent were observed at the Pretoria Saltpan crater, too, and resulted in complex structures in the upper rim.
Overall the structures observed at the Pretoria Saltpan crater are all typical of a simple bowl-shaped meteorite crater of these dimensions, as was shown by using Meteor Crater and Odessa Crater for comparison.

Figure 9.9 Rotated mega-block on the rim of Meteor Crater. Photograph taken looking towards the centre of the crater. The usual concentric orientation of the sediments is seen here to have been rotated by as much as 90° resulting in a radial orientation. The diagonal width of the photographed area is approximately 4 metres.

Crater and projectile dimensions

Melosh (1989) noted that transient simple bowl-shaped craters on planetary bodies are morphologically similar, having a depth/diameter ratio of between 1/5 (0.2) and 1/3 (0.33). Using drill-core information, together with reasonable erosional assumptions, shows that the Pretoria Saltpan crater had a transient cavity (the cavity which forms at the end of the excavation stage; Melosh, 1989) depth of approximately 250 metres (using information from the drill-core) and a transient cavity diameter of approximately 1000 metres (the diameter of the transient cavity is less than the final crater diameter as a result of slumping of the inner crater walls). This results in a depth/diameter ratio of 0.25, which is well within the above range for simple bowl-shaped impact structures.

According to Dence et al. (1977), an approximate relation between crater diameter (D) in kilometres and impact energy (E) in kilotons of TNT (1 kiloton TNT = 4.186×10^{12} Joules; Dence et al., 1977) is given by

$$D = 0.1\sqrt[3]{E} \qquad (9.1)$$

Since the kinetic energy (KE) released on impact is given by

$$KE = \tfrac{1}{2}mv^2 \qquad (9.2),$$

the diameter varies with the cube root of the mass of the impacting meteorite. For the Pretoria Saltpan crater with a diameter of about 1.1 kilometres, equation 9.1 gives the impact energy (E) for the Saltpan impact event as 1331 kilotons TNT. Using equation 9.2 and the minimum and maximum values of 11.2 km/s and 72.8 km/s (Buchwald, 1975) for final impacting velocities for a meteorite having the calculated energy above, the minimum and maximum masses for the projectile that caused the Saltpan crater can be constrained to 2,1 and 88,8 tons, respectively. The maximum density for the proposed meteorite is that of an iron meteorite (7.9 g/cm^3), and the minimum density is that of a type I carbonaceous chondrite (2.2 gm/cm^3). For the reasonable minimum and maximum velocity (Glass, 1982) and mass values, and upper and lower density limits for the projectile, four different diameter values can be calculated for the projectile that

could form an impact crater of the size of the Pretoria Saltpan (shown in Table 9.1; all calculations assume a meteorite of spherical shape and vertical impact). Geochemical studies (Koeberl et al., 1993a) indicate that a chondritic projectile is the most likely type of projectile to have caused the Saltpan crater. Therefore, the table also shows what are believed to be reasonable values (assuming a stony meteorite composition: density of 3.5 g/cm^3 and velocity of 25 km/s, gives a diameter of 21.3 metres), which are well within the range of the obtained maximum and minimum values.

Velocity (km/s)	Mass (tons)	Density (g/cm^3)	Diameter (metres)
11.2	88,832	2.2	42.6
		7.9	27.8
72.8	2,102	2.2	12.2
		7.9	8.0
25	17,829	3.5	21.3

Table 9.1 Range of possible densities and diameters calculated using a minimum velocity, a maximum velocity and a probable velocity for the Saltpan projectile. All calculations use an estimated impact energy of 1331 kilotons TNT, calculated using equation 9.1 (Dence et al., 1977).

Geophysical implications

Identifying a structure solely on the basis of geophysical evidence can be ambiguous. Nevertheless, the geological data obtained from the drillcore (Partridge et al., 1993), were confirmed by the geophysical results from the structure. Gravity and magnetic observations may be primary geophysical indicators of impact structures, which, however, have to be confirmed through additional geological observations.

The results of the only gravity reconnaissance carried out over the crater prior to this study (Fudali et al., 1973) failed to support an impact origin. Although no singular rule exists for the relation between impact crater size and character or magnitude of geophysical anomalies (Pilkington and Grieve, 1992), the negative gravity anomaly determined over the Pretoria Saltpan crater is within reasonable limits of that expected for an impact crater of such size (compare also with Fudali, 1979). The depth extent of the low-density allochthonous breccia zone can be estimated and modelled to coincide with the actual drill core observation. Density modelling has shown that the crater structure is essentially a near-surface disturbance which dies out abruptly in intensity with radial distance from the centre of the structure. The final gravity model is in excellent agreement with the observed stratigraphic column for the central borehole (Reimold et al., 1992).

The magnetic signature over the main crater produced no evidence of any magnetic volcanic material or pipe (for example kimberlite) which may have been thought to exist below the crater fill. This again is in agreement with petrographic findings on drillcore samples that preclude a significant contribution from volcanic rocks to the unconsolidated suevitic breccia (Reimold et al., 1992).

The small circular feature to the southeast of the main crater, which could represent a satellite or twin crater because of it's vicinity to the main crater, its perfectly circular shape which is completely different to the normally encountered shapes of other pans in the Transvaal, and its absolutely unique regional presence, does not show geophysical signatures typical of impact craters. Application of geophysical techniques unfortunately did not establish the true nature of this feature, but a rough depth section with lithological breaks at 0.7 metre and 26 metre depths was determined. The lower depth is thought to represent the lower contact between depression-fill and floor material (probably Nebo granite) beneath the structure. A drilling program is definitely required in order to explain the inconclusive geophysical results and to solve the open question as to the nature of this feature.

Petrology and chemical results

The alkali and mafic intrusives found at the crater site were believed by a number of authors (for example: Wagner, 1922; Feuchtwanger, 1973; Wallace, 1979) to be unique to the crater area and therefore related to the cratering process. Petrological and chemical (major and trace element) investigations have matched the various rock types from the crater area to those of the crater environs and the Pienaars River Alkaline Complex. These investigations have shown that the alkaline and mafic rocks found at the crater are common in the surrounding region. Furthermore, no signs of volcanic feeder-dykes were encountered in the drill-core into the crater centre, which would be expected if the crater was the cause of any of the intrusives found at the crater.

McNerney et al. (1992) suggested that the Greenview alkaline lamprophyre, which was shown in this study to be similar to the lamprophyres from the crater and crater environs, should be considered as a possible southward extension of the Pienaars River Alkaline Complex. From these observations it is apparent that the Pienaars River Alkaline Complex may influence a greater area than was previously thought to be the case, and that the Saltpan crater is actually situated on the northwestern extension of this alkaline complex. Outcrop in the crater environs is scarce and weathering is severe (which was also noted by Milton and Naeser, 1971). Therefore, it is probable that small bodies of carbonatite do occur in the crater environs, but remained hidden because of weathered granite overburden.

Impact cratering-related deformation and shock metamorphism

The observations on the drill-core breccia have shown the presence of shocked particles, and, aided by geophysical results, have delineated the extent of a thick breccia lens in the interior of the circular structure (Figure 9.2). However, evidence of shock and rock deformation diminishes rapidly with depth, as soon as the fractured and the undeformed crater floor are reached.

The absence of coesite, stishovite, and shatter cones at this structure do not rule out an impact origin. Other small astroblemes, such as West Hawk Lake, commonly failed to show these criteria (Short, 1970). Meteorite fragments, in general, occur only at relatively

young craters where meteorite material has not been completely vaporized during impact, or subsequently destroyed by erosion and chemical weathering (Short, 1970). In the absence of readily identifiable meteoritic material, shock metamorphism has to be used as the main meteorite impact criterion (Dence, 1968). Reimold et al. (1992) noticed an enrichment of glasses and sulphide spherules in siderophile elements and Cr. This they attributed to the possible contamination of the breccia by part of the projectile.

Carter et al. (1986; 1990) claimed that planar deformation features can occur in explosive volcanic environments. However, Alexopoulos et al. (1988) and Grieve et al. (1990) have shown that the character of shock-produced planar deformation features is well established and is distinct from that of lamellar micro-structures produced in other high strain environments. A wide diversity of shock effects was observed in quartz grains both from the core and from selected rim breccia samples. According to Robertson and Grieve (1977), diagnostic shock metamorphic effects should not be expected to be formed in the rocks from the rims of small simple craters. Nevertheless, a few breccia samples found on the rim displayed planar deformation features in quartz grains (Chapter 6). The abundant petrographic evidence for shock metamorphism, covering the full range of shock pressures between circa 15 and 45 GPa in quartz and feldspar minerals, is unequivocal proof for the origin of the Pretoria Saltpan crater by meteorite impact (Reimold et al., 1991, 1992).

Grieve and Cintala (1992) predicted approximately $1x10^{-3}$ km^3 of impact melt for an impact crater of the dimensions of the Saltpan. Using 1.14% by volume glass fragments and spherules in the 56 metre thick breccia zone (Reimold et al., 1992) and an average diameter of the breccia zone of 40 metres result in a melt volume of $1x10^{-3}$ km^3, which is identical to the prediction by Grieve and Cintala (1992). The true average diameter of this breccia zone is, however, thought to be 100 metres which would give a much larger ($6x10^{-3}$ km^3) impact melt volume. Even though the figures used to determine the impact melt volume are approximate values, the results roughly agree with the order of magnitude calculated by Grieve and Cintala (1992). It should also be noted that a large fraction of melted rock may have been dispersed as part of the ejecta, as assumed for West Hawk Lake crater (Short, 1970).

Geochronological results

According to Grieve and Pesonen (1992), there is a clear bias in the ages of terrestrial impact craters, with over 50% of known craters having ages of less than 200 Ma. This reflects the effect of erosion, which removes the topographic and geologic expression of an impact crater. Clearly, the relatively small Pretoria Saltpan crater must be young, due to its excellent state of preservation. In fact, its excellent state of preservation alone makes it extremely unlikely that the structure can be older than the Pleistocene, which was even recognised by Fudali et al. (1973). This observation is in agreement with ages obtained by Partridge et al. (1993), Storzer et al. (1993), and Koeberl et al. (1993b) for the cratering event of about 200 ka (cf. Chapter 8). Rb-Sr chronology on intrusives from the crater area, crater environs, and the Roodeplaat Complex yields ages between 1200 and 1350 Ma. Therefore, there is a very long time gap between the last endogenic activity that has occurred in the entire study area surrounding the crater and the cratering event.

The currently known cratering record (Koeberl, 1994) for Africa comprises the data in Table 9.2. From this it is clear that the number of known impact structures in Africa is significantly less than the number of impact craters known for North America and Europe (Grieve and Pesonen, 1992) of relatively much smaller aerial extent. Clearly, a large number of impact craters still remain to be discovered in Africa.

Name	Country	Diameter (km)	Age(Ma)
Amguid	Algeria	0.45	<0.1
Aorounga	Chad	12.6	?
Aouelloul	Mauritania	0.36	3.1±0.3
B.P. Structure	Libya	2.8	<120
Bosumtwi	Ghana	10.5	1.1±0.2
Highbury	Zimbabwe	15-25	<1800
Kalkkop	South Africa	0.64	<5
Oasis	Libya	11.5	<120
Ouarkziz	Algeria	3.5	<70
Pretoria Saltpan	South Africa	1.13	0.2
Roter Kamm	Namibia	2.5	3.7±0.3
Talemzane	Algeria	1.75	<3
Tenoumer	Mauritania	1.9	2.5±0.5
Tin Bider	Algeria	6	<70
Vredefort	South Africa	140	1970±100

Table 9.2 The currently known cratering record for Africa (Koeberl, 1994).

CHAPTER 10 CONCLUSIONS

Young and well-preserved impact craters such as the Pretoria Saltpan are rare in the terrestrial cratering record. The Saltpan crater, therefore, provided an excellent opportunity for a structural analysis of such a crater. Further work was required with respect to the distribution of the lithologies and the occurrence of alkaline rocks in an otherwise granitic terrane. The geology of the crater environs and the possibility that mafic and alkaline lithologies could be a regional phenomenon and not be restricted to the crater, have been disregarded in previous work. This study has shown that the Pretoria Saltpan crater occurs in an area of alkaline activity, the age of which has been determined at about 1.3 Ga. The cratering event is significantly younger at about 220 ka ago.

The evidence of a high degree of crater circularity, a topographically high rim, a flat crater floor, which is lower than the surrounding area, the lack of associated volcanic material combined with the evidence of shock metamorphism, prove an impact origin. Petrographic and well documented structural observations have also met and demonstrated all the criteria which have been observed at other impact structures, such as Meteor Crater, Arizona. Thus, an origin by impact for the Pretoria Saltpan crater is the only reasonable explanation for the existence of this crater and its characteristics. The petrographic and structural observations on the crater, as well as the new geological data, are all in agreement with an impact origin for the Pretoria Saltpan structure.

REFERENCES

Alexopoulos, J.S., Grieve, R.A.F. & Robertson, P.B. (1988). Microscopic lamellar deformation features in quartz: Discriminative characteristics of shock-generated varieties. *Geology*, 16, p. 796-799.

Alvarez, L.W., Alvarez, W., Asaro, F. & Michel, H.V. (1980). Extraterrestrial cause for the Cretaceous-Tertiary extinction. *Science*, 208, p. 1095-1108.

Ashton, P.J. & Schoeman, F.R. (1983). Limnological studies on the Pretoria Salt Pan, a hypersaline maar lake. *Hydrobiologica*, 99, p. 61-73.

Bischoff, L. & Oskierski, W. (1987). Fractures, pseudotachylite veins and breccia dykes in the crater floor of the Rochechouart impact structure, SW-France, as indicator of crater forming processes. In *Research in Terrestrial Impact Structures*, ed. J. Pohl. Vieweg Publ., Braunschweig-Wiesbaden, Germany, p. 5-29.

Bischoff, L. & Oskierski, W. (1988). The surface structure of the Haughton impact crater, Devon Island, Canada. *Meteoritics*, 23, p. 209-220.

Bohor, B.F., Foord, E.E., Modreski, P.J. & Triplehorn, D.M. (1984). Mineralogical evidence for an impact event at the Cretaceous/Tertiary boundary, *Science*, 224, p. 867-869.

Bohor, B.F., Modreski, P.J. & Foord, E.E. (1987). Shocked quartz in the Cretaceous/Tertiary boundary clays: Evidence for a global distribution. *Science*, 236, p. 705-708.

Bond, G.W. (1946). A geochemical survey of the underground water supplies of the Union of South Africa. *South Africa Geol. Survey Mem.*, 41, 208 pp.

Brandt, D. (1991). A detailed study of the recent sedimentation at the Pretoria Salt Pan. B.Sc. Hon. Project, Dept. of Geology, Univ. of the Witwatersrand (unpubl.), 91 pp.

Brown, R.W., Allsopp, H.L., Bristow, J.W. & Smith, C.B. (1989). Improved precision of Rb-Sr dating of kimberlitic micas: an assessment of a leaching technique. *Chem. Geol.* (Isotope Geosc. Section), 79, p. 125-136.

Buchwald, V.F. (1975). Handbook of Iron Meteorites, 3 Volumes. University of California Press, 1418 pp.

Bunch, T.E. (1968). Some characteristics of selected minerals from craters. In *Shock Metamorphism of Natural Materials,* eds. B.M. French & N.M. Short, Mono Book Corp., Baltimore, p. 41 - 432.

Carter, N.L., Officer, C.B., Chesner, C.A. & Rose, W.I. (1986). Dynamic deformation of volcanic ejecta from the Toba caldera: Possible relevance to the Cretaceous/Tertiary boundary phenomena. *Geology,* 14, p. 380-383.

Carter, N.L., Officer, C.B. & Drake, C.L. (1990). Dynamic deformation of quartz and feldspar: Clues to causes of some natural crises. *Tectonophysics,* 71, p. 373-391.

Coertze, F.J., Burger, A.J., Walraven, F., Marlow, A.G. & MacCaskie, D.R. (1978). Field relations and age determinations in the Bushveld Complex. *Trans. geol. Soc. S. Afr.,* 81, p. 1-11.

Cullers, R.L. & Graf, J.L. (1984). Rare earth elements in igneous rocks of the continental crust: predominantly basic and ultrabasic rocks. In *Rare Earth Element Geochemistry,* ed. P. Henderson, Vierweg Publ., Amsterdam, p. 237-268.

Davis, J.L. & Annan, A.P. (1989). Ground penetrating radar for high resolution mapping of soil and rock stratigraphy. *Geophys. Prospect.,* 37, p. 531-551.

De Laubenfels, M.W. (1965). Dinosaur extinction: one more hypothesis. *J. Paleontol.*, 30, p. 207-218.

Dence, M.R. (1968). Shock zoning at Canadian craters: petrography and structural implications. In *Shock Metamorphism of Natural Materials*, eds. B.M. French & N.M. Short, Mono Book Corp., Baltimore, p. 169-184.

Dence, M.R., Grieve, R.A.F. & Robertson, P.B. (1977). Terrestrial impact structures: principal characteristics and energy considerations. In *Impact and Explosion Cratering*, eds. D. J. Roddy, R. O. Pepin & R. B. Merrill, Pergamon Press, New York, p. 247-275.

Egglington, B.M. & Harmer, R.E. (1991). GEODATE: a program for the processing and regression of isotope data using IBM-compatible microcomputers. *CSIR Manual EMA-H 9101*, Pretoria, 57 pp.

Faure, G. (1977). *Principles of Isotope Geology*. John Wiley & Sons, Inc., 464 pp.

Feuchtwanger, T. (1973). *Zoutpan: A carbonatite-alkaline volcano*. B.Sc. Hons. Proj., Dept. of Geology, Univ. Witwatersrand, Johannesburg, (unpubl.), 41 pp.

French, B.M. & Short, N.M. (Eds.) (1968). *Shock Metamorphism of Natural Materials*. Mono Book Corp., Baltimore, Maryland, 644 pp.

Frey, H. (1980). Crustal evolution of the early earth: the role of major impacts. *Precambrian Research*, 10, p. 195-216.

Fudali, R.F. (1979). Gravity Investigations of Wolf Creek Crater, Western Australia. *J. Geol.*, 87, p. 55-67.

Fudali, R.F., Gold, D.P., & Gurney, J.J. (1973). The Pretoria Salt Pan: Astrobleme or Cryptovolcano ? *J. Geol.*, 81, p. 495-507.

Gault, D.E., Quaide, W.L. & Oberbeck, V.R. (1968). Impact Cratering Mechanics and Structures. In *Shock Metamorphism of Natural Materials*, eds. B.M. French & N.M. Short, Mono Book Corp., Baltimore, p. 87-99.

Glass, B. P. (1982). *Introduction to Planetary Geology.* Cambridge University Press, New York, 469 pp.

Grieve, R.A.F. (1980). Impact bombardment and its role in proto-continental growth on the early earth. *Precambrian Research*, 10, p. 217-247.

Grieve, R.A.F. & Cintala, M.J. (1992). An analysis of differential impact melt-crater scaling and implications for the terrestrial impact record. *Meteoritics*, 27, p. 526-538.

Grieve, R.A.F. & Pesonen, L.J. (1992). The terrestrial impact cratering record. *Tectonophysics*, 216, p. 1-30.

Grieve, R.A.F., Sharpton, V.L. & Stöffler, D. (1990). Shocked minerals and the K/T controversy. *EOS Trans. Am. Geophys. Union*, 71, p. 1792.

Harmer, R.E. (1985). Rb-Sr isotopic study of units of the Pienaars River Alkaline Complex, north of Pretoria, South Africa. *Trans. Geol. Soc. S. Afr.*, 88, p. 215-223.

Heinrich, E.W. (1965). *Microscopic Identification of Minerals.* McGraw-Hill Inc., New York, 414 pp.

Henderson, R.C. and Zeitz, I. (1948). Analysis of total magnetic intensity anomalies produced by point and line sources. *Geophysics*, 13, p. 1-3.

Hörz, F. (1965). Untersuchungen an Riesgläsern. *Beitr. Mineral. Petrogr.*, 11, p. 621-661.

Hörz, F. & Ahrens, T.J. (1969). Deformation of experimentally shocked biotite. *Amer. J. Sci.*, 267, p. 1213-1229.

Jeppe, F. (1868). Die Transvaalsche oder S. A. Republik nebst einem Anhang: Dr. Wangemann's Reise in Südafrika. *Petermann's Geogr. Mitt. Erg.*, 24, 24 pp.

Kerr, S.J., Stanistreet, I.G. & Partridge, T.C. (1993). The sedimentary facies record from the Pretoria Saltpan crater. *S. Afr. J. Sci.*, 89, p. 372-374.

Koeberl, C. (1993). Instrumental neutron activation analysis of geochemical and chosmochemical samples: A fast and proven method for small sample analysis. *Journal of Radioanalytical and Nuclear Chemistry*, 168, p. 47-60.

Koeberl, C. (1994). African meteorite impact craters: characteristics and geological importance. *Journal of African Earth Sciences*, in press.

Koeberl, C., Kluger, F. & Kiesl, W. (1987). Rare earth element determinations at ultratrace abundance levels in geologic materials. *Journal of Radioanalytical and Nuclear Chemistry*, 112, p. 481-487.

Koeberl, C., Reimold, W.U. & Shirey, S.B. (1994a). Saltpan Impact Crater, South Africa: geochemistry of target rocks, breccias, and impact glasses, and osmium isotope systematics. *Geochimica et Cosmochimica Acta*, in press.

Koeberl, C., Storzer, D. & Reimold, W.U. (1994b). The age of the Saltpan impact crater, South Africa. *Meteoritics*, 28, in press.

Le Bas, M.J., Le Maitre, R.W., Streckeisen, A. & Zanettin, B. (1986). A chemical classification of volcanic rocks based on the total alkali-silica diagram. *J. Petrol.*, 27, p.745-750.

Leonard, F.C., (1946). Authenticated meteorite craters of the world: a catalog of provisional co-ordinate numbers for the meteoritic falls of the world. *Meteoritics,* 1, Univ. New Mexico. Publ., 54 pp.

McClay, K. (1987). *The Mapping of Geological Structures.* Open University Press, London, 161 pp.

McLaren, D.J. (1970). Time, life, and boundaries. *J. Paleontol.,* 44, p. 801-815.

McNerney, N., Dippenaar, K. & Snyman, C.P. (1992). The geology of the Greenview lamprophyric breccia vent. *S. Afr. J. Geol.,* 95, p. 194-202.

Melosh, H.J. (1989). *Impact Cratering: A Geologic Process.* Oxford University Press Inc., Oxford, 245 pp.

Milton, D.J. & Naeser, C.W. (1971). Evidence for an impact origin of the Pretoria Salt Pan, South Africa. *Nature Phys. Sci.,* 229, p. 211-212.

Nakamura, N. (1974). Determination of REE, Ba, Fe, Mg, Na and K in carbonaceous and ordinary chondrites. *Geochim. Cosmochim. Acta.,* 38 p. 757-775.

Nicolaysen, L.O., De Villiers, J.W.L., Burger, A.J. & Strelow, F.W.E. (1958). New measurements relating to the absolute age of the Transvaal System and the Bushveld Igneous Complex. *Trans. geol. Soc. S. Afr.,* 61, p. 137-163.

Nockolds, S.R., Knox, R.W.O'B. & Chinner, G.A. (1978). *Petrology for Students.* Cambridge University Press, Cambridge, 435 pp.

Norrish, K. & Hutton, J.T. (1969). An accurate X-ray spectrographic method for the analysis of a wide range of geological samples. *Geochim. Cosmochim. Acta,* 33, p. 431-453.

Oosthuyzen, E.J. & Burger, A.J. (1964). Radiometric dating of intrusives associated with the Waterberg System. *Ann. Geol. Surv. S. Afr.*, 3, p. 87-106.

Partridge, T.C., Reimold, W.U. & Walraven, F. (1990). The Pretoria Zoutpan Crater: First results from the 1988 drilling project. *Meteoritics*, 25, p. 396.

Partridge, T.C., Kerr, S.J., Metcalfe, S.E., Scott, L., Talma, A.S. & Vogel, J.C. (1993). The Pretoria Saltpan: a 200,000 year Southern African lacustrine sequence. *Palaeogeography, Palaeoclimatology, Palaeoecology,* 101, p. 317-337.

Peters, L.J. (194?). The direct approach to magnetic interpretation and its application. *Geophysics,* 14, p. 3.

Pilkington, M. & Grieve, R.A.F. (1992). The geophysical signature of terrestrial impact craters. *Reviews of Geophysics,* 30, p. 161-181.

Pilon, J.A., Grieve, R.A.F. & Sharpton, V.L. (1991). The subsurface character of Meteor Crater, Arizona, as determined by ground probing-radar. *J. Geophys. Res.*, 96 (15), p. 563-576.

Pohl, J., Bleil, U. & Hornemann, U. (1975). Shock magnetization and demagnetization of basalt by transient stress up to 10 kbar. *J. Geophys.*, 41, p. 23-41.

Reimold, W.U. & Hörz, F. (1986). Textures of experimentally shocked (5.1-35.5 GPa) Witwatersrand quartzite. *Lunar Planet. Sci. XVII,* p. 703-704, Lunar and Planet. Institute, Houston.

Reimold, W.U. & Koeberl, C. (1992). Pretoria Saltpan impact crater: impact glasses and sulphide spherules. *Lunar Planet. Sci. XXIII,* p. 1139-1140, Lunar and Planet. Institute, Houston.

Reimold, W.U., Oskierski, W., & Huth, J. (1987). The pseudotachylite from Champagnac in the Rochechouart meteorite crater, France. *Proc. Lunar Planet. Sci Conf. 17th, J. Geophys. Res.,* 92, p. E737-E748.

Reimold, W.U., Koeberl, C., Kerr, S.J. & Partridge, T.C. (1991). The Pretoria Saltpan - the first firm evidence for an origin by impact. *Lunar Planet. Sci. XXII,* pp. 1117-1118, Lunar and Planet. Inst., Houston.

Reimold, W.U., Koeberl, C., Partridge, T.C. & Kerr, S.J. (1992). Pretoria Saltpan crater: Impact origin confirmed. *Geology* 20, p. 1079-1082.

Robertson, P.B. & Grieve, R.A.F. (1977). Shock attenuation at terrestrial impact structures. In *Impact and Explosion Cratering,* eds. D.J. Roddy, R.O. Pepin & R.B. Merrill. Pergamon, New York, p. 687-702.

Robertson, P.B., Dence, M.R. & Vos, M.A. (1968). Deformation in rock-forming minerals from Canadian craters. In *Shock Metamorphism of Natural Materials,* eds. B.M. French and N.M. Short. Mono Book Corp., Baltimore, Md., p. 433-452.

Rock, N.M.S. (1991). *Lamprophyres.* Blackie, Glasgow, 285 pp.

Roddy, D.J., Shuster, S.H., Kreyenhagen, K.N. & Orphal, D.L. (1980). Computer code simulations of the formation of Meteor Crater, Arizona: Calculations MC-1 and MC-2, *Proc. Lunar Planet. Sci. Conf. 11th,* p. 2275-2307.

Rohleder, H.P.T. (1933). The Steinheim basin and the Pretoria Salt Pan: Volcanic or meteoritic origin? *Geol. Mag.,* 70, p. 489-498.

Schneider, H. (1971). Deformation und Umwandlung von Biotiten aus Gesteinen des Nördlinger Rieskraters durch Stosswellenmetamorphose. Dissertation, Tübingen.

Schreiner, G.D.L. (1958). Comparison of the ^{87}Rb-^{87}Sr ages of the red granite of the Bushveld Complex from measurements on the total rock and separated mineral fractions. *Proc. Roy. Soc. London,* Ser. A, 245, p. 112-117.

Schreiner, G.D.L., & Van Niekerk, C.B. (1958). The age of a Pilanesberg dike from the central Witwatersrand. *Trans. geol. Soc. S. Afr.,* 61, p. 198-199.

Scott, L. (1988). The Pretoria Saltpan: A unique source of Quaternary palaeoenvironmental information. *South African Journal of Science,* 84, p. 560-562.

Sharpton, V.L. & Grieve, R.A.F. (1990). Meteorite impact, cryptoexplosion, and shock metamorphism; a perspective on the evidence at the K/T boundary. *Geol. Soc. Am., Special Paper,* 247, p. 301-318.

Shoemaker, E.M. (1960). Penetration mechanics of high velocity meteorites, illustrated by Meteor Crater, Arizona. *Internat. Geol. Congr., 21st Session,* pt. 18, Copenhagen, p. 418-434.

Shoemaker, E.M. (1963). Impact mechanics at Meteor Crater, Arizona. In *The Moon, Meteorites, and Comets,* eds. B.M. Middlehurst & G.P. Kuiper (The Solar System, vol. 4.). University of Chicago Press, Chicago and London, p. 301-336.

Shoemaker, E.M. & Eggleton, R.E. (1961). Terrestrial features of impact origin. In *Proc. Geophysical Lab./Lawrence Radiation Crat. Symp.*, ed. M.D. Milo, p. A1-A27.

Short, N.M. (1970). Anatomy of a meteorite impact crater: West Hawk Lake, Manitoba, Canada. *Geol. Soc. Am. Bull.,* 81, p. 609-648.

Smith, C.B. (1983). *Rubidium-strontium, uranium-lead, and samarium-neodynium isotopic studies of kimberlite and related mantle-derived xenoliths.* Ph.D. thesis, Univ. Witwatersrand, Johannesburg, (unpubl.), 436 pp.

Smith, C.B., Allsopp, H.L., Kramers, J.D., Hutchinson, G. & Roddick, J.C. (1985). Emplacement ages of Jurassic-Cretaceous South African kimberlites by the Rb-Sr method on phlogopite and whole-rock samples. *Trans. Geol. Soc. S. Afr.*, 88, p. 249-266.

Snelling, N.J. (1963). Age determination unit. *Ann. Rep. Overseas geol. Surv.*, p. 30.

South African Committee for Stratigraphy (SACS). (1980). Stratigraphy of South Africa. Part I (comp. L.E. Kent). Lithostratigraphy of the Republic of South Africa, South West Africa/Namibia, and the Republics of Bophuthatswana, Transkei and Venda. *Handbk. Geol. Surv. S. Afr.*, 8, 690 pp.

Steiger, R.H., & Jäger, E. (1977). Subcommission on Geochronology: Convention on the use of decay constants in geo- and cosmochronology. *Earth Planet. Sci. Lett.*, 36, p. 359-362.

Stöffler, D. (1972). Deformation and transformation of rock-forming minerals by natural and experimental shock-processes, I. Behaviour of minerals under shock compression. *Fortschr. Miner.*, 49, p. 50-113.

Stöffler, D. (1974). Deformation and transformation of rock-forming minerals by natural and experimental shock processes, II. Physical properties of shocked minerals. *Fortschr. Miner.*, 51 (2), p. 256-289.

Stöffler, D., Ewald, U., Ostertag, R. & Reimold, W.U. (1977). Research drilling Nördlingen 1973 (Ries): composition and texture of polymict breccias. *Geol. Bavarica.*, 75, p. 163-189.

Storzer, D., Koeberl, C., & Reimold, W.U. (1993). The age of the Pretoria Saltpan impact crater, South Africa. *Lunar Planet. Sci. XXIV*, p. 1365-1366, Lunar and Planet. Inst., Houston.

Trollope, A. (1878). *South Africa.* Balkema, Cape Town, 504 pp. (reprinted edition edited by J.H. Davidson, 1973).

Urey, H. (1973). Comet collisions and geological periods. *Nature,* 242, p. 32-33.

Vacquier, V., Steenland, N.C., Henderson, R.G. and Zeitz, I. (1951). Interpretation of Aeromagnetic Maps. *Geol. Soc. of America, Mem.* 47, New York.

Van Niekerk, C.B. (1962). The age of the Gemspost Dyke from the Venterspost gold mine. *Trans. Geol. Soc. S. Afr.,* 65, p. 105-111.

Verwoerd, W.J. (1967). The Carbonatites of South Africa and South West Africa. *Handb. Geol. Surv. S. Afr.,* 6, 292 pp.

Wagner, P.A., (1922). The Pretoria Saltpan. *Geol. Surv. S. Afr. Mem.,* 20, 136 pp.

Wallace, R.C. (1979). Note on some of the mafic ejecta from the Pretoria Saltpan. *Trans. Geol. Soc. S. Afr.,* 79, p. 191-196.

Walraven, F. & Hattingh, E. (1993). Geochronology of the Nebo Granite, Bushveld Complex. *S. Afr. J. Geol,* 96, p. 31-41.

Walraven, F., Burger, A.J. & Allsopp, H.L. (1982). Summary of age determinations carried out during the period April 1981 to March 1982. *Ann. Geol. Surv. S. Afr.,* 16, p. 107-114.

Walraven, F., Retief, E.A., Burger, A.J. & de V. Swanepoel, D.J. (1987). Implications of new U-Pb zircon age dating on the Nebo Granite of the Bushveld Complex. *S. Afr. J. Geol.,* 90, p. 344-351.

Wyllie, P.J. (1966). Experimental studies of carbonatite problems: the origin and

differentiation of carbonatite magmas. In *Carbonatites*, eds., O.F. Tuttle & J. Gittins, Richard Clay Ltd., Suffolk, p. 311-352.

APPENDIX A : MAJOR ELEMENT ANALYSES OF THE STUDY SAMPLES

1) Samples from the mapped area (data in wt%)

Sample No.	SiO_2	TiO_2	Al_2O_3	Fe_2O_3	MnO	MgO	CaO	Na_2O	K_2O	P_2O_5	LOI	TOTAL
2 #	52.02	1.12	14.10	10.33	0.23	2.49	4.54	0.60	7.91	1.55	4.19	99.07
14 *	37.92	6.88	7.42	22.69	0.42	4.06	7.61	0.00	2.97	0.71	9.74	100.42
41 *	39.67	5.94	6.33	19.07	0.30	7.55	13.92	0.41	2.40	0.59	3.59	99.75
76 #	50.02	1.24	13.99	10.89	0.27	2.34	6.28	4.51	2.94	1.74	4.87	98.99
104 *	39.18	0.79	13.43	25.74	0.41	3.90	5.25	0.92	1.63	0.24	9.19	100.67
107 =	23.92	0.34	5.15	11.48	0.75	7.75	19.76	0.00	3.24	1.32	25.85	99.56
109 *	39.58	5.91	5.87	19.37	0.32	8.23	13.73	0.34	1.46	0.55	4.960	100.31
4 #	39.46	9.05	9.28	25.25	0.17	2.90	1.05	0.00	2.05	0.74	10.17	100.12
19 *	35.32	5.92	5.92	19.87	0.46	5.22	13.71	0.00	2.14	0.55	10.66	99.78
22 #	57.67	1.35	17.04	8.85	0.03	0.97	0.09	0.00	9.85	0.03	4.05	99.93
23 #	48.45	12.30	14.93	11.19	0.18	1.45	0.08	0.00	5.61	0.06	5.56	99.82
40 +	48.45	1.12	14.04	10.05	0.14	3.16	7.50	3.50	5.75	1.52	4.80	100.01
53 *	40.07	5.78	5.73	18.29	0.28	8.14	14.40	0.00	2.59	0.53	4.04	99.84
72 x	73.54	0.26	9.49	7.38	0.21	0.32	0.24	1.71	4.46	0.12	1.86	99.58
95 =	11.85	1.22	1.34	9.63	0.78	4.16	36.94	0.00	0.03	1.16	32.34	99.44
P o	49.29	0.85	22.01	12.32	0.12	1.94	1.34	3.98	4.78	0.10	3.35	100.06
21-C *	38.76	5.36	14.43	17.15	0.20	3.26	0.87	0.16	3.48	0.46	14.76	98.89
21-E *	43.42	5.32	6.94	18.12	0.33	7.75	9.52	1.00	2.85	0.59	4.26	100.09
21-I(2) *	47.83	4.91	11.87	18.50	0.24	2.46	0.50	0.00	6.28	0.08	6.41	99.08
21-I(3) *	49.24	4.67	10.87	15.36	0.25	3.92	3.52	3.23	3.65	0.65	4.39	99.74
21-B -	75.75	0.14	5.65	1.90	0.02	0.17	0.12	0.00	2.43	0.04	12.80	99.02
23-D *	39.03	5.60	6.14	18.79	0.34	7.25	13.83	0.51	3.03	0.55	4.83	99.91
SP-GR ♦	76.58	0.12	11.44	1.99	0.07	0.16	0.54	3.28	4.99	0.06	0.60	99.81
ZP-BR x	57.80	0.14	9.98	13.89	0.32	1.69	5.25	1.06	2.47	0.14	7.40	100.14
ZP-1 ♦	72.4	0.25	12.2	3.1	-	-	0.65	3.3	5.6	0.03	0.7	98.23
ZP-4 x	80.2	0.26	8.1	4.2	0.02	0.3	0.3	1.2	3.6	0.04	1.2	99.42

Total Fe as Fe_2O_3

* Lamprophyre = Carbonatite o Albitic Gneiss Xenolith
\# Trachyte ♦ Granite - Quartz-rich Vein
\+ Phonolite x Granite Breccia

2) Samples from the Pienaars River Alkaline Complex

Sample	SiO_2	TiO_2	Al_2O_3	Fe_2O_3	MnO	MgO	CaO	Na_2O	K_2O	P_2O_5	LOI	TOTAL
R1-Roodeplaat	56.17	0.61	14.55	9.72	0.18	5.45	6.87	3.50	2.05	0.12	2.05	101.27
R2-Roodeplaat	68.32	0.77	11.96	8.49	0.10	0.93	2.11	1.99	3.23	0.24	1.62	99.76
R3-Roodeplaat	58.05	1.17	17.67	6.8	0.17	1.84	3.60	5.17	3.01	0.35	1.10	98.91
R4-Roodeplaat	57.70	0.62	18.58	3.97	0.16	0.60	3.73	5.48	4.94	0.04	3.38	99.20
R5-Roodeplaat	58.29	1.12	18.21	6.50	0.14	1.57	3.26	5.30	3.10	0.35	1.06	98.91
R6-Roodeplaat	55.31	0.94	14.31	8.04	0.46	0.60	3.39	5.15	8.44	0.06	2.39	99.09
R7-Roodeplaat	56.68	1.75	13.84	13.78	0.35	2.93	1.33	4.24	0.10	0.18	3.67	98.85
R8-Roodeplaat	59.38	1.04	16.05	7.46	0.82	0.28	0.05	0.00	13.95	0.09	2.01	100.32
R8A-Rd.plaat	53.28	0.52	18.98	5.76	0.36	0.91	3.04	2.52	8.74	0.04	5.38	99.52
R9-Roodeplaat	37.52	3.96	10.02	14.28	0.20	6.67	12.25	1.60	0.31	0.43	12.60	99.84
R10-Rd.plaat	52.91	0.76	15.73	9.00	0.14	7.58	9.54	1.68	1.12	0.09	1.12	99.66
R11-Rd.plaat	53.32	0.48	15.93	9.16	0.15	6.77	10.28	1.80	0.83	0.08	0.62	99.41
KLIPDRIFT	49.82	0.90	15.26	11.74	0.20	7.75	10.19	1.50	0.82	0.10	0.88	99.16
LEEUW-KRAAL	57.96	0.92	18.26	4.40	0.19	0.71	1.77	7.59	5.57	0.14	1.58	99.09

3) Water and carbon contents of selected samples from the study area (given in wt%)

Sample Number	Water	Carbon
21-I(2)	6.64	0.11
22	3.92	0.19
23	5.47	0.21
21-C	12.60	0.08
R9	4.09	9.52
107	1.35	7.03
95	1.60	32.72
19	3.53	8.56
107	1.94	27.41

APPENDIX B : MICROPROBE RESULTS OF LAMPROPHYRE PYROXENES

(data in wt%)

Sample No.	SiO_2	TiO_2	Al_2O_3	FeO	MnO	MgO	CaO	Na_2O	K_2O	Cr_2O_3	NiO	TOTAL
21-E*	51.11	1.99	1.41	7.43	0.18	13.66	22.93	0.60	-	-	-	99.31
23-D*	51.87	1.63	2.01	7.78	0.26	14.28	22.23	0.70	0.04	0.01	-	100.81
109#	50.73	1.88	1.58	7.16	0.19	13.46	23.00	0.47	0.03	-	0.11	98.61
53(1)#	50.22	1.38	1.21	6.04	0.11	14.32	23.07	0.49	-	0.13	0.07	97.04
53(2)#	49.87	1.33	1.20	5.47	0.06	14.76	23.15	0.50	-	0.26	0.06	96.66

* Crater Environ Samples
\# Crater Rim Samples

APPENDIX C : TRACE ELEMENT RESULTS

1) Samples from the mapped area (data in ppm)

Sample No.	Rb	Sr	Y	Zr	Nb	V	Cr	Co	Ni	Cu	Zn	Ba
2	292	288	66	592	184	101	13	11	17	19	136	2201
14	123	988	43	519	161	413	184	52	186	169	166	2220
41	171	1057	33	448	138	405	205	48	148	287	1188	970
76	77	210	31	582	191	100	19	6	15	11	115	345
104	110	52	97	874	88	237	478	53	72	6	409	160
107	117	478	259	511	84	73	36	4	25	1	157	141
109	124	1010	30	414	128	417	268	59	161	267	126	642
4	79	583	252	640	217	307	212	25	191	289	296	1741
19	147	1088	39	423	128	418	304	50	171	256	125	992
22	530	54	133	769	189	87	17	6	18	12	100	777
23	324	245	214	929	290	422	27	19	66	216	192	3063
40	229	518	24	662	158	93	12	2	14	17	121	837
53	188	954	31	412	124	379	263	57	163	264	132	1254
72	128	60	89	343	59	37	3	1	7	0	39	762
95	14	379	36	123	30	146	59	20	32	8	58	27
P	505	120	79	180	17	164	185	25	52	14	170	787
21-C	152	233	1207	594	150	355	739	20	215	81	739	1159
21-E	148	868	47	539	195	326	220	49	172	246	145	1992
21-I(2)	237	673	172	574	191	271	97	18	92	177	1120	4636
21-I(3)	158	300	214	478	176	263	100	31	119	159	152	1535
21-B	79	12	76	219	9	16	10	7	6	7	38	540
23-D	412	883	54	411	123	389	148	50	119	315	126	1428
ZP-1	167	-	69	321	19	12	4	7	7	0	52	1121
Zp-4	128	-	64	348	20	16	24	8	12	bd	49	805

2) Samples from the Pienaars River Alkaline Complex

Sample	Rb	Sr	Y	Zr	Nb	V	Cr	Co	Ni	Cu	Zn	Ba
R1-Roodeplaat	125	340	21	117	4	170	216	32	72	18	173	650
R2-Roodeplaat	93	187	42	281	13	46	5	15	5	5	121	1137
R3-Roodeplaat	74	1638	23	465	112	35	15	9	7	9	98	1195
R4-Roodeplaat	213	263	43	783	149	33	4	7	4	4	117	458
R5-Roodeplaat	81	1702	22	145	107	39	4	9	7	23	87	1232
R6-Roodeplaat	294	725	109	2203	459	149	26	0	8	3	505	2332
R7-Roodeplaat	1	235	39	3018	643	103	26	4	37	31	347	687
R8-Roodeplaat	371	79	61	1530	378	41	4	5	8	1	531	952
R8A-Roodeplaat	277	317	46	1047	167	64	19	3	6	4	311	540
R9-Roodeplaat	16	640	19	252	84	333	498	41	130	148	92	258
R10-Roodeplaat	46	309	19	90	6	176	363	37	83	56	71	278
R11-Roodeplaat	30	280	14	62	4	164	43	35	114	37	68	214
KLIPDRIFT	58	268	19	77	6	259	213	44	150	127	80	292
LEEUWKRAAL	137	1641	46	811	140	36	nd	8	342	2	102	1192

APPENDIX D: RESULTS OF INSTRUMENTAL NEUTRON ACTIVATION ANALYSIS

Data in ppm, except as noted

(Analyses by C. Koeberl, Institute of Geochemistry, University of Vienna)

	SP-95 Carb.	SP-137 Carb.	SP-104 Lamp.	SP-109 Lamp.	SP-21-E Lamp.	SP-21-I Lamp.	SP-22 Trachyte	SP-76 Trachyte	SP-R8A Microsyen.
From:	Crater	Crater	Crater	Crater	Environs	Environs	Crater	Crater	Roodeplaat
Na (%)	0.016	0.15	0.43	0.56	1.32	0.17	0.17	3.77	2.14
K (%)	0.074	2.48	1.21	1.11	2.84	4.46	7.01	2.39	6.39
Sc	10.1	9.02	18.5	34.9	29.7	25.3	4.55	3.31	0.31
Cr	67.7	75.4	376	282	266	127	29.3	22.1	6.1
Fe (%)	6.61	7.96	17.3	13.4	11.6	12.8	5.91	7.63	3.83
Co	30.1	12.8	12.3	76.9	61.9	41.1	9.78	15.2	2.72
Ni	37	105	80	180	180	175	50	31	15
Zn	70	181	410	193	180	1120	116	113	296
Ga	6.2	13.4	30	11	19	16.1	25	32	18
As	2.28	3.14	2.39	2.64	5.72	19.6	1.44	1.49	1.49
Se	0.4	1.3	0.9	1.2	1.1	0.7	0.5	0.41	1.55
Br	0.28	0.42	0.28	0.23	0.33	0.38	0.52	0.19	0.32
Rb	5.1	124	113	124	134	233	515	79.9	271
Sr	387	487	50	1030	900	775	40	216	314
Zr	130	788	780	421	340	692	679	532	885
Ag	0.08	0.11	0.08	0.29	0.61	0.61	0.17	0.07	0.06
Sb	0.25	0.67	0.58	0.36	0.64	1.37	0.41	0.35	0.65
Cs	0.098	0.26	2.12	13.1	7.64	3.55	6.61	0.98	1.36
Ba	47	276	92	339	871	2540	318	190	296
La	26.4	203	61.6	104	218	279	45.3	37.8	196
Ce	56.2	375	110	207	303	292	89.4	77.6	297
Nd	28.3	198	56.6	102	145	241	51.2	49.1	74.5
Sm	6.36	42.7	12.6	15.4	24.6	43.7	12.8	12.2	10.2
Eu	1.41	6.82	1.99	4.42	5.41	7.64	1.73	2.01	2.17
Gd	7.6	38	16	15	14	34	16.2	6.7	6.1
Tb	1.32	6.98	2.73	2.53	1.86	5.49	2.98	1.03	1.02
Dy	7.9	46	17.2	12	10	29	19	6.3	7.1
Tm	0.65	4.37	1.51	0.61	0.72	2.1	1.81	0.56	0.63
Yb	4.11	31.3	10.1	2.21	3.85	11.7	12.9	3.15	4.66
Lu	0.57	4.14	1.45	0.27	0.47	1.54	1.91	0.45	0.63
Hf	2.05	14.1	14.5	9.64	11.8	13.1	13.9	11.7	21.3
Ta	2.34	5.65	1.55	8.46	12.4	12.9	15.9	14.1	2.29
W	1.36	1.48	1.11	0.93	1.31	1.39	1.51	1.64	5.85
Ir (ppb)	<2	<1.5	<2	<1	<1.5	<2	<2	<2	<0.8
Au (ppb)	5.8	0.8	3.3	1.2	0.8	0.9	0.8	10.4	2.4
Hg	0.22	<0.4	<0.5	<0.24	<0.33	0.21	<0.5	0.06	0.38
Th	7.13	213	29.8	11.2	20.6	22.1	36.1	14.8	33.2
U	5.64	35.8	11.6	3.35	8.96	9.39	10.1	3.25	9.48

APPENDIX E: Rb-Sr DATING RESULTS ON A CRATER RIM LAMPROPHYRE
(Wairaven, unpubl.)

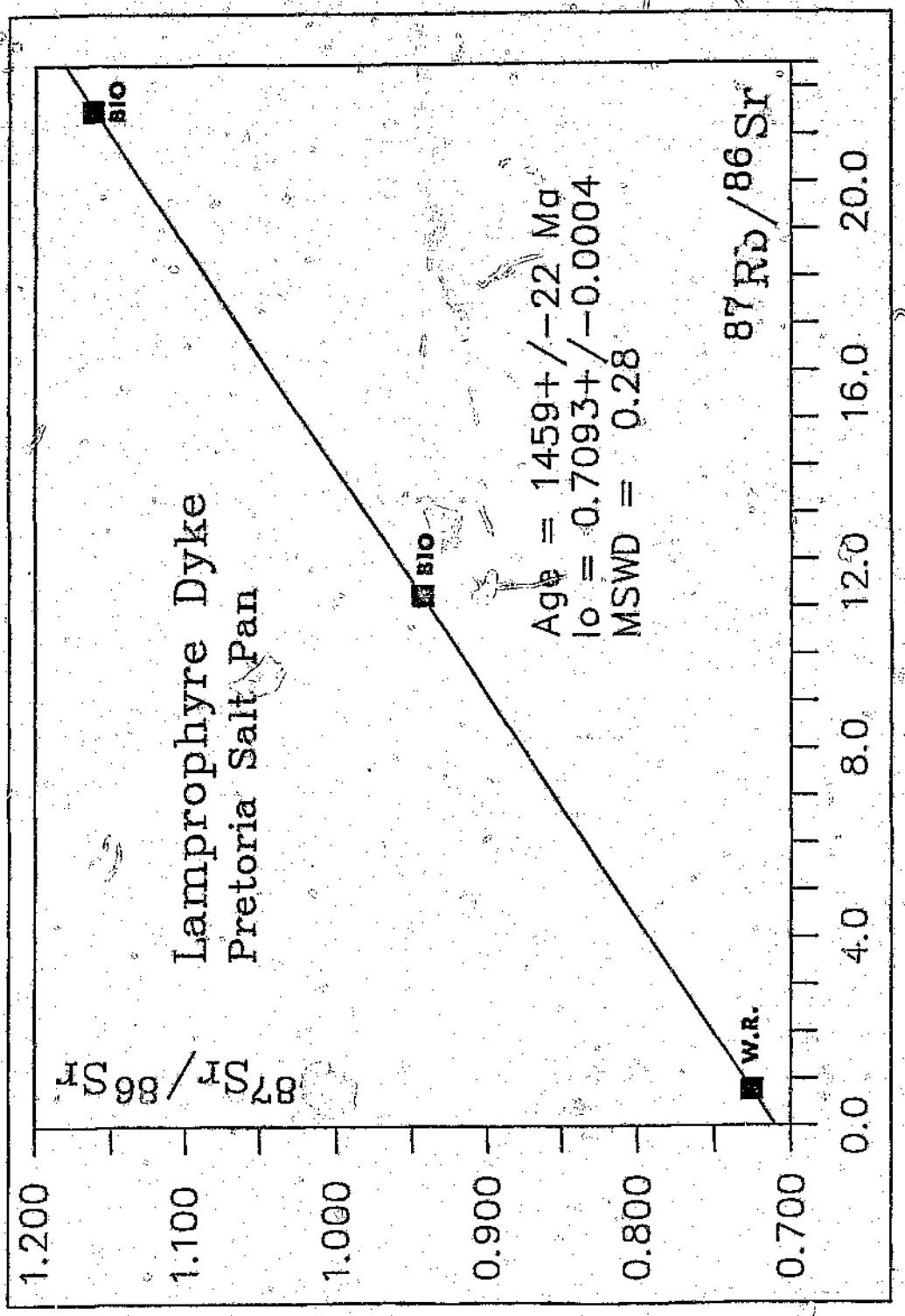

APPENDIX F: FISSION TRACK AGE OF IMPACT GLASS FRAGMENTS SEPARATED FROM MELT BRECCIAS. (Storzer et al., 1992)

Section No.	No. of Particles	Area Scanned	D_t	Age (ka)
10	83	3.61	0.55	107±76
11	59	2.70	1.85	361±161
12	27	1.76	1.14	222±157
13	87	3.24	1.54	301±135
14	52	1.74	0.58	112±112
15	91	2.72	1.10	215±124
16	57	1.06	0.94	183±183
TOTAL		16.83	1.13	220±52

Geology of the Region around the Pretoria Saltpan Crater

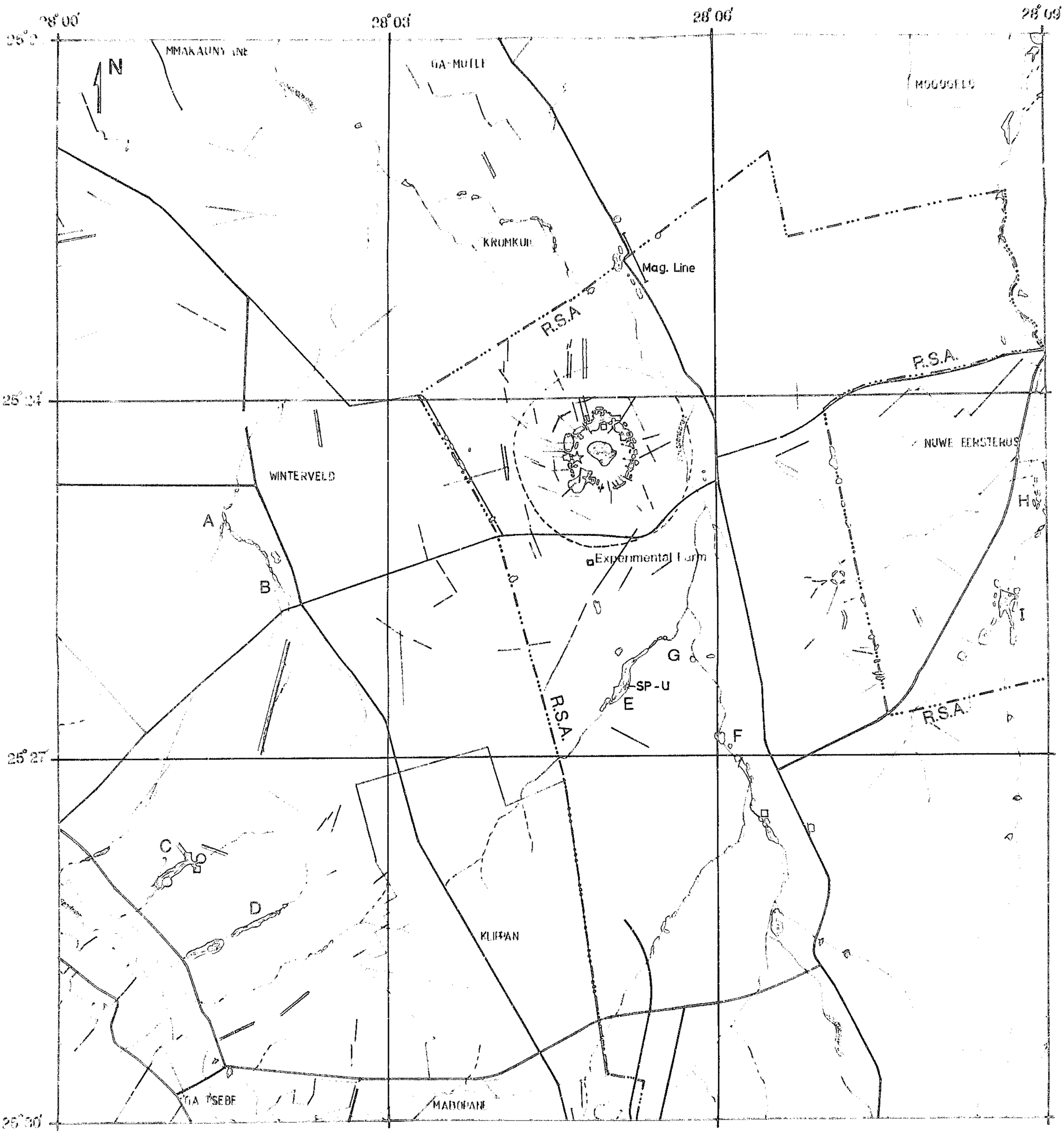

Compiled by Dion Brandt 1992–1993

28° 05' E

25° 24' 30" S

Rim Section

0 50 100 150 m

- Brine Lake
- Mud (Max. Lake Transgression)
- Granite Derived Sands
- Coarse Granitic Scree
- Karoo Grits
- Lamprophyre
- Trachyte
- Carbonatite
- Granite

- Vertical Dip
- Fault
- Bore Hole
- Trig. Beacon
- Drainage Channel
- Planetabled Area

Geology of the Pretoria Saltpan (Zoutpan) Crater

Compiled by
Dion Brandt 1992–1993

28° 05' E

25° 24' 30" S

Ring Section

0 50 100 150 m

- Brine Lake
- Mud (Max. Lake Transgression)
- Granite Derived Sands
- Coarse Granitic Scree
- Karoo Grits
- Lamprophyre
- Trachyte
- Carbonatite
- Granite

- Vertical Dip
- Fault
- Bore Hole
- Trig. Beacon
- Drainage Channel
- Planetabled Area

Geology of the Pretoria Saltpan (Zoutpan) Crater

Compiled by
Dion Brandt 1992-1993